

Thèse de Doctorat, soutenue à Aix-Marseille Université
Prévue le 29 Avril 2022 par

Farah Mustapha

Interrogation of Mechanotransduction in Early T cell Spreading



Discipline: Biologie / Santé

Spécialité: Immunologie

École doctorale: ED 62 – Sciences de la vie et de la santé

Effectuée au Laboratoire Adhésion et Inflammation (LAI), Aix Marseille University, LAI UMR 61, Inserm, UMR_S 1067, CNRS, UMR 7333, Marseille, F-13288, France, et au Centre Interdisciplinaire de Nanoscience de Marseille (CINAM), CNRS- AMU UMR 7325, Marseille, F-13288, France

Composition du jury

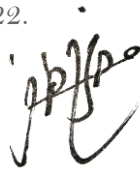
| | |
|--|------------------------|
| Dr. Jérémie Rossy Universität Konstanz | Rapporteur |
| Dr. Paolo Pierobon Institut Curie, Paris | Rapporteur |
| Prof. Janis Burkhardt University of Pennsylvania | Examinatrice |
| Dr. Claire Hivroz Institut Curie | Présidente du jury |
| Prof. Mossadek Talby Aix Marseille Université | Invité |
| Dr. Torsten Müller JPK Instruments/Bruker | Invité |
| Dr. Pierre-Henri Puech LAI | Directeur de thèse |
| Dr. Kheya Sengupta CINAM | Co-directrice de thèse |

*This project has received funding from the European Union's Horizon 2020 research and innovation programme under the Marie Skłodowska-Curie grant agreement No713750. Also, it has been carried out with the financial support of the Regional Council of Provence- Alpes-Côte d'Azur and with the financial support of the A*MIDEX (n° ANR- 11-IDEX-0001-02), funded by the Investissements d'Avenir project funded by the French Government, managed by the French National Research Agency (ANR).*

Affidavit

I, undersigned, Farah Mustapha, hereby declare that the work presented in this manuscript is my own work, carried out under the scientific direction of Pierre-Henri Puech and Kheya Sengupta, in accordance with the principles of honesty, integrity and responsibility inherent to the research mission. The research work and the writing of this manuscript have been carried out in compliance with both the French national charter for Research Integrity and the Aix-Marseille University charter on the fight against plagiarism. This work has not been submitted previously either in this country or in another country in the same or in a similar version to any other examination body.

Marseille, February 24th, 2022.

A handwritten signature in black ink, appearing to be 'Farah Mustapha', written in a cursive style.

Liste de publications et participation aux conférences

1) Liste des publications¹ réalisées dans le cadre du projet de thèse :

1. Mechanical Forces in T cell Biology. Mustapha F, Sengupta K, Puech P. Book Chapter, In: Immunology and Cancer Biology (2022).
2. May the force be with your (immune) cells: An introduction to traction force microscopy in Immunology. Mustapha F, Sengupta K, Puech P. Frontiers in Immunology (2022).
3. Cellular forces during early spreading of lymphocytes on ultra-soft substrates. Mustapha F, Pelicot M, Torro R, Sengupta K, Puech P. ELife (In submission).
4. Protocol for measuring weak cellular traction forces using well-controlled ultra-soft polyacrylamide gels. Mustapha F, Sengupta K, Puech P. Star Protocols, Cell Press (2022).
5. Rapid viscoelastic changes are a hallmark of early leukocyte activation. Zak A, Merino-Cortés S, Sadoun A, Mustapha F... Husson J. Biophysical Journal (2021).
6. Dissecting T-cell mechanosensing at molecular and cellular scales. Sadoun A, Mustapha F, Ndao O, Eich G, Hamon Y, Limozin L, Puech P. Wiley Analytical Science (2020).

2) Participation aux conférences² et écoles d'été au cours de la période de thèse :

1. ImmunoBiophysics EMBO Workshop- Virtual Meeting- 2021
2. Interdisciplinary Doctoral Day- Marseille, France- 2019
3. 2nd Mechanobiology Meeting- Quy Nhon, Vietnam- 2018

¹ Cette liste comprend les articles publiés, les articles soumis à publication et les articles en préparation ainsi que les livres, chapitres de livre et/ou toutes formes de valorisation des résultats des travaux propres à la discipline du projet de thèse. La référence aux publications doit suivre les règles standards de bibliographie et doit être conforme à la charte des publications d'AMU.

² Le terme « conférence » est générique. Il désigne à la fois « conférence », « congrès », « workshop », « colloques », « rencontres nationales et/ou internationales » ... etc.

Indiquer si vous avez fait une présentation orale ou sous forme de poster.

Résumé

Les lymphocytes T sont activés lorsque les récepteurs membranaires des lymphocytes T (TCR) reconnaissent les peptides antigéniques étrangers présentés par les complexes majeurs d'histocompatibilité (pCMH) des cellules présentatrices d'antigènes (CPA) au sein d'une interface cellule-cellule spécialisée appelée "synapse immunologique" (SI). De nombreuses recherches décrivent l'aspect biochimique de cette interaction, identifiant les réseaux de ligands sécrétés, les récepteurs de surface cellulaire, les voies de signalisation intracellulaire et les facteurs de transcription en jeu. Néanmoins, cela ne suffit pas à complètement élucider le(s) mécanisme(s) précis de l'activation des lymphocytes T.

Ces dernières années, il est apparu que les forces mécaniques générées au niveau de la SI sont essentielles à la bonne activation des lymphocytes T. En effet, on sait maintenant que les cellules T ne sont pas seulement sensibles mais aussi réactives aux forces et ce de l'échelle moléculaire (par le biais du TCR et des molécules d'adhésion, e.g. LFA-1) à l'échelle cellulaire. A cela manque une compréhension détaillée de la transmission de l'information mécanique à travers ces échelles.

À cette fin, le concept à la base de mon projet était d'étudier si et comment les forces cellulaires, transmises par certaines molécules, influencent l'activation précoce des cellules T. Pour ce faire, nous avons choisi de remplacer la cellule présentatrice d'antigène (CPA) par des gels de polyacrylamide mous. Sachant que les CPA couvrent une plage de rigidité ($\sim 0,4\text{--}2$ KPa) définie en fonction de leur type et de leur statut dans le processus d'inflammation, la première partie de ma thèse a été consacrée à la production de gels ayant l'élasticité la plus faible possible dans cette gamme (400 Pa), et fonctionnalisés avec des anticorps activateurs contre le TCR/CD3, CD28 (molécule co-stimulatrice) et LFA-1 (molécule d'adhésion). L'élasticité des gels a été déterminée par indentation à l'aide de microscopie à force atomique (AFM), tandis que l'homogénéité et la densité des molécules adsorbées ont été quantifiées par microscopie à épifluorescence.

Nous avons ensuite étudié l'étalement des cellules et la modulation des propriétés mécaniques des cellules T Jurkat Lifeact-GFP (actine marquée avec GFP) lors de leur interaction avec des gels d'élasticités différentes (0.4-200 KPa), mais fonctionnalisés avec le même anticorps activateur contre le TCR/CD3. Par la suite, nous avons utilisé les gels les plus souples (400 Pa et 2 KPa) pour étudier, à l'aide de microscopie à force de traction (TFM), les contraintes générées et les énergies exercées par les cellules T Jurkat (type sauvage), les cellules T Jurkat Lifeact-GFP et les cellules T Jurkat Lck-GFP (cytosquelette et membrane marquée à la GFP). À notre connaissance, de telles mesures à des élasticités aussi faibles et à des stades aussi précoces de l'interaction n'ont jamais été rapportées auparavant. Il est intéressant de noter que nos mesures de TFM dynamiques ont révélé de nouveaux profils de forces au cours du temps, modulés selon mécanique et la fonctionnalisation du substrat, et également influencés par les modifications génétiques des cellules où des rapporteurs fluorescents sont introduits dans la membrane ou dans le cytosquelette.

Enfin, nous avons étendu nos expériences TFM aux cellules T primaires, plus précisément aux cellules T humaines mémoire, naïves et stimulées, dans le but d'observer si une différence entre les énergies et entre les contraintes exercées par ces trois sous-types peut être détectée.

Mots clés: Lymphocytes T, cellules présentatrices d'antigènes, forces mécaniques, microscopie à force de traction

Abstract

T cells are activated when the membrane bound T cell receptors (TCRs) recognize the foreign antigenic peptides presented by the major histocompatibility complexes (pMHCs) of antigen presenting cells (APCs) within a specialized cell-cell interface termed the “Immunological Synapse” (IS). Today, an extensive body of research exists describing the biochemical aspect of this interaction, identifying the networks of secreted ligands, cell surface receptors, intracellular signaling pathways, and transcriptional factors at play. Unfortunately, this has not been sufficient to unravel the precise mechanism(s) of T-cell activation.

In recent years, it has become apparent that the mechanical forces generated at the IS are essential for the proper activation of T cells. Indeed, T cells are now known to be not only sensitive but also responsive to forces acting at both the molecular (through the TCR and adhesion molecules e.g. LFA-1) and cellular scale. What is lacking is a detailed comprehension of the transmission of the mechanical information across these scales.

To this end, the concept behind my project was to investigate if and how cellular forces, transmitted through certain molecules, influence early T cell activation. To do so, we chose to substitute the antigen presenting cell (APC) with surrogate polyacrylamide gels. Knowing that APCs span a defined stiffness range (~ 0.4 – 2 KPa) depending on their type and status in the inflammation process, the first part of my PhD was dedicated to producing gels with the lowest possible elasticity within that range (400 Pa), and functionalized with activating antibodies against the TCR/CD3, CD28 (co-stimulatory molecule) and LFA-1 (adhesion molecule). The elasticity of the gels was determined by indentation using Atomic Force Microscopy, and the homogeneity and density of the coated molecules was verified using epifluorescence microscopy.

We then studied the spreading and the modulation of the mechanical properties of Jurkat Lifeact-GFP T cells (actin labeled with GFP) when interacting with gels of different elasticities (0.4–200 KPa) but functionalized with the same activating antibody against the TCR/CD3. After that, we employed the softest gels (400 Pa and 2 KPa) for studying, using traction force microscopy (TFM), the generated stresses and the energies exerted by Jurkat T cells (wild-type), Jurkat Lifeact-GFP T cells and Jurkat Lck-GFP T cells (cytoskeleton and membrane labeled with GFP). Similar measurements at such low elasticities, and during such early stages of interaction, have never been reported before to our knowledge. Interestingly, our dynamic TFM measurements revealed new patterns of force application over time, that are modulated as a function of substrate mechanics and functionalization, and that are also impacted by the genetic manipulation of cells to introduce fluorescent reporters at the membrane or in the cytoskeleton.

Finally, we have also extended our TFM experiments to primary T cells, specifically Memory, Naive and Stimulated human T cells, in the aim of observing if any difference in the stresses and energies exerted between these three subtypes can be detected.

Keywords: T lymphocyte, antigen presenting cell, mechanical forces, traction force microscopy

Acknowledgements

To my jury members, **Claire Hivroz**, **Janis Burkhardt**, **Jérémie Rossy**, and **Paolo Pierobon**, I am truly honored, and frankly a bit terrified, to have my work evaluated by researchers of your caliber. Thank you for generously taking the time out of your schedules to read my manuscript and partake in my defense. My manuscript may not be the most flashing, I am aware, however, I truly do hope that you find it an interesting read.

To my invitees, **Mossadek Talby** and **Torsten Müller**, you were under no obligation to be part of my jury, however, you both accepted without hesitation. You have been part of this journey since the very beginning. It makes me quite happy that you will be there to see it till the very end.

To my co-supervisor **Kheya Sengupta**, I have always found it quite inspiring and motivating to watch women in STEM lead the way, working with you was of no exception to that. Thank you for your invaluable feedback, encouraging words (that were much needed at certain times), and most importantly for telling Pierre to stop when he was being a bit too Pierre.

To my supervisor **Pierre-Henri Puech**, well, we made it, a bit of battle wounds, scars and emotional trauma, but nevertheless, here we are, still standing. When we first met, I was an immunology student with no background whatsoever in biophysics, and somehow, yesterday, I found myself arguing with you about the influence of mechanical forces on TCR triggering. I have you to thank for that. Thank you for recognizing my potential and constantly pushing me forward, especially during the times when I felt completely out of my element, not to mention your endless repertoire of dad jokes that always made me laugh (or roll my eyes) and the countless packets of instant ramen noodles and choco prince you have thrown my way. I shall leave you with this: “Be afraid. Be very afraid”.

To my **LAI family**, those of you who are still here and those of you who have left, I can honestly say there was never a dull moment with you, constant laughter, debates and sometimes fights, but what family does not have those. Being a part of this lab has pushed me to grow, as a research, and a person, and so, I would like to thank you. I would like to personally thank our lab director **Olivier Theodoly** for fostering this environment, creating and funding “Friday beer sessions”, and constantly supplying frozen pizza for us night owl students, our lab engineer **Martine Pelicot** for being the lab version of Clark Kent, and finally to my colleague and good friend **Achyuth Acharya**, for tolerating my never-ending ranting and helping me push through the finish line.

To my Marseille family, **Emily**, **Luis**, **Giulia**, **Enrico**, **Natalie**, and **Annalisa**, it has been my absolute privilege to share this journey with you, you have truly made it worthwhile. Who would have thought that between tequila mornings and raclette nights, I would build such beautiful and strong friendships... Thank you for being there for me, celebrating my

highs, and supporting me during my lows (as you may know, they were quite low), and most importantly, thank you for being my home away from home.

To my **Valentine**, thank you for being my person these past three years (in and outside the lab), for sharing the dumbest albeit funniest conversations with me, for understanding my crazy and matching it, for never saying no to sharing a bottle of red wine (or three) with me, and for believing in me and pushing me forward at times when I simply wanted to give up. It goes without saying that you are built in my future, with our home, on our farm, with our llamas.

To my siblings, **Taha, Rami, Samah, and Abbas**, if I were to be asked who inspires me in life, my answer would be you. Thank you for teaching me what unconditional love is.

To my **Mom and Dad**, I owe everything I am today to you two. This thesis, similar to my previous and future work, is dedicated to you.

To the newest addition to our family, **baby Raphael**, good luck!

Special shout out to our **T cell army**, I do not get excited about anyone or anything the way I get excited when I talk about you (to the person reading this, it's pathetic, I am aware).



Patrolling



Checking



Acting

*Oh what I would give for
an hour of sleep right
now...*

Initial Project Proposal and Objectives³

T cells are activated when the membrane bound T cell receptors (TCRs) recognize the foreign antigenic peptides presented by the major histocompatibility complexes (pMHCs) of antigen presenting cells (APCs), within a specialized cell-cell interface termed the “Immunological Synapse” (IS). Today, an extensive body of research exists describing the biochemical aspect of this interaction, identifying the networks of secreted ligands, cell surface receptors, intracellular signaling pathways, and transcriptional factors at play. Unfortunately, this has not been sufficient to unravel the precise mechanism(s) underlying T-cell activation. In recent years, it has become apparent that the mechanical forces generated at the T cell-APC interface are essential for the proper activation of T cells. Indeed, T cells are now known to be not only sensitive but also responsive to forces acting at both the molecular (for example through the TCR and adhesion molecules such as LFA-1) and cellular scale. What is lacking still is a detailed comprehension of the transmission of the mechanical information across these scales. To this end, the concept behind this project was to investigate if and how cellular forces, transmitted through certain molecules, influence early T cell activation.

As such, we had proposed to employ T cell interaction with “artificial APCs”, in the form of nano-/micro-patterned elastic substrates, as a paradigm of the T cell-APC interface. We intended to evaluate the physical/mechanical properties of the cell-substrate interaction and their influence on T cell activation, and to then encode them into quantitative parameters, directly implementable into testable T cell activation models.

The project was initially divided into 3 objectives of gradual experimental complexity and biological implications:

1. ***Design ultra-soft substrates mimicking APC elasticity***– elastomers of defined and variable elasticities functionalized with the controlled distribution of ligands (against TCR, LFA-1, and co-receptors), and measure T cell spreading dynamics on these substrates.
2. ***Measure cell generated forces*** during and after T cell spreading, on the designed substrates, *via* traction force microscopy (TFM).
3. ***Quantify activation levels*** on designed substrates and under force, in order to provide data for theoretical models derived from current works of LAI and CINAM, which aim in the long term to describe mechanotransduction from molecular to cellular level in the frame of T cell activation.

³ We thought it was important to include this page as to provide a reference for comparison between what was initially proposed and what has been achieved in the frame of this PhD project.

Manuscript Outline

After a brief glance into the immune system, with a more detailed focus on the role and biology of T cells, each chapter represents an article or review that has been either accepted or submitted to peer review journals. As such, each chapter possesses its own reference body and the reader may find duplicated content in different sections.

The first review concerns mechanical forces in T cell immunology. There, we try to summarize the existing body of literature that unveils the implications of forces, acting on either specific molecules or on the cell itself, in the early recognition, activation, and function of T cells. We describe how forces help T cells decipher their micro-environment, and throughout different stages of their lives. We conclude this part by highlighting the missing link between the molecular and cellular scales, which is still rather unclear and remains the subject of many works.

A short chapter presents a command work that was initially made as technical note for JPK Instruments/Bruker, the non-academic partner in this project, and turned into a web-based publication for Wiley around the use of the different force-based techniques that the LAI possesses and uses to investigate T cell mechanobiology.

Then, we include a second review on the main technique around which this project revolves, Traction Force Microscopy (TFM). We describe the importance of measuring forces in cell biology, in the frame of mechanotransduction studies, as well as the difficulties of measuring immune cell forces. We take a quick peek into certain biophysical tools that have been reported in literature with their field of application: single molecule studies, single cell scale or between cells. We then summarize the different modalities that the term TFM represents and showcase the most common of them. Then, we point the reader towards the importance of experimental, technical and analytical details that ultimately condition the conclusions that can be drawn. Finally, we highlight the latest advancements in the world of TFM, including the use of molecular reporters and the recovery forces in three dimensions.

The third article, published in 2022 in Star Protocols, replaces the “material and methods” section. We detail the entire process we have set in place to obtain ultra-soft, reproducible polyacrylamide (PAA) gels for TFM. All the materials are given in a comprehensive table at the end of the article. We also present our data processing strategy, which is based around open-source and homemade solutions that we provide to the community through GitHub repositories. We discuss in depth the analysis parameters and their influence on the output data, and include some caution points, and potential variants of the protocols, that one can follow to adapt to the experimental needs and available materials. Here, we demonstrate our methodology on human peripheral blood mononuclear cells (PBMCs) obtained from blood bags.

The fourth article contains a large body of the data obtained in this project. We apply our experimental strategies to study early forces generated by Jurkat T cells when interacting

with ultra-soft PAA gels mimicking the antigen presenting cell (APC) surface by its composition. Here, we complete the previously presented protocol by showing the technical details behind gel characterization (using Atomic Force Microscopy (AFM) indentation and fluorescence microscopy). Importantly, we reveal new patterns of force application over time- sigmoidal, intermittent and fluctuating- that are modulated as a function of substrate mechanics and functionalization, and that are also impacted by the genetic manipulation of cells to introduce fluorescent reporters at the membrane or in the cytoskeleton. We conclude this article by proposing some possible explanations for the reported behaviors, that may have previously impaired the observation of low forces during early Jurkat interactions, and provide words of caution on the impact of minute details on mechanotransduction studies, in particular for T cells.

We then include a small chapter about the characterization of model APC cells (COS-APC) that were used in a previous PhD project in the LAI (A. Sadoun, defended in 2018) in order to answer the questions of a referee from the Biophysical Journal concerning the mechanical modulation of COS-APCs as a function of the presented antigen; the study showed that after a few seconds of contact with an activating surface, being a bead or a cell, the lymphocyte stiffens and gets more viscous on timescales smaller than the one to reach, for example, calcium flux, a hallmark of early T cell activation. Our added experiments proved that, indeed, in this system, the effects observed at the COS-APC-T cell interface were mainly due to the T cell mechanical response to the specific stimulus delivered by the APCs.

The final chapter displays our ongoing work on human primary T cells that have been isolated from PBMCs obtained from blood bags. We use the same methodology, as that described previously, to investigate if any differences in the intensities and profiles of force exertion can be observed between the three subtypes: memory, effector, and naïve. Though the data presented hints towards a possible difference, it is simply a preliminary study and further experimentation is needed to draw firm conclusions.

We follow our final chapter with a short section on some envisioned experimental perspectives aiming to further push the biology over the biophysics in the frame of our TFM experiments. As a primary objective, we propose to overlap calcium flux detection with traction force measurement to try to correlate force with exertion with early T cell activation.

Finally, we conclude on the work done in the past 3 years, and present more general perspectives regarding the field of immuno-biophysics of T cell activation.

Table of Contents

| | |
|---|-----|
| A Brief Glance into the Immune System | 21 |
| Adaptive and Innate Immune Responses | 22 |
| A closer look into T cell activation | 23 |
| Mechanical Forces in T cell Biology | 37 |
| Looking Back on History | 38 |
| Integrins: The prototypic mechanoreceptors | 40 |
| The TCR as a mechanosensor | 41 |
| The TCR-pMHC bond can exhibit complex behaviors | 42 |
| Mechanosensitivity feature of the TCR conserved at the pre-TCR level | 43 |
| Sensing and exerting forces on the cellular level | 44 |
| T cells can sense and react to substrate stiffness | 47 |
| T cells can sense and react to ligand mobility | 49 |
| How to relay the message? | 50 |
| Concluding remarks | 51 |
| Dissecting T-cell mechanosensing at molecular and cellular scales | 60 |
| Overview | 60 |
| Introduction | 60 |
| Materials and Methods | 61 |
| Evaluation of TCR recognition at the single molecule scale, on living T cells | 61 |
| Real-time combination of AFM and fluorescence microscopy | 62 |
| Characterization of substrates for interaction with T cells | 63 |
| Characterization of model antigen presenting cells | 63 |
| T lymphocyte/antigen presenting cell forces | 63 |
| Measuring T cell cortical tension by pulling membrane tethers | 64 |
| Conclusions and Perspectives | 65 |
| May the force be with your (immune) cells | 70 |
| Introduction | 71 |
| Making invisible forces visible | 73 |
| Continuous versus discrete anchoring | 73 |
| From 2D TFM to 3D TFM | 75 |
| Making the right material choices | 76 |
| Quantifying displacements | 78 |
| Mapping forces | 80 |
| Improved detection in 2D (and 3D) | 81 |
| Insights into T cell biology from TFM data | 82 |
| Molecular sensors for force measurements | 84 |
| Conclusion and perspectives | 85 |
| Protocol for measuring weak cellular traction forces using well-controlled ultra-soft polyacrylamide gels | 97 |
| BEFORE YOU BEGIN | 98 |
| STEP-BY-STEP METHOD DETAILS | 99 |
| Part 1: Production of Ultra-Soft Polyacrylamide Gels | 99 |
| Part 2: Image Acquisition | 104 |
| Expected outcomes | 106 |

| | |
|---|-----|
| Quantification and statistical analysis (optional) | 106 |
| Part 3: Data Analysis | 107 |
| Limitations | 111 |
| Troubleshooting | 112 |
| Cellular forces during early spreading of T lymphocytes on ultra-soft substrates | 119 |
| Introduction | 120 |
| 1. Characterization of soft PAA gels with and without nano-beads | 122 |
| 2. Cell adhesion, spreading, and mechanics are modulated by PAA gels elasticity | 125 |
| 3. Early spreading on very soft gels reveals three distinct force application behavior | 127 |
| 4. Stress vectors are initially pointing outwards while the cell spreads, then reverse their direction at longer time intervals | 132 |
| 5. Fluorescent reporters may modulate TFM energy patterns | 132 |
| Conclusion | 134 |
| Material and methods | 136 |
| Rapid viscoelastic changes are a hallmark of early leukocyte activation | 153 |
| Mechanics of COS-APC cells as a function of peptide loading | 153 |
| Extension to human primary T cells: A preliminary study | 159 |
| Important limitations of the Jurkat T cell line | 159 |
| Questions arising from our previous work | 161 |
| Cells and reagents | 161 |
| Results and discussion | 162 |
| Concluding Remarks and Perspectives | 169 |

A Brief Glance into the Immune System

Biologists have long been fascinated by the ability of living beings to maintain their own stability. Hippocrates even named the principle *Vis medicatrix naturae* - the healing power of nature, meaning the intrinsic ability of the body to heal itself. This phenomenon implies that there are certain forces within the body that function in preserving the integrity of the organism and thus sustain life. This concept of homeostasis was first proposed by Claude Bernard in 1878. He explained that the organs of living beings bathe in a fluid matrix; the “milieu interne” or the internal environment. This internal environment is maintained and modulated by the organism itself. Bernard added “*all the vital mechanisms, however varied they may be, have only one object, that of preserving constant the conditions of life in the internal environment.*”

The human body is an open system in a state of continuous flux; it is in constant interface with the surrounding environment, with external stimuli creating internal disturbances and oscillations, and with many biochemical and biophysical reactions and processes occurring at the same time. Nevertheless, this complex non-equilibrium system is maintained at a near steady state, and these oscillations are kept within a narrow range, not just by continuous input and output, but also by the automatic intervention of the immune system (Marques et al. 2016). However, this is a fragile steady state, as we have seen in the epidemics and pandemics of the past, and the ongoing Coronavirus disease (COVID-19) pandemic.

In retrospect, every organism currently existing on the planet has needed to develop a plethora of defense strategies to fend off an almost limitless number of potential invaders, from microbes, viruses, fungi, and parasites, to toxins, allergens, and pollutants. It is this inherent need to preserve the self that forced hosts to evolve what we refer to today as “immunity”. While at one point it was thought that only complex multicellular organisms possess immunity, we now know that it exists in most life forms (Major and Complex 2001; Loker 2012; Boehm and Swann 2014). Immunity could be something as simple as the peptidoglycan or cell wall in bacteria, cellulose fibers in plants, and epithelial layers in mammals, or as sophisticated as the clustered regularly interspaced short palindromic repeats/Caspase (CRISPR/Caspase) complexes in bacteria, RNA-induced silencing complex/argonaut (RISC/ago) complexes in plants, and T cell receptor/ major histocompatibility complex (TCR/MHC) complexes in mammals (Murphy, Travers, and Walport 2008).

Admittedly, similar to other evolutionary phenomena, the complexity of the immune system has in many ways progressed in tandem with the complexity of the host itself. In other words, systems of increasing structural complexity require even more complex systems to safeguard them. As such, the human immune system arguably represents the most daunting example of complexity in biology. This complexity exists on at least three levels: First, there is the great diversity of the differentiated states of the cells, from the highly specialized lymphocytes of the adaptive immunity, to the multitude of cells participating in the innate

immunity. Second, there is the state of responsiveness of these individual cells to the chemical and physical cues to which they are subjected, a phenomenon that can be classified under the term “tuning”. Third, there is the almost limitless array of distinctive specificities exhibited by lymphocytes, coupled with the much more restricted, yet still considerable, diversity of recognition elements of the innate immune system. The complexity is further amplified by the anatomical structure of the immune system; these already highly interactive cells exist in virtually every bodily tissue and they interact with the cells of those tissues in ways that regulate their function as well.

Adaptive and Innate Immune Responses

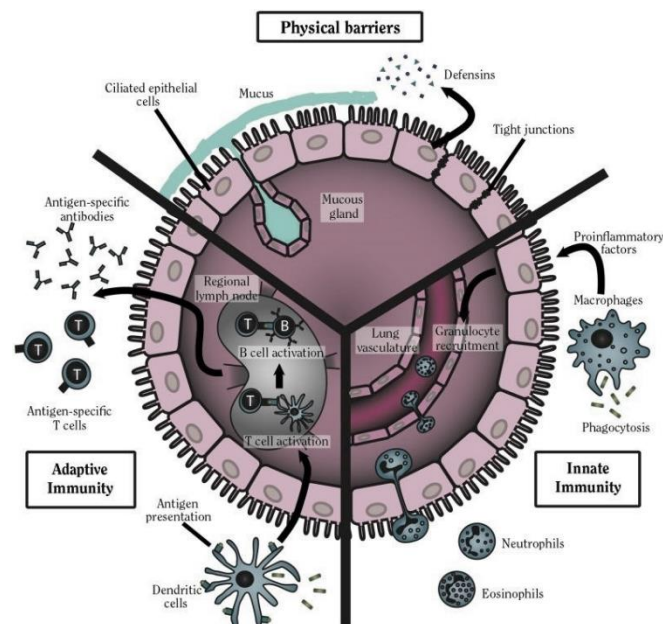


Fig. 1, adapted from (United States Surgeon General 2014): Schematic depicting the interplay between natural physical barriers that the body possesses, the first line, rapid responses that the innate system can bring to control infections and the second line, a very refined and sensitive adaptive immune system which possess various mechanisms to maintain body homeostasis. This representation allows to underline the interplay, constant and at many scales, between the different systems, here for lung defense.

Historically, immune functions have been conceptually divided into two separate domains, innate defenses and adaptive ones. The innate immune response comprises a collection of hard-wired responses encoded by genes in the host's germ line, and that recognize molecular patterns presented by invaders that are not present in the host. Thus, as its name implies, cells of the innate immune response, such as neutrophils, eosinophils, basophils, macrophages, monocytes, dendritic cells and mast cells, “know” how to combat a range of potential pathogens without being specifically notified or trained in advance. As such, they are the first responders at the scene of an environmental breach. It is noteworthy to mention that the innate immune system extends well beyond membrane bound receptors and cytoplasmic proteins that bind molecular patterns, to include physical barriers, such as epithelial cell layers expressing tight cell-cell contacts (tight junctions, cadherin-mediated cell interactions, and others), mucus layers covering the epithelium in the respiratory,

gastrointestinal and genitourinary tracts, epithelial cilia that sweep away the aforementioned mucus layers, as well as soluble proteins and bioactive small molecules (such as complement proteins, defensins, ficolins, cytokines, chemokines, lipid mediators of inflammation, reactive free radical species, and bioactive amines and enzymes that also contribute to tissue inflammation) (Fig. 1).

The adaptive immune response on the other hand, involves only a few types of cells, primarily T and B lymphocytes, and comprises responses encoded by gene elements that somatically rearrange to assemble antigen-specific binding receptors from intact T cell receptor (TCR) and immunoglobulin (B cell antigen receptor; Ig) genes. The assembly of such receptors from a collection of a few hundred germ-line-encoded gene elements enables the production of a repertoire of T and B cells expressing millions of different antigen receptors, each with a potentially unique specificity for a different antigen. Even though lymphocytes are viewed as the “*crème de la crème*” of the immune system, with their ability to specifically and effectively eradicate threats, they are few in number, and so responding cells must first and foremost proliferate before mounting an effective response. This goes to explain why adaptive responses generally unfold temporally after innate ones, and further emphasizes the indispensability of innate immunity in controlling the early stages of infection before lymphocytes are mobilized. Another signature attribute of the adaptive response is its ability to manifest immune memory, whereby adaptive responses produce long-lived dormant lymphocytes that can re-exhibit effector functions rapidly after another encounter with their specific antigen, even decades after the initial sensitizing encounter.

Although these two systems may appear at first glance to be contrasting, functionally independent arms of the host defenses, they actually act together, with innate immune cells allowing for the *proper activation* of adaptive immune cells. In fact, the principle process that governs the progression from an innate to an adaptive immune response is the activation of T cells by antigen presenting cells (APCs, such as dendritic cells and macrophages) (Fig. 2, left).

A closer look into T cell activation

In order for naive T cells, CD4+ or CD8+, to be activated, they first need to interact with a cognate antigen. However, unlike B cells, T cells are incapable of recognizing “free” or soluble antigens. They can only recognize, via their T cell receptors (TCRs), antigens that have been internalized (by phagocytosis, endocytosis, or pinocytosis), enzymatically processed, and presented by APCs via carrier molecules referred to as major histocompatibility (MHC) complexes (either class I or class II MHC complexes)⁴ (Lanzavecchia 2007). Typically, the antigens presented by the MHC molecules are peptides,

⁴ It is important to note that here we are referring to the dominant population of T cells expressing α/β TCRs, opposite to the less defined γ/δ TCR-expressing population of T cells that do play important roles as a first line of defense on mucosal surfaces, however, are activated in a MHC-independent manner and thus lack the infamous antigen specificity conventionally associated with lymphocytes.

short stretches of amino acids (eight to 30), originating from the internal (self antigens) or external environment (non-self/foreign antigens) of the cell presenting them.

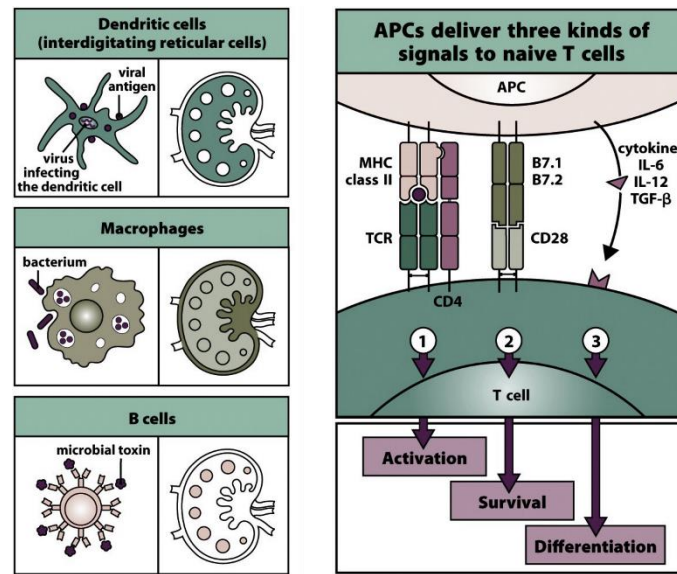


Fig. 2, adapted from (Murphy, Travers, and Walport 2008). Left, professional APCs which can be found in a lymph node, with their preferred targets. Right, such APCs have to deliver, for the activation to be complete, three signals to naive T cells, which will turn them from naive to effector T cells, ready for action.

Actually, T cells are continuously testing APCs as they move between the lymph nodes and the blood. In a simplified view, each TCR somehow measures the affinity of its interaction with the peptide-MHC (pMHC) and provides an intracellular read-out which determines the subsequent response. Note that this description, which relies essentially on the biochemistry of the interactions between molecules and was accepted for a long time, has been recently questioned and represents, in fact, an oversimplified version of T cell activation, as it neglects the biophysical factors at play. This will be further discussed and elaborated upon in the next chapter.

If the T cell does not encounter activating signals, it moves on. Conversely, in the event that it does recognize a cognate pMHC, the TCR-pMHC interaction will provide a partial signal, or what we now refer to as “signal 1” for activation. Full activation necessitates a “signal 2” which is triggered by the engagement of co-stimulatory molecules in the T cell-APC interface, such as CD28-B7, LFA-1-ICAM-1, and CD2-LFA-3. “Signal 2” is thought to amplify the intracellular signaling initiated by “signal 1”. However, receiving “signal 1” in the absence of a costimulator can drive T cells into an anergic state of prolonged non-responsiveness, or even apoptosis (Fig 2, right).

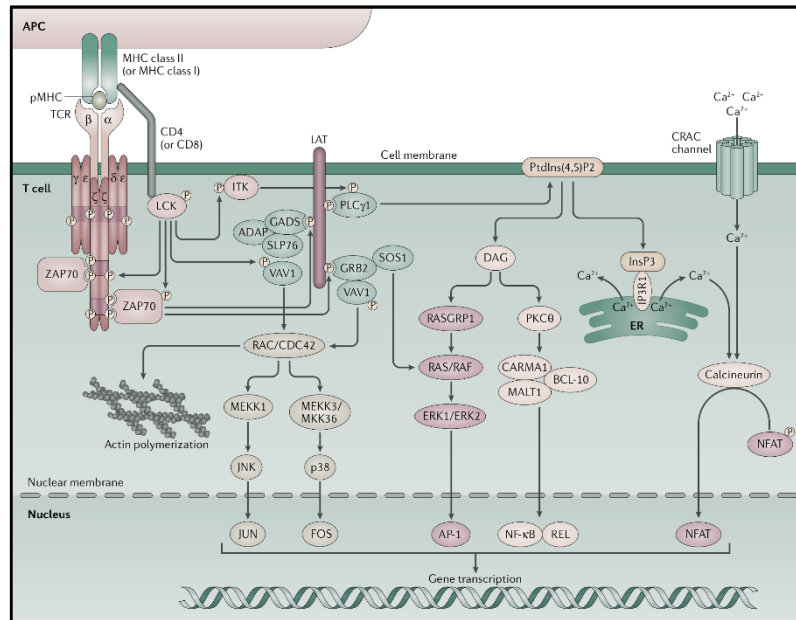


Fig. 3, adapted from (Gaud, Lesourne, and Love 2018). Signaling pathways following TCR triggering the recognition of a cognate antigen. The phosphorylation/de-phosphorylation events mentioned below permit the assembly of the large molecular signaling complex LAT signalosome (Linker for Activation in T cells). Activation of LAT-associated effector molecules results in calcium fluxes, a hallmark of early T cell activation. Calcium-driven transcription factors will then enter the nucleus and modify the cellular program, leading to T cell proliferation, migration, cytokine production and effector function. Of note, the LAT signalosome implicates CDC42 (cell division control protein 42 homologue) which itself interacts with WASP (Wiskott-Aldrich syndrome protein) and Arp2/3 (Actin Related Protein 2/3) (Janssen et al. 2016; Sun et al. 2019). This interaction overlaps the TCR signaling pathways with the actin cytoskeleton, thus linking mechanotransduction and T cell activation (Blumenthal and Burkhardt 2020; Comrie and Burkhardt 2016; Basu and Huse 2017; Huse 2017).

On its own, the TCR (which has short intracytoplasmic tails) is not capable of transmitting “signal 1” into the cell. It needs the assistance of the invariant transmembrane accessory chains with which it is associated, the CD3 complex- a protein complex incorporating transmembrane CD3 γ , CD3 δ , and CD3 ϵ chains, plus a largely intracytoplasmic homodimer of two CD3 ζ chains (Fig. 3). The cytoplasmic portions of each of these chains contain sequence motifs designated immunoreceptor tyrosine-based activation motifs (ITAMs). Upon the receipt of “signal 1”, and under the appropriate conditions (primarily the presence of costimulation), the key tyrosines in the CD3 chain ITAMs will undergo phosphorylation by the now activated, due to CD45 exclusion, receptor-associated kinase lymphocyte protein tyrosine kinase (Lck). The protein tyrosine kinase ZAP-70 will then be recruited to the phosphorylated ITAMs where it is activated by phosphorylation as well. Activated Lck, Fyn, and ZAP-70 will then initiate an activation cascade involving multiple downstream substrates including LAT and SLP-76. In turn, activation of these proteins will lead to the stimulation of phospholipase C (PLC γ 1). PLC γ 1 will hydrolyze phosphatidylinositol 4,5-bisphosphate (PIP2) to produce the second messengers

diacylglycerol (DAG) and inositol trisphosphate (IP₃). DAG will activate PKC θ and the MAPK/Erk pathways, both promoting the activation of transcription factor NF- κ B, while IP₃ will trigger the release of Ca²⁺ from the ER, promoting the entry of extracellular Ca²⁺ into cells through calcium release-activated Ca²⁺ (CRAC) channels. Finally, Calcium-bound calmodulin (Ca²⁺/CaM) will activate the phosphatase calcineurin, inducing IL-2 gene transcription through the transcription factor NFAT (Murphy, Travers, and Walport 2008; Gaud, Lesourne, and Love 2018).

Feedback regulation at several points within these pathways will result in different outcomes, depending on cell type, the environment, and the signals incorporated from other cell surface receptors (e.g. CD28). However, successful T cell activation will culminate in the activation of genes that will first drive T cell clonal expansion, and then their differentiation into one of several alternative functional phenotypes: Th1, Th2, Th17, and follicular helper T cells that help activate both humoral immune responses (B cell help) and cellular responses (delayed type hypersensitivity responses, others), or cytotoxic T cells that kill infected cells and tumor cells, or regulatory T cells (T regs) that act to down modulate immune responses.

Although we have only highlighted here a few key molecular players involved in T cell activation, in reality, the T cell-APC interaction involves the assembly of a highly intricate and specialized structure, termed the “Immunological Synapse” (IS), that encompasses numerous accessory receptor-ligand bonds, including CD4/CD8-MHC II/I , CD2-LFA-3, and LFA-1-ICAM 1 bonds (Fig. 4).

The canonical IS was first documented in the 1990s by Monks et al. who observed the clustering and segregation of proteins at the T cell-APC contact zone into three radially symmetric compartments, referred to as supramolecular activation clusters (SMAC) (Monks et al. 1998; Grakoui et al. 1999). In this “bull’s eye” structure, the TCR accumulates in the central area, forming the central SMAC (cSMAC). The peripheral SMAC (pSMAC) then surrounds the cSMAC in an adhesive ring where the integrin LFA-1 segregates, and finally, the distal SMAC (dSMAC) encloses in turn the pSMAC in a filamentous actin (F-actin) rich zone where the transmembrane tyrosine phosphatase CD45 is localized (Freiberg et al. 2002). With the development of powerful imaging techniques that offered higher degrees resolution, several revisions were later made to the original definition of the SMACs. Primarily, cognate antigen recognition by the TCR was shown to trigger the assembly of TCR microclusters (MCs) (clusters containing >10 TCRs each) that formed at the dSMAC and then moved centripetally through the pSMAC to the cSMAC (Choudhuri and Dustin 2010).

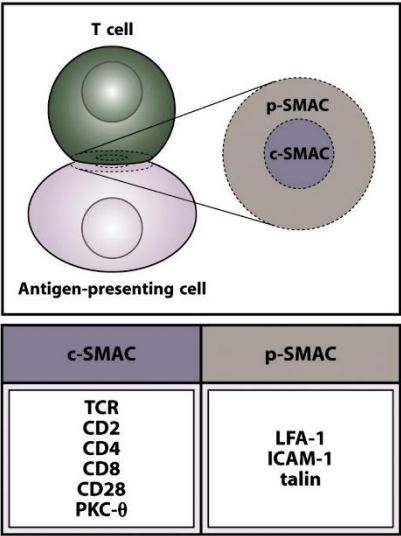


Fig. 4, modified from (Murphy, Travers, and Walport 2008). The immune synapse displays SMAC organization, based on the relative sizes of the molecules or molecular ligand/receptor couples. The cSMAC encompasses the shortest molecules which are mainly signaling related (TCR, coreceptors -on the T cell side). The pSMAC, stabilizes the structure by adhesion molecules, linked to the actin cytoskeleton (LFA-1). Long molecules, such as CD45 are excluded from c- and pSMAC into the dSMAC, most likely facilitating activation by removing phosphatases from the cSMAC (Cartwright, Griggs, and Davis 2014).

The perplexing process of TCR Triggering

For decades, the focus of T cell biologists had been directed towards identifying the networks of secreted ligands, cell surface receptors, intracellular signaling pathways, and transcriptional factors mediating T cell activation (Murphy, Travers, and Walport 2008). Despite this wealth of knowledge that has been accumulated, to this day, the mechanism by which the TCR is triggered is still largely unknown and highly controversial. The challenge in explaining this phenomenon lies in the highly unusual features that TCR antigen recognition possesses, in comparison to other cell surface recognition events.

First, TCR triggering must be extremely sensitive as to identify a particular pMHC against a very noisy environmental background of endogenous self-peptides MHCs, many of which may involve the same MHC molecule (Huppa and Davis 2013). In fact, TCRs can be triggered in response to a single pMHC within the contact area (Huang J Immunity 2013). Second, the TCR must be able to efficiently discriminate between self and non-self pMHCs, even though the TCRs are cross-reactive and are likely to bind a fraction of self pMHCs with affinities that are not much lower than that for non-self pMHCs (Palmer and Naeher 2009). Finally, TCR triggering must occur despite the great diversity in TCR-pMHC bindings, resulting from the variability of peptide sequences and TCR complementarity-determining region 3 (CDR3) loops.

Over the last 10 to 15 years, the unique, and quite frankly perplexing, features of the TCR-pMHC interaction have inspired numerous researchers to put forth several models for

TCR triggering. Generally, these models invoke one of three behaviors: Aggregation, conformational change, or redistribution/segregation of the TCR-CD3 complex (Fig 5).

In theory, if the TCR-CD3 complexes were to aggregate, the increased proximity of the associated Lck molecules would most likely result in the activation of the other receptors within the aggregate, by trans-autophosphorylation, and thus amplify T cell signaling, even upon encountering a single cognate pMHC. Two models have been proposed to explain the mechanism underlying this aggregation. The first one, known as the *co-receptor heterodimerization model*, posits that the CD4/CD8 co-receptors bind to the same cognate pMHC as the TCR, thereby bringing Lck into close proximity with the CD3 ITAMs, consequently mediating their phosphorylation. However, given that TCR triggering has been shown to occur in the complete absence of the coreceptors (Schilham et al. 1993), this indicates that heterodimerization could not be essential for this process.

Alternatively, the second *pseudodimer model* suggests that while one TCR binds a cognate pMHC, a second one binds a self-pMHC, and as such, a pseudodimer is formed by the binding of the self-pMHC CD4/CD8 coreceptor to the cognate pMHC. This model is particularly appealing as first, a high proportion of self pMHCs seem to enhance cognate pMHC recognition. Second, it addresses the problem of the overwhelming abundance of self-pMHCs in comparison to cognate pMHCs. It is true that TCR microclusters (MCs, aggregates of > 10 TCRs and are enriched in signaling molecules such as Lck, ZAP70, LAT, and SLP-76) have been visualized, however they appear to assemble seconds after TCR triggering and before calcium fluxing (Bunnell 2002, Yokosuka 2005, Krummel 2000), which implies that TCR MCs are most likely a product of signaling rather than the cause of it. This however does not reflect the importance of TCR MCs in sustaining TCR signaling (Kumari et al. 2020).

Other models have proposed that pMHC binding induces conformational changes in the TCR/CD3 complex, at the level(s) of the TCR ectodomains and/or CD3 ectodomains and/or CD3 cytoplasmic domains, that consequently trigger signaling. Indeed, some studies have reported subtle conformational changes in the membrane-proximal AB loop of the TCR α constant (C α) domain (Kjer-Nielsen et al. 2003), and showed that mutations of residues in the AB loop inhibited TCR antigen recognition (Beddoe et al. 2009). However, this raises two new questions. First, how can such a conformational change occur with every TCR- cognate pMHC interaction considering the great diversity at the TCR-pMHC binding interface? One could easily imagine that a mechanical force acting on the TCR-pMHC would be a very plausible and realistic explanation. Second, how can a conformational change at the level of the TCR ectodomains be transduced into the cell? Based on the observation that mutations in the AB loop affect TCR dimerization (Kuhns et al. 2010), it has been proposed that conformational changes in the AB loop of the TCR C α domain regulate TCR dimerization, which thus takes us back to the aggregation-based models.

Alternatively, based on observations drawn from a compilation of reports, it has been proposed that conformational changes applied to the CD3 cytoplasmic domain instead regulate TCR triggering. Specifically, cognate pMHC binding is thought to expose CD3

ITAMs, that are otherwise hidden inside the lipid bilayers, for phosphorylation by Lck. It is quite fascinating that this hypothesis was drawn 20 years ago, and only recently a study using fluorescence resonance energy transfer (FRET) showed that, under force, the TCR is capable to deciphering subtle structural differences between different peptides, and that potency of the peptide appears to directly regulate the amount of CD3 conformational change and the degree of the CD3 ζ chain dissociation from the inner membrane leaflet and consequently the exposure of its ITAMs to phosphorylation (Sasmal et al. 2019).

Finally, a third mechanism postulated for TCR triggering relies on the redistribution or segregation of the TCR-CD3 complex from other cell surface receptors at the T cell-APC interface in response to cognate-pMHC binding. This proposition is built on the fact that the TCR-CD3 complex interacts with two types of molecules, ones that enhance its activation, such as Lck, and ones that suppress its activation, such as CD45. Lck has been found to be constitutively active in naive T cells. This implies that the level of phosphorylation of CD3 ITAMs, and consequently TCR triggering, is mainly controlled by constitutively active phosphatases. If the TCR-CD3 complex, Lck and CD45 were to be spatially redistributed with respect to each other, this would tip the de-/phosphorylation balance in favor of one or the other.

The kinetic segregation model proposes that cognate pMHC binding traps the TCR-CD3 complex within a close contact zone that subsequently excludes large inhibitory molecules such as CD45. The two primary pieces of evidence supporting this model are that first, CD45 has been shown to be excluded from areas of TCR triggering (Varma et al. 2006) and second, the truncation of the large CD45 ectodomain does in fact inhibit TCR triggering (Lin and Weiss 2003). The only shortcoming of this model, however, is that it relies solely on molecule-ectodomain size-based segregation. Small ectodomains have in fact been shown to induce CD45 exclusion from TCR MCs (Douglass and Vale 2005), and alternatively, small endo-domains (of CD43) as well have resulted in poor exclusion (Allenspach et al. 2001). Even though these observations have been made at the MC and IS levels, which precede TCR triggering, they suggest that molecular sorting may not rely completely on size. Interestingly enough, recent studies have revealed the existence of microvilli (highly dynamic F-actin rich finger-like structures) covering the surface of T cells and that appear to be implicated in the dynamic surveying of the APC surface and the force driven penetration of the APC glycocalyx (Cai et al. 2017). What is even more interesting is that these structures were later shown to colocalize TCR MCs (Kumari et al. 2020). Together, these features make microvilli ideal sites for TCR triggering. At the time of proposition of the kinetic segregation model, we lacked the advanced imaging techniques that would allow the characterization of such dynamic structures, however, now that we have detected them, maybe the model needs to be modified to accommodate also for actin-driven microvilli to bring the TCR-pMHC into close proximity instead of relying only on the size-based exclusion of large inhibitory phosphatases such as CD45 (Comrie and Burkhardt 2016).

The lipid raft model on the other hand, suggests that the binding of cognate pMHC instead leads to the association of the TCR-CD3 complex to lipid rafts, that are rich in certain molecules (such as Lck) and deficient in others (such as CD45), consequently promoting CD3

ITAMs phosphorylation; pMHC binding to TCR-CD3 alters its lipid environment by clustering TCR-CD3 complexes. Even though the existence of lipid rafts has been proven and several studies have reported an important role for them in TCR signal transduction, the role of lipid rafts in TCR triggering is still highly controversial (Hashimoto-Tane et al. 2010).

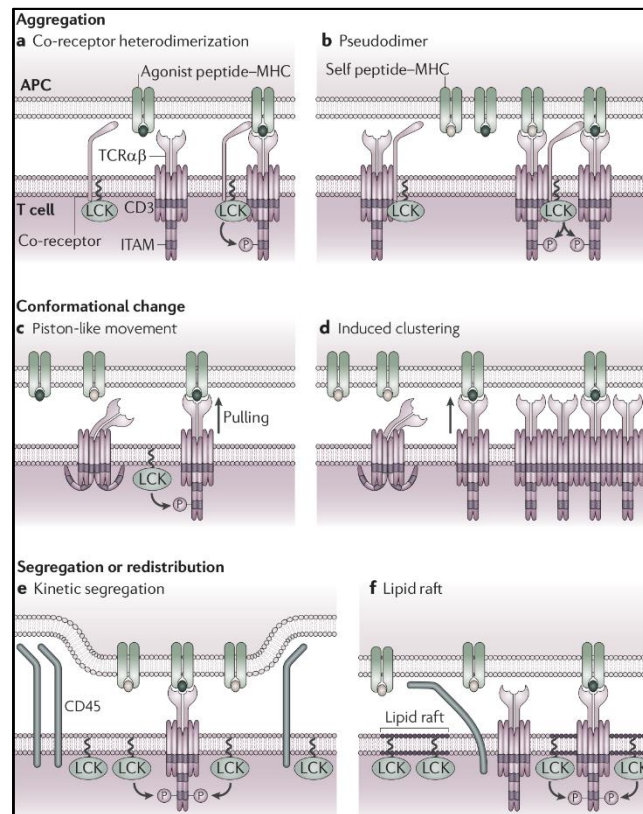


Fig. 5, adapted from (van der Merwe and Dushek 2011). Putative mechanisms, based on structural, colocalization or mutation experiments to explain TCR signaling specificity, sensitivity, and robustness. Note that these plausible views of what may happen at the molecular scale do not take fully into account the dynamic nature of the interface, hence the fact that the represented molecules may be subjected to forces, either pushing the two opposing cellular membranes together, or, to the contrary, pulling them away. These physical, mechanical constraints are now believed to be essential for the unique features of the TCR triggering (Liu et al. 2014; Zhu et al. 2019; Basu and Huse 2017; Huse 2017; Puech and Bongrand 2021; Limozin and Puech 2019).

Although three different mechanistic models for TCR triggering have been presented separately here, it is highly likely that this process invokes a combination of these mechanisms instead of simply one. However, even if combined, these models would still be incomplete as they would lack one critical aspect of T cell life and function: Mechanical forces. By simply observing the T cell-APC interaction, one would realize how dynamic the process is, involving successive cycles of pushing and pulling events. Even outside of the context of antigen recognition and T cell activation, T cells lead intensely *“physical”* lives, constantly adhering, deforming, and migrating in diverse roiling environments. Ergo, it is not unworlly to presume that mechanical forces, originating from the inside and the outside of the cell, are in fact detrimental in shaping T cell behavior, on different scales of length and time. Building on

this note, the next chapter has been dedicated to portraying the influence of mechanical forces on T cell biology.

References

- Allenspach, E. J., P. Cullinan, J. Tong, Q. Tang, A. G. Tesciuba, J. L. Cannon, S. M. Takahashi, R. Morgan, J. K. Burkhardt, and A. I. Sperling. 2001. 'ERM-Dependent Movement of CD43 Defines a Novel Protein Complex Distal to the Immunological Synapse'. *Immunity* 15 (5): 739–50. [https://doi.org/10.1016/s1074-7613\(01\)00224-2](https://doi.org/10.1016/s1074-7613(01)00224-2).
- Basu, Roshni, and Morgan Huse. 2017. 'Mechanical Communication at the Immunological Synapse'. *Trends in Cell Biology* 27 (4): 241–54. <https://doi.org/10.1016/j.tcb.2016.10.005>.
- Beddoe, Travis, Zhenjun Chen, Craig S. Clements, Lauren K. Ely, Simon R. Bushell, Julian P. Vivian, Lars Kjer-Nielsen, et al. 2009. 'Antigen Ligation Triggers a Conformational Change within the Constant Domain of the Alphabeta T Cell Receptor'. *Immunity* 30 (6): 777–88. <https://doi.org/10.1016/j.immuni.2009.03.018>.
- Blumenthal, Daniel, and Janis K. Burkhardt. 2020. 'Multiple Actin Networks Coordinate Mechanotransduction at the Immunological Synapse'. *The Journal of Cell Biology* 219 (2). <https://doi.org/10.1083/jcb.201911058>.
- Boehm, Thomas, and Jeremy B. Swann. 2014. 'Origin and Evolution of Adaptive Immunity'. *Annual Review of Animal Biosciences* 2 (1): 259–83. <https://doi.org/10.1146/annurev-animal-022513-114201>.
- Burbach, Brandon J, Ricardo B Medeiros, and Kristen L Mueller. 2007. 'T-Cell Receptor Signaling to Integrins'. *Immunological Reviews* 218: 65–81.
- Cai, En, Kyle Marchuk, Peter Beemiller, Casey Beppler, Matthew G. Rubashkin, Valerie M. Weaver, Audrey Gérard, et al. 2017. 'Visualizing Dynamic Microvillar Search and Stabilization during Ligand Detection by T Cells'. *Science* 356 (6338): eaal3118–eaal3118. <https://doi.org/10.1126/science.aal3118>.
- Callan-Jones, Andrew C, and Raphaël Voituriez. 2016. 'Actin Flows in Cell Migration: From Locomotion and Polarity to Trajectories'. *Current Opinion in Cell Biology* 38 (February): 12–17. <https://doi.org/10.1016/j.ceb.2016.01.003>.
- Cartwright, Adam N R, Jeremy Griggs, and Daniel M Davis. 2014. 'The Immune Synapse Clears and Excludes Molecules above a Size Threshold'. *Nature Communications* 5: 5479–5479. <https://doi.org/10.1038/ncomms6479>.
- Choquet, Daniel, Dan P Felsenfeld, and Michael P Sheetz. 1997. 'Extracellular Matrix Rigidity Causes Strengthening of Integrin–Cytoskeleton Linkages'. *Cell* 88 (1): 39–48. [https://doi.org/10.1016/S0092-8674\(00\)81856-5](https://doi.org/10.1016/S0092-8674(00)81856-5).
- Choudhuri, Kaushik, and Michael L. Dustin. 2010. 'Signaling Microdomains in T Cells'. *FEBS Letters* 584 (24): 4823–31. <https://doi.org/10.1016/j.febslet.2010.10.015>.
- Comrie, William A., and Janis K. Burkhardt. 2016. 'Action and Traction: Cytoskeletal Control of Receptor Triggering at the Immunological Synapse'. *Frontiers in Immunology* 7 (March). <https://doi.org/10.3389/fimmu.2016.00068>.
- Douglass, Adam D., and Ronald D. Vale. 2005. 'Single-Molecule Microscopy Reveals Plasma Membrane Microdomains Created by Protein-Protein Networks That Exclude or Trap Signaling Molecules in T Cells'. *Cell* 121 (6): 937–50. <https://doi.org/10.1016/j.cell.2005.04.009>.
- Freiberg, Benjamin A., Hannah Kupfer, William Maslanik, Joe Delli, John Kappler, Dennis M. Zaller, and Abraham Kupfer. 2002. 'Staging and Resetting T Cell Activation in SMACs'. *Nature Immunology* 3 (10): 911–17. <https://doi.org/10.1038/ni836>.

- Gaud, Guillaume, Renaud Lesourne, and Paul E. Love. 2018. 'Regulatory Mechanisms in T Cell Receptor Signalling'. *Nature Reviews Immunology*, 1–13. <https://doi.org/10.1038/s41577-018-0020-8>.
- Grakoui, A., S. K. Bromley, C. Sumen, M. M. Davis, A. S. Shaw, P. M. Allen, and M. L. Dustin. 1999. 'The Immunological Synapse: A Molecular Machine Controlling T Cell Activation.' *Science* 285 (5425): 221–27.
- Hashimoto-Tane, Akiko, Tadashi Yokosuka, Chitose Ishihara, Machie Sakuma, Wakana Kobayashi, and Takashi Saito. 2010. 'T-Cell Receptor Microclusters Critical for T-Cell Activation Are Formed Independently of Lipid Raft Clustering'. *Molecular and Cellular Biology* 30 (14): 3421–29. <https://doi.org/10.1128/MCB.00160-10>.
- Huppa, Johannes B., and Mark M. Davis. 2013. 'The Interdisciplinary Science of T-Cell Recognition'. In *Advances in Immunology*, 119:1–50. Elsevier. <https://doi.org/10.1016/B978-0-12-407707-2.00001-1>.
- Huse, Morgan. 2017. 'Mechanical Forces in the Immune System'. *Nature Reviews Immunology* 17 (11): 679–90. <https://doi.org/10.1038/nri.2017.74>.
- Janssen, Erin, Mira Tohme, Mona Hedayat, Marion Leick, Sudha Kumari, Narayanaswamy Ramesh, Michel J. Massaad, et al. 2016. 'A DOCK8-WIP-WASp Complex Links T Cell Receptors to the Actin Cytoskeleton'. *Journal of Clinical Investigation* 126 (10): 3837–51. <https://doi.org/10.1172/JCI85774>.
- Kjer-Nielsen, Lars, Craig S. Clements, Anthony W. Purcell, Andrew G. Brooks, James C. Whisstock, Scott R. Burrows, James McCluskey, and Jamie Rossjohn. 2003. 'A Structural Basis for the Selection of Dominant Alphabeta T Cell Receptors in Antiviral Immunity'. *Immunity* 18 (1): 53–64. [https://doi.org/10.1016/s1074-7613\(02\)00513-7](https://doi.org/10.1016/s1074-7613(02)00513-7).
- Kuhns, M. S., A. T. Girvin, L. O. Klein, R. Chen, K. D. C. Jensen, E. W. Newell, J. B. Huppa, et al. 2010. 'Evidence for a Functional Sidedness to the TCR'. *Proceedings of the National Academy of Sciences* 107 (11): 5094–99. <https://doi.org/10.1073/pnas.1000925107>.
- Kumari, Sudha, Michael Mak, Yeh-Chuin Poh, Mira Tohme, Nicki Watson, Mariane Melo, Erin Janssen, Michael Dustin, Raif Geha, and Darrell J Irvine. 2020. 'Cytoskeletal Tension Actively Sustains the Migratory T-cell Synaptic Contact'. *The EMBO Journal* 39 (5). <https://doi.org/10.15252/embj.2019102783>.
- Lanzavecchia, Antonio. 2007. 'Pillars Article: Antigen-Specific Interaction between T and B Cells. 1985.' *Journal of Immunology (Baltimore, Md. : 1950)* 179 (11): 7206–8.
- Limozin, Laurent, and Pierre-Henri Puech. 2019. 'Membrane Organization and Physical Regulation of Lymphocyte Antigen Receptors: A Biophysicist's Perspective'. *The Journal of Membrane Biology* 252 (4–5): 397–412. <https://doi.org/10.1007/s00232-019-00085-2>.
- Lin, Joseph, and Arthur Weiss. 2003. 'The Tyrosine Phosphatase CD148 Is Excluded from the Immunologic Synapse and Down-Regulates Prolonged T Cell Signaling'. *The Journal of Cell Biology* 162 (4): 673–82. <https://doi.org/10.1083/jcb.200303040>.
- Liu, Baoyu, Wei Chen, Brian D. Evavold, and Cheng Zhu. 2014. 'Accumulation of Dynamic Catch Bonds between TCR and Agonist Peptide-MHC Triggers T Cell Signaling'. *Cell* 157 (2): 357–68. <https://doi.org/10.1016/j.cell.2014.02.053>.
- Loker, Eric S. 2012. 'Macroevolutionary Immunology: A Role for Immunity in the Diversification of Animal Life'. *Frontiers in Immunology* 3 (March): 25. <https://doi.org/10.3389/fimmu.2012.00025>.

- Major, The, and Histocompatibility Complex. 2001. 'Immunology: Comparative Immunology of Mammals', 1–4.
- Marques, Rafael Elias, Pedro Elias Marques, Rodrigo Guabiraba, and Mauro Martins Teixeira. 2016. 'Exploring the Homeostatic and Sensory Roles of the Immune System'. *Frontiers in Immunology* 7 (March): 125. <https://doi.org/10.3389/fimmu.2016.00125>.
- Merwe, P. Anton van der, and Omer Dushek. 2011. 'Mechanisms for T Cell Receptor Triggering'. *Nature Reviews Immunology* 11 (1): 47–55. <https://doi.org/10.1038/nri2887>.
- Monks, Colin R. F., Benjamin A. Freiberg, Hannah Kupfer, Noah Sciaky, and Abraham Kupfer. 1998. 'Three-Dimensional Segregation of Supramolecular Activation Clusters in T Cells'. *Nature* 395 (6697): 82–86. <https://doi.org/10.1038/25764>.
- Murphy, Ken, Paul Travers, and Mark Walport. 2008. *Janeway's Immunobiology 7th Edition*. Edited by Garland Science.
- Palmer, Ed, and Dieter Naeher. 2009. 'Affinity Threshold for Thymic Selection through a T-Cell Receptor-Co-Receptor Zipper'. *Nature Reviews. Immunology* 9 (3): 207–13. <https://doi.org/10.1038/nri2469>.
- Puech, Pierre-Henri, and Pierre Bongrand. 2021. 'Mechanotransduction as a Major Driver of Cell Behaviour: Mechanisms, and Relevance to Cell Organization and Future Research'. *Open Biology* 11 (11): 210256. <https://doi.org/10.1098/rsob.210256>.
- Sasmal, Dibyendu K., Wei Feng, Sobhan Roy, Peter Leung, Yanran He, Chufan Cai, Guoshuai Cao, et al. 2019. 'TCR–PMHC Bond Conformation Controls TCR Ligand Discrimination'. *Cellular & Molecular Immunology*, September. <https://doi.org/10.1038/s41423-019-0273-6>.
- Schilham, M. W., W. P. Fung-Leung, A. Rahemtulla, T. Kuendig, L. Zhang, J. Potter, R. G. Miller, H. Hengartner, and T. W. Mak. 1993. 'Alloreactive Cytotoxic T Cells Can Develop and Function in Mice Lacking Both CD4 and CD8'. *European Journal of Immunology* 23 (6): 1299–1304. <https://doi.org/10.1002/eji.1830230617>.
- Sun, Xizi, Yin Wei, Pamela P. Lee, Boxu Ren, and Chaohong Liu. 2019. 'The Role of WASp in T Cells and B Cells'. *Cellular Immunology* 341 (July): 103919. <https://doi.org/10.1016/j.cellimm.2019.04.007>.
- United States Surgeon General. 2014. 'The Health Consequences of Smoking – 50 Years of Progress: A Report of the Surgeon General: (510072014-001)'. American Psychological Association. <https://doi.org/10.1037/e510072014-001>.
- Varma, Rajat, Gabriele Campi, Tadashi Yokosuka, Takashi Saito, and Michael L. Dustin. 2006. 'T Cell Receptor-Proximal Signals Are Sustained in Peripheral Microclusters and Terminated in the Central Supramolecular Activation Cluster'. *Immunity* 25 (1): 117–27. <https://doi.org/10.1016/j.immuni.2006.04.010>.
- Zhu, Cheng, Wei Chen, Jizhong Lou, William Rittase, and Kaitao Li. 2019. 'Mechanosensing through Immunoreceptors'. *Nature Immunology* 20 (10): 1269–78. <https://doi.org/10.1038/s41590-019-0491-1>.

Mechanical Forces in T cell Biology

Farah Mustapha ^{1,2,3,4,5}, Kheya Sengupta ^{4,5, *}, Pierre-Henri Puech ^{1,2,3,4, *}

Affiliations:

Laboratoire Adhésion et Inflammation (LAI)

¹ Aix Marseille University, LAI UM 61, Marseille, F-13288, France.

² Inserm, UMR_S 1067, Marseille, F-13288, France.

³ CNRS, UMR 7333, Marseille, F-13288, France.

CENTURI

⁴ CENTURI, Turing Center for Living systems, Marseille, France

Centre Interdisciplinaire de Nanoscience de Marseille (CINAM)

⁵ CNRS - AMU UMR 7325, Marseille, F-13288, France

* To whom correspondence should be addressed:

sengupta@cinam.univ-mrs.fr; pierre-henri.puech@inserm.fr

Abstract:

The fate of the adult human body, in terms of tissue development and homeostasis, is governed by how well its cells interact with one another, and with their environment. While the biochemical aspect of such interactions has been extensively studied for decades, their mechanical features, have only more recently captured the attention of cell biologists. Such an oversight becomes particularly notable when studying immune cells that experience different mechanical milieus during their life cycles- from primary/secondary/tertiary lymphoid organs and peripheral tissues displaying variable substrate rigidities, to the blood and lymphatic circulatory systems presenting complex hydrodynamic forces- and that are capable of exerting a substantial amount of force against their interacting surfaces. Indeed, mechanical cues, both dynamic forces and spatial features, have been shown to regulate the development, activation, differentiation and expansion of immune cells. T cells in specific, however, depict a unique paradigm of mechano-immunomodulation as the T cell receptor (TCR) itself has been shown to both sense and convert forces into biochemical signals, as well as induce force exertion following triggering. Consequently, it is only reasonable to imagine that incorporating mechanical cues into our “classical” view of T cell biology will help us better understand and manipulate their behavior, and more importantly, address the still unresolved mystery of their activation. In this chapter, we will review the existing body of knowledge showcasing the influence of mechanical forces on certain T cell surface and cytoplasmic proteins, the process of force generation during T cell interactions, how these forces come into play in T cell biology, and finally the ability of T cells to sense and respond to substrate stiffness and ligand mobility.

Keywords: Force, T cell, T cell receptor, Mechano-immunomodulation, Activation

Looking Back on History

In all forms of life, survival depends on the ability to adapt to environmental stresses, including mechanical stimuli such as external physical forces. It is a requirement so fundamental that it is at the core of all biological designs; virtually all organisms have evolved structures from the macro (organs, tissues) to the micro (cells) and even down to the nanoscale (molecular assemblies, single proteins) that are not only sensitive, but also responsive to forces.

The biological effects of these forces are perhaps most evident in the context of physical structure and activity- the skeleton provides structural support to sustain the force of gravity. The skin provides a protective barrier that is maintained upon the application of external stretch. Even the simplest of physiological functions, such as respiration and circulation, require the generation of forces. This could explain why the earliest understanding and quantifications of these forces were focused on the organism and organ levels. In 1917, biologist D'Arcy Thompson published his book 'On Growth and Form', in which he discussed how mechanical forces contribute to the shape and size of living organisms [1]. Near contemporaries of Thompson, Cecil Murray and Julius Wolff, proved respectively that shear stress controls the size of blood vessels [2] and that mechanical loading increases the thickness and density of bone [3].

This goes to show that the study of the interplay between physical forces and biological function dates back to well before the term 'mechanobiology' was even coined. Today, there is a general consensus that cells constantly sense the various mechanical cues (e.g. force, stress, strain, rigidity, topology and adhesiveness) of their micro-environment, via a process called 'mechanosensing'. They then translate these cues into biochemical signals such as modified binding affinity, altered phosphorylation state, and/or a conformational change; a process called 'mechanotransduction'.

These features are ubiquitous among different cell types and find themselves at the core of many physiological functions; in particular, it has been demonstrated that they are instrumental for key moments of immune cell life and function [4]. For decades, immunological research had focused on identifying the networks of secreted ligands, cell surface receptors, intracellular signaling pathways, and transcriptional factors mediating the immune response [5]. These networks have been predominantly regarded as chemical in nature, largely because the individual molecules that make them up have been characterized by their non-covalent molecular interactions and/or enzymatic activity. Though this chemical description may not be incorrect, it neglects the influence of physical cues, in particular mechanical forces, on signaling networks, as well as the influence of signaling networks on the mechanical environment within and outside of the cell. Such an oversight becomes particularly relevant when studying immune cells whose lives are intensely "physical": regularly deforming, migrating through tight interstitial spaces, adhering under shear flow, and forming stable interfaces (known as immunological synapses; ISs) with other cells [6] (Figure1). Effectively, this means that the receptor-ligand interactions that govern immune cell function are likewise being subjected to and influenced by the same mechanically

tempestuous microenvironment. And, given that several cell surface proteins (e.g. integrins) are known to be strongly connected to the actin cytoskeleton, which is in turn connected to other intracellular proteins, this makes the molecular machinery involved in signal transduction ideal for relaying physical information about the extracellular environment into the cell, as well as translating biochemical signals inside the cell into physical forces exerted against that environment [7,8].

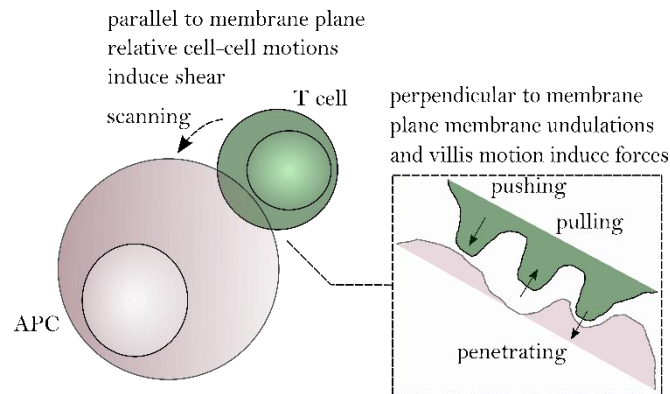


Fig. 1. Origins and orientations of forces at the cellular and molecular scales in T cell recognition and function.

Exemplifying the importance of mechanosensing and mechanotransduction in their development and function are T cells, key players of the adaptive immune system [9]. Broadly speaking, T cells can be divided into three categories; Cytotoxic T cells that directly kill virally infected cells and cancer cells, and Helper and Regulatory T cells that activate and tune the effector functions of other cells in the immune system. In either case, T cells carry out the formidable task of identifying a particular cognate peptide bound to the major histocompatibility complex (pMHC) (Figure 2A), against a very noisy environmental background of endogenous self-peptides MHCs, many of which involve the same MHC molecule [10]. They do so even though the T cell receptors (TCRs) are cross-reactive and typically low in affinity when measured in isolation. One would expect that such high-fidelity decisions would be time consuming, however, T cells scan numerous antigen presenting cells (APCs) in a very short time (\sim a few minutes) so that the immune system can react fast enough and avoid any potential significant damage to the body. The ability of T cells to perform their function properly while simultaneously abiding by all these constraints has baffled the scientific community for many years. Over the last decade, mechano-sensing/transduction has been proposed to be the missing puzzle piece in our understanding of T cell function [11,12]. Different players may have different roles, as we will exemplify further on.

Integrins: The prototypic mechanoreceptors

As in any architectural structure, if mechanical load is to be transmitted across the cell surface into the cell, the simplest manner to do so would be through pliable structural elements that are physically interconnected [13]. Given that integrins link either the ECM or integrin ligands on other cells (through their extracellular domains) to the actin-cytoskeleton (through their cytoplasmic tails and adapter molecules) (Figure 2B), they represent excellent candidates for both mechanosensing and mechanotransduction. In fact, the demonstration that integrins are indeed mechanoreceptors was made almost three decades ago in a series of elegant experiments using magnetic twisting cytometry, where twisting ligand-bearing beads bound to $\beta 1$ integrins caused endothelial cells to stiffen [14].

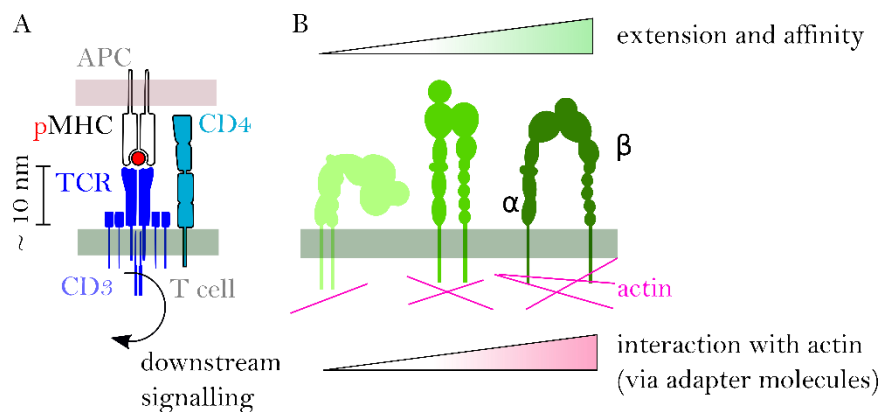


Figure 2: Key mechanosensory molecules for T cells. A: TCR interacts with peptide bearing MHC of an APC and directs the specificity of the adaptive immune response through signaling via the phosphorylation of CD3 cytoplasmic tails. B: Integrins can modulate their extension and interaction with the cytoskeleton depending on forces acting on them (outside-in signaling) or in response to e.g. T cell activation through the TCR (inside-out signaling) [15].

T cells specifically rely heavily on integrins, whether it is for adhesion during trafficking from the bloodstream, migration within tissues, immune synapse formation, or for signaling and cell polarization [16]. Lymphocyte function-associated antigen-1 (LFA-1) is the predominant integrin on T cells, binding intercellular adhesion molecule-1 and -2 (ICAM-1 and ICAM-2) on partner cells (APCs or endothelial cells) [5]. Like other members of the integrin family, LFA-1 is a heterodimer comprising one α and one β chain, each containing a long, stalk-like extracellular domain, a transmembrane helix, and a short intracellular tail responsible for interacting with cytoplasmic signaling and cytoskeletal proteins [17].

The affinity of LFA-1 to ICAMs, however, is intimately coupled to its conformation, which is in turn set by the cell activation status [18]. In the cell resting state, LFA-1 exhibits a low affinity, bent conformation in which its ligand binding pockets are oriented towards the plasma membrane. In the presence of activating TCR signals during immune synapse formation, specific protein complexes (e.g. talin and kindlins) assemble on the cytoplasmic tails of the α and β chains and drive them apart [19]. The conformational change induces the extension of the extracellular domain, thus allowing ligand recognition. Although this

extended conformation is capable of ligand binding, it can only do so at intermediate affinity. In fact, TCR signaling alone is insufficient to unlock the full binding potential of LFA-1 [20].

Only under applied tangential force, originating from the actin cytoskeleton (further elaborated later on), and transferred to integrins via interactions between cytoskeletal adaptors, such as talin, and the tail of the β subunit, does LFA-1 reach peak binding affinity (~ 100 fold increase) [21,22], a clear signature of catch-bond behavior. Catch bonds are an unusual kinetic behavior of ligand receptor interactions where the exertion of a physical force on a molecular complex counter-intuitively prolongs its bond lifetime, in contrast to the so called ‘ordinary’ slip bonds, where force intuitively shortens bond lifetime. Indeed, similar to other integrins [23], LFA-1 binding with ICAM-1 behaves as a catch bond [24].

Interestingly enough, the engagement of LFA-1 alone does not generate any measurable forces or intracellular signaling [25]. This observation suggests that the mechanosensing/transduction capacity of T cells could not be limited to conventional adhesion molecules such as integrins.

The TCR as a mechanosensor

In the event that a cognate pMHC on an APC is encountered, TCR signaling will rapidly convert the ligand-binding event to the phosphorylation of up to 10 immunoreceptor tyrosine-based activation motif elements (ITAMS) in the cytoplasmic tails of the associated CD3 complexes. The ensuing signaling cascade ultimately results in developmental decisions, effects, or functions [26]. Unfortunately, our current knowledge of this signaling cascade far exceeds our limited understanding of how it is initiated upon TCR-pMHC binding.

The TCR-pMHC interaction is probably among the weakest protein-protein interactions that can initiate an effective biological response [27]. The affinity of a TCR binding to a pMHC is only around 10^{-4} – 10^{-6} M [28], about 1000 times weaker than a typical antigen-antibody binding (10^{-6} – 10^{-10} M [29]). Aside, shape-complementarity at the TCR-pMHC interface has been shown to be extremely poor [30]. Despite that, the TCR is still capable of discriminating as few as one to ten non-self antigens in a sea of endogenous self antigens that are presented by the same self-MHC molecule on the APC surface, and even a single pMHC is thought to be sufficient to trigger efficient TCR signaling and subsequent T cell activation [31]. All of this begs the question: How can a seemingly weak interaction simultaneously achieve such levels of specificity and sensitivity?

In an attempt to answer this question, in 2008, Ma and colleagues proposed a ‘receptor deformation model’ for TCR signaling. In this model, TCR signaling is initiated by significant conformational changes in the TCR/CD3 complex, induced by a pulling force originating from the cytoskeleton of the T cell and transmitted through pMHC-TCR binding interactions with enough strength to resist rupture [32]. Essentially, providing a mechanistic explanation to the specificity and sensitivity of the TCR.

A year later, Kim and colleagues provided the first concrete proof that the TCR behaves as a mechanosensor [19]. They used optical tweezers (OT) and nuclear magnetic resonance (NMR) techniques to characterize the distinct functional consequences of several anti-CD3 monoclonal antibodies (mAbs) binding to T cells. In parallel, they quantified Ca^{2+} levels as a measure of T cell activation. The NMR cross-correlation analysis showed that agonist Abs (i.e. those capable of triggering calcium fluxes) bind CD3 in a diagonal fashion, in comparison to CD3 Abs that do not trigger downstream signaling which bind CD3 in an upright mode (perpendicular to cell membrane plane). Interestingly enough, perpendicularly binding Abs were still capable of activating T cells but only when a significant tangential force, of ~ 50 piconewtons (pN), i.e. ~ 10 - 12 times the thermal agitation limit, was applied by OT. Based on these observations, the authors proposed a model in which external tangential forces generated following pMHC ligation during the scanning of the APC by the T cell, allow TCRs to mechanically sense and then transduce the first activation signals.

The TCR-pMHC bond can exhibit complex behaviors: The catch bond proposition

In 2014, Liu and colleagues connected yet another piece of the puzzle [33]. Using biomembrane force probes (BFPs), they showed that the lifetime of the bond between a TCR and its specific pMHC was prolonged by the application of a ~ 10 pN force, indicative of catch-bond behavior. Such a complex response was also associated with more robust and long-lived cellular calcium fluxes, suggesting that catch bond formation may be required for stronger T cell activation. By contrast, the affinity of non-specific TCR-pMHC bonds peaked at zero force, indicative of slip-bond behavior. OT experiments using DNA tethers further revealed that it is in fact the FG loop of the constant domain of the β chain that allosterically controls the V domain modules' catch bond lifetime and peptide discrimination, through a force-driven conformational transition [34]. Collectively, these findings demonstrated that by eliciting antigen-specific catch bonds, external forces may amplify the power of T cell antigen discrimination by separating agonist pMHCs that induce catch bonds from non-specific pMHCs that exhibit only slip bonds.

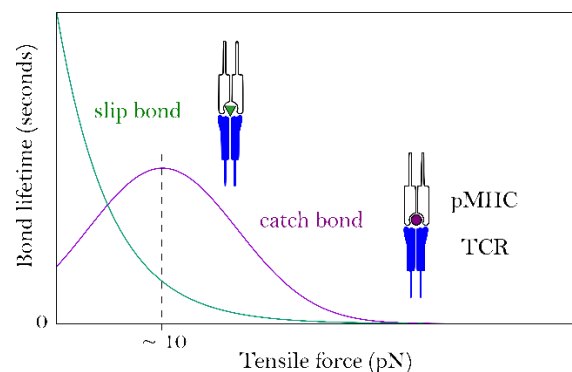


Figure 3: Different bond behaviors that have been proposed to play a role in antigen discrimination during the TCR-pMHC interaction. Slip bonds, whose lifetime only decreases when subjected to increasing forces, vs. catch bonds whose lifetime increases when subjected to increasing forces, up to a certain maximum limit (which has been estimated to be ~ 10 pN).

for TCR/pMHC), beyond which the lifetime decreases as a function of force, similar to slip bond behavior [33].

While catch bonds have been observed in a broad range of molecules, TCR-pMHC catch bonds are still enigmatic, as their origin is still a matter of debate; numerous reports employing purely acellular systems have demonstrated that, outside the cellular context, the TCR does not exhibit catch bond behavior [35]. Aside, how can a tangential (to the membrane) force applied to the TCR-pMHC bond make it stronger? The same group attempted to answer this question using an integrated approach of steered molecular dynamics (SMD) simulation, MTs, and BFPs [36]. Their results showed that forces acting on the TCR-agonist pMHC complex induced a conformational change in the MHC that subsequently increased the length of the complex. Specifically, the increased force experienced by the TCR-agonist pMHC bond uncoupled the α -chain β 2-microglobulin (β 2m) interdomain interaction, resulting in a 5–10 nm extension of the MHC. They proposed that such pronounced extension would not only stabilize the TCR-agonist pMHC bond but also promote the formation of new interactions after forces rupture the preexisting ones. Based on these results, the authors hypothesized that, in the case of agonist pMHCs, the forces acting on the TCR-agonist pMHC complex would induce a conformational change in the MHC, ultimately stabilizing the complex and creating a catch bond. The catch bond would then endow the TCR with the power to sensitively discriminate between peptides (self and non-self), plus, the increased chance of bond formation would make T cell activation easier. Nevertheless, this still does not explain the discrepancy observed by [35] and more work will be needed to clarify (i) if the catch bond behavior is indeed essential for T cell activation and (ii) if it is in fact a hallmark of TCR-cognate pMHC bonds, where is it originating from.

Mechanosensitivity feature of the TCR conserved at the pre-TCR level

Even before the TCR, force-based discrimination, is thought to be conserved in its developmental precursor, the pre-TCR, for the selection of efficient TCRs. Early thymic progenitors (ETPs; uncommitted thymic cells retaining some myeloid, NK and little if any B lineage potential) enter the corticomedullary junction of the thymus as double-negative cells (DN, stages DN1 to 4), lacking the expression of both CD4 and CD8, as well as the full T cell receptor (whether TCR $\alpha\beta$ or TCR $\gamma\delta$). For the $\alpha\beta$ T cell lineage, a surrogate preT- α chain (denoted pT α , which lacks V α of final TCR $\alpha\beta$) is expressed on the surface of DN2 cells in place of the α chain seen in the final $\alpha\beta$ TCR. Shortly after, the cells enter the DN3 stage where they synthesize the TCR β chain and express it on their surface in association with the pT α chain, forming what is known as the pre-TCR receptor [37]. Signaling through this pre-TCR marks the first major checkpoint in early thymic development, referred to as β -selection, whereby only DN cells with productive TCR β are selected to continue their development. The question here is how does pre-TCR signaling occur?

Initially, pre-TCR signaling was thought to be ligand-autonomous [38,39] and purely dependent on pT α charge-based receptor oligomerization [40]. That theory was readily

discredited by Mallis and colleagues [41] who showed through NMR and BFP experiments that the pre-TCR, just like its mature form, and through the β chain alone, is capable of recognizing its respective pMHC (albeit with a broader specificity than its final TCR $\alpha\beta$ form), as well as triggering calcium fluxes. Using OT, the same group later showed that this pre-TCR-pMHC recognition occurs specifically through the V β hydrophobic patch, in partnership with the C β FG loop of the TCR β , and that the recognition is in-fact force-sensitive [42]. Indeed, the pre-TCR-pMHC interaction, similar to the TCR-pMHC one, was shown to exhibit features of catch bond behavior. Diminishing bond strength and/or bond lifetime (through mutating either the V β or the C β FG loop) negatively impacted pre-TCR ligand discrimination and ultimately reduced post-DN3 thymocyte proliferation and developmental progression (Li et al. 2021).

These observations show that only under force is pre-TCR signaling induced during β -selection. In this sense, the β repertoire is tuned prior to the $\alpha\beta$ repertoire final tuning, with mechanotransduction through the β subunit serving as the first checkpoint towards ensuring a functional TCR. As for the diminished ligand specificity of the pre-TCR in comparison with that of the final $\alpha\beta$ TCR, it is possible that the broader ligand focus allows the β chain to interact with multiple self-pMHC ligands in the pMHC-rich stromal environment, affording DN3 growth/survival advantage to pMHC binding competent preTCRs and imprinting self-reactivity in the developing repertoire. Thus, DN progression selects for a self-reactive repertoire early in development. The V β patch may contribute to this behavior, relaxing peptide specificity requirements and functioning as a surrogate V α domain whose replacement at the double positive (DP) stage (signaling through the pre-TCR marks the end of DN3 stage and the transition into the DP stage where the cells stop β chain rearrangement, undergo a period of proliferation, and begin to express both CD4 and CD8) where by an actual V α domain then imposes more precise peptide recognition. Negative selection, that corresponds to the final selection before T cells leave the thymus where only DP T cells that bind self-antigens at low affinity survive, therein purges high pMHC self-reactivity while maintaining a low self-pMHC bias.

Sensing and exerting forces on the cellular level: The role of the actomyosin cytoskeleton

Moving up from the molecular to the cellular level, mechanical forces play a very important role in T cell function. However, before diving into that, one should first address how forces are generated and sensed on the cellular scale. Ultimately, mechano-sensing/transduction, on any scale, and force exertion are tightly linked processes. Mechanically induced conformational changes, just as those described for activating the pMHC-TCR and LFA-1-ICAM bonds, only occur under the influence of force. Ergo, mechanotransduction necessitates that the cell exerts and receives forces from its environment. Conversely, force exertion is itself regulated by feedback from mechanosensing pathways, as we will see later on.

Cells exert forces against their environments via dynamic cytoskeletal remodeling; the cytoskeleton is a polymer network composed of three distinct biopolymers: actin, microtubules, and intermediate filaments. Typically, it is the filamentous actin (F-actin) cytoskeleton that bears the brunt of the mechanical load; It is a highly dynamic structure that undergoes continuous reorganization in response to external mechanical cues. This feature is what enables the cell to rapidly change its elastic properties and what consequently endows it with the capacity to apply forces against a substrate and move [44]. The classical model for F-actin dependent force exertion involves myosin motors consuming chemical energy in the form of ATP and walking on actin filaments in a general three-step process of binding, power stroke, and unbinding. This process is continuously repeated and leads to the generation of a contractile force (actomyosin contractile force) [44]. Although actomyosin contractility was initially characterized in muscle cells, it is now clear that it is a universal mechanism for force generation in most eukaryotic cells, fueling a wide range of processes including adhesion, division and motility. With that being said, it is important to note that actin polymerization alone, in the absence of myosin motors, does also generate force. However, such protrusive forces are far less characterized, most likely because they are easily masked by the long-lasting, contractile ones [43].

Whether it is protrusive or contractile, in order for forces to propagate from the cytoskeleton onto the extracellular environment (substrate or cell), both parties have to be linked through adhesive contact points. The most characterized of such contact points are focal adhesions (FAs); FAs constitute large protein assemblies in which transmembrane adhesion receptors (e.g. integrins) and F-actin are bridged via a specialized layer of cytoplasmic scaffolding proteins (e.g. paxillin, vinculin, talin...) [45]. The size, composition, and structure of such adhesion sites are directly dependent on the mechanical forces that they are subjected to, whether it is from actomyosin contractility or from the extracellular environment. This explains why FAs are readily observed for fibroblasts cultured on stiff supports, while similar prominent contacts are harder to detect in-vivo, where the extracellular matrix (ECM) is much more compliant [46]. Interestingly, the process of building FAs from initial adhesion receptors is intricately coupled to the activity of intracellular signaling cascades, not through their possession of enzymatic activity, rather, their capacity to recruit specific, “classical” adhesion signaling components to the growing FAs [47]. For example, in the case of integrin mediated adhesions, the focal adhesion kinase (FAK) recruited to the FA site regulates diverse downstream signaling pathways, including those promoting cell growth and survival [48].

It has to be underlined that, unlike large adherent cells such as the fibroblasts mentioned above, many immune cells, among which the T cells, do not form distinct FAs-like structures in vitro or in vivo. Rather, they form transient adhesive contacts that contain cell surface receptors, F-actin, and cytoplasmic proteins such as the ones typically found in FAs. These contacts likely serve as sites for force exertion during migration and cell-cell interactions [4].

The most straightforward way in which cellular forces could contribute to T cell function is through enabling their migration and trafficking. Typically, as a cell moves on a substrate (whether it is the ECM or simply a cover slide), it experiences external forces, mainly the viscous force/resistance from the surrounding medium and cell-substrate interaction forces,

as well as internal forces that are generated by the cytoskeleton. In T cells, as in most animal cells, the cytoskeleton is the essential component in creating these motility-driving forces, and in coordinating the entire process of movement: First, a cell propels the membrane forward by growing the actin network at its leading edge, creating an F-actin rich lamellipodium. Second, it adheres to the substrate (for example through integrin adhesions in T cells) at the leading edge and deadheres (releases) at the cell body and rear of the cell (also known as uropod). Finally, the cell propels forward by the F-actin retrograde flow generated against the adhesive contacts present at the base of the leading edge of the cell; retrograde flow describes the variable movement of actin filaments rearward with respect to the substrate, generally in the direction opposite to cell movement [43] and it is caused by actin polymerization against the plasma membrane, which drives the growing fibers backwards, and myosin contractility, which collapses the leading edge F-actin network into linear bundles [4].

Aside from motility, cellular forces come into play at different time points in T cell activation. To begin with, the most basic requirement for T cell activation is for the TCR to interact with the pMHC. This may seem trivial to point out, however, there are physical barriers that make this interaction not as straightforward; The TCR-pMHC bonds (10-15 nm) are much smaller than individual TCR and APC glycocalyx proteins, such as the T cell receptor tyrosine phosphatases CD45 (28-50 nm) and CD148 (47-55 nm), and even LFA-ICAM bonds (45-50 nm for the couple). Though models such as the kinetic segregation one [49] were originally put forth to explain how the T cell overcomes these barriers, there still remains several key issues that the model does not account for [50]. Recently, Cai et al. combined time-resolved lattice light-sheet microscopy and quantum dot-enabled synaptic contact mapping microscopy to show how highly dynamic T cell F-actin-rich microvilli colocalized with TCR microclusters (MCs; upon ligand binding, TCRs coalesce into signaling microclusters containing >10 receptors each), and in the absence of external stimulus, scanned the entire area of opposing cells and surfaces (coated with antagonist/agonist pMHCs and ICAM-1) before and during antigen recognition, at a time frame (≈ 1 min) similar to that recorded for T cell-APC contacts in vivo [51]. These observations, coherent with earlier ones [52], suggest that T cell microvilli, with an average length of 380 nm, can promote TCR signaling by surpassing the size-related restrictions, penetrating the glycocalyx, and bringing the TCR into close proximity with the pMHCs. Additionally, one could imagine that the applied F-actin protrusive forces would further stabilize low affinity TCR-pMHC bonds, and with the microvilli containing pre-clustered TCRs, it would provide an easy access platform for signal amplification, explaining the high sensitivity of T-cells to low numbers of pMHC antigens.

After TCR engagement, actin polymerization at the T cell-APC contact zone commences. The membrane deformation resulting from such polymerization forces allows the T cell to spread over the APC. This spreading process is critical as it not only allows the T cell to scan a larger area of the APC and thus increases the efficiency of antigen sampling [53], but it also exerts force on the receptor-ligand pairs engaged, such as the mechanosensitive TCR-pMHC and LFA-1-ICAM-1/2 bonds, further enhancing peptide discrimination and TCR activation.

As the T cell reaches its maximal spreading area, the same actin polymerization forces, combined with myosin contractility, create retrograde flow. Forces originating from this

retrograde flow organize the various TCR MCs and signaling molecules present at the T cell-APC contact zone, and order them into the infamous spatially symmetric bullseye structure of the IS [54]. To be more specific, the TCR MCs are swept towards the center of the contact by retrograde F-actin centripetal flow at the periphery and then by myosin II dependent actin arcs closer to the center, leading to the formation of the cSMAC (central supramolecular activation cluster) surrounded by a ring of integrins (LFA-1/ICAM bonds) in the pSMAC (peripheral supramolecular activation cluster). The interruption of F-actin centripetal flow eradicates TCR MC signaling within seconds, further confirming that force exertion is imperative for maintaining proper TCR activation. Interestingly enough though, the same actin machinery described above may also break TCR-pMHC bonds, allowing the serial engagement of the same pMHC with the other TCRs present in the TCR MC, consequently augmenting TCR signaling.

Once the IS is established, it has to be maintained for a long enough period of time (up to hours) to enable the proper activation of the T cell. This is a particularly difficult task as T cells are already highly motile cells and the T cell-APC interaction occurs in non-static conditions. By monitoring the T cell cytoskeletal organization during their interaction with both APCs and APC mimetic surfaces, Kumari et al. found that antigen recognition triggered the formation of actin foci (by the help of Wiskott–Aldrich syndrome protein) at the T cell-APC-substrate contact that, with the assistance of myosin II contractility, generated and sustained intracellular tension within the T cell that maintained the stability and symmetry of the IS for the activation time frame [55].

Finally, in an elegant series of experiments combining pMHC and ICAM-1 coated on beads bared by deformable micropipettes and on micropillar arrays, Basu et al. demonstrated that mechanical forces at the IS potentiate cytotoxic T cell (CTL) cytotoxicity: CTLs destroy target cells by secreting a mixture of the protein perforin and granzyme proteases, where perforin forms pores in the target cell membrane that enable granzymes to access the cytoplasm and induce apoptosis [56]. Specifically, their study revealed that altering the membrane tension of the CTLs using pharmacological drugs or osmotic shock strongly perturbed the pore-forming activity of perforin. Similarly, altering the membrane tension of the target cell by changing substrate stiffness modulated CTL killing, with cells on stiffer substrates exhibiting a higher sensitivity to perforin-induced pore formation. Taken together, these results point towards a model in which forces at the IS promote CTL killing by straining the target cell membrane, thus facilitating the formation of perforin pores. Considering that several reports have correlated transformation and malignancy with cellular softening, this work puts forth a very compelling hypothesis in which tumor cells modulate their mechanical properties to relief forces at the IS and thus evade the immune system [4,57].

T cells can sense and react to substrate stiffness

Just as we do when we use our fingers to apply pressure on an object, T cells exert forces to test their mechanical environment, particularly stiffness. Pioneering work by Judokusumo et al. initially documented this property by stimulating naïve CD4+ mouse T cells with polyacrylamide gels of different rigidities, and functionalized with activating antibodies

against CD3 and CD28 [58]. Their experiments revealed that T cells exhibited stronger activation, quantified as IL-2 secretion, with increasing substrate rigidities (over the range of 10-200 KPa), and that this mechano-sensing/transduction ability was largely affiliated with the TCR/CD3 complex rather than CD28. Intriguingly, this “stiffness sensitivity” property was observed only when the anti-CD3 antibody was immobilized onto the surface of the gel, rather than added as a soluble solution, and it was lost upon myosin inhibition. These observations are in accordance with the now commonly accepted idea that antigen receptors pull against their ligands for optimal signaling. Conversely, similar experiments done by O'Connor et al. on polydimethylsiloxane substrates with the same functionalization but using a different rigidity range (100-200 KPa), showed that naïve CD4+ human T cells were stimulated and proliferated more on softer substrates in comparison to stiffer ones [59]. Taken together, these studies suggest a possible biphasic response to stiffness sensitivity. Another crucial piece of information came from Tabdanov et al. who employed a combination of activating anti-CD3 antibody and ICAM-1 functionalized flat micropatterned PDMS substrates (5 KPa- 2000 KPa) and micropillar arrays to delineate the contributions of both the TCR/CD3 complex and LFA-1 in stimulated CD4+ human T cell activation [60]. In these experiments, early T cell activation, measured by the total phosphor-tyrosine levels, was weaker on soft substrates than on rigid ones. Though this stiffness sensitivity was observed in the absence of LFA-1 engagement, it was enhanced by its presence.

Even more interestingly, their results also highlighted a mechanical cooperation between the TCR/CD3 and LFA-1-ICAM-1 systems, whereby actin nucleation downstream of TCR signaling sustained the growth of the LFA-1 dependent actin network, which in turn provided the cytoskeletal tension to allow mechanical sensing, T-cell spreading and enhanced TCR activation.

Similar experiments were later repeated but on substrates with stiffnesses of more physiologic relevance in terms of T cell function, considering that APCs display a stiffness range between ≈ 200 Pa and 2 KPa [61]. Notable of which were those performed by Hui et al. [62,63] who used poly-l-lysine-antiCD3-coated soft polyacrylamide gels (1- 5 KPa) to demonstrate the contributions of actin polymerization and myosin contractility, as well as dynamic microtubules, to force generation and maintenance during enhanced green fluorescent protein (eGFP)-actin expressing Jurkat T cell activation (quantified as phosphotyrosine signaling). Their results, similar to what was originally documented by Judokusumo et al., showed that T cells exhibited higher levels of activation on stiffer gels in comparison to softer ones.

Though these studies are difficult to directly compare because they differ in substrate chemistry, antibody/protein immobilization, stiffness ranges, and more importantly the T cell types/subtypes used, they do overall reveal that T cells possess the inherent ability to sense stiffness. This, at least partly, explains their modified behaviors in mechanically distinct interactions, whether it is different APCs that have been activated by different stimuli and present a varying repertoire of agonist/non-agonist pMHCs, or endothelial cells in blood vessels, or infected/tumor cells inside tissues. Even if the change in stiffness between these surfaces may seem quite modest and inconsequential, it is nevertheless sensed and responded to by T cells. Wahl et al. recently proposed a model in which increased substrate stiffness

heightens the TCR-pMHC resistance to cytoskeletal forces and thus increases T cell spreading and activation, that is to a certain limit, beyond which the tension on the bonds becomes too high and breaks them, which consequently decreases spreading and weakens T cell activation [64].

T cells can sense and react to ligand mobility

Aside from stiffness sensitivity, T cells have also been shown to be sensitive to ligand mobility [65]. The interaction between a T cell and an APC necessitates extensive cytoskeletal and lipid membrane composition changes for both cells, as to allow for the spatial ligand/receptor re-ordering mentioned above. In an innovative approach, Mossman et al. investigated the impact of ligand mobility on T cell signaling by creating “artificial APCs” where nanofabricated 10–20 nm high chromium barriers were assembled on pMHC and ICAM-1 coated supported lipid bilayers [66]; set up as is, the bilayer would allow for free lipid diffusion, however, the barriers would block the movement of proteins with larger cytoplasmic domains, and more importantly, TCR MCs. Interestingly, trapping the TCR clusters in the in the IS periphery (as opposed to their natural position in the cSMAC of the IS) augmented early TCR-associated phosphotyrosine signaling and cytoplasmic Ca^{2+} levels in the spatially constrained IS in comparison to the native ones. In a similar approach, but playing on the lipid bilayer composition instead of using chromium barriers for limiting ligand mobility, Hsu et al. revealed that tyrosine phosphorylation and persistent elevation of cytoplasmic Ca^{2+} was in fact more pronounced for T cells (Jurkat and naïve or stimulated CD4^{+} murine) on mobile membranes than on less mobile ones [67]. Though these two studies seem contradictory, the immobilization of the TCRs differed between the two systems; in the former, the chromium barriers completely trapped the TCR clusters in the periphery, on the other hand, the latter still permitted the diffusion of TCRs but at a slower rate. This could underline a complex mechanism, potentially reliant on the spatial and temporal parameters of ligand constriction, by which T cell sensitivity to ligand mobility impacts T cell activation. However, this would require further experimentation to decipher.

More recently, pioneering work done by Bukhardt and colleagues [30,68] revealed that dendritic cell (DC) maturation- a process characterized by an increase in DC cortical stiffness- induced a dramatic actin-dependent decrease in ICAM-1 mobility. The reported decrease in ICAM-1 mobility helped generate a counterforce that drove the centripetal flow of the actomyosin network in the T cells spreading over the APC. This flow, in turn, recruited LFA-1 to the IS, maintained it in a high affinity conformation, and consequently promoted efficient binding to ICAM-1. One could imagine that since LFA-1 connects the extra- and intra-cellular compartments, similar to other integrins, the tension on LFA-1 will also affect the dynamics of the underlying T cell actin network [69]; since the TCR is thought to be interacting with said network, this will indirectly influence tension on the TCR, potentially modulating TCR signaling [13]. This work is of particular importance as firstly, it explains how LFA-1 reaches peak binding affinity necessary for proper T cell activation, and secondly, it suggests that cells can regulate intercellular communication by altering the physical status of the signaling molecules in question, rather than just their expression level or spatial localization.

How to relay the message?

Although the influence of mechanical forces on the specificity and sensitivity of antigen recognition by the TCR is coming to light, how information regarding TCR-antigen binding is relayed into the cell still remains unclear [70].

As mentioned above, TCR signaling propagates across the membrane through the CD3 intracellular domains, specifically through ITAM phosphorylation. In their unphosphorylated state, ITAM chains have been shown to be buried in the hydrophobic interior of the membrane, hence inaccessible to Src kinases. Ligand binding by the TCR has been recently proposed to induce conformational change in the CD3 chains, extending them and exposing their ITAMs to phosphorylation [71]. Although there are currently no definitive studies directly linking mechanical forces applied onto the TCR protein to this CD3 ζ conformational change (e.g. are the forces needed pushing/pulling on the complex to unlock it, similar to an umbrella?), a recent study using fluorescence resonance energy transfer (FRET) showed that the TCR, under force, is able to decipher structural subtle differences between peptides by different bond conformations, independent of binding affinity and kinetics. Peptide potency then appears to directly regulate the amount of conformational change, which in turn dictates the degree of dissociation of the CD3 (ζ chain) from the inner membrane leaflet and consequently the exposure of its ITAMs to phosphorylation [72].

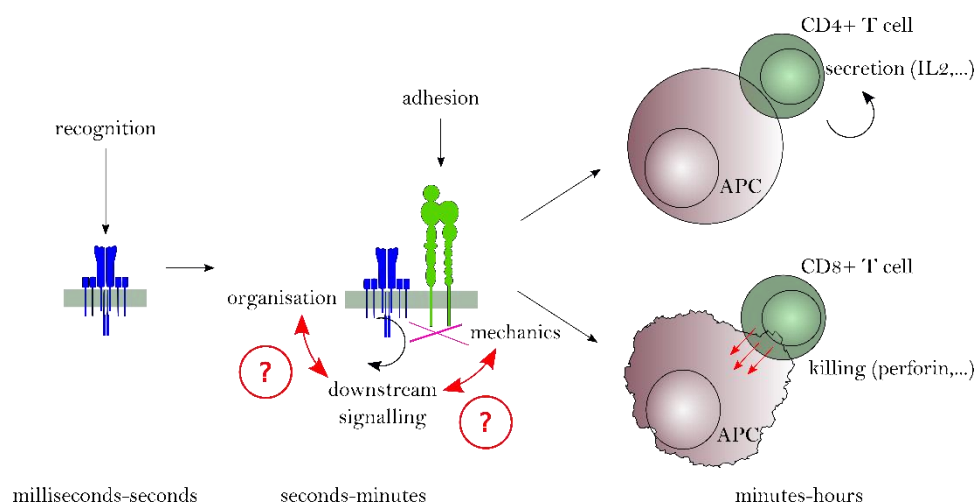


Figure 4: Typical time scales for signal propagation and consequences. The question marks indicate the interactions between different cell biology “modules” [73] that still need clarification in order to fully understand the entire process of T cell mechanotransduction and activation.

Another important question to address is the link between the different scales (Figure 4), particularly the TCR and the actin cytoskeleton. As mentioned previously, in adherent cells, the maintenance, growth and signaling through FAs are completely dependent on cytoskeletal forces. As such, FAs act as mechano-sensors/transducers bridging transmembrane adhesion receptor binding and actin flow with cell signaling. It is intriguing to imagine that the TCR MCs serve similar purposes. Using novel ratiometric tension probes, Ma et al. have

demonstrated that TCRs undergoing clustering within the first few minutes of stimulation experience tension in the pN range [74,75]. It is thus highly likely that TCR clustering is stabilized by the underlying F-actin network or even through direct tethering of the TCR complex to cortical actin. Interestingly, the force-sensing protein lymphocyte-specific Crk-associated substrate (Cas-L) has recently been proposed by Santos et al. to mechanically link TCR MCs to the underlying actin network [76]. Their experiments showed that Cas-L participates in a positive feedback loop whereby, upon TCR triggering, Cas-L localized to the TCR MCs undergoes actin-polymerization dependent activation (through phosphorylation), leading to Ca^{2+} signal amplification, regulation of TCR MC transport, inside-out integrin signaling, as well as actomyosin contraction [76].

Concluding remarks

Besides the mechano-sensitive/transductive abilities of the TCR and integrins, there are several other membrane receptors, ion channels, cytoskeletal proteins, and transcriptional factors that are thought to be also affected by mechanical forces. For example, pulling forces on bound Notch receptors during endocytosis of Notch ligands induce a conformational change in Notch that ultimately drives early thymic progenitors to commit to the T cell lineage [77,78] and mechanical stretch of the membrane during IS formation activates Piezo channels, thereby triggering Ca^{2+} flux and regulating TCR signaling [79].

What is truly interesting is that these different elements do not function in isolation, but rather as parts of a complex mechanical signaling network with cross-talks and feedback loops, that ultimately regulates T cell mechanics, gene expression, and behavior. The challenge, now that some of the key elements have been described separately, is to understand how these mechano-signaling components and pathways are intertwined and integrated across time and length scales, and in different intra-cellular compartments, to shape the T cell response [7,73]. To take the TCR and LFA-1 as an example, Bernard and colleagues attempted to decipher the mechanical link between these two molecules by imaging T cells on anti-TCR Ab micropatterned soluble lipid bilayers (SLBs) [80]. Their results showed that the TCRs do in fact aggregate into MCs that colocalize with the anti-TCR Ab patterns, however, the clusters do not move (by the means of retrograde actin flow) to the center of the contact area, as seen during the formation of the central supramolecular activating complex of the IS. Only upon the addition of ICAM-1 to the SLBs, do the TCR MCs centralize with the actin and form a peripheral ring around them. This study, in addition to many others [60,81,82], supports a model in which the actin cytoskeleton couples the TCR and LFA-1 in a positive feedback loop that coordinates IS formation and growth. It also puts forward a very exciting concept of the actin cytoskeleton acting as a mechanical intermediate that integrates force-dependent signals coming from different receptor-ligand interactions, and then coordinates outgoing responses over large distances [50].

Over the last decade, a sturdy foundation has emerged for measuring and interpreting mechanical forces in T cells. Nevertheless, the field remains in its infancy, we still don't know much- for example, how are mechanical forces transferred and integrated across different molecules, different scales, different time intervals, and different partner cells- however, what

is becoming more and more apparent is that forces represent a fundamental component of the T cell response that can no longer be ignored. It is our hope that the literature and arguments presented in this review raise awareness to this emerging area of research in T-cell biology. It is also worth noting that the concepts presented here for T cells apply to all immune cell types, with basic similar phenomena and subtle differences for other lymphocytes such as B cells and NK cells, but also APCs such as dendritic cells, macrophages and neutrophils [4,6].

Acknowledgments

Part of this work was supported by institutional grants from INSERM, CNRS and Aix-Marseille University to the LAI and CINAM.

FM was supported by a PhD grant from the European Union's Horizon 2020 research and innovation programme under the Marie Skłodowska-Curie grant agreement No713750, with the financial support of the Regional Council of Provence- Alpes-Côte d'Azur and with of the A*MIDEX (n° ANR- 11-IDEX-0001-02), funded by the Investissements d'Avenir project funded by the French Government, managed by the French National Research Agency (ANR).

References

1. Thompson, D'Arcy Wentworth. *On Growth and Form*. Revised ed. édition. New York: Dover Publications Inc. 1992.
2. Murray CD. 'The Physiological Principle of Minimum Work: I. The Vascular System and the Cost of Blood Volume'. *Proceedings of the National Academy of Sciences of the United States of America*. 1926; 12: 207–214.
3. Teichtahl, Andrew J, Anita E Wluka, Pushpika Wijethilake, Yuanyuan Wang, et al. 'Wolff's Law in Action: A Mechanism for Early Knee Osteoarthritis'. *Arthritis Research & Therapy*. 2015; 17: 207.
4. Huse, Morgan. 'Mechanical Forces in the Immune System'. *Nature Reviews Immunology*. 2017; 17: 679–690.
5. Murphy, Ken, Paul Travers, Mark Walport. *Janeway's Immunobiology 7th Edition*. Edited by Garland Science. 2008.
6. Zhang, Xuexiang, Tae-Hyung Kim, Timothy J Thauland, Hongjun Li, et al. 'Unraveling the Mechanobiology of Immune Cells'. *Current Opinion in Biotechnology*. 2020; 66: 236–245.
7. Limozin, Laurent, Pierre-Henri Puech. 'Membrane Organization and Physical Regulation of Lymphocyte Antigen Receptors: A Biophysicist's Perspective'. *The Journal of Membrane Biology*. 2019; 252: 397–412.
8. Malissen, Bernard, Pierre Bongrand. 'Early T Cell Activation: Integrating Biochemical, Structural, and Biophysical Cues'. *Annual Review of Immunology*. 2015; 33: 539–561.
9. Rossy, Jérémie, Julia M Laufer, Daniel F Legler. 'Role of Mechanotransduction and Tension in T Cell Function'. *Frontiers in Immunology*. 2018; 9.
10. Huppa, Johannes B, Mark M Davis. 'The Interdisciplinary Science of T-Cell Recognition'. In *Advances in Immunology*. 2013; 119: 1–50.
11. Paegeon, Sophie V, Matt A Govendir, Daryan Kempe, Maté Biro. 'Mechanoimmunology : Molecular-Scale Forces Govern Immune Cell Functions'. 2018; 29: 1919–1926.
12. Rushdi, Muaz, Kaitao Li, Zhou Yuan, Stefano Travaglini, et al. 'Mechanotransduction in T Cell Development, Differentiation and Function'. *Cells*. 2020; 9.
13. He, Hai-Tao, Pierre Bongrand. 'Membrane Dynamics Shape TCR-Generated Signaling'. *Frontiers in Immunology*. 2012; 3: 90.
14. Wang N, JP Butler, DE Ingber. 'Mechanotransduction across the Cell Surface and through the Cytoskeleton'. *Science (New York, N.Y.)*. 1993; 260: 1124–1127.
15. Springer, Timothy A, Michael L Dustin. 'Integrin Inside-out Signaling and the Immunological Synapse'. *Current Opinion in Cell Biology*. 2012; 24: 107–115.
16. Gérard, Audrey, Andrew P Cope, Claudia Kemper, Ronen Alon, et al. 'LFA-1 in T Cell Priming, Differentiation, and Effector Functions'. *Trends in Immunology*. 2021; 42: 706–722.
17. Luo, Bing-Hao, Christopher V Carman, Timothy A Springer. 'Structural Basis of Integrin Regulation and Signaling'. *Annual Review of Immunology*. 2007; 25: 619–647.
18. Dustin ML, TA Springer. 'T-Cell Receptor Cross-Linking Transiently Stimulates Adhesiveness through LFA-1.' *Nature*. 1989; 341: 619–624.
19. Kim, Sun Taek, Koh Takeuchi, Zhen-Yu J Sun, Maki Touma, et al. 'The Alphanbeta T Cell Receptor Is an Anisotropic Mechanosensor'. *J Biol Chem*. 2009; 284: 31028–31037.
20. Feigelson, Sara W, Ronit Pasvolsky, Saso Cemurski, Ziv Shulman, et al. 'Occupancy of

- Lymphocyte LFA-1 by Surface-Immobilized ICAM-1 Is Critical for TCR- but Not for Chemokine-Triggered LFA-1 Conversion to an Open Headpiece High-Affinity State.' *Journal of Immunology* (Baltimore, Md.: 1950). 2010; 185: 7394—7404.
21. Astrof, Nathan S, Azucena Salas, Motomu Shimaoka, JianFeng Chen, et al. Springer. 'Importance of Force Linkage in Mechanochemistry of Adhesion Receptors'. *Biochemistry*. 2006; 45: 15020—15028.
 22. Friedland, Julie C, Mark H Lee, David Boettiger. 'Mechanically Activated Integrin Switch Controls Alpha5beta1 Function'. *Science* (New York, N.Y.). 2009; 323: 642—644.
 23. Kong, Fang, A Paul Mould, Martin J Humphries, Cheng Zhu. 'Demonstration of Catch Bonds between an Integrin and Its Ligand'. *Cell*. 2009; 185: 1275—1284.
 24. Chen, Wei, Jizhong Lou, Cheng Zhu. 'Forcing Switch from Short- to Intermediate- and Long-Lived States of the AA Domain Generates LFA-1/ICAM-1 Catch Bonds'. *Journal of Biological Chemistry*. 2010; 285: 35967—35978.
 25. Husson, Julien, Karine Chemin, Armelle Bohineust, Claire Hivroz, et al. 'Force Generation upon T Cell Receptor Engagement'. Edited by Javed N. Agrewala. *PLoS ONE*. 2011; 6: e19680.
 26. Smith-Garvin, Jennifer E, Gary A Koretzky, Martha S Jordan. 'T Cell Activation'. *Annu Rev Immunol*. 2009; 27: 591—619.
 27. Chakraborty, Arup K, Arthur Weiss. 'Insights into the Initiation of TCR Signaling'. *Nature Immunology*. 2014; 15: 798—807.
 28. Rudolph, Markus G, Robyn L Stanfield, Ian A Wilson. 'How TCRs Bind MHCs, Peptides, and Coreceptors'. *Annu Rev Immunol*. 2006; 24: 419—466.
 29. Sundberg, Eric J, Roy A Mariuzza. 'Molecular Recognition in Antibody-Antigen Complexes'. *Advances in Protein Chemistry*. 2002; 61: 119—160.
 30. Rossjohn, Jamie, Stephanie Gras, John J Miles, Stephen J Turner, et al. 'T Cell Antigen Receptor Recognition of Antigen-Presenting Molecules'. *Annual Review of Immunology*. 2015; 33: 169—200.
 31. Huang, Jun, Mario Brameshuber, Xun Zeng, Jianming Xie, et al. 'A Single Peptide-Major Histocompatibility Complex Ligand Triggers Digital Cytokine Secretion in CD4(+) T Cells'. *Immunity*. 2013; 39: 846—857.
 32. Ma, Zhengyu, Paul A Janmey, Terri H Finkel. 'The Receptor Deformation Model of TCR Triggering'. *The FASEB Journal*. 2008; 22: 1002—1008.
 33. Liu, Baoyu, Wei Chen, Brian D Evavold, Cheng Zhu. 'Accumulation of Dynamic Catch Bonds between TCR and Agonist Peptide-MHC Triggers T Cell Signaling'. *Cell*. 2014; 157: 357—368.
 34. Das, Dibyendu Kumar, Yinnian Feng, Robert J Mallis, Xiaolong Li, et al. 'Force-Dependent Transition in the T-Cell Receptor β -Subunit Allosterically Regulates Peptide Discrimination and PMHC Bond Lifetime'. *Proceedings of the National Academy of Sciences*. 2015; 112: 1517—1522.
 35. Limozin, Laurent, Marcus Bridge, Pierre Bongrand, Omer Dushek, et al. 'TCR-PMHC Kinetics under Force in a Cell-Free System Show No Intrinsic Catch Bond, but a Minimal Encounter Duration before Binding'. *Proceedings of the National Academy of Sciences of the United States of America*. 2019; 116: 16943—16948.
 36. Wu, Peng, Tongtong Zhang, Baoyu Liu, Panyu Fei, et al. 'Mechano-Regulation of Peptide-MHC Class I Conformations Determines TCR Antigen Recognition'. *Molecular*

Cell. 2019; 73: 1015–1027.e7.

37. Carpenter, Andrea C, Rémy Bosselut. ‘Decision Checkpoints in the Thymus’. *Nature Immunology*. 2010; 11: 666–673.

38. Irving BA, FW Alt, N Killeen. ‘Thymocyte Development in the Absence of Pre–T Cell Receptor Extracellular Immunoglobulin Domains’. *Science (New York, N.Y.)*. 1998; 280: 905–908.

39. Yamasaki, Sho, Takashi Saito. ‘Molecular Basis for Pre–TCR–Mediated Autonomous Signaling’. *Trends in Immunology*. 2007; 28: 39–43.

40. Smelty, Philippe, Céline Marchal, Romain Renard, Ludivine Sinzelle, et al. ‘Identification of the Pre–T–Cell Receptor Alpha Chain in Nonmammalian Vertebrates Challenges the Structure–Function of the Molecule’. *Proceedings of the National Academy of Sciences of the United States of America*. 2010; 107: 19991–19996.

41. Mallis, Robert J, Ke Bai, Haribabu Arthanari, Rebecca E Hussey, et al. ‘Pre–TCR Ligand Binding Impacts Thymocyte Development before $\alpha\beta$ TCR Expression’. *Proceedings of the National Academy of Sciences*. 2015; 112: 201504971–201504971.

42. Das, Dibyendu Kumar, Robert J Mallis, Jonathan S Duke–Cohan, Rebecca E Hussey, et al. ‘Pre–TCRs Leverage V β CDRs and Hydrophobic Patch in Mechanosensing Thymic Self–Ligands’. *Journal of Biological Chemistry*. 2016; 291: jbc.M116.752865–jbc.M116.752865.

43. Ananthakrishnan, Revathi, Allen Ehrlicher. ‘The Forces behind Cell Movement’. *International Journal of Biological Sciences*. 2007; 3: 303–317.

44. Salvi, Alicia M, Kris A DeMali. ‘Mechanisms Linking Mechanotransduction and Cell Metabolism’. *Current Opinion in Cell Biology*. 2018; 54: 114–120.

45. Chen, Christopher S, John Tan, Joe Tien. ‘Mechanotransduction at Cell–Matrix and Cell–Cell Contacts’. *Annual Review of Biomedical Engineering*. 2004; 6: 275–302.

46. Prager–Khoutorsky, Masha, Alexandra Lichtenstein, Ramaswamy Krishnan, Kavitha Rajendran, et al. ‘Fibroblast Polarization Is a Matrix–Rigidity–Dependent Process Controlled by Focal Adhesion Mechanosensing’. *Nature Cell Biology*. 2011; 13: 1457–1465.

47. Welf, Erik S, Christopher E Miles, Jaewon Huh, Etai Sapoznik, et al. ‘Actin–Membrane Release Initiates Cell Protrusions’. *Developmental Cell*. 2020; 55: 723–736.e8.

48. Schlaepfer, David D, Steven K Hanks, Tony Hunter, Peter van der Geer. ‘Integrin–Mediated Signal Transduction Linked to Ras Pathway by GRB2 Binding to Focal Adhesion Kinase’. *Nature*. 1994; 372: 786–791.

49. Davis, Simon J, P Anton van der Merwe. ‘The Kinetic–Segregation Model: TCR Triggering and Beyond’. *Nat Immunol*. 2006; 7: 803–809.

50. Comrie, William A, Janis K Burkhardt. ‘Action and Traction: Cytoskeletal Control of Receptor Triggering at the Immunological Synapse’. *Frontiers in Immunology*. 2016; 7.

51. Cai, En, Kyle Marchuk, Peter Beemiller, Casey Beppler, et al. ‘Visualizing Dynamic Microvillar Search and Stabilization during Ligand Detection by T Cells’. *Science*. 2017; 356: eaal3118–eaal3118.

52. Brodovitch, Alexandre, Pierre Bongrand, Anne Pierres. ‘T Lymphocytes Sense Antigens within Seconds and Make a Decision within One Minute’. *Journal of Immunology (Baltimore, Md.: 1950)*. 2013; 191: 2064–2071.

53. Brodovitch, Alexandre, Eugene Shenderov, Vincenzo Cerundolo, Pierre Bongrand, et al. ‘T Lymphocytes Need Less than 3 Min to Discriminate between Peptide MHCs with Similar TCR–Binding Parameters’. *European Journal of Immunology*. 2015.

54. Blumenthal, Daniel, Janis K Burkhardt. 'Multiple Actin Networks Coordinate Mechanotransduction at the Immunological Synapse'. *The Journal of Cell Biology*. 2020; 219.
55. Kumari, Sudha, Michael Mak, Yeh-Chuin Poh, Mira Tohme, et al. 'Cytoskeletal Tension Actively Sustains the Migratory T-cell Synaptic Contact'. *The EMBO Journal*. 2020; 39.
56. Basu, Roshni, Benjamin M Whitlock, Julien Husson, Judy Lieberman, et al. 'Cytotoxic T Cells Use Mechanical Force to Potentiate Target Cell Killing Cytotoxic T Cells Use Mechanical Force to Potentiate Target Cell Killing'. *Cell*. 2016; 165: 100—110.
57. Basu, Roshni, Morgan Huse. 'Mechanical Communication at the Immunological Synapse'. *Trends in Cell Biology*. 2017; 27: 241—254.
58. Judokusumo, Edward, Erdem Tabdanov, Sudha Kumari, Michael L Dustin, et al. 'Mechanosensing in T Lymphocyte Activation'. *Biophysical Journal*. 2012; 102: L5—7.
59. O'Connor, Roddy S, Xueli Hao, Keyue Shen, Keenan Bashour, et al. 'Substrate Rigidity Regulates Human T Cell Activation and Proliferation.' *Journal of Immunology (Baltimore, Md. : 1950)*. 2012; 189: 1330—1339.
60. Tabdanov, Erdem, Sasha Gondarenko, Sudha Kumari, Anastasia Liapis, et al. 'Micropatterning of TCR and LFA—1 Ligands Reveals Complementary Effects on Cytoskeleton Mechanics in T Cells'. *Integrative Biology (United Kingdom)*. 2015; 7: 1272—1284.
61. Bui, Nathalie, Michael Saitakis, Stéphanie Dogniaux, Oscar Buschinger, et al. 'Human Primary Immune Cells Exhibit Distinct Mechanical Properties That Are Modified by Inflammation'. *Biophysical Journal*. 2015; 108: 2181—2190.
62. Hui, King Lam, Lakshmi Balagopalan, Lawrence E. Samelson, Arpita Upadhyaya. 'Cytoskeletal Forces during Signaling Activation in Jurkat T—Cells'. *Molecular Biology of the Cell*. 2015; 26: 685—695.
63. Hui, King Lam, Arpita Upadhyaya. 'Dynamic Microtubules Regulate Cellular Contractility during T—Cell Activation'. *Proceedings of the National Academy of Sciences*. 2017; 114: E4175—4183.
64. Wahl, Astrid, Céline Dinet, Pierre Dillard, Aya Nassereddine, et al. 'Biphasic Mechanosensitivity of T Cell Receptor—Mediated Spreading of Lymphocytes'. *Proceedings of the National Academy of Sciences*. 2019; 116: 5908—5913.
65. Dillard, Pierre, Rajat Varma, Khaya Sengupta, Laurent Limozin. 'Ligand—Mediated Friction Determines Morphodynamics of Spreading T Cells'. *Biophysical Journal*. 2014; 107: 2629—2638.
66. Mossman, Kaspar D, Gabriele Campi, Jay T Groves, Michael L Dustin. 'Altered TCR Signaling from Geometrically Repatterned Immunological Synapses.' *Science*. 2005; 310: 1191—1193.
67. Hsu, Chih—Jung, Wan—Ting Hsieh, Abraham Waldman, Fiona Clarke, et al. 'Ligand Mobility Modulates Immunological Synapse Formation and T Cell Activation'. *PloS One*. 2012; 7: e32398.
68. Comrie, William A, Shuixing Li, Sarah Boyle, Janis K Burkhardt. 'The Dendritic Cell Cytoskeleton Promotes T Cell Adhesion and Activation by Constraining ICAM—1 Mobility'. *The Journal of Cell Biology*. 2015; 208: 457—473.
69. Jankowska, Katarzyna I, Edward K Williamson, Nathan H Roy, Daniel Blumenthal, et al. 'Integrins Modulate T Cell Receptor Signaling by Constraining Actin Flow at the Immunological Synapse'. *Frontiers in Immunology*. 2018; 9.

70. Harrison, Devin L, Yun Fang, Jun Huang. 'T--Cell Mechanobiology: Force Sensation, Potentiation, and Translation'. *Frontiers in Physics*. 2019; 7.
71. Lee, Mark S, Caleb R Glassman, Neha R Deshpande, Hemant B Badgandi, et al. 'A Mechanical Switch Couples T Cell Receptor Triggering to the Cytoplasmic Juxtamembrane Regions of CD3 ζ '. *Immunity*. 2015; 43: 227—239.
72. Sasmal, Dibyendu K, Wei Feng, Sobhan Roy, Peter Leung, et al. 'TCR—PMHC Bond Conformation Controls TCR Ligand Discrimination'. *Cellular & Molecular Immunology*. 2019.
73. Puech, Pierre--Henri, Pierre Bongrand. 'Mechanotransduction as a Major Driver of Cell Behaviour: Mechanisms, and Relevance to Cell Organization and Future Research'. *Open Biology*. 2021; 11: 210256.
74. Ma, Victor Pui--Yan, Yang Liu, Lori Blanchfield, Hanquan Su, et al. 'Ratiometric Tension Probes for Mapping Receptor Forces and Clustering at Intermembrane Junctions'. *Nano Letters*. 2016; 16: 4552—4559.
75. Liu, Yang, Lori Blanchfield, Victor Pui--Yan Ma, Rakieb Andargachew, Kornelia Galior, et al. 'DNA--Based Nanoparticle Tension Sensors Reveal That T--Cell Receptors Transmit Defined PN Forces to Their Antigens for Enhanced Fidelity'. *Proceedings of the National Academy of Sciences*. 2016; 113: 5610—5615.
76. Santos, Luís C, David A Blair, Sudha Kumari, Michael Cammer, et al. 'Actin Polymerization--Dependent Activation of Cas--L Promotes Immunological Synapse Stability'. *Immunology and Cell Biology*. 2016; 94: 981—993.
77. Wang X, T Ha. 'Defining Single Molecular Forces Required to Activate Integrin and Notch Signaling'. *Science*. 2013; 340: 991—994.
78. Luca, Vincent C, Byoung Choul Kim, Chenghao Ge, Shinako Kakuda, et al. 'Notch--Jagged Complex Structure Implicates a Catch Bond in Tuning Ligand Sensitivity'. *Science*. 2017; 355: 1320—1324.
79. Liu, Chinky Shiu Chen, Deblina Raychaudhuri, Barnali Paul, Yogaditya Chakrabarty, et al. 'Cutting Edge: Piezo1 Mechanosensors Optimize Human T Cell Activation'. *The Journal of Immunology*. 2018; 200: 1255—1260.
80. Benard, Emmanuelle, Jacques A Nunès, Laurent Limozin, Kheya Sengupta. 'T Cells on Engineered Substrates: The Impact of TCR Clustering Is Enhanced by LFA--1 Engagement'. 2018; 9: 1—12.
81. Chen, Yunfeng, Lining Ju, Muaz Rushdi, Chenghao Ge, et al. 'Receptor--Mediated Cell Mechanosensing'. *Molecular Biology of the Cell*. 2017; 28: 3134—3155.
82. Verma, Navin Kumar, Dermot Kelleher, Email Alerts. 'Not Just an Adhesion Molecule: LFA--1 Contact Tunes the T Lymphocyte Program'. 2018.

Dissecting T-cell mechanosensing at molecular and cellular scales

A. Sadoun, F. Mustapha, O Ndao, G Eich, Y Hamon, L Limozin and PH Puech

Published online in April 2020

I participated in the following small review that was commanded to us by JPK Instruments/Bruker as a Technical Report available on their website (see below). This was part of our interaction with JPK Instruments/Bruker as they were one of my non-academic partners in my PhD project. It was then turned into an online Wiley publication based on a proposition from Wiley. I present hereafter the non-edited text of the second version.

Overview

T cells play an essential role in the immune response. Atomic Force Microscopy (AFM) is ideal for investigating T-cell receptor (TCR) binding to antigen peptides on cell surfaces, T lymphocyte activation and TCR signaling. AFM, alone and in combination with Optical Tweezers, can be used to investigate the mechanosensory properties of T cells, characterize the surfaces T cells come in contact with, and the mechanics and forces involved in the immune response. AFM can also be combined with fluorescence microscopy to characterize, in real-time, intracellular signals generated when the proteins present on the cell surface are stimulated.

Introduction

The key function of T lymphocytes during an immune response is to scan the surface of surrounding cells and detect, via the membrane T cell receptor (TCR), the presence of foreign peptide antigens on antigen presenting cells (APC) among the many self-peptides presented by the Major Histocompatibility Complexes (MHC). A TCR-peptide-MHC (pMHC) interaction is required for the activation of T-cells and subsequent actions, such as proliferation, which is the essence of the adaptive immune response. In addition, TCR-pMHC interactions constantly provide “survival signals” in order to maintain a steady population of memory cells, which constitute our long-term immunity. [1]

TCR dependent signaling must therefore be both rapid and sensitive in order to efficiently detect the presence of very low numbers of foreign peptide antigens, and at the same time filter out self-peptide/MHC generated ‘noise’, so as not to harm healthy cells and normal tissue. The different ways TCR-peptide-MHC binding events are processed by the cellular signaling machinery of the lymphocytes remains a critically important question for both the development and the function of the adaptive immune response.

In particular, a lot of effort has been made to quantify (i) the kinetics of the TCR-peptide-MHC bonds, (ii) the number of interacting partners, (iii) the type and role of co-stimulatory molecules, (iv) the spatial organization of the activating molecules, and (v) the contribution of other physical parameters, such as the forces exerted on the molecular bonds^[2].

For this reason, the cytoskeletal architecture of T cells appears to play an ever more central role in their recognition and activation properties, but this needs to be further clarified and quantified. It allows the T cells to exert forces on the APC, down to the single molecule scale. It has been proposed that these forces are a key factor in the capacity of T cells to selectively and sensitively recognize foreign peptides and in their activation. T cells can feel the overall rigidity of the substrate they are in contact with and, in addition to its biochemical properties, use it as a supplementary signal. It is thought that, to a certain extent, mechanotransduction plays a role in the activation of T cells, from the molecular scale to a more global cellular scale^[3].

As a result, the aim of our investigations is to examine how the micro- and nano-organization of activation-related surface molecules affect or are affected by the micro-mechanical properties of T cells (such as recognition, adhesion, elasticity, membrane tension) using advanced biophysical techniques based on force application/measurement such as Atomic Force Microscopy (AFM) or Optical Tweezers (OT). These techniques allow the measurement of cell elasticity, viscosity and adhesion during signaling.

OT and nano-indentation by AFM allow the investigator to gain quantitative information about the elasticity and viscoelasticity of cells. Membrane tension can be measured by using AFM or OT to pull tethers from the membrane.

In this article, we will go into detail on how both AFM and OT can be important tools in the field of immuno-mechanics.

Materials and Methods

Evaluation of TCR recognition at the single molecule scale, on living T cells

In a first attempt to understand which physical parameters are recognized by T cells when they come in contact with an antigen presenting cell, we designed a single molecule study to determine the probability of adhesion and the forces of detachment at the surface of living lymphocytes. We used SMFS (Single Molecule Force Spectroscopy) with soft AFM cantilevers and tips decorated with recombinant pMHC molecules (Fig. 1).

We used them to probe the mechanics of the T cell under very low forces and for very short periods of contact time (~ 100 msec). This resulted in infrequent recognition events. By varying the peptide load in the pocket of the MHC, we showed that recognition was indeed specific, but that the rupture forces we observed under the experimental conditions were not peptide-dependent^[4].

It was later shown, via techniques using softer springs (a laser for OT; a Red Blood Cell for a biomembrane force probe) that indeed, the TCR can behave as a mechanosensory molecule. The forces that the T cell feel via the TCR are now thought to help recognition be highly specific and rapid^[5].

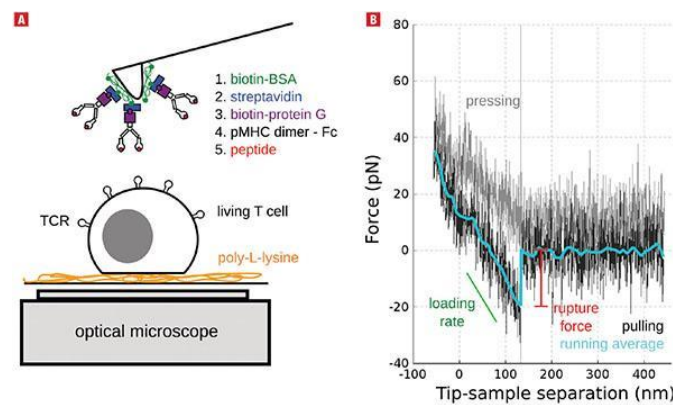


Figure 1. SMFS of TCR/pMHC bond. A: Schematics of the experiments on living T cell hybridoma, with the methodology used to decorate AFM cantilevers with pMHC. B: Typical single molecule separation event, showing the very low specific forces (~ 20 pN) that were recorded, to be compared to larger forces obtained for classical adhesion molecules. Adapted from^[4].

Real-time combination of AFM and fluorescence microscopy

We performed AFM indentation of T cells simultaneously with intracellular Ca^{2+} fluorescence imaging to gain quantitative information on the forces at play during the different activation phases^[6].

We used an original internal timer signal and AFM based mechanical stimulation to apply a mechanical stimulation that can, in addition, be made specific via, e.g., anti CD3 antibodies. We have developed micro-manipulation techniques to decorate AFM cantilevers with beads of diameters ranging from one to $50\ \mu\text{m}$ in order to control the shape and size of the stimulating surface. Stimulation can be performed with either continuous contact or with a succession of timed, short stimulations in order to dissect how the “signaling black box” answers the same specific signal, but with a specified spatial or temporal distribution. This approach, in a way, is a typical physicist method for dissecting the “transfer function” of an unknown system. Here, biology allows us to interfere with the “black box” thanks to the use of mutants or molecules that can impact specific parts of the signaling cascades or functions.

We also developed protocols to record the modification of the mechanical properties of T cells with optogenetic tools, for example, photoactivatable Rac, a small GTP-ase protein^[6].

Characterization of substrates for interaction with T cells

Two AFM modes can be used to characterize the topology or the mechanical properties of an artificial substrate which will interact with the T cells. Firstly, the substrate can be imaged at the nanoscale and its roughness^[7] or surface structure observed, e.g. using micro-contact printing or nano-scale patterns^[8]. Secondly, when preparing soft polymeric substrates or soft gels, substrate indentation or force mapping can be used to precisely characterize the mechanical properties of the substrate the cell is exposed to at the subcellular scale using a thin tip/small scan range, or at the cellular scale using a bead for cellular contact/larger scan range. We observed that the mechanical properties of the substrate may lead to unconventional spreading behavior of the T cells depending on the molecular decoration of the surface^[9].

Characterization of model antigen presenting cells

We shaped model APCs (COS-7 cells,^[9]) on stamped fibronectin, while preventing the adhesion and activation of the T cells around them. Micropatterns were used to pull on the edge of the cell to create a large lamellipodium that was thin enough to observe the early contacts of T cells through it, using advanced surface microscopies such as TIRF (with membrane labelled T cells) or RICM (without any labelling).

This structure allows us to have a fully controlled, fluid, cellular environment, the composition of which is controllable by transfection and is closer to physiological conditions than textured substrates and supported lipid bilayer approaches^[10]. The 3D topography of the lamellipodium was characterized using different pattern sizes and a combination of TIRF, confocal (membrane, cytoskeleton), multi-color RICM reconstruction in conjunction with AFM imaging and force mapping^[11]. We also used classical AFM indentation to characterize the Young's modulus of different populations of COS cells expressing different receptors and molecules in regard to T cell mechanics (unpublished data, consistent with ^[12]).

T lymphocyte/antigen presenting cell forces

In order to simulate physiological situations more accurately, we approached the APC vs. T cell situation by attaching a model APC (a transfected COS-7 cell,^[9]) to an AFM cantilever and brought it in contact with a (Ca²⁺ reporter loaded) T cell of known shape^[9]. This method, called Single Cell Force Spectroscopy (SCFS)^[14], allows the evaluation of the contact mechanics between cells, the evolution of the contact and the forces needed for separation, from single molecules to entire cell scales. It has recently been applied to T cell/APC contact over long contact times and after formation of the immune synapse^[13], but

only adhesion at the cellular scale was recorded, early activation of the cells was not simultaneously observed.

Combining SCFS with our technique of simultaneous AFM/fluorescence to record the activation pattern before, during and after contact, the early physical determinants of T cell activation can be analyzed, such as which forces are required or created by T cells to integrate a biochemical or biomechanical signal (Fig. 2). Depending on the contact times, the molecules involved and potential signaling required to reinforce the cell/cell adhesion, such approaches may need an extended piezo range (up to 100 μm or even more). It may also be necessary to coordinate the fluorescence-detecting lens with a supplementary piezo, all of which is possible with the JPK CellHesion module^[14], an add-on of the JPK NanoWizard AFM. Cell/cell adhesion forces, numbers and separation distances are indeed larger compared to usual SCFS (cell vs. substrate) experiments, requiring adaption of the spring constant of the cantilever in order to be able to record the forces, and importantly, the pulling range, which is usually limited to 10–15 μm in conventional AFMs.

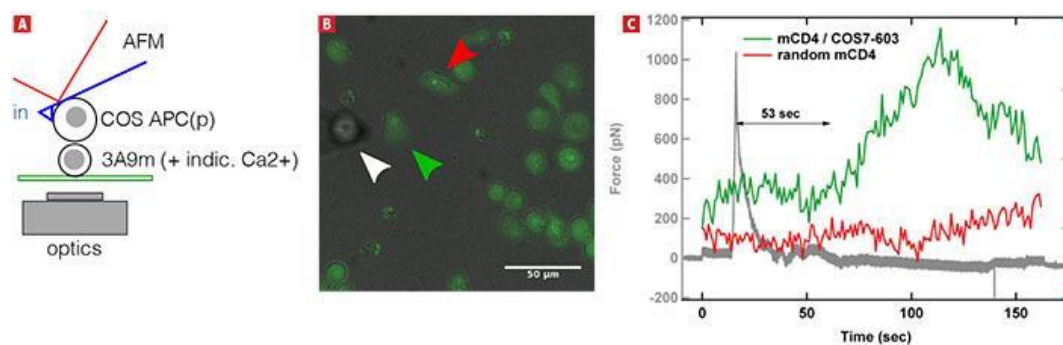


Figure 2. SCFS coupled to fluorescence microscopy. A: Schematics of the experiments, where a calcium reporter loaded T cell, gently immobilized on a PLL coated surface, is brought into contact with an APC attached to an AFM lever. B: Superposition of transmission and fluorescence images, with the APC (white arrowhead), the contacted T cell (green arrowhead) and a control/non contacted T cell (red arrowhead). C: Force signal, presented with the fluorescence signal emitted by contacted and control T cells. The rise in calcium follows the contact, as detected by force rise, by ~ 1 min, which is coherent with literature.

Measuring T cell cortical tension by pulling membrane tethers

Using, e.g. lectin decorated cantilevers, membrane tubes or tethers can be pulled using AFM. Cortical cell tension can be estimated based on the force needed to extract them from the cell, and, using drug-induced perturbation of the cell cytoskeleton in a parallel experiment, the cell's membrane tension and the interaction energy between the membrane and the cytoskeleton can be evaluated^[15, 16].

Using Optical Tweezers (for us, the JPK NanoTracker 2), the resolution in force can be increased compared to AFM, and such experiments can be performed in combination with fluorescence imaging of the membrane (Fig. 3). As a result of the very low noise level ($\sim \text{pN}$), detailed observation of the mechanics of tube pulling is possible. A long pulling distance can

be mandatory: T cells are rather small ($\sim 10\ \mu\text{m}$ in diameter) but tethers can be pulled that are up to $10\ \mu\text{m}$ or even $20\ \mu\text{m}$ long, depending on the experimental conditions.

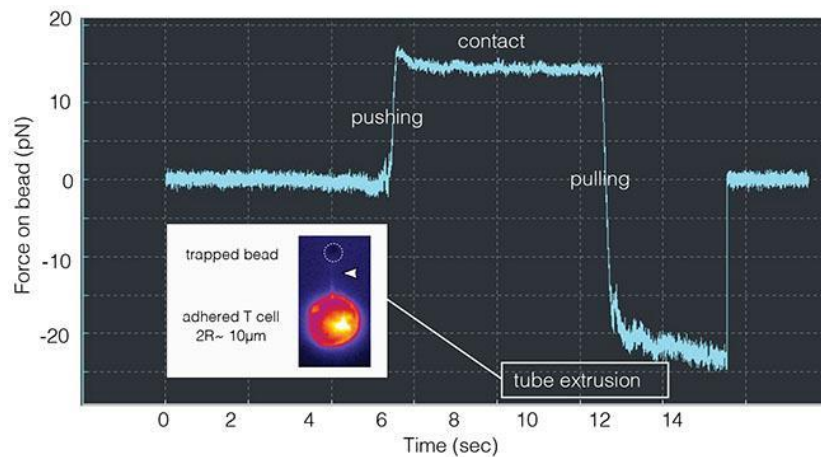


Figure 3. Membrane tube pulling using OT. A lectin-coated bead is used to contact a PLL immobilized T cell, and to pull a long membrane tether, as denoted by a force plateau in the retraction (« pulling ») part of the force curve vs. Time. Insert: Fluorescence monitoring of the membrane tube (white arrowhead), using a mutant cell line, the membrane of which is fluorescent.

Conclusions and Perspectives

T cells have mechanosensory properties that range from their characteristic TCR molecule to the whole cell scale^[2]. Here, we have presented several examples which show that AFM, in imaging or force mode, is a highly interesting tool for characterizing the surfaces that T cells come in contact with, or the mechanics and forces of the T cells themselves.

AFM can also be combined with fluorescence microscopy to characterize, in real-time, some of the intracellular signals that are generated when the proteins present on the cell surface are stimulated. When used in combination with OT, a detailed characterization of cellular mechanics (Young's modulus, tension, and by using oscillating mechanical modes G' and G'' - dynamic shear modulus) can be obtained. Information on the sub-membrane organization of the cytoskeleton can also be obtained by varying the shape and size of the indenter over different scales.

Very interesting possibilities arise when the systems are combined: (i) fluorescence and AFM or OT in real-time^[6] could for example lead to the characterization of the transfer function of the membrane/surface protein system. When AFM imaging is used in combination with fluorescence microscopy, 3D functional structures on the cell surface can be revealed^[14]. (ii) Combining AFM with OT in a single system allows the reproduction of environments more similar to physiological ones, as one can assess the interaction between a T cell and an antigen presenting cell using SCFS, and when a helper, secondary T cell is brought into contact, the modulation of the recognition forces can be recorded^[17]. All in all, the use of

nano-force tools is full of promise for the emerging fields of immuno-biophysics and immuno-mechanics.

References

- Murphy, Ken, Paul Travers, and Mark Walport. 2008. *Janeway's Immunobiology* 7th Edition. Edited by Garland Science.
- Limozin, Laurent, and Pierre-Henri Puech. 2019. 'Membrane Organization and Physical Regulation of Lymphocyte Antigen Receptors: A Biophysicist's Perspective'. *The Journal of Membrane Biology* 252 (4–5): 397–412. <https://doi.org/10.1007/s00232-019-00085-2> SMASH.
- Wahl, Astrid, Céline Dinot, Pierre Dillard, Aya Nasserredine, Pierre-Henri Puech, Laurent Limozin, and Kheya Sengupta. 2019. 'Biphasic Mechanosensitivity of T Cell Receptor-Mediated Spreading of Lymphocytes'. *Proceedings of the National Academy of Sciences of the United States of America* 116 (13): 5908–13. <https://doi.org/10.1073/pnas.1811516116> SMASH.
- Puech, Pierre-Henri, Damien Nevoltris, Philippe Robert, Laurent Limozin, Claude Boyer, and Pierre Bongrand. 2011. 'Force Measurements of TCR/PMHC Recognition at T Cell Surface'. Edited by Daniel J. Muller. *PLoS ONE* 6 (7): e22344. <https://doi.org/10.1371/journal.pone.0022344> SMASH.
- Huse, Morgan. 2017. 'Mechanical Forces in the Immune System'. *Nature Reviews Immunology* 17 (11): 679–90. <https://doi.org/10.1038/nri.2017.74> SMASH.
- Cazaux, Séverine, Anaïs Sadoun, Martine Biarnes-Pelicot, Manuel Martinez, Sameh Obeid, Pierre Bongrand, Laurent Limozin, and Pierre-Henri Puech. 2016. 'Synchronizing Atomic Force Microscopy Force Mode and Fluorescence Microscopy in Real Time for Immune Cell Stimulation and Activation Studies'. *Ultramicroscopy* 160 (January): 168–81. <https://doi.org/10.1016/j.ultramic.2015.10.014> SMASH.
- Lo Schiavo, Valentina, Philippe Robert, Zohar Mishal, Pierre-Henri Puech, Francesco Gentile, Paolo Decuzzi, Pierre Bongrand, and Laurent Limozin. 2013. 'Transient Adhesion Mediated by Ligand-Receptor Interaction on Surfaces of Variable Nanotopography'. *International Journal of Nanotechnology* 10 (5–7): 404–18. <https://doi.org/10.1504/IJNT.2013.053512> SMASH.
- Pi, Fuwei, Pierre Dillard, Laurent Limozin, Anne Charrier, and Kheya Sengupta. 2013. 'Nanometric Protein-Patch Arrays on Glass and Polydimethylsiloxane for Cell Adhesion Studies'. *Nano Letters*, June. <https://doi.org/10.1021/nl401696m> SMASH.
- Salles A, Billaudeau C, Sergé A, Bernard A-M, Phélipot M-C, Bertaux N, et al. 2013. 'Barcoding T Cell Calcium Response Diversity with Methods for Automated and Accurate Analysis of Cell Signals (MAAACS)'. *PLoS Comput Biol* 9(9): e1003245. <https://doi.org/10.1371/journal.pcbi.1003245> SMASH
- Dillard, Pierre, Rajat Varma, Kheya Sengupta, and Laurent Limozin. 2014. 'Ligand-Mediated Friction Determines Morphodynamics of Spreading T Cells'. *Biophysical Journal* 107 (11): 2629–38. <https://doi.org/10.1016/j.bpj.2014.10.044> SMASH.
- Dejardin, Marie-Julie, Arnaud Hemmerle, Anaïs Sadoun, Yannick Hamon, Pierre-Henri Puech, Kheya Sengupta, and Laurent Limozin. 2018. 'Lamellipod Reconstruction by Three-Dimensional Reflection Interference Contrast Nanoscopy (3D-RICN)'. *Nano Letters*, September. <https://doi.org/10.1021/acs.nanolett.8b03134> SMASH.
- Bufl, Nathalie, Michael Saitakis, Stéphanie Dogniaux, Oscar Buschinger, Armelle Bohineust, Alain Richert, Mathieu Maurin, Claire Hivroz, and Atef Asnacios. 2015. 'Human Primary

- Immune Cells Exhibit Distinct Mechanical Properties That Are Modified by Inflammation'. *Biophysical Journal* 108 (9): 2181–90. <https://doi.org/10.1016/j.bpj.2015.03.047> SMASH
- Hosseini, Babak H., Ilia Louban, Dominik Djandji, Guido H. Wabnitz, Janosch Deeg, Nadja Bulbuc, Yvonne Samstag, Matthias Gunzer, Joachim P. Spatz, and Günter J. Hammerling. 2009. 'Immune Synapse Formation Determines Interaction Forces between T Cells and Antigen-Presenting Cells Measured by Atomic Force Microscopy'. *Proceedings of the National Academy of Sciences of the United States of America* 106 (42): 17852–57. <https://doi.org/10.1073/pnas.0905384106> SMASH.
- Puech, Pierre-Henri, Kate Poole, Detlef Knebel, and Daniel J Muller. 2006. 'A New Technical Approach to Quantify Cell-Cell Adhesion Forces by AFM.' *Ultramicroscopy* 106 (8–9): 637–644. <https://doi.org/10.1016/j.ultramic.2005.08.003> SMASH.
- Diz-Muñoz, Alba, Michael Krieg, Martin Bergert, Itziar Ibarlucea-Benitez, Daniel J. Muller, Ewa Paluch, and Carl-Philipp Heisenberg. 2010. 'Control of Directed Cell Migration In Vivo by Membrane-to-Cortex Attachment'. Edited by William A. Harris. *PLoS Biology* 8 (11): e1000544. <https://doi.org/10.1371/journal.pbio.1000544> SMASH.
- Sadoun, Anaïs, and Pierre-Henri Puech. 2017. 'Quantifying CD95/Cl-CD95L Implications in Cell Mechanics and Membrane Tension by Atomic Force Microscopy Based Force Measurements'. *Methods in Molecular Biology* (Clifton, N.J.) 1557: 139–51. https://doi.org/10.1007/978-1-4939-6780-3_14 SMASH.
- Chen, Jiahuan, Anutosh Ganguly, Ashley D Mucsi, Junchen Meng, Jiacong Yan, Pascal Detampel, Fay Munro, et al. 2017. 'Strong Adhesion by Regulatory T Cells Induces Dendritic Cell Cytoskeletal Polarization and Contact-Dependent Lethargy'. *Journal of Experimental Medicine*, 1–12. <https://doi.org/10.1084/jem.20160620> SMASH.

May the force be with your (immune) cells: An introduction to traction force microscopy in Immunology.

Farah Mustapha ^{1,2,3,4,5}, Kheya Sengupta ^{4,5,*}, Pierre-Henri Puech ^{1,2,3,4,*}

Affiliations:

Laboratoire Adhésion et Inflammation (LAI)

¹ Aix Marseille University, LAI UM 61, Marseille, F-13288, France.

² Inserm, UMR_S 1067, Marseille, F-13288, France.

³ CNRS, UMR 7333, Marseille, F-13288, France.

CENTURI

⁴ Turing Center for Living systems, Marseille, France

Centre Interdisciplinaire de Nanoscience de Marseille (CINAM)

⁵ CNRS - AMU UMR 7325, Marseille, F-13288, France

* To whom correspondence should be addressed:

sengupta@cinam.univ-mrs.fr; pierre-henri.puech@inserm.fr

Abstract:

For more than a couple of decades now, “force” has been recognized as an important physical parameter that cells employ to adapt to their microenvironment. Whether it is externally applied, or internally generated, cells use force to modulate their various actions, from adhesion and migration to differentiation and immune function. T lymphocytes use such mechano-sensitivity to decipher signals when recognizing cognate antigens presented on the surface of antigen presenting cells (APCs), a critical process in the adaptive immune response. As such, many techniques have been developed and used to measure the forces felt/exerted by these small, solitary and extremely reactive cells to decipher their influence on diverse T cell functions, primarily activation. Here, we focus on traction force microscopy (TFM), in which a deformable substrate, coated with the appropriate molecules, acts as a force sensor on the cellular scale. This technique has recently become a center of interest for many groups in the “ImmunoBiophysics” community and, as a consequence, has been subjected to refinements for its application to immune cells. Here, we present an overview of TFM, the precautions and pitfalls, and the most recent developments in the context of T cell immunology.

Keywords: Immune system, T cell, Antigen presenting cell, Mechanosensitivity, Traction Force Microscopy

Introduction

The adult human body has approximately 10^{13} cells, and its fate, in terms of tissue and organ development and homeostasis, depends on how well these cells interact with one another and with their environment (see, for example (1–4) and references therein). A wealth of cell biology reports has documented the biochemical aspect of these interactions, identifying the networks of secreted ligands, cell surface receptors, intracellular signaling pathways, and transcriptional factors at play. However, as cells live in a physical world, the mechanical aspect of such interactions cannot be neglected. Indeed, the last few decades of research have confirmed that cells do sense the mechanical forces arising from their environment; they actively respond to them through mechanically driven biological actions, such as adhesion, migration, division, differentiation, and even apoptosis - a process termed mechanotransduction (4). Mechanotransduction appears to be present in almost all interactions between a given cell and its environment, including immune cells.

For T lymphocytes, the initiation of an adaptive immune response necessitates the interaction of naive T cells with antigen presenting cells (APCs). This interaction starts with the T cell receptor (TCR) recognizing an antigenic peptide presented on the major histocompatibility complex (pMHC) of the APC. Once the TCR binds to a cognate pMHC, the T cell can be seen applying cycles of pushing and pulling forces on the APCs. These forces, generated from the rapid reorganization of the T cell cytoskeleton upon activating stimuli, may participate in the formation of a specialized cell-cell interface termed the “Immunological Synapse” (IS), encompassing additional receptor-ligand pairs. Through these interactions, the APC relays a highly orchestrated series of signals that drive T cell activation, proliferation, and eventual differentiation (3).

In recent years, it has become increasingly clear that the mechanical forces generated at the IS are essential for the proper activation of T cells; several of the cell surface receptors participating in the IS are mechanosensitive proteins, and the forces originating from the constant remodeling of the cytoskeleton play an important role in regulating them (5–7). It has been also proposed that both the amplitude and the time evolution of the forces applied through the TCR contribute to rapid discrimination of the antigenic peptides (8). Moreover, there is evidence suggesting that T cells and APCs use mechanical forces as a form of communication to transmit information across the synapse (2).

Thus, given the substantial impact of mechanical forces on the behavior of T cells, and knowing that even comparatively moderate defects in T cell activation can lead to autoimmune diseases on one hand, and immunodeficiency on the other, it comes as no real surprise that elucidating the precise mechanisms underpinning mechanotransduction is of significant interest to researchers in the area of fundamental and applied immunology, and biophysics. Clearly, a knowledge of both the intracellular and extracellular forces is required. Owing to this demand, the last two decades have witnessed a burst in novel experimental methods that have been employed to quantify cellular forces (4, 8, 9). These include, but are not limited to, Atomic Force Microscopy (AFM), Optical Tweezers (OT), Bio-membrane Force Probes (BFP), and Traction Force Microscopy (TFM) (Figure 1, and references within the caption).

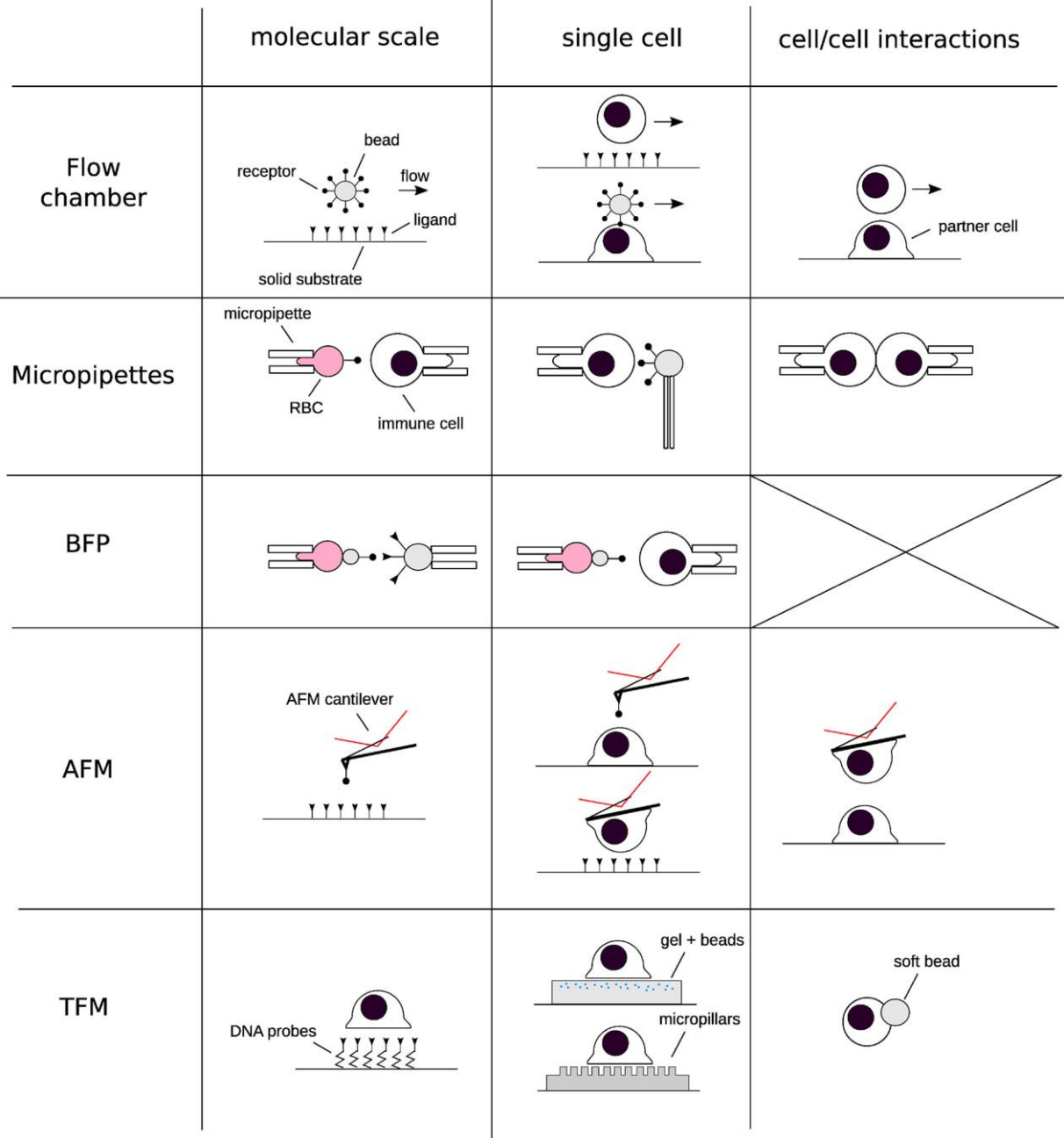


FIGURE 1 Schematics of the techniques that have been used for deciphering the implications of forces in immunology at different scales of space (from molecular to cell/cell interactions) and times. Each row represents a “group” of similar techniques, and each column a given spatial scale. A selection of references corresponding to each technique, restricted to their application to immune cells: Flow chamber: (10–12) Micropipettes: (13–16). Biomembrane Force Probe: (17–20). Atomic Force Microscopy: (21–26) Traction force microscopy and related techniques: (27–36).

This review will focus on methods that are now collectively known as Traction Force Microscopy (TFM). TFM is essentially a technique that permits the quantification of cellular traction forces via the non-invasive optical imaging of deformations induced by the cell. Though the term was initially used to refer to the forces exerted by adherent cells on 2D linear

elastic substrates (37), it has since been adapted for quantification of three dimensional (tangential and normal) forces exerted onto 2D, 2.5D and 3D substrates.

Making invisible forces visible

Broadly speaking, forces are not an experimentally directly accessible quantity; they have to be inferred from the fact that they create some type of deformation or motion. The relation between deformation/motion and force is described by the classical laws of physics, one such example being Hooke's law for the deformation of a linear elastic spring: $F = k \Delta x$, where F is the force, k is the spring constant and Δx is the extension of the spring. Without a measurement of Δx , no statement on F would be possible (k is a constant that can be obtained from a calibration experiment). In order to measure Δx , the relaxed reference state of the spring in the absence of any force has to be known.

Consequently, all measurements of cellular forces must start with the identification of a suitable strain gauge and incorporating it into a cell culture setup. One straightforward way of doing so is by replacing the traditional glass or plastic cell culture plates with a substrate capable of deforming under force. The earliest attempt at this was by Harris et al. who used a thin silicon rubber to show that fibroblasts generated elastic wrinkles when crawling (38). They named the force "traction", comparing it to "the traction an automobile's wheel exerts on the highway surface". However, because wrinkling is an inherently non-linear and complex process, the forces couldn't be accurately quantified.

Continuous versus discrete anchoring

Despite this seminal experiment remaining a rather qualitative observation, it inspired the design and development of alternative systems capable of quantitatively measuring traction forces. Nearly two decades later, in 1999, Dembo and Wang officially introduced "Traction Force Microscopy" – TFM – as a method to quantify forces exerted by adherent cells on compliant substrates (37). They replaced the silicon membranes with thicker, linearly elastic, hydrogels and adopted fluorescent beads as fiducial markers, instead of relying on wrinkles to report substrate deformation (Figure 2A). Above all, these changes replaced the generally nonlinear and mathematically complex description of wrinkle formation with a classical, linear, continuum mechanics model from material science (39, 40), thus opening the way for systematic force measurement.

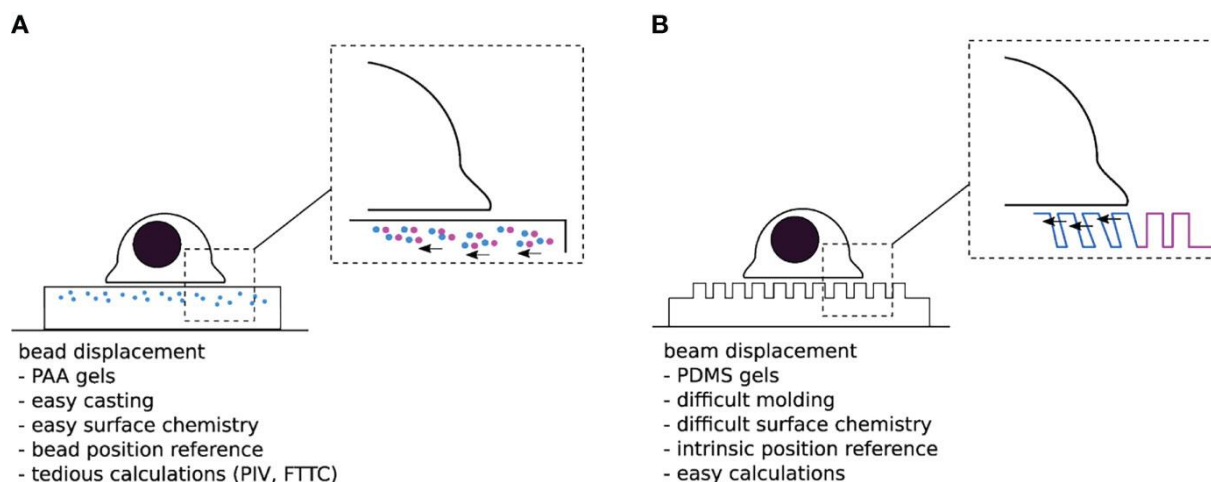


FIGURE 2 (A) “Traditional” TFM with PAA gels doped with sub-resolution fluorescent beads. One difficulty is to assess the non-perturbed bead position either at the beginning or the end of the experiment. (B) Micropillar based TFM. The typical size of a pillar is $1\mu\text{m}$ diameter over $10\mu\text{m}$ length, for a $1\mu\text{m}$ interpillar distance, and a hexagonal compact 2D distribution—the numbers given here are typical orders of magnitude for these parameters). The unmolding step in the substrate fabrication process can be quite delicate, while the force localization and calculation are rather trivial.

In an attempt to further simplify the computationally intensive force calculations required for continuous hydrogels, Tan and colleagues introduced an elegant alternative system for TFM in 2003 (41). Theirs consisted of cylindrical polymeric pillar arrays, fabricated by soft lithography, where cellular forces can be laterally decoupled in a series of local strain gauges; once cells adhere to the protein-coated pillar tops, they bend them away from their unloaded position. By estimating this deformation and applying the classical beam bending theory, one can then calculate the local traction forces exerted by the cells (Figure 2B) (41, 42). Despite the obvious advantage of using such discrete adhesive surfaces (i.e., load-free reference position is readily available and the deflection of a given pillar only depends on the force applied to that particular pillar), the pillars themselves represent a major flaw in the system: They impose arbitrary restrictions on the size, shape, and location of cellular adhesions, and consequently control where and how cells transmit force (43, 44). In addition, if the cell makes adhesive protrusions that extend into the substrate beyond the very top of the pillars, the classical calculation is not applicable. Thus, even though forces can be elegantly calculated using such a system, it remains unclear how these calculations relate to those actually transmitted in the native cellular environment.

Though the pillar arrays system suffered from several intrinsic limitations, it is crucial to highlight that the concept behind it served as a foundation to build a number of new approaches that translated the “reference free” and “computationally easy” force reconstruction onto flat 2D TFM substrates. These include the micro-patterning of cell adhesive islands (45, 46), the lithographic photoresist of ordered arrays (47, 48), as well as the nano-patterning of quantum dots (QDs) on linearly elastic substrates (49). Using these technologies, a regularized grid of reporter structures allows the determination of deformation of continuous 2D substrates without the need of a reference frame. However, as

these patterns may represent the only sites where cells can exert force, similar to the pillars, the artificial constraint on cell force location will impact the physiological relevance.

From 2D TFM to 3D TFM

Whether it's the continuous hydrogels from Dembo and Wang, or the pillar arrays from Tan and colleagues, both systems were originally developed with the aim of quantifying forces generated by adherent cells on 2D substrates. This was based on the assumption that cellular forces are predominantly tangential (in-plane, x, y), and that the forces normal to the substrate (out-of-plane, z) are negligible (50). However, since then, it has become evident that cells interacting with adherent substrates exert forces in 3D, and that the out-of-plane traction components are often comparable to the tangential ones (51, 52).

To account for these realizations, classical 2D TFM has been extended to 2.5D and 3D TFM (53–56).

2.5D TFM refers to the measurement of tangential and normal cellular forces exerted onto 2D substrates, not to be confused with “true 3D” TFM that quantifies forces exerted in 3D space (substrate). Nevertheless, in either case, by obtaining both the in- and out- of plane displacement fields of fiducial markers (e.g., fluorescent beads or patterns) using high-resolution image processing, for example through z-stack or astigmatic imaging (56), one can then reconstruct the “3D” force fields exerted by the cells.

While resolving normal traction forces is in itself difficult, given that it requires significant computational power, in addition to an appropriate imaging modality (discussed below), 3D TFM in specific comes with its unique set of challenges. Typically, in 3D TFM, cells (e.g., fibroblasts) are encapsulated within a deformable 3D extracellular matrix (ECM) scaffold material (e.g., collagen or fibrin fibers), pre-loaded with fluorescent beads (57). Unlike in 2D and 2.5D TFM, where the synthetic substrates can be fully characterized, biopolymers such as ECM materials are mechanically complex (57); they are constantly being synthesized, degraded and remodeled by cells. It is thus difficult to discern whether the recorded deformations are caused by one of those processes or by actual cellular forces. Besides, natural ECM is composed of fibers with highly non-linear force-extension relationships, meaning extracting traction forces from deformations is not possible using classical mechanics approaches. An innovative solution around these difficulties was put forth by Legant et al. who performed 3D-TFM with polyethylene glycol (PEG) hydrogels, incorporating domains that allowed for both adhesion (fibronectin RGD binding domain) and degradation (matrix metalloproteinase susceptible linkers) by the embedded cells (58). It is important to note that 3D TFM is not quite physiologically relevant when studying lymphocytes, potentially more so for other immune cells such as macrophages.

Another noteworthy innovative TFM adaptation involves the use of deformable hydrogel microparticles for force quantification (35). Though this approach does not follow the classical definition of either 2.5D or 3D TFM, since neither the substrates are 2D, nor are the cells encapsulated, it does allow the quantification of tangential and normal forces applied to a

sphere of adjustable size, and can therefore be quite intriguing for the investigation of cell-cell interactions. For example, studying T cell-APC and cytotoxic T cell-infected cell interactions where membrane tension is essential for immune synapse stabilization (59) and perforin (a hydrophobic protein that forms pores in the target cell membrane) secretion (60).

Making the right material choices

Despite the many exciting developments in the broad field of TFM, the most commonly used system to measure cellular traction forces remains the one designed by Dembo and Wang in 1999: TFM on continuous and linearly elastic substrates embedded with fluorescent beads (37) (Figure 3). The most popular substrates used in this system are polyacrylamide gels (PAGs) and polydimethylsiloxane elastomers (PDMS, also called silicone). However, two unique features have given PAGs an edge over their counterparts. First, PAGs span an excellent range of elasticities (62). By simply varying the concentrations of acrylamide and N,N'-methylenebisacrylamide-the building blocks of PAGs- while retaining the same surface chemistry, the stiffness of the PAG can be adjusted to mimic that of most biological tissues (typically from 100 Pa to 100 kPa). Second, PAGs are generally non-fouling, meaning they are nearly inert as adhesive substrates. The same chemical stability and non-adherence that allows the usage of PAGs for the electrophoretic separation of nucleic acids and proteins, also guarantees that neither cell surface receptors nor adhesive proteins present in the serum can bind directly to the gel. Consequently, only molecules covalently grafted on the gel surface can act as ligands for the cells (29). In comparison, different formulations of PDMS are required for it to span a similar range [1 KPa- 1 MPa, 'Q-gel' is the more suitable choice for low elasticities and 'Sylgard' for the high ones; (63)]. Additionally, being extremely hydrophobic, PDMS requires supplementary passivation to prevent the non-specific adsorption of proteins onto its surface.

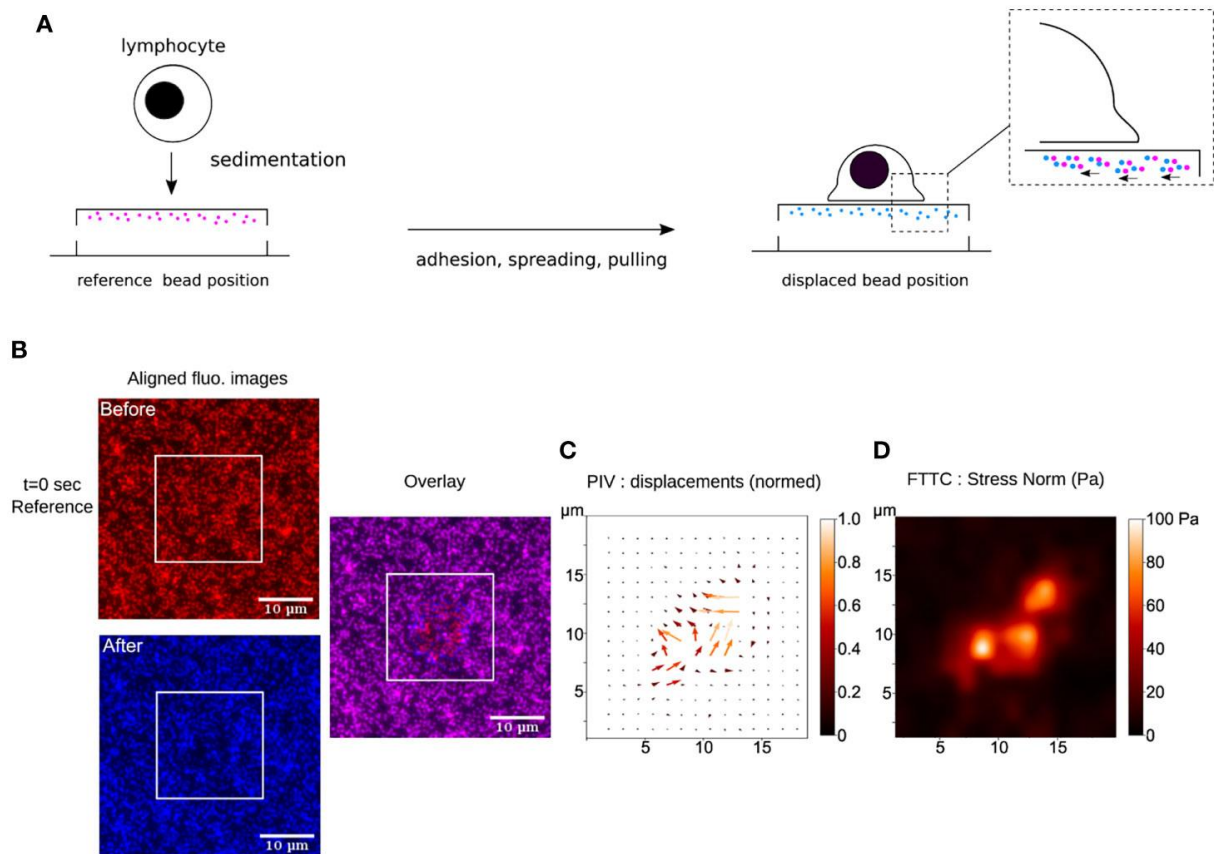


FIGURE 3 (A) Schematics of TFM for the study of early interactions of a primary human T lymphocyte with an ultra-soft APC-mimicking PAG doped with fluorescent nanobeads. (B) Raw fluorescence images, before and after the cell has landed, aligned to remove sample lateral drift. These ROIs are cut from original large field epifluorescence movies. The white squares indicate where a T lymphocyte has landed, as observed in bright-field transmission microscopy (not shown). The overlay shows the displacement of the beads due to cellular force. (C) Result of PIV calculation (over the zone delimited by the white square, where the cell sits) showing the constructed vector map of bead displacement field, taking $t=0$ sec frame (before the cell has landed) as the cell-/stress-free reference. The displacements have been normalized. (D) Result of FTTC calculation showing the gaussian smoothed map of stress norm. The data presented here has been processed using open-source softwares (Fiji/ImageJ (61), Python), following (29).

It is generally accepted that the experimental setup used for TFM has a great influence on the achievable result, both in accuracy and quality. Thus, regardless of the chosen material, a number of key considerations must be taken into account when designing a TFM substrate.

First, the thickness of the substrate needs to be sufficient. “Cells may not see or hear”, but they can certainly “feel” their surroundings and sense a collective stiffness. Just like the princess in Hans Anderson’s fairy tale who felt a small pea beneath a stack of soft mattresses, cells too can feel the stiffness of a rigid support buried beneath a soft layer, even if they’re not in direct contact with it. The soft layer, in this case the substrate, must be sufficiently thick such that the cells feel and respond to its softness rather than the rigidity of the underlying glass.

Second, the stiffness of the substrate must be tuned to fit the biological system under investigation. Different cell types exert forces over a wide range, and thus the chosen stiffness must be able to manifest the exerted forces as an appropriate deformation. On one hand, if the substrate is too stiff, the cells will not be capable of effectively deforming it, resulting in insufficient bead displacement, and rendering the calculation of force impossible. On the other hand, if the substrate is too soft, then the bead displacement may be too large, thus breaching the linear-response regime and making the linear-elastic theory inapplicable. A starting point for cells hitherto unexplored in terms of force measurements, is to consider the elasticity data reported for cells or tissues that the cells under consideration interact with. For example, when working on T cells, a stiffness such as the one reported for antigen presenting cells may be the appropriate starting choice (64).

Third, considerations of roughness and porosity are important. Given the cross-linked nature of PAA and PDMS, their stiffness is related to the mesh size of their molecular polymer network; the stiffer they are, the smaller the mesh size. Thus, an additional restriction would be that the substrate must be stiff enough to grant the formation of a sufficiently small mesh size capable of trapping the beads inside of it. It is important to note that mesh size may also influence the surface density of the functionalized proteins (65).

Fourth, the density of the fiducial markers needs to be optimal. Bead density in the substrate, of course in conjunction with the optical technique chosen for observation, directly determines the accuracy of force recovery (61). Thus, it must be carefully chosen in accordance with the spatial scale, the magnitude of the forces being measured, and the image analysis method to be used later. The density of the beads must be high enough to capture the spatial intricacies of the traction force field. If the bead density is too low, then in certain areas the deformation may go unreported and thus the traction information may be incomplete. Alternatively, if the bead density is too high, the image of the beads may overlap and nearby beads may not be resolved, thus concealing details of their relative displacement.

Quantifying displacements

The fundamental principle behind TFM has remained the same since its conception: when cells adhere or migrate over sufficiently compliant substrates, they exert traction forces that can deform said substrate. These deformations are spatially and temporally mapped by monitoring the changes in lateral position of sub-resolution fluorescent beads embedded just below the cell accessible, functionalized surface.

In order to measure cell traction forces, (at least) two images of the substrate have to be acquired: One image of the bead field while the substrate is subjected to cellular forces (i.e., the stressed state) and another image of the bead field in the absence of cellular forces (i.e., the relaxed state). The image of the beads in their relaxed state can either be obtained before cell engagement (28, 66) or after cell detachment using EDTA or cocktails of proteolytic enzymes such as Trypsin or Accutase (67). Provided that the substrate is linearly elastic, the beads should return back to their relaxed state once the cells, and therefore the exerted forces, have

been removed. The displacement caused by the cells can then be computed by comparing the bead positions in the stressed state to that in the relaxed state.

There are currently two main approaches to perform this comparison, either by localizing and tracking each individual bead, also known as single-particle tracking (SPT, (68, 69)), or by correlating displacements with regions of an image, also known as particle image velocimetry (PIV, (70)).

SPT identifies and tracks individual bead centroids by utilizing single particle localization algorithms. Basically, these algorithms scan all the pixels in the relaxed image to identify the pixel coordinates of the fluorescent beads (referred to as pixel intensity maxima). For each bead that is tracked, a box of pixels centered around the maximum intensity pixel is designated. The relative pixel intensities in that box serve as a “fingerprint” for the tracked bead, which is then used to find the coordinates of the corresponding “fingerprint” in the stressed image. This process is repeated for every bead in the image. Usually such procedures are able to track the bead displacements with submicron resolution (71).

Alternatively, one can forgo identifying and tracking individual bead centroids, and instead use PIV to calculate and project displacements on a grid, using image cross-correlation. To do that, both rest and stressed images have to be first partitioned into small interrogation windows. The pattern of an interrogation window in the first image is correlated with a region of equal size in the second image that is shifted pixel-wise in the vicinity of the location of the interrogation window of the first image. The result of this operation is a local correlation map of a specific bead pattern. The position of the maximum correlation value within this map is the most probable displacement of the bead pattern of this specific interrogation window.

Because PIV requires the image to be divided into smaller regions, some of the displacement occurring in the sub-regions might be lost. To minimize this loss, the selection of a “correct” PIV window is critical. If the window is too large, fine detail regarding the bead displacement will be lost, and the overall resolution of the force will be compromised. Alternatively, if the window is too small, such that it contains no distinguishable features (eg. a too small number of beads or even no beads to the extreme limit), the correlation between frames will be unreliable and prone to error due to the creation of non-existing displacement. Such a choice is influenced by the density of beads but also by the scale of the features one expects to record.

Both of these approaches have their own limitations, and they can also be combined (30, 69). SPT potentially yields higher accuracy but may introduce incorrect bead matches between the relaxed and stressed images which contaminate the true displacement data. PIV on the other hand is robust against mismatches as well as sample drift in the z direction, however, it is doubtful to obtain comparable lateral accuracy and resolution. Nevertheless, they have both been utilized in 2D TFM with minimal modifications. The question of which approach to use depends on the expected nature of the forces. For example, in the case of focal adhesion forming cells where forces are likely to result in a collective motion of a group of beads, it would probably be more appropriate and practical to use an approach that depends on image cross correlation instead of individual bead displacement.

Mapping forces

The final step in TFM is to convert displacements into a map of cellular traction stresses or forces. In other words, a relationship, derived from the physics of materials, is needed to describe the deformation of a material in response to a force applied onto its surface. Although this conversion fundamentally requires solving a stress-strain problem, several approaches have been developed to do so, the two main ones being the forward approach and the inverse approach.

The forward approach is more straightforward and computationally efficient. As the name suggests, the stress tensor is calculated directly from a three-dimensional displacement field, using the constitutive law of the material, and the surface traction is calculated from the 3D stress field (72). One major advantage for this method is that it can be easily applied to nonlinear, viscoelastic, or other material constitutive properties without having to modify the general mathematical framework. Nevertheless, there are two major trade-offs to using it. First, a 3D or quasi 3D displacement field is needed and second, noise effects may become very important. In traditional 2D TFM where fluorescent beads are embedded in the substrate, the stress field is not known immediately at the cell-substrate interface, it's rather measured at the layer of beads closest to the interface. Consequently, in order to calculate the forces experienced at the true substrate interface, some method of extrapolation must be implemented to estimate the stress field at the interphase from that at bead level. This estimation might introduce significant error if one can't ensure that a large enough number of beads is present quite near to the substrate surface.

One way to address this concern is to adopt the inverse approach. In this approach, the traction field becomes a convolution of the displacement field and Green's function. It's important to note that the utilization of Green's function imposes several key assumptions. First, forces are mainly exerted along the substrate surface rather than normal to it. Second, the substrate is estimated to be a 2D elastic plane extending laterally to infinity (a semi-infinite half space). Third, the strains are small and thus the substrate deforms under a linear elastic regime. Lastly, the substrate material remains homogeneous in both relaxed and stressed states. Even if all these assumptions are experimentally met, the inverse approach still suffers from two major limitations. First, upon inversion, the calculated forces become very sensitive to high frequency fluctuations (i.e., noise) in the displacement data. To solve this problem, a pre-smoothing, also known as regularization, must be implemented to obtain a reasonable solution (73)). The regularization coefficient must be carefully chosen so as to provide a balance between how well the solution fits the noise-distorted experimental displacement data and the overall magnitude of the traction forces. If the solution is over-regularized, the data will become over-smoothed and the resolution of the recovered forces will be lost. Alternatively, if the data is under-regularized, the solution will overfit the noise in the displacement and will thus be a false representative of the traction forces. Secondly, the computation needed to solve the inverse problem and implement the additional regularization steps is quite time-consuming and computationally expensive. The most common and general way to solve this problem is by using Fourier Transform Traction Cytometry (FTTC) whereby, essentially the

integrated displacements are transformed into Fourier Space and the calculations are performed using matrix multiplications.

Improved detection in 2D (and 3D)

The accuracy and resolution of TFM ultimately depend on the spatio-temporal resolution of the optical microscopy technique with which it is accompanied. The spatial resolution is a limit imposed by the resulting finite size of the point spread function (PSF) associated with each fluorescent bead. At high densities, the PSF of the beads begin to overlap, hindering the reliable tracking of their displacement. Similarly, the temporal resolution also influences the ability to reference and track individual beads over time. Not to mention that at low time resolutions, dynamic processes are concealed, whereas at higher time resolution, requiring more frequent imaging, phototoxicity as well as photobleaching become a concern. As such, experimentalists often find themselves forced into a trade-off between spatial and temporal resolution.

The first straightforward attempt to partially overcome these limitations came from Sabass et al. who proposed to incorporate fluorescent beads of two different colors to increase the allowed bead density while decreasing the noise and irregularities in bead tracking (69, 74). To further improve the spatial resolution of TFM from the micron to the submicron scale, Colin-York et al. combined super-resolution stimulated emission depletion (STED) microscopy with TFM (2D STED-TFM) (75). STED-TFM allowed a 5-fold improvement in the resolution of the tracked bead displacement field, yielding a much finer recovery of force compared to standard laser scanning confocal microscopy. This step forward however, came at the expense of increasing the image acquisition time to a few minutes for each field of view due to the STED scanning. Additionally, the high laser intensity required for fluorescence depletion diminished the biocompatibility of this approach. The same group later addressed these problems by developing live-cell super-resolution 3D SIM-TFM, a technique combining structured illumination microscopy (SIM) and TFM. Because SIM is a wide-field technique, it does not rely on image raster scanning, and thus, unlike STED, allowed faster acquisition times (11 ms per frame, 15 frames per super-resolution image in 3D mode), and at a significantly lower fluorescence excitation light, thus increasing the number of images that can be acquired at a given time frame while minimizing the effects of photobleaching (76, 77).

To overcome the need for the axial scanning required for the 3D imaging of the beads using 3D SIM-TFM, and further increase the speed of acquisition, they later combined TFM with 2.5D astigmatic imaging (aTFM) and SIM in total internal reflection fluorescence microscopy mode (TIRF-SIM) (56). Astigmatic imaging allowed the 3D information in the $\sim 1 \mu\text{m}$ zone surrounding the focal plane to be inferred from a single wide-field image, rather than having to perform multi-frame z-stack acquisitions, thus increasing image acquisition to up to 90 ms per SIM image frame, while the use of TIRF reduced the contribution of out-of-plane fluorescence and enhanced the overall quality (contrast) of the images. In their most recent work, they extended TIRF-SIM to 2D (2D TIRF-SIM-TFM), demonstrating a >2 fold

increase in spatial resolution and >10 fold increase in temporal resolution in comparison to traditional TFM (78).

There are two main limitations that appear when using 3D SIM-TFM and TIRF-SIM-TFM (2.5D and 2D). Firstly, they necessitate the use of high numerical aperture objectives with narrow working distances which consequently diminishes the imaging depth and limits the thickness of the substrate that can be used. This is particularly problematic in TFM since, as mentioned previously, the substrate must be sufficiently thick to eliminate any mechanical influence coming from the underlying glass. Secondly, imaging the substrate-cell interface requires that the substrate has a refractive index similar to that of glass, such as PDMS (variety Qgel for example, (63)), which in itself comes with its own set of constraints, primarily the limited elasticity range that can be achieved. PAGs, having a refractive index similar to that of water, are therefore not directly amenable to such refined techniques.

It is also noteworthy that the availability of such advanced microscopy systems is likely limited by prohibitively high costs, either on the material side or on the development time needed to set them up, which often limits experimentalists to more classical fluorescence (epi or confocal) and phase-contrast microscopy. Normally, this would rule out the possibility of recovering 3D traction forces since traditional 2D imaging systems suffer from a relatively high degree of out-of-focus light-scattering. However, Hazlett et al. found an interesting strategy to get around that difficulty (54). They embedded a single dense layer of fluorescent beads on the PAG surface, and then obtained volumetric images of the beads by deconvolving the experimental epifluorescence images acquired using the PSF collected from a single bead in the images. Using SPT, they managed to quantify 3D volumetric bead displacements, and consequently, 3D stress fields.

Insights into T cell biology from TFM data

In this section, we present a few prominent examples of recent insights gained into the workings of T cells thanks to TFM studies.

One of the earliest experiments implementing TFM for T cell studies examined the complementary roles of CD3 (parts of the TCR complex, responsible for signal transmission across the membrane) and CD28 (a costimulatory molecule participating T cell activation) in mechanosensing during primary human CD4+ T cell activation. Using PDMS pillar arrays presenting activating antibodies against CD3/or pMHCs and/or CD28, Bashour et al. confirmed that antigen recognition does in fact involve force exertion. They recorded traction forces of around 100 pN, exerted specifically through the TCR-CD3 complex, and which could be augmented with co-stimulation through the engagement of PI3K signaling pathways (27).

To examine the interplay between activation and adhesion, Tabdanov et al. also employed PDMS pillar arrays, but functionalized with activating anti-CD3 antibody +/- ICAM-1 instead (79). Their experiments showed that the incorporation of ICAM-1 significantly increased the cellular contractile stresses exerted by Jurkat T cells, in comparison to those recorded when only the TCR/CD3 complex was engaged. Combined with their experiments

on micropatterned surfaces, their work highlighted a mechanical cooperation between the TCR/CD3 and LFA-1-ICAM-1 systems, whereby actin nucleation (governed by Arp2/3) downstream of TCR signaling sustained the growth of the LFA-1 dependent actin network, which in turn then provided the cytoskeletal tension to allow mechanical sensing, T-cell spreading and enhanced TCR activation.

Focusing further on the influence of the T cell cytoskeleton, Hui et al. used enhanced green fluorescent protein (eGFP)–actin expressing Jurkat T cells and poly-L-lysine-anti-CD3-coated polyacrylamide gels, to demonstrate the contribution of actin polymerization and myosin contractility in force generation and maintenance during T cell activation (28). With this system, they recorded peak stresses reaching 20–30 Pa and a total force of a few nanonewtons and showed that the EGFP-actin Jurkat T cells exerted larger forces on polyacrylamide gels of increased stiffness. This came in contrast to Bashour et al.'s work (27), where no change in traction force per pillar as a function of pillar stiffness was observed. Building on these results, the same group later utilized the same system to showcase the role of dynamic microtubules in regulating force generation at the T cell-substrate interface, through suppressing Rho contractility and actin flow (80).

Another study highlighting the role of actin in T cell force generation, was that of Savinko et al. (81) employing silicone-based gel substrates coated solely with ICAM-1. In these experiments, knocking out the actin-binding protein filamin A dropped the traction stresses exerted by mouse CD4+ effector T cells by approximately 50% (from ≈ 50 Pa to ≈ 25 Pa).

Linking cytoskeletal forces and effector function, Tamazalit et al. used PDMS pillar arrays presenting cognate p-MHC-I to show that CD8+ T lymphocytes employ F-actin rich protrusions, generated by Wiskott-Aldrich Syndrome protein (WASP) and the Arp2/3 actin nucleation complex, for synaptic force exertion and cytotoxic function (perforin and granzyme release; granzymes are proteases that induce cell apoptosis) - A process they termed as “mechano-potential” (82).

In an innovative approach, Vorselen et al. studied the interaction of eGFP-actin expressing cytotoxic T lymphocytes (CTLs) with activating (quantified as Ca^{2+} influx) soft (~ 300 Pa) deformable polyacrylamide microparticles (DAAM-particles, ≈ 15 μm in diameter) functionalized with cognate pMHCs and ICAM-1. Interestingly, using this technique, the shear stresses (~ 100 Pa) detected in the contact area (8 μm in diameter) between the CTLs and the microparticles were directed outwards, and as time progressed, localized indentations i.e., normal traction forces (up to 200 Pa, 0.5 nN total force) started forming within that area (35).

Similarly, Aramesh et al. also adopted an unconventional strategy to study both tangential and normal forces generated by T cells. Instead of using microparticles-doped gels however, they performed a functionalized bead assay whereby anti-CD3 and/or anti-CD28-functionalized 200 nm neutravidin-conjugated beads were bound onto the surface of biotinylated poly(ethylene glycol)diacrylate (PEGDA) gels or PDMS-based QGel, and Jurkat T cells were left to interact with them (55). In accordance with Bashour et al.'s observations

(27), their experiments also showed that co-stimulation by CD28 does in fact enhance T cell forces, reaching up to 10 nN forces, and not surprisingly, the increased force generated correlated with increased Ca^{2+} influx, i.e., increased activation. However, what was truly intriguing about their data was that single T cell microvilli were targeting single beads, and within that T cell-microvilli contact, actin was forming a vortex-like ring structure where the TCR was enriched and CD45 was excluded. This comes in line with previous reports suggesting that the size-mediated exclusion of CD45 from the IS shifts the ITAM phosphorylation–dephosphorylation balance, thereby triggering TCR signaling (83).

Though this section has focused on the existing literature regarding T lymphocytes studies using TFM, several other immune cell types have been investigated using the same methodologies, often though to a lesser extent. These include neutrophils (31), B cells (30, 66), dendritic cells (84) and macrophages (36).

Molecular sensors for force measurements

All the techniques mentioned thus far represent macroscopically large strain gauges that measure force maps generated by the cell, at the (sub)cellular scale. The same principle can be implemented at the nanoscale to measure the force borne by a specific molecule, through the interaction of a single receptor and ligand: provided that mechanical properties can be evaluated at the molecular scale, deformations of individual molecules, such as the extension of protein domains or DNA molecules, can be converted into forces. To this end, a great deal of effort has been dedicated over the last decade into the development of molecular force sensors (32, 85–87). These may not formally qualify as TFM but are included here because of their immense importance and potential.

The principal components of these sensors are deformable molecules that are sensitive to molecular tension, and that are labeled with a dye, a dye–quencher pair, or a dye–dye pair. Once force is applied onto the construct, its configuration will change, and consequently the fluorescent activity of the sensor will change as well. Thus, the experienced molecular force will eventually be reported as surface fluorescence loss, fluorescence gain, or Förster resonance energy transfer (FRET) efficiency change (88). Note that, similar to the substrates used in classical TFM, the responsivity range of the deformable molecule should match the range of the molecular force transmitted by the molecule under investigation.

While most common molecular force sensors are coated onto surfaces and are thus used to report the forces applied by cells onto said surfaces, another type can be used to measure forces inside cells. Typically, these constitute mechanosensitive proteins that have been engineered with fluorophore pairs and expressed in living cells; As they experience force, the separation distance between the fluorophores, and consequently the FRET efficiency, is altered, allowing for the real time measurement of intracellular forces across single molecules (89, 90).

Although such sensors provide an immediate readout of molecular forces, for several reasons, interpreting the obtained signals might not be as straightforward. First the effective

spring constant of the elastic linker might depend on the local environment in the cell, even if previously calibrated by single-molecule force spectroscopy experiments (by Atomic Force Microscopy, Optical or magnetic Tweezers (91). Second, the fluorescent signal is a sensitive function of domain separation and relative orientation, thus, a direct conversion into force can be problematic (92, 93). Third, it is difficult to control the number of engaged sensors, consequently, the fluorescent signal cannot easily be integrated over a larger region. Not to mention that using such a technique allows the recovery of only the norm of the force exerted and not the exact direction of said force. Therefore, advanced molecular force sensors can be expected to complement, but not fully replace, traditional TFM in the future.

Conclusion and perspectives

The last two decades have witnessed an upsurge in the development of a wide variety of techniques for probing cell generated forces. Though they have not been discussed in this review, they have been described in great detail elsewhere (See for example, for immune cells, (2, 8)). Despite their growing availability, such advanced biophysical techniques still require specialized skills and often expensive tools that are still far from becoming routine laboratory equipment in biology labs, unlike conventional molecular biology tools for examining gene expression and protein concentration. Perhaps the simplest of these techniques, and the one that is rapidly leading its way towards standardization, is TFM. Most likely, TFM has gained such wide adoption by the mechanobiology community because of its ease of implementation and longstanding history.

However, if we disregard for a brief moment its attractive simplicity, we will see that TFM suffers from very serious caveats. Primarily, the computational analysis required for tracking displacements and recovering force maps is quite complex, nuanced and difficult to validate. Even marginal errors in retrieving bead displacement will introduce large errors into the final stress and force fields. Moreover, as explained above, extracting force fields from displacement fields is a mathematically ill-posed problem that will introduce noise into the final measurements, and will thus necessitate regularization. Since there is not a “standard” regularization factor, which is quite logical since this value will depend on several experimental and numerical parameters, which are not uniform (e.g., bead size, bead density, substrate stiffness, cellular forces, and imaging parameters, methodology for calculating the beads displacements ...), one could end up with either over-smoothed, or alternatively, under-regularized data, which does not faithfully represent the exerted cellular traction forces. Given such variable experimental and analysis protocols, comparing experimental values obtained in different laboratories becomes very difficult, especially, as is the case for any quantification of living systems, since biological diversity, such as cell culture conditions and cell passage number, may also impact the scatter in measured values.

Potentially, the only way to overcome these challenges is by utilizing reproducible and accessible standardized protocols, as well as implementing open source softwares for data analysis. Several startup companies that sell prefabricated substrates exist today, which is a partial step towards standardization - though in our experience their rigidities need to be verified by the end user. Python, ImageJ/Fiji, and even Matlab scripts are now available online

for calculating stresses, force maps and energies from bead images (see for example <https://sites.google.com/site/qingzongtseng/tfm>, <https://github.com/topics/traction-force-microscopy>, https://github.com/MBPPlab/TFM_v1). Though this does not completely solve the problem, it is a step in the right direction towards standardization.

To further complexify the picture, the generation of mechanical forces by biological systems are space and time scales dependent, from cells, down to single molecules and up to entire organisms, lasting less than a few seconds up to hours and even over their whole lifetime. For example, looking at T cell activation, certain processes such as actin turn-over occur at the order of seconds, while others may take several minutes, such as the building of the IS, or more. Another important point is that, in-vivo, cells are interacting with different substrates/other cells and are constantly integrating the myriad of biochemical and physical signals rising from their microenvironment. Trying to recapitulate such intricate physiological conditions is extremely challenging, and so it remains difficult to understand how forces measured in-vitro, on mechanically simplified substrates, relate to those existing in living tissues or organs. A prominent example in T cell studies is that every interaction of a T cell with APCs will be made under different mechanical conditions as pointed out by Bufi et al. (64) leading to adaptation in experimental parameters, such as the substrate rigidity in TFM to accommodate for a precise encounter to be studied.

Therefore, before opting for one technique or the other, an investigator needs to make several critical decisions: (1) in-vivo or in-vitro (2) 2D, 2.5D or 3D, (3) spatial resolution-nanoscale or microscale- and/or temporal resolution-sub second, second, or minutes, (4) molecular scale forces or cellular scale forces. Another key point is deciding whether one time point quantification, and thus one force value, will suffice, or whether the process is dynamic and will require time-lapse measurements. We have specifically highlighted this point in our recent work using TFM on ultra-soft PAGs which showed that T cells exhibit distinct dynamic stress and energy patterns (29).

With the pace at which the field of mechanobiology is growing, it is not unreasonable to imagine that the next-generation tools for quantifying cellular forces will exhibit an extended range of measurable forces, an improved spatio-temporal resolution, and will re-create a more complex cellular microenvironment that will allow cells to experience a dynamically changing set of biochemical and physical conditions, more representative of that occurring in in-vivo settings. Though this may sound quite alluring, one has to keep in mind that the more complex our questions and experiments become, the more difficult it will be to extract meaningful correlations and determine clear cause-effects relations. There will always be a series of more or less arbitrary trade-offs.

Perhaps the most exciting and currently achievable experimental approach in the world of TFM revolves around combining simultaneous measurement techniques. This could be through merging fluorescent molecular force sensors with classical 2D TFM, to have a better understanding of how forces propagate between the molecular and cellular scales. It could also be through the simultaneous quantification of cellular/molecular forces with signaling cascades, eg. using live phosphorylation (94) or calcium reporters (95, 96), to yield

a more complete picture of how force generation and biochemical events are integrated across different scales. Ultimately, studying the mechanobiology of cells in general, but of immune cells and T cells in particular, will be the route to enhancing our understanding of the role of mechanobiology in health and disease (2, 4), and hopefully we will one day be able to translate this wealth of knowledge into next-generation diagnoses and treatments.

Author contributions

All authors listed have made a substantial, direct, and intellectual contribution to the work and approved it for publication.

Acknowledgments

The project leading to this publication has received some funding from France 2030, the French Government program managed by the French National Research Agency (ANR-16-CONV-0001) and from Excellence Initiative of Aix-Marseille University - A*MIDEX. Part of this work was also supported by institutional grants from Inserm, CNRS and Aix-Marseille University to the LAI and from CNRS and Aix-Marseille University to the CINAM.

FM was supported as a PhD grant by the European Union's Horizon 2020 research and innovation programme under the Marie Skłodowska-Curie grant agreement No713750, with the financial support of the Regional Council of Provence- Alpes-Côte d'Azur and with of the A*MIDEX (n° ANR- 11-IDEX-0001-02), funded by the Investissements d'Avenir project funded by the French Government, managed by the French National Research Agency (ANR).

Conflict of interest

The authors declare that the research was conducted in the absence of any commercial or financial relationships that could be construed as a potential conflict of interest.

Publisher's note

All claims expressed in this article are solely those of the authors and do not necessarily represent those of their affiliated organizations, or those of the publisher, the editors and the reviewers. Any product that may be evaluated in this article, or claim that may be made by its manufacturer, is not guaranteed or endorsed by the publisher.

References

1. Hannezo E, Heisenberg C-P. Mechanochemical feedback loops in development and disease. *Cell* (2019) 178(1):12–255. doi: 10.1016/j.cell.2019.05.052
2. Huse M. Mechanical forces in the immune system. *Nat Rev Immunol* (2017) 17(11):679–90. doi: 10.1038/nri.2017.74
3. Basu R, Huse M. Mechanical communication at the immunological synapse. *Trends Cell Biol* (2017) 27(4):241–545. doi: 10.1016/j.tcb.2016.10.005
4. Puech P-H, Bongrand P. Mechanotransduction as a major driver of cell behaviour: Mechanisms, and relevance to cell organization and future research. *Open Biol* (2021) 11(11):2102565. doi: 10.1098/rsob.210256
5. Comrie WA, Burkhardt JK. Action and traction: Cytoskeletal control of receptor triggering at the immunological synapse. *Front Immunol* (2016) 7:68. doi: 10.3389/fimmu.2016.00068
6. Blumenthal D, Burkhardt JK. Multiple actin networks coordinate mechanotransduction at the immunological synapse. *J Cell Biol* (2020) 219(2): e201911058. doi: 10.1083/jcb.201911058
7. Chabaud Mélanie, Paillon Noémie, Gaus K, Hivroz C. Mechanobiology of antigen-induced T cell arrest. *Biol Cell* (2020) 112(7):196–2125. doi: 10.1111/ boc.201900093
8. Liu B, Kolawole EM, Evavold BD. Mechanobiology of T cell activation: To catch a bond. *Annu Rev Cell Dev Biol* (2021) 37(1):65–875. doi: 10.1146/annurevcellbio-120219-055100
9. Limozin L, Puech P-H. Membrane organization and physical regulation of lymphocyte antigen receptors: A biophysicist's perspective. *J Membrane Biol* (2019) 252(4–5):397–412. doi: 10.1007/s00232-019-00085-2
10. Limozin L, Bridge M, Bongrand P, Dushek O, Merwe PAvd, Robert P. TCRPMHC kinetics under force in a cell-free system show no intrinsic catch bond, but a minimal encounter duration before binding. *Proc Natl Acad Sci United States America* (2019) 116(34):16943–485. doi: 10.1073/pnas.1902141116
11. Vitte J, Pierres A, Benoliel A-M, Bongrand P. Direct quantification of the modulation of interaction between cell- or surface-bound LFA-1 and ICAM-1. *J Leukoc Biol* (2004) 76(3):594–6025. doi: 10.1189/jlb.0204077
12. Vitte J, Benoliel A-M, Eymeric P, Bongrand P, Pierres A. Beta-1 integrinmediated adhesion may be initiated by multiple incomplete bonds, thus accounting for the functional importance of receptor clustering. *Biophys J* (2004) 86(6):4059– 745. doi: 10.1529/biophysj.103.038778
13. Husson J, Chemin K, Bohineust A, Hivroz C, Henry N. Force generation upon T cell receptor engagement'. edited by javed n. agrewala. *PloS One* (2011) 6 (5):e196805. doi: 10.1371/journal.pone.0019680
14. Sawicka A, Babataheri A, Dogniaux Stéphanie, Barakat AI, GonzalezRodriguez D, Hivroz C, et al. Micropipette force probe to quantify single-cell force generation: Application to T-cell activation. *Mol Biol Cell* (2017) 28 (23):3229–395. doi: 10.1091/mbc.E17-06-0385
15. Sung K-LP, Sung LA, Crimmins M, Burakoff SJ, Chien S. Determination of junction avidity of cytolytic T cell and target cell. *Sci New Ser* (1986) 234 (4782):1405–8. doi: 10.1126/science.3491426
16. Chen W, Zarnitsyna VI, Sarangapani KK, Huang J, Zhu C. Measuring receptor–ligand binding kinetics on cell surfaces: From adhesion frequency to thermal fluctuation methods. *Cell Mol Bioengineering* (2008) 1(4):276–885. doi: 10.1007/s12195-008-0024-8

17. Chen W, Evans EA, McEver RP, Zhu C. Monitoring receptor-ligand interactions between surfaces by thermal fluctuations. *Biophys J* (2008) 94 (2):694–7015. doi: 10.1529/biophysj.107.117895
18. Evans E, Kinoshita K. Using force to probe single-molecule receptor cytoskeletal anchoring beneath the surface of a living cell. *Methods Cell Biol* (2007) 83(07):373–965. doi: 10.1016/S0091-679X(07)83016-0
19. Kinoshita K, Leung A, Simon S, Evans E. Long-lived, high-strength states of ICAM-1 bonds to B2 integrin, II: Lifetimes of LFA-1 bonds under force in leukocyte signaling. *Biophys J* (2010) 98(8):1467–755. doi: 10.1016/j.bpj.2009.12.4316
20. Liu B, Chen W, Evavold BD, Zhu C. Accumulation of dynamic catch bonds between TCR and agonist peptide-MHC triggers T cell signaling. *Cell* (2014) 157 (2):357–685. doi: 10.1016/j.cell.2014.02.053
21. Marshall BT, Long M, Piper JW, Yago T, McEver RP, Zhu C. Direct observation of catch bonds involving cell-adhesion molecules. *Nature* (2003) 423 (6936):190–93. doi: 10.1038/nature01605
22. Puech P-H, Nevoltris D, Robert P, Limozin L, Boyer C, Bongrand P. Force measurements of TCR/PMHC recognition at T cell surface. *PloS One* (2011) 6(7): e223445. doi: 10.1371/journal.pone.0022344
23. Rico Félix, Chu C, Abdulreda MH, Qin Y, Moy VT. Temperature modulation of integrin-mediated cell adhesion. *Biophys J* (2010) 99(5):1387–965. doi: 10.1016/j.bpj.2010.06.037
24. Hu KH, Butte MJ. T cell activation requires force generation. *J Cell Biol* (2016) 213(5):535–425. doi: 10.1083/jcb.201511053
25. Lim TS, Mortellaro A, Lim CT, Hämmerling GünterJ, Ricciardi-Castagnoli P. Mechanical interactions between dendritic cells and T cells correlate with T cell responsiveness. *J Immunol* (Baltimore Md.: 1950) (2011) 187(1):258–655. doi: 10.4049/jimmunol.1100267
26. Zak A, Merino-Cortés SV, Sadoun Anaïs, Mustapha F, Babataheri A, Dogniaux Stéphanie, et al. Rapid viscoelastic changes are a hallmark of early leukocyte activation. *Biophys J* (2021) 120(9):1692–704. doi: 10.1016/j.bpj.2021.02.042
27. Bashour KT, Gondarenko A, Chen H, Shen K, Liu X, Huse M, et al. CD28 and CD3 have complementary roles in T-cell traction forces. *Proc Natl Acad Sci* (2014) 111(6):2241–465. doi: 10.1073/pnas.1315606111
28. Hui KL, Balagopalan L, Samelson LE, Upadhyaya A. Cytoskeletal forces during signaling activation in jurkat T-cells. *Mol Biol Cell* (2015) 26(4):685–955. doi: 10.1091/mbc.E14-03-0830
29. Mustapha F, Sengupta K, Puech P-H. Protocol for measuring weak cellular traction forces using well-controlled ultra-soft polyacrylamide gels. *STAR Protoc* (2022) 3(1):1011335. doi: 10.1016/j.xpro.2022.101133
30. Kumari A, Pineau J, Sáez PJ, Maurin M, Lankar D, Roman MS, et al. Actomyosin-driven force patterning controls endocytosis at the immune synapse. *Nat Commun* (2019) 10(1):2870. doi: 10.1038/s41467-019-10751-7
31. Henry SJ, Chen CS, Crocker JC, Hammer DA. Protrusive and contractile forces of spreading human neutrophils. *Biophys J* (2015) 109(4):699–7095. doi: 10.1016/j.bpj.2015.05.041
32. Blanchard AT, Salaita K. Emerging uses of DNA mechanical devices. *Science* (2019) 365(6458):1080–81. doi: 10.1126/science.aax3343

33. Hong J, Ge C, Jothikumar P, Yuan Z, Liu B, Bai Ke, et al. A TCR mechanotransduction signaling loop induces negative selection in the thymus. *Nat Immunol* (2018) 19(12):1379–90. doi: 10.1038/s41590-018-0259-z
34. Spillane KM, Tolar P. DNA-based probes for measuring mechanical forces in cell-cell contacts: Application to b cell antigen extraction from immune synapses. *Methods Mol Biol* (2018) 1707:69–80. doi: 10.1007/978-1-4939-7474-0_5
35. Vorselen D, Wang Y, de Jesus MM, Shah PK, Footer MJ, Huse M, et al. Microparticle traction force microscopy reveals subcellular force exertion patterns in immune cell–target interactions. *Nat Commun* (2020) 11(1). doi: 10.1038/s41467-019-13804-z
36. Vorselen D, Barger SR, Wang Y, Cai W, Theriot JA, Gauthier NC, et al. Phagocytic “Teeth” and myosin-II “Jaw” power target constriction during phagocytosis. *ELife* (2021) 10:e68627. doi: 10.7554/eLife.68627
37. Dembo M, Wang YL. Stresses at the cell-to-Substrate interface during locomotion of fibroblasts. *Biophys J* (1999) 76(4):2307–16. doi: 10.1016/S0006-3495(99)77386-8
38. Harris AK, Wild P, Stopak D. Silicone rubber substrata: A new wrinkle in the study of cell locomotion. *Sci (New York N.Y.)* (1980) 208(4440):177–79. doi: 10.1126/science.6987736
39. Style RW, Boltyanskiy R, German GK, Hyland C, MacMinn CW, Mertz AF, et al. Traction force microscopy in physics and biology. *Soft Matter* (2014) 10 (23):4047–555. doi: 10.1039/C4SM00264D
40. Ferrari A. Recent technological advancements in traction force microscopy. *Biophys Rev* (2019) 11(5):679–81. doi: 10.1007/s12551-019-00589-0
41. Tan JL, Tien J, Pirone DM, Gray DS, Bhadriraju K, Chen CS. Cells lying on a bed of microneedles: An approach to isolate mechanical force. *Proc Natl Acad Sci* (2003) 100(4):1484–89. doi: 10.1073/pnas.0235407100
42. Hur SS, Jeong JiH, Ban MJ, Park JH, Yoon JK, Hwang Y. Traction force microscopy for understanding cellular mechanotransduction. *BMB Rep* (2020) 53 (2):74–815. doi: 10.5483/BMBRep.2020.53.2.308
43. Schoen I, Hu W, Klotzsch E, Vogel V. Probing cellular traction forces by micropillar arrays: Contribution of substrate warping to pillar deflection. *Nano Lett* (2010) 10(5):1823–305. doi: 10.1021/nl100533c
44. Schwarz US, Soine JérômeRD. Traction force microscopy on soft elastic substrates: A guide to recent computational advances. *Biochim Biophys Acta – Mol Cell Res* (2015) 1853(11):3095–104. doi: 10.1016/j.bbamcr.2015.05.028
45. Polio SR, Rothenberg KE, Stamenović D, Smith ML. A micropatterning and image processing approach to simplify measurement of cellular traction forces. *Acta Biomaterialia* (2012) 8(1):82–885. doi: 10.1016/j.actbio.2011.08.013
46. Canović EP, Seidl DT, Polio SR, Oberai AA, Barbone PE, Stamenović D, et al. Biomechanical imaging of cell stiffness and prestress with subcellular resolution. *Biomechanics Modeling Mechanobiol* (2014) 13(3):665–785. doi: 10.1007/s10237-013-0526-8
47. Balaban NQ, Schwarz US, Riveline D, Goichberg P, Tzur G, Sabanay I, et al. Force and focal adhesion assembly: A close relationship studied using elastic micropatterned substrates. *Nat Cell Biol* (2001) 3(5):466–72. doi: 10.1038/35074532
48. Merkel R, Kirchgeßner N, Cesa CM, Hoffmann B. Cell force microscopy on elastic layers of finite thickness. *Biophys J* (2007) 93(9):3314–235. doi: 10.1529/biophysj.107.111328

49. Bergert M, Lendenmann T, Zündel M, Ehret AE, Panozzo D, Richner P, et al. Confocal reference free traction force microscopy. *Nat Commun* (2016) 7 (1):12814. doi: 10.1038/ncomms12814
50. Vogel V, Sheetz M. Local force and geometry sensing regulate cell functions. *Nat Rev Mol Cell Biol* (2006) 7(4):265–755. doi: 10.1038/nrm1890
51. Delanoë-Ayari H, Rieu JP, Sano M. 4D traction force microscopy reveals asymmetric cortical forces in migrating Dictyostelium cells. *Phys Rev Lett* (2010) 105(24):248103. doi: 10.1103/PhysRevLett.105.248103
52. Bastounis E, Meili R, Álvarez-González Begoña, Francois J, del Álamo JC, Firtel RA, et al. Both contractile axial and lateral traction force dynamics drive amoeboid cell motility. *J Cell Biol* (2014) 204(6):1045–615. doi: 10.1083/jcb.201307106
53. Burnette DT, Shao L, Ott C, Pasapera AM, Fischer RS, Baird MA, et al. A contractile and counterbalancing adhesion system controls the 3D shape of crawling cells. *J Cell Biol* (2014) 205(1):83–96. doi: 10.1083/jcb.201311104
54. Hazlett L, Landauer AK, Patel M, Witt HA, Yang J, Reichner JS, et al. Epifluorescence-based three-dimensional traction force microscopy. *Sci Rep* (2020) 10(1):165995. doi: 10.1038/s41598-020-72931-6
55. Aramesh M, Mergenthal S, Issler M, Plochberger B, Weber F, Qin X-H, et al. Functionalized bead assay to measure three-dimensional traction forces during Tcell activation. *Nano Lett* (2021) 21(1):507–14. doi: 10.1021/acs.nanolett.0c03964
56. Li Di, Colin-York H, Barbieri L, Javanmardi Y, Guo Y, Korobchevskaya K, et al. Astigmatic traction force microscopy (ATFM). *Nat Commun* (2021) 12 (1):21685. doi: 10.1038/s41467-021-22376-w
57. Song D, Dong Li, Gupta M, Li L, Klaas O, Loghin A, et al. Recovery of tractions exerted by single cells in three-dimensional nonlinear matrices. *J Biomechanical Eng* (2020) 142(8):0810125. doi: 10.1115/1.4046974
58. Legant WR, Choi CK, Miller JS, Shao L, Gao L, Betzig E, et al. Multidimensional traction force microscopy reveals out-of-Plane rotational moments about focal adhesions. *Proc Natl Acad Sci USA* (2013) 110(3):881–65. doi: 10.1073/pnas.1207997110
59. Kumari S, Mak M, Poh Y-C, Tohme M, Watson N, Melo M, et al. Cytoskeletal tension actively sustains the migratory T-cell synaptic contact. *EMBO J* (2020) 39(5):e102783. doi: 10.15252/embj.2019102783
60. Basu R, Whitlock BM, Husson J, Lieberman J, Kam LC, Huse M, et al. Cytotoxic T cells use mechanical force to potentiate target cell killing cytotoxic T cells use mechanical force to potentiate target cell killing. *Cell* (2016) 165(1):100–10. doi: 10.1016/j.cell.2016.01.021
61. Martiel J-L, Leal A, Kurzawa L, Balland M, Wang I, Vignaud Timothée, et al. Measurement of cell traction forces with ImageJ. *Methods Cell Biol* (2015) 125:269–87. doi: 10.1016/bs.mcb.2014.10.008
62. Tse JR, Engler AJ. Preparation of hydrogel substrates with tunable mechanical properties. *Curr Protoc Cell Biol* (2010) 47(1):105.16.1–10.16.16. doi: 10.1002/0471143030.cb1016s47
63. Wahl A, Dinet Céline, Dillard P, Nassereddine A, Puech P-H, Limozin L, et al. Biphasic mechanosensitivity of T cell receptor-mediated spreading of lymphocytes. *Proc Natl Acad Sci* (2019) 116(13):5908–135. doi: 10.1073/pnas.1811516116
64. Bufi N, Saitakis M, Dogniaux Stéphanie, Buschinger O, Bohineust A, Richert A, et al. Human primary immune cells exhibit distinct mechanical properties that are modified by

- inflammation. *Biophys J* (2015) 108(9):2181–905. doi: 10.1016/j.bpj.2015.03.047
65. Wen JH, Vincent LG, Fuhrmann A, Choi YuS, Hribar KC, Taylor-Weiner H, et al. Interplay of matrix stiffness and protein tethering in stem cell differentiation. *Nat Mater* (2014) 13(10):979–875. doi: 10.1038/nmat4051
66. Kumari A, Pineau J, Lennon-Duménil A-M, Balland M, Pierobon P. Traction force microscopy to study b lymphocyte activation. *JoVE (Journal Visualized Experiments)* (2020) 161:e60947. doi: 10.3791/60947
67. Charrier EE, Asnacios A, Milloud R, Mets RDe, Balland M, Delort F, et al. Desmin mutation in the c-terminal domain impairs traction force generation in myoblasts. *Biophys J* (2016) 110(2):470–805. doi: 10.1016/j.bpj.2015.11.3518
68. Sergé A, Bertaux N, Rigneault Hervé, Marguet D. Dynamic multiple-target tracing to probe spatiotemporal cartography of cell membranes. *Nat Methods* (2008) 5(8):687–945. doi: 10.1038/nmeth.1233
69. Sabass B, Gardel ML, Waterman CM, Schwarz US. High resolution traction force microscopy based on experimental and computational advances. *Biophys J* (2008) 94(1):207–5. doi: 10.1529/biophysj.107.113670
70. Fu S, Biwolé P-H, Mathis C. A comparative study of particle image velocimetry (PIV) and particle tracking velocimetry (PTV) for airflow measurement. *ICFDT 2015 : 17th International Conference on Fluid Dynamics and Thermodynamics* (2015) 9(1):6.
71. Kraning-Rush CM, Carey SP, Califano JP, Reinhart-King CA. Quantifying traction stresses in adherent cells. *Methods Cell Biol* (2012) 110:139–78. doi: 10.1016/B978-0-12-388403-9.00006-0
72. Blumberg JW, Schwarz US. Comparison of direct and inverse methods for 2.5D traction force microscopy. *PloS One* (2022) 17(1):e02627735. doi: 10.1371/journal.pone.0262773
73. Mulligan JA, Bordeleau François, Reinhart-King CA, . Adie SG. Traction force microscopy for noninvasive imaging of cell forces. *Adv Exp Med Biol* (2018) 1092:319–49. doi: 10.1007/978-3-319-95294-9_15
74. Plotnikov SV, Sabass B, Schwarz US, Waterman CM. High-resolution traction force microscopy. *Methods Cell Biol* (2014) 123:367–94. doi: 10.1016/B978-0-12-420138-5.00020-3
75. Colin-York H, Eggeling C, Fritzsche M. Dissection of mechanical force in living cells by super-resolved traction force microscopy. *Nat Protoc* (2017) 12 (4):783–965. doi: 10.1038/nprot.2017.009
76. Colin-York H, Javanmardi Y, Skamrahl M, Kumari S, Chang VT, Khuon S, et al. Cytoskeletal control of antigen-dependent T cell activation. *Cell Rep* (2019) 26 (12):3369–3379.e5. doi: 10.1016/j.celrep.2019.02.074
77. Colin-York H, Javanmardi Y, Barbieri L, Li Di, Korobchevskaya K, Guo Y, et al. Spatiotemporally super-resolved volumetric traction force microscopy. *Nano Lett* (2019) 19(7):4427–34. doi: 10.1021/acs.nanolett.9b01196
78. Barbieri L, Colin-York H, Korobchevskaya K, Li Di, Wolfson DL , Karedla N, et al. Two-dimensional TIRF-SIM–traction force microscopy (2D TIRF-SIMTFM). *Nat Commun* (2021) 12(1):2169. doi: 10.1038/s41467-021-22377-9
79. Tabdanov E, Gondarenko S, Kumari S, Liapis A, Dustin ML, Sheetz MP, et al. Micropatterning of TCR and LFA-1 ligands reveals complementary effects on cytoskeleton mechanics in T cells. *Integr Biol (United Kingdom)* (2015) 7(10):1272– 845. doi:

10.1039/c5ib00032g

80. Hui KL, Upadhyaya A. Dynamic microtubules regulate cellular contractility during T-cell activation. *Proc Natl Acad Sci* (2017) 114(21):E4175–835. doi: 10.1073/pnas.1614291114

81. Savinko T, Guenther C, Uotila LM, Asens ML, Yao S, Tojkander S, et al. Filamin a is required for optimal T cell integrin-mediated force transmission, flow adhesion, and T cell trafficking. *J Immunol* (Baltimore Md.: 1950) (2018) 200 (9):3109–165. doi: 10.4049/jimmunol.1700913

82. Tamzalit F, Wang MS, Jin W, Tello-Lafoz M, Boyko V, Heddlestone JM, et al. Interfacial actin protrusions mechanically enhance killing by cytotoxic T cells. *Sci Immunol* (2019) 4(33):eaav5445. doi: 10.1126/sciimmunol.aav5445

83. Aramesh M, Stoycheva D, Sandu I, Ihle SJ, Zünd T, Shiu J-Y, et al. Nanoconfinement of microvilli alters gene expression and boosts T cell activation. *Proc Natl Acad Sci* (2021) 118(40):e2107535118. doi: 10.1073/pnas.2107535118

84. Bendell AC, Williamson EK, Chen CS, Burkhardt JK, Hammer DA. The Arp2/3 complex binding protein HS1 is required for efficient dendritic cell random migration and force generation. *Integr Biol* (2017) 9(8):695–7085. doi: 10.1039/c7ib00070g

85. Jurchenko C, Salaita KS. Lighting up the force: Investigating mechanisms of mechanotransduction using fluorescent tension probes. *Mol Cell Biol* (2015) 35 (15):2570–825. doi: 10.1128/MCB.00195-15

86. Liu Y, Galior K, Ma VP-Y, Salaita K. Molecular tension probes for imaging forces at the cell surface. *Accounts Chem Res* (2017) 50(12):2915–245. doi: 10.1021/acs.accounts.7b00305

87. Liu Z, Liu Y, Chang Y, SeyfHR, Henry A, Mattheyses AL, et al. Nanoscale optomechanical actuators for controlling mechanotransduction in living cells. *Nat Methods* (2016) 13(2):143–465. doi: 10.1038/nmeth.3689

88. Schmid J, Birbach A. Fluorescent proteins and fluorescence resonance energy transfer (FRET) as tools in signaling research. *Thromb Haemostasis* (2007) 97(03):378–845. doi: 10.1160/TH06-08-0472

89. Grashoff C, Hoffman BD, Brenner MD, Zhou R, Parsons M, Yang MT, et al. Measuring mechanical tension across vinculin reveals regulation of focal adhesion dynamics. *Nature* (2010) 466(7303):263–66. doi: 10.1038/nature09198

90. Nordenfelt P, Elliott HL, Springer TA. Coordinated integrin activation by actin-dependent force during T-cell migration. *Nat Commun* (2016) 7(1):13119. doi: 10.1038/ncomms13119

91. Zhong BL, Vachharajani VT, Dunn AR. STReTCh: A strategy for facile detection of mechanical forces across proteins in cells. *Preprint Bioengineering* (2022). doi: 10.1101/2021.12.31.474658

92. Gayrard Charlene, Borghi N. FRET-based molecular tension microscopy. *Methods* (2016) 94:33–42. doi: 10.1016/j.ymeth.2015.07.010

93. Kong HJ, Polte TR, Alsberg E, Mooney DJ. FRET measurements of cell traction forces and nano-scale clustering of adhesion ligands varied by substrate stiffness. *PNAS* (2005) 102(12):4300–5. doi: 10.1073/pnas.0405873102

94. Cadra S, Gucciardi A, Valignat M-P, Theodoly O, Vacaflores A, Houtman JCD, et al. ROZA-XL, an improved FRET based biosensor with an increased dynamic range for visualizing zeta associated protein 70 KD (ZAP-70) tyrosine kinase activity in live T cells. *Biochem Biophys Res Commun* (2015) 459(3):405–105. doi: 10.1016/j.bbrc.2015.02.117

95. Sadoun Anaïs, Biarnes-Pelicot M, Ghesquiere-Dierickx L, Wu A, Théodoly O, Limozin L,

- et al. Controlling T cells spreading, mechanics and activation by micropatterning. *Sci Rep* (2021) 11(1):67835. doi: 10.1038/s41598-021-86133-1
96. Mank M, Griesbeck O. Genetically encoded calcium indicators. *Chem Rev* (2008) 108(5):1550–645. doi: 10.1021/cr078213v
- Roles in T-Cell Traction Forces.' *Proceedings of the National Academy of Sciences* 111 (6): 2241–46. <https://doi.org/10.1073/pnas.1315606111>.

Protocol for measuring weak cellular traction forces using well-controlled ultra-soft polyacrylamide gels

Farah Mustapha ^{1,2,3,4,5,6}, Kheya Sengupta ^{4,5,7*}, Pierre-Henri Puech ^{1,2,3,4,7*}

Affiliations:

Laboratoire Adhésion et Inflammation (LAI)

¹ Aix Marseille University, LAI UM 61, Marseille, F-13288, France.

² Inserm, UMR_S 1067, Marseille, F-13288, France.

³ CNRS, UMR 7333, Marseille, F-13288, France.

CENTURI

⁴ Turing Center for Living systems, Marseille, France

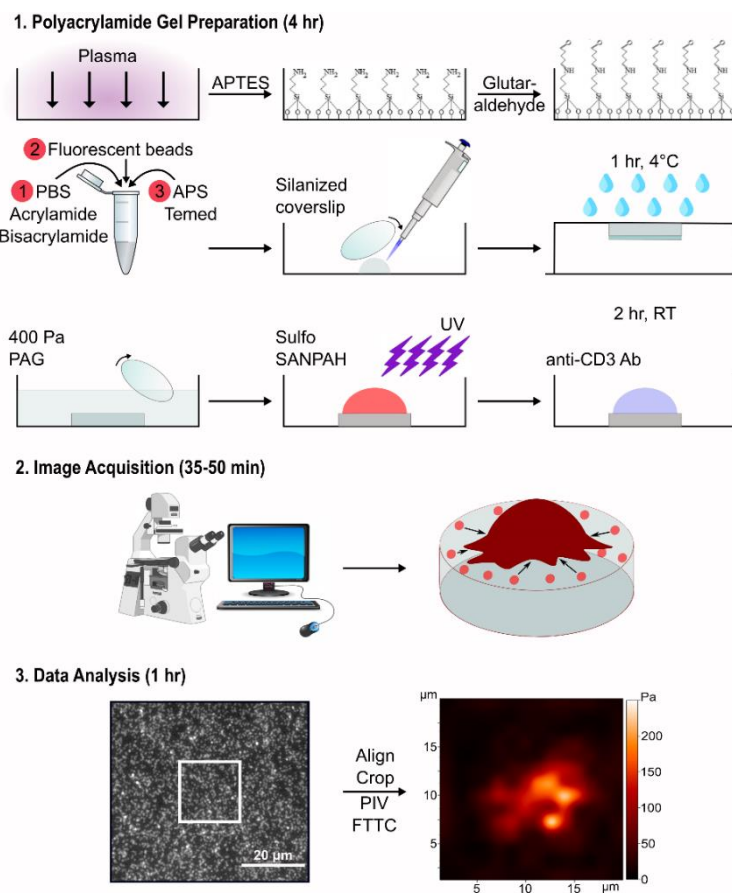
Centre Interdisciplinaire de Nanoscience de Marseille (CINAM)

⁵ CNRS - AMU UMR 7325, Marseille, F-13288, France

⁶ Technical contact

⁷ Lead contact

*Correspondence: sengupta@cinam.univ-mrs.fr, pierre-henri.puech@inserm.fr



Summary

Traction force microscopy (TFM) has been implemented in the study of cellular forces for more than two decades now. However, the reproducible fabrication of ultra-soft substrates dedicated for the faithful detection of weak cellular stresses remains a challenge to this day. Here, we describe a simple in-vitro TFM protocol using ultra-soft protein-coated polyacrylamide gels and widefield fluorescence microscopy. The protocol is complemented with in-house scripts for data analysis, allowing readers to easily quantify traction forces when studying cell mechanobiology.

BEFORE YOU BEGIN

Despite the numerous exciting developments in the field of Traction Force Microscopy (TFM), the most commonly used system to measure cellular forces remains fairly similar to the one designed by Dembo and Wang in 1999 (Dembo and Wang, 1999): TFM on continuous and linearly elastic substrates embedded with fluorescent beads. The most popular of these substrates are polyacrylamide gels (PAGs) and polydimethylsiloxane silicone (PDMS) elastomers. In the protocol described here, we favor polyacrylamide gels over their counterparts for two main reasons. First, the stiffness of PAGs can be easily adjusted to mimic that of soft biological tissues (on the order of 100 Pa), which applies very well to our systems of interest, namely immune cells. Second, PAGs are generally non-fouling, meaning neither cell surface receptors nor adhesive proteins present in the serum can bind directly to the gel, only molecules covalently grafted on the gel surface can act as ligands for the cells.

The PAGs produced using this protocol exhibit several key specifications. First, they are sufficiently thick ($\approx 80 \mu\text{m}$) such that the cells feel and respond to the softness of the gels rather than the rigidity of the underlying glass. Second, they have a well characterized and homogeneous Young's modulus of $\approx 400 \text{ Pa}$, specifically chosen for studying weak forces similar to those generated by immune cells. This rigidity is neither so high that the cells are incapable of significantly deforming the gel, nor so low that the resulting large deformation breaches the linear-response regime, making the linear-elastic theory underlying TFM inapplicable. It is also important to mention that PAGs with this stiffness have a sufficiently small mesh size capable of entrapping sub-resolution (200 nm) fluorescent beads within it. Finally, the gels have a lateral bead density corresponding to about four beads in an area of $2.5 \times 2.5 \mu\text{m}^2$ ($16 \times 16 \text{ px}^2$), carefully chosen in accordance with the lateral distribution and the magnitude of the forces being measured, as well as the quantitative image analysis method employed.

Here, we use this optimized protocol for measuring the traction forces exerted by peripheral blood mononuclear cells (PBMCs), however, we have successfully employed it for different subtypes of primary T cells and Jurkat T cells as well.

STEP-BY-STEP METHOD DETAILS

Part 1: Production of Ultra-Soft Polyacrylamide Gels

Given the toxic and hazardous nature of several of the chemicals mentioned in part 1, we highly recommend that the following steps are performed under a chemical fume hood.

a. Preparation of amino-silanized glass-bottom fluorodish(es)

Timing: 1 hr

There are two reasons behind specifically choosing these fluorodishes for PAG casting. First, they have an optical quality glass bottom with a thickness of 0.17 mm, making the visualization of the gel on inverted microscopes with high magnification objectives quite easy. Second, they are individually packed and gamma sterilized which decreases the number of steps and time needed for activating them.

- i. Plasma clean the sterile fluorodish for 2 min at high settings.

Note 1: For our experiments we use residual air plasma. As mentioned above, the fluorodishes are already sterile. This step is an additional precaution to help increase the surface energy of the glass surface to better bond with the reagent added in the next step.

Note 2: Given that we are using fluorodishes, which are glass-bottom plastic dishes, for casting the PAGs, we cannot use harsh chemicals for activating them. This is why we chose to use a plasma cleaner in this step. In the case of in-availability of a plasma cleaner, we suggest replacing the fluorodishes with glass coverslips and activating them with a piranha solution (sulfuric acid- hydrogen peroxide). We have successfully done this several times.

- ii. Immediately add 1 ml of 5% APTES diluted in Milli Q water to the activated fluorodish surface. Allow the APTES to react for 5min. After 5 min, remove the remaining liquid APTES from the fluorodish, flip it upside down on a clean paper towel and allow it to dry for 10min.

CRITICAL: APTES is highly sensitive to moisture and should be stored by filling the pocket of gas in the bottle with inert gas such as nitrogen or argon, preferentially at 4°C. If it is stored at 4°C, it should be brought to $\approx 25^{\circ}\text{C}$ before usage. The elevated temperature will enhance the covalent attachment and self-assembly of APTES to the glass during the silanization reaction. The diluted solution should always be prepared fresh. Do not keep any unused solution.

- iii. Rinse the fluorodish with running Milli Q water for 30 sec to remove the remaining APTES from step 2.

Note: It is essential to completely remove any trace of unreacted APTES for it will react with the glutaraldehyde used in step 3 and form an orange-brown precipitate. This precipitate fluoresces under UV light and may therefore interfere with fluorescence imaging of either the beads or the cells (if fluorescently labeled) during the experiment.

iv. Add 1 ml of 0.5% glutaraldehyde in Milli Q water to the fluorodish and let it sit for 30 min.

CRITICAL: Using APTES alone to bind the polyacrylamide gel to the glass surface is not reproducible. Thus, following the APTES treatment with glutaraldehyde will help further activate the amino silanized surface and ensure the covalent attachment of the polyacrylamide gel to the glass surface.

v. Aspirate the remaining glutaraldehyde from the fluorodish and rinse it again with running Milli Q water.

Pause Point: After this step the fluorodishes can either be (a) dried and used immediately for polyacrylamide gel casting, (b) stored in water at 4°C for up to a week or (c) dried and stored under desiccation for up to a month. We preferentially used options (a) and (b).

b. Preparation of chloro-silanized coverslip(s)

Timing: 2 hr 30 min

vi. Sonicate (ELMAULTRASONIC S 30 H) the 12 mm glass coverslips for 30 min in 2% Hellmanex (diluted in Milli Q water) twice and then for another 30 min in Milli Q water twice. Rinse the coverslips with running Milli Q water for 1 min in between each sonication.

vii. Plasma clean the coverslips for 2 min at high settings.

Note 1: As mentioned above, for our experiments we use residual air plasma. This step is needed to help increase the surface energy of the coverslips to better bond with the reagent added in the next step.

Note 2: In the case of in-availability of a plasma cleaner, we suggest activating the coverslips with a piranha solution (sulfuric acid- hydrogen peroxide). We have successfully done this several times.

viii. Immediately cover the activated coverslip surface with undiluted Sigmacote (as provided by the manufacturer) and allow it to react for 5 min. After 5 min, remove the excess Sigmacote solution by capillarity with an absorbing paper (eg, Kimwipe) and let the coverslips air-dry for 10 min protected from light and dust.

CRITICAL: Sigmacote is a chlorinated silane and thus, similar to APTES, has to be stored under an inert gas atmosphere at 4°C and has to be brought back to $\approx 25^{\circ}\text{C}$ before usage.

ix. Rinse the coverslips with running distilled water

Pause Point: After this step, the coverslips can either be dried and used immediately, or stored under desiccation to be used later.

c. Preparation of soft polyacrylamide gels

Timing: 20 min

There are numerous reports of acrylamide/bis-acrylamide formulations that can be used to produce PAGs with a wide range of stiffness. We have adapted ours from the commonly used and cited protocol published (Tse and Engler, 2010). The Young's modulus of the PAGs was verified using Atomic Force Microscopy in mapping mode using a JPK Instruments Nanowizard I, equipped with a JPK Instruments Petri Dish heating system set at 37°C. To do so, we used Brucker Instruments MLCT cantilevers that we modified by gluing beads on their tip, by micromanipulation, the size of which is comparable to that of a lymphocyte (diameter $\approx 10\ \mu\text{m}$, (Sadoun et al., 2021)). We made $48 \times 48\ \mu\text{m}^2$ laterally resolved maps of the modulus on several regions (at least 3) on the gels to ensure the lateral homogeneity of this crucial parameter. By performing these measurements regularly, we ensured that our PAG preparation protocol was stable and reproducible.

- i. Prepare the polyacrylamide gel premix by mixing acrylamide and bis-acrylamide to their desired concentrations in either Milli Q water or PBS in an eppendorf tube. To obtain ultra-soft polyacrylamide gels ($\approx 400\ \text{Pa}$ PAG), mix $75\ \mu\text{l}$ Acrylamide (40%) with $30\ \mu\text{l}$ Bis-acrylamide (2%) and $895\ \mu\text{l}$ PBS. To generate gels with different stiffness, refer to (Tse and Engler, 2010).

Note 1: It is important to note that using PBS instead of Milli Q water will slightly increase the elastic modulus of the gel. This can be quantified by AFM measurements.

Note 2: It is preferable to mix the precursors, APS and TEMED, directly before polymerizing the gels since that will limit and control their exposure to oxygen, ensuring a better reproducibility of the final gel stiffness.

- ii. Add 0.7% total volume of 200 nm fluorescent beads ($7\ \mu\text{l}$) to the premix.

Note: The beads used in this protocol are carboxylate-modified with an orange fluorescence (excitation wavelength of 540/560 nm). Before use, the beads have to be cleaned using a Slide-A-Lyzer Dialysis Device 10 KDa to remove any chemicals present in the bead solution that might interfere with polymerization of the gel. Since the beads used here are of very small size ($\sim 200\ \text{nm}$), dialysis is the safest method to ensure the thorough cleaning of the beads without creating any aggregates.

- iii. Add 1% total volume of Ammonium persulfate (APS, $10\ \mu\text{l}$) and 0.1% total volume of Tetramethylethylenediamine (TEMED, $1\ \mu\text{l}$) to gel solutions.

CRITICAL: APS has to be either freshly prepared or previously aliquoted and stored at -20°C otherwise the polymerization of the gel will be disrupted. Similarly, TEMED that has been stored for a long time or that hasn't been stored properly will have the same effect.

- iv. Quickly vortex the polymerizing solution for 20 sec and pipette 5 μ l of the polymerizing gel into the center of the fluorodish and sandwich it with the chloro-silanized coverslip, with the treated side facing the gel.

Note 1: If the coverslip was treated properly, the polymerizing gel should wet it perfectly without any need for supplementary manipulation.

Note 2: The volumes mentioned above should theoretically create a 40 μ m thick gel, however the real height of the gel was observed to be \approx 80 μ m when measured using a motorized optical microscope stage system. This discrepancy is due to the fact that gels swell after polymerization, and so the height of the gel cannot be directly calculated from the volume of the cast polymerizing solution. Also, the degree of PAG swelling varies with each acrylamide/bis-acrylamide formulation and cannot be easily predicted, thus, it is important to measure or at least estimate the height of the resulting gel before using it for TFM. The gel must be sufficiently thick such that it can freely deform due to cellular forces without the influence of the underlying glass. As a consequence, the increased gel thickness might impose a limit on the type of microscopy and objectives (depending on their working distance) that can later be used for visualization.

- v. Close the fluorodish lid, flip it upside down to allow the beads to move towards the surface, surround it with wet tissue paper, place it in a closed-light protected chamber (e.g. large petri dish covered with aluminum foil), and then allow it to polymerize for 1 hr at 4°C.

CRITICAL: Surrounding the fluorodish with wet tissue-papers will provide enough humidity to prevent the gel from drying out and cracking during the polymerization process. Shorter polymerization times may result in insufficient polymerization of all available monomers and may cause the mechanical properties of the hydrogels to vary from the values noted here and/or be heterogeneous over the gel surface. Monitoring the state of the unused solution in the eppendorf, for example by poking it with a needle can help estimate the degree of polymerization of the gel.

Refer to Troubleshooting 1: Gels do not polymerize.

- vi. Fill the fluorodish with PBS (or water) for 20 min before carefully peeling off the coverslip using the tip of a needle or tweezers.
- vii. Rinse the gel twice by submersion, each time for 5 min in PBS (or water) to remove any unpolymerized acrylamide.

Pause Point: At this point, the gels can be stored in PBS (or water) at 4°C for up to a week before usage. Although the gel looks ‘polymerized’ after 1 hr, there’s a deeper level of polymerization that takes place within the first 12 hrs of gel casting. Thus, it is preferable to use the gel only after this time interval has lapsed and the cross-linking has been completed.

Refer to Troubleshooting 2: Gels crack.

Part 1d: Gel functionalization

Timing: 2 hr

Before the cells can be deposited, the desired proteins that will drive the interactions between the cells and the gel need to be first immobilized onto the gel surface. PAGs are known to be nearly inert, and thus they do not readily adsorb proteins. One way to overcome this is to covalently link the proteins of interest to the PAG surface using a heterobifunctional protein cross-linker called sulfo-SANPAH. Sulfo-SANPAH contains an amine-reactive N-hydroxysuccinimide (NHS) ester on one side and a UV photoactivatable nitrophenyl azide on the other. Once a sulfo-SANPAH-coated gel is exposed to a UV light source with a wavelength between 320 and 365 nm, the nitrophenyl azide group will form a nitrene group that will bind to the polyacrylamide gel, and the sulfosuccinimidyl group will react with the primary amino groups of proteins to form stable amide bonds.

- i. Remove PBS or water from pre-silanized fluorodish.
- ii. Add 250 μ l of 0.5 mg/ml sulfo-SANPAH (prepared in 50 mM HEPES, pH 8.5) to the surface for the gel and expose it to 365 nm UV radiation for 2 min at 100% power in a UV-KUB 2 oven. Repeat this step twice with a PBS rinsing step in between.

Note 1: Sulfo-SANPAH is highly unstable in aqueous solutions and is light sensitive. Thus, it either has to be previously aliquoted and stored at -80°C (where it can be kept for up to 6 months, shielded from light at all times) or stored as powder and prepared immediately before gel functionalization. After sulfo-SANPAH has been exposed to UV, it should change its color from orange red to brown. It is also important to take care when choosing the UV source: we observed that broad-spectrum UV lamps/ovens are likely to bleach the fluorescent beads used here.

Note 2: When the hydrogels are later used for TFM, non-specific binding of cellular proteins and media proteins to unlinked sulfo-SANPAH sites does not take place because the reaction happens only when the pH is around 8.5, and the pH of the cell medium is usually between 7 and 7.4.

- iii. Rinse the gel 3 times with PBS to ensure that all unbound sulfo-SANPAH has been removed.
- iv. Add an appropriate amount of the desired protein onto the surface of the activated gel, and incubate this solution for either 2 hrs at 25°C or for 12 hrs at 4°C .

Note: For our experiments, we used a final concentration of 30 $\mu\text{g}/\text{ml}$ of the antibody OKT3. A primary concern when using PAGs is the variability of ligand density and the homogeneity of ligand coating, especially given their inert and porous nature. Thus, to optimize the coating protocol to the end user's specific proteins and conditions, a quantification step is necessary. One way to perform this quantification is by using a fluorescently labeled protein to both relate the measured signal to the amount of protein from reference standards and to

inspect the relative lateral homogeneity of the coating (González et al., 2019). Fluorescently labeled proteins can be added in this step instead of their unlabeled counterparts and can then be imaged after incubation using fluorescence microscopy. Nevertheless, it is preferable *not* to use a fluorescence label for the proteins, especially one with absorption/emission spectra too close to the one of the beads to avoid creating background noise via bleed-through which may compromise the fine detection of bead displacement.

Part 2: Image Acquisition

Timing: 15-30 min/sample

1. Once the incubation period is over, rinse the gel gently with a 37°C preheated medium 3 times, leaving the gel immersed in medium after the last rinse (≈ 2 ml of medium), and then transfer the fluorodish to an inverted widefield fluorescence microscope. We used a Zeiss Axiovert 200 microscope equipped with a 40 x NA0.9 air objective, a CoolSnap HQ2 camera (Photometrics), a LED illumination system (Colibri 2, Zeiss) with suitable filter sets (Cazaux et al., 2016), and a petri dish heater module (JPK Instruments) that allows setting the temperature at the desired value, with a stability of a fraction of a degree.

Pause Point: Leave the gel to equilibrate at the desired temperature (in our case 37°C) for at least 20 min before starting image acquisition. This reduces the potential drifts due to thermal expansion of the substrate or the microscope stage. The mentioned time interval may need to be adapted to every setup used, in particular for thermal equilibration.

Note: In all TFM experiments, at least two images of the substrate have to be acquired: One image of the bead field while the substrate is subjected to cellular forces (i.e. stressed state) and another image of the bead field in the absence of cellular forces (i.e. relaxed state). In our setup, the fluorodishes are firmly fixed onto the microscope with the petri dish heater module. This enables us to start the image acquisition *before* the addition of the cells, consequently giving us the relaxed state of the gel at the start of the experiment. This corresponds also to our goal of studying the early stages of immune cell mechanotransduction.

2. Start image acquisition using an appropriate software. In our case, we used Zen software (Zeiss) that controls the Colibri 2 diodes system and the camera.

Note: Since we are interested in the dynamics of early immune cell spreading, our image acquisition only lasts between 15 and 30 min, and instead of taking only two images (relaxed and stressed), we acquire time-lapse TFM movies, at a typical interval of 1 frame every 5s, by capturing image doublets of the cells in phase-contrast (20 ms exposure time) and orange fluorescent microspheres (excitation ≈ 488 nm, 200ms exposure time) over the course of the mentioned time frame. Since the layer of microspheres is only a couple of micrometers beneath the gel surface (due to the flipping of the gel during the polymerization step), the cells will still be easily visualized and tracked while the focus is set on the bead layer.

3. Remove any excess medium (if there is any, depending on the desired final concentration of the cells), and gently pipette the cells onto the gel.

Note 1: For our experiments, we typically add a final concentration of 0.75 million cells/2 ml in complete RPMI media containing 10% fetal bovine serum (FBS), 1% glutamax, 1% penicillin streptomycin and 2.5% HEPES. Remove 1 ml of medium, add the 0.75 million cells/0.5 ml onto the center of the gel and then add the remaining 1.5 ml of medium around the gel center. Note that the final concentration of cells used needs to be adjusted based on the cell type at hand and the forces they exert; it is crucial that the stress fields exerted by the cells are spatially separate. Also, the cells are always sub-cultured 12 hrs before the experiment so as to not agitate them the day of the experiment. Keeping culture conditions strict is an important point for ensuring the comparison between different days of experimentation and for subsequent statistical pooling of the data.

Note 2: A common method to obtain the relaxed reference state of the beads is to carefully detach the cells at the end of the experiment, for example using Triton X-100, SDS, Trypsin, or accutase solutions, wait until substrate deformation is fully reversed, and then capture an image of the beads. In this case, the risk of accidentally moving the sample from its position is greatly augmented, which complicates data analysis, sometimes even rendering it impossible. However, in case of encountering significant drift during step 3, this method could be used instead.

Expected outcomes

A successful run should have cells interacting with the substrate at the end of the experiment (Figure 1).

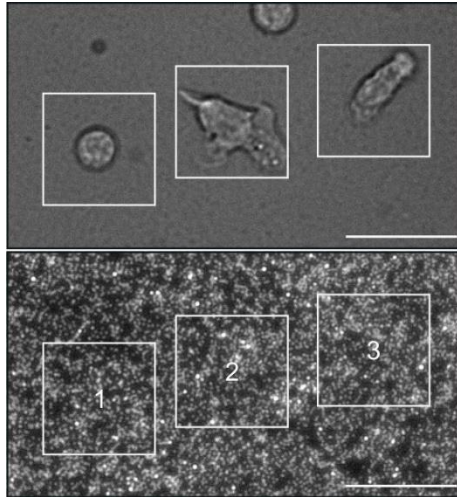


Figure 1: Transmission image of PBMCs (top) and fluorescent image of beads (bottom). Inserts: white squares indicating sub-image zones cropped and used for the PIV and FTTC calculations. Scale bar 20 μm .

Quantification and statistical analysis (optional)

For the data analysis and the post-processing, we chose to use open source softwares and programming languages. We use the last version of Fiji (Schindelin et al., 2012) which is a meta-package of ImageJ (used as of 13/11/21, v1.53c), with specialized plugins available either on Fiji/ImageJ website, programmer's website or GitHub repository (see below). For Python, we use the latest release of Anaconda Python distribution (<https://www.anaconda.com>, used as v3.8.8) which contains all the needed packages for data science applications, together with an IDE (Spyder) and the Jupyter notebook system utilized in this protocol. We perform our analysis on 64 bits Linux PCs (Ubuntu 18.04; Linux Mint 20.2).

Part 3: Data Analysis

The computer configuration we used for data analysis was a Dell Precision 3640 Tower, with an Intel i9-10900K (20) @ 5.300GHz CPU and 64Go RAM under Ubuntu Linux 18.04. We have also successfully performed the analysis on a Dell XPS 13 9370 laptop, with a Intel i7-8550U (8) @ 4.000GHz CPU and 16Go RAM, under Ubuntu Linux 18.04 or Linux Mint 20.2.

Timing: 1 hr/sample

Having imaged the sample, one can then extract the cellular traction stresses from the collections of images obtained. This arduous, calculation intensive process encompasses four key steps:

1. Sample Drift Correction

Typically, images taken one after the other may present a slight drift, however, this drift becomes especially evident when acquiring images over a larger time frame and at a relatively high frequency such as in our experiments. Sample drift is of two kinds, either a focus drift (i.e. along the z-axis) caused by small temperature variations between the sample and the objective (in particular in the case of an immersion lens), or a lateral drift (i.e. along the x-y plane), caused by stage instability or dilatation, for example. The z drift is somehow less problematic than the lateral one since it can be either automatically controlled by an autofocus, or z-scan acquisition with further detection of the best focus image (e.g. using the ImageJ macro from <https://sites.google.com/site/qingzongtseng/find-focus>), or manually adjusted at given time points throughout the acquisition period. The x-y drift on the other hand cannot be easily experimentally predicted or corrected, only minimized by suitable motion and temperature control, and thus can severely corrupt the true displacement data. Consequently, before one can faithfully measure cell-induced bead displacement, the frame to frame drift generated due to whole-sample translation, and sometimes rotation, must first be calculated and then subtracted from the total bead displacement to properly align the images.

- a. Install and open Fiji -> Import video of the fluorescent beads -> Save video as .tif or .czi in a separate folder named “**images**” -> Open Set Scale and properly calibrate the images -> Install the TrackMate plugin -> Open Plugins -> Open Tracking -> Run TrackMate -> Extract “Track Displacement” -> Save the pop-up table titled “Spots in tracks statistics” as “**trajectories.csv**”

Note: TrackMate (Tinevez et al., 2017) is a tool for automated single particle tracking; It assigns each fluorescent bead an identity (based on its coordinates) over the given frames and then reconstructs the trajectories of each bead in the form of a track. We use the full frame $220 \times 164 \mu\text{m}^2$ ($1392 \times 1040 \text{ px}^2$) images (16 bits coded on 12 bits) in this step since they contain a large number of beads that can be detected and tracked, which helps increase the accuracy of the measured drift.

- b. Create an empty folder named “**aligned**” and then run the following Jupyter notebook: <https://github.com/remyeltorro/SPTAlign>. The now aligned frames will appear in the “**aligned**” folder.

Note 1: The script mentioned above utilizes the trajectories obtained from the previous step to perform a sample drift correction. Since the average shift is often on a subpixel scale, the script applies the shift in Fourier Space: It first direct Fourier transforms the image, applies the shift using Scipy Fourier shift function, and then inverse Fourier transforms the image. The first frame of the movie is chosen as the frame of reference (since the cells are not present yet) and consequently all the following frames are aligned to the coordinates of the fluorescent beads in the first frame.

Note 2: The same trajectories can be used to correct the drift on the cell movie since we do not change the objective and filter-set between the bead-field and cell images.

2. Cropping Regions of Interest

- a. Open the drift-corrected bead image sequence in Fiji and search for the areas with bead displacements.

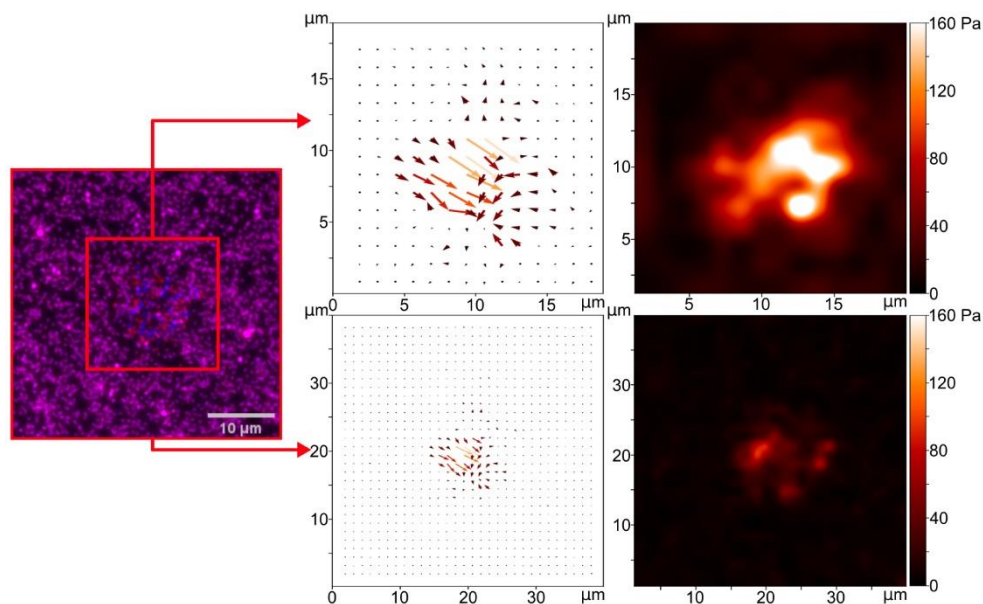


Figure 2: Effect of the selected image size ($20 \times 20 \mu\text{m}^2$ vs. $40 \times 40 \mu\text{m}^2$) for the PIV and FTTC calculations on the constructed vector map of bead displacement and the gaussian smoothed map of stress norms, using the same PIV parameters and regularization factor.

Note: Large bead displacements are easily caught by eye, however, low magnitude forces (for example those caused by Jurkat T cells) cause small bead displacements that can be difficult to detect by eye. In these cases, monitoring the position of the cells can be quite beneficial since one could simply project the position of the cells onto the bead images and limit the search for bead displacement to those areas.

- b. Install the ROI-1click tools (<https://imagej.net/plugins/roi-1-click-tools>) in Fiji -> Open the ROI-1 click tools -> Choose the appropriate selection size (explained below) -> Select the regions where the beads are visibly moving by clicking the pointer once at the center of the movement -> Leave the ROI manager containing all the selections open (this is crucial for the next step)

Note: Choosing the right selection size is highly dependent on the experimental data itself. The chosen region should be centered around the cell, but it should not necessarily be limited to the cell outline; In most cases, substrate deformation by cellular forces is not confined to the area directly underneath the cell, and so some bead movement can be detected in the margins outside the cell outline, due to the continuous elastic nature of the gel. Consequently, constricting the region for force detection to that underneath the cell and neglecting the displacement occurring outside of it will not be a true representation of the real force exerted by the cell. Additionally, if in fact the force does extend outside the cell outline and the bead displacement does not go down to zero at the boundary of the cropped image, some so-called “ringing” artifacts (oscillations) will appear at the boundary and will introduce errors into the final reconstituted force field. Alternatively, if the cropped region is too large, then the stresses will be diluted over an area where a substantial number of beads will be immobile (not experiencing any force, just background noise). In this case, one runs the risk of severely dampening the signal to noise ratio which ultimately would not be a true representation of the real force exerted by the cell (Figure 2).

- c. Load the Multicrop macro ([1-PHP-multicrop.ijm](https://github.com/phpuech/TFM) from <https://github.com/phpuech/TFM>) in Fiji -> Click Run -> Double click on the “aligned” folder -> Click Run. The cropped full-length image sequences of the selections will now appear in the “aligned” folder, each in a separate folder named “segment_n” where n goes from 0 to the total number of selections present.

3. Calculating Bead Displacement Field and Traction Force Field

- a. Install the PIV Plugin and the FTTC Plugin from <https://sites.google.com/site/qingzongtseng/imagejplugins> in Fiji -> Open the macro [2-PHP-TFM-loops-modified.ijm](https://github.com/phpuech/TFM) from <https://github.com/phpuech/TFM> in the Macro editor in Fiji -> Input the following parameters: Interrogation Windows (**IW1, IW2, IW3**), Search Windows (**SW1, SW2, SW3**), Vector spacing between the IWs (**VS1, VS2, VS3**), **Poisson’s ratio** (0.5 for PAG), the **Young’s modulus** of the gel (in Pascal), **Pixel size**, **Width** and **Height** of the cropped image (in pixels), **Correlation threshold** value and **Regularization Factor** -> Click Run -> Double click on the “aligned” folder -> Click Run. The PIV and FTTC text files will now appear in a “save” subfolder for each “segment_n” in the “aligned” folder.

Refer to Troubleshooting 3: Poor lateral resolution of the stress maps due to inappropriate choice of PIV and FTTC parameters

Note 1: The PIV Plugin calculates the bead displacement field from the bead images, and then the FTTC Plugin reconstructs the traction force field from the displacement data. Since the PIV and FTTC Plugins only process two images at a time and our experimental data consists of movies (made up of ≈ 200 frames), this Fiji/ImageJ macro was written to consecutively run the two plugins over the full length image sequences of all the segments in the aligned folder, always taking the first frame in each segment as the reference frame.

Note 2: If you open the PIV Plugin, three options will appear: Cross-correlation iterative PIV (also known as conventional PIV), Basic iterative PIV (also known as template matching PIV), and Advanced iterative PIV (an extension of the Basic iterative PIV). The macro linked here implements the Advanced iterative PIV: The images are divided into two types of windows, Interrogation Windows (IWs) and larger Search Windows (SWs). In each iteration, the displacement is calculated by a normalized correlation coefficient algorithm, so that an IW from image 1 is compared to the SW in image 2 to find the required shift of image 1 to have the best overlap between images 1 and 2. Up to three iterations can be performed, going from coarse to fine scale, with each iteration taking into account the displacement field measured previously. A correlation threshold, ranging from +1 (exact match) to -1 (zero correlation), is manually defined to filter out low correlation matches resulting from IWs with an insufficient number of beads. Thus, even if the pre-shift given by one of the PIVs is partly inaccurate, the best matched vectors depicted by a significant correlation peak (equal or higher than the threshold) are displayed in the final cross-correlation result, while other vectors with a correlation value lower than the threshold are replaced by the median value of the surrounding neighbors.

4. Post-Processing

In order to visualize and quantify the bead displacement data and the stress field data in the PIV and FTTC text files:

Open the following Python script: [3-PHP-Reconstruct-Energy-Plots.py](https://github.com/phpuech/TFM) from <https://github.com/phpuech/TFM> in Spyder IDE -> Input the **source** of the segment folders -> Input the **dt** (time interval between frames), **VS3**, **Calibration factor** from (to convert px to μm), **image size** (in px) -> Choose which parameters you would like to plot (**map of the displacement vectors, histogram of the displacement norm, map of the stress vectors, discrete map of the stress norm, Energy plot, Stress sum plot**) -> Adjust the output parameters of the plots as needed -> Run the script.

Note 1: The stress norm is defined, at each position of the reconstituted stress field, as the norm of the stress vector obtained by the FTTC macro. The stored energy is calculated as the sum of the scalar products of the displacement vectors and force vector (i.e. the stress times the area on which it applies) as in (Butler et al., 2002). The maps show the lateral distribution of a given parameter, and possibly the orientation of the vectors, while an “average” parameter plot focuses more on the time evolution of the global behavior of the cells.

Note 2: This Python code generates quiver plots (maps of arrows, color coded for their norm values) and histograms for the displacement parameter, as well as heatmaps (color coded for the norm of the vectors at a given position) for the stress parameter. This is recursively done for each “**segment_n**” present in the “**aligned**” folder in one go, allowing for a faster processing of a given experiment. It also generates Y vs time plots, where Y is the sum or the mean or the median of the stress norms over the images or the stored energy over the images. The reconstructed maps of the displacement vectors, histograms of the displacement norm and the PIV text files will appear in a “**PIV**” folder while the reconstructed maps of the stress vectors, discrete maps of the stress norm, energy plots, stress sum plots, and the FTTC text files will appear in an “**FTTC**” folder, both in a subfolder called “**save**” for each “**segment_n**”.

Note 3: We implemented this Python script because we are interested in observing the dynamics of the stress exerted by the cells, however, to generate vector plots for the bead displacement and the stress for a specific time point, a simple alternative would be to use the PIV and FTTC visualization tools available at <https://sites.google.com/site/qingzongtseng/imagejplugins>.

Note 4: For the post processing, as for the PIV and FTTC calculations, we choose *not* to apply a mask corresponding to the projection, at each time point, of the cells. Such a mask is used as a way to exclude the zones where the beads are expected not to move, which, as mentioned before, will impact the stress field calculated by decreasing the signal to noise ratio. Some reports arbitrarily extend the data processing zone to include a margin around the area occupied by the cell, amounting to 10% of the cell area, to account for beads that may move since they are close to the cell margin and hence within the deformation field of the continuous elastic gel. We preferred to minimize the number of assumptions by using a “one image size” fits all approach for a given condition, in order to compare between different cells and cell types.

This is our end point. The maps and plots can be either used as such or the corresponding data can be accessed as text files for further analysis of any kind.

Limitations

First and foremost, since these ultra-soft gels are produced specifically for weak forces, cells that exert high forces are not suitable for study using these gels. Ideally, the rigidity of the PAGs should be optimized for every specific cell type and condition.

Another problem that arises for all PAG-based TFM, due to the hydrophilic, as well as porous nature of polyacrylamide, is that the thickness of the resulting gel is very hard to control. In this protocol, the gels have a relatively stable thickness of $\approx 80 \mu\text{m}$. Thick gels preclude low working distance objectives, and as a result many high magnification and high numerical aperture oil objectives cannot be used. Not to mention that PAGs have roughly the same refractive index as water, which consequently also eliminates the possibility of performing

surface microscopies (e.g. Reflection Interference Contrast Microscopy, Total Internal Reflection Fluorescence Microscopy).

Additionally, given the high hydrophilicity of PAGs in general, but of soft PAGs, microcontact printing and patterning of proteins onto the gels will be extremely challenging.

Finally, using the set-up described here, a 2D substrate with embedded beads, we are limited to measuring forces exerted in tangential (in-plane) directions (X, Y). Forces that may be applied normal to the substrate (out-of-plane) will be very hard, if not impossible, to assess. Some recent reports have proposed to use additional beads to derive these forces (Aramesh et al., 2021).

Troubleshooting

Problem 1: Gels do not polymerize reproducibly

Manufacturing gels of very low elastic moduli is a very sensitive process. Even minor perturbations of the chemical integrity of the reactants can modify, slow or even disrupt the full polymerization reaction. Most commonly, this problem is due to a malfunction of the initiators, APS and TEMED, or to additives present in the fluorescent microsphere solution incorporated in the gel premix.

Potential solution:

Solution 1: Prepare fresh APS for each experiment or properly aliquot it and store it at -20°C prior to experimentation. APS is very hygroscopic and begins to degrade almost immediately when dissolved in water.

Solution 2: Renew the TEMED at least every 6 months and make sure it is tightly closed and stored under inert gas (such as Argon and Nitrogen gas) at 4°C during that time interval. TEMED is very hygroscopic and subject to oxidation as well. As it accumulates water and reacts with it over time, it will gradually lose its catalytic activity.

Solution 3: Thoroughly clean the fluorescent beads before they are incorporated in the gel. The fluorescent microsphere solution contains some chemicals that may inhibit the polymerization reaction. We recommend washing by dialysis for 12 hrs.

Problem 2: Gels crack

The presence of beads in the gels, in combination with the flipping of the fluorodishes, may lead to the formation of visible cracks in the gels. When this happens, the beads will accumulate in the cracks, perturbing the otherwise uniform dispersion of the beads in the surrounding regions and rendering the gel unusable.

Potential solution:

Increase the level of humidity during the polymerization process. We recommend surrounding the fluorodishes with wet tissue-papers during that time interval.

Problem 3: Poor lateral resolution of the stress maps due to inappropriate choice of PIV and FTTC parameters

Potential solution:

Choose correct PIV and FTTC parameters as described below.

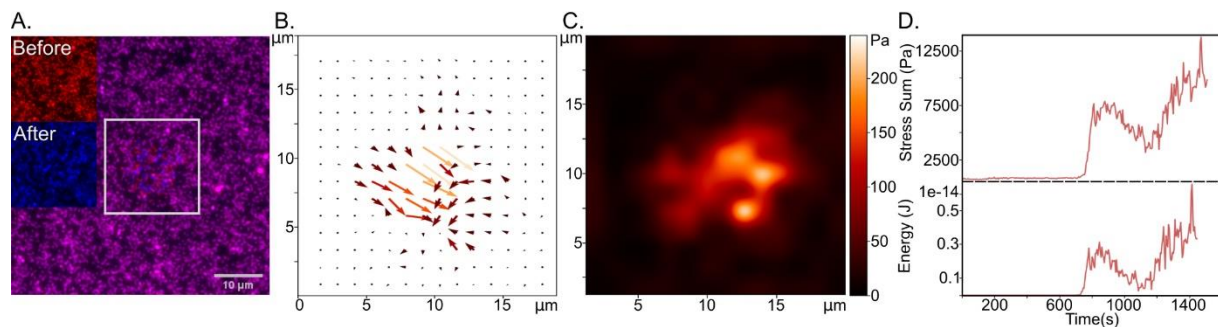


Figure 3: A. Merged images of beads at $t = 0$ min (red) and $t = 20$ min (blue). Inserts: reference image in red at $t = 0$ min, stressed image in blue at $t = 20$ min, white square indicating sub-image zone cropped and used for the PIV and FTTC calculations. B. Vector map of bead displacement obtained for $t = 20$ min after the PIV calculations over the sub-images. C: Gaussian smoothed map of stress norms obtained for $t = 20$ min after the FTTC calculations over the sub-images. D: Curves representing the sum of stresses (top) and the energy (bottom) over the sub-images vs. the time duration of the experiment.

First, start by choosing the size of the IW in the final iteration (IW₃). The smaller the IW, the higher the resolution of the forces. However, if the IW gets too small, the discernable features (fluorescent beads) in the window will become less and less numerous, making the correlation unreliable and prone to error. As a rule of thumb, **the smallest IW must contain on average 3 - 4 beads, or more** (Martiel et al., 2015). Second, choose the size of the SW₃. In general, the SW should be larger than the IW. The simplest and probably most computationally efficient option is to **set the SW₃ to be double the size of the IW₃**. Do not set the SW₃ and the IW₃ to the same value, as the PIV program will turn automatically into Basic Iterative PIV mode, which is less precise, and hence not recommended (see <https://sites.google.com/site/qingzongtseng/tfm>). Third, choose the VS, which effectively represents the spacing between the IWs. Again, the simplest and probably most computationally efficient option is to **set the VS to be half the size of the IW**. Once the final iteration values have been inputted, proceed to the remaining iterations. To run three iterations, one option is to double the values of IW₃, SW₃ and VS₃ to get IW₂, SW₂ and VS₂, and then similarly double the values of IW₂, SW₂ and VS₂ to get IW₁, SW₁ and VS₁. To limit the number of iterations performed, set the IWs and SWs to zero. Remember that the previous PIVs with the larger IWs and SWs only serve as a guide for finding the correlation peak. For example, for the 128 x 128px² (equivalent to 20 x 20 μm²) bead image

shown in Figure 3 and Method Video S2, the following PIVs were used: IW1= 64 SW1= 128 VS1= 32, IW2= 32 SW2= 64 VS2= 16, IW3= 16 SW3= 32 VS3= 8.

Next, set the correlation threshold. This value defines to what extent the program should keep the correlation result. A high correlation threshold value will leave only the vectors resulting from highly matched IWs, while other vectors with correlation value lower than the threshold will be interpolated by the surrounding values (replaced by the median value of the 8 neighbors). Typically, **the recommended correlation threshold is 0.6** (Q. Tseng, personal communication and (Martiel et al., 2015), above which the displacement between the IWs is considered to represent an actual bead displacement.

Finally, set the Regularization Factor for the FTTC. This factor can be viewed as a noise-smoothing parameter (Han et al., 2015). The degree of regularization must be carefully chosen such that it provides a balance between how well it fits the noise-distorted experimental displacement data (coming from erroneous PIV evaluations and/or effective experimental noise) and the overall magnitude of the traction forces. If the data is over-regularized, the stress field will become over-smoothed and the resolution of the recovered stress, both in direction and magnitude, will be lost. Alternatively, if the data is under-regularized, the program will overfit the noise in the displacement and will thus be a false representative of the traction forces. For our data, we tested a large number of possible values coherent with literature (references; starting with 0, as a reference, and then ranging from 10^{-12} to 10^{-7}). We found that a **regularization factor of $9e-10$** fits our data best, which corresponds well with the one used in (Tseng et al., 2012), upon which our codes are based.

RESOURCE AVAILABILITY

Lead contact

Further information and requests for resources and reagents should be directed to and will be fulfilled by the lead contact, Pierre-henri Puech (pierre-henri.puech@inserm.fr).

Materials availability

This study did not generate new unique reagents.

Data and code availability

Images and data sets used here can be obtained from the authors upon request.

Softwares can be obtained from online resources (for Fiji/ImageJ and Plugins, see text). Specific Fiji/ImageJ and Python codes can be found online on <https://github.com/phpuech/TFM> and <https://github.com/remyeltorro/SPTAlign>

SUPPLEMENTAL INFORMATION

Supplemental information can be found online at <https://doi.org/10.1016/j.xpro.2022.101133>.

Method Video S1. **The first 25 min of a PBMC interacting with a very soft anti-CD3 coated PAG**, related to the expected outcome section. The movie is 1 frame every 5 sec.

Method Video S2. **The displacement of fluorescent beads inside a 400 Pa PAG with the corresponding vector maps of bead displacement and gaussian smoothed maps of stress norms**, related to part 3 step 4. The movie is 1 frame every 5 sec.

ACKNOWLEDGMENTS

The authors thank the INSERM Cell Culture Facility (PCC). Part of this work was supported by institutional grants from INSERM, CNRS, and Aix-Marseille University to the LAI and CINAM. F.M. was supported by a PhD grant from the European Union's Horizon 2020 research and innovation program under the Marie Skłodowska-Curie grant agreement No 713750, with the financial support of the Regional Council of Provence- Alpes-Co[^]te d'Azur and with of the A*MIDEX (n ANR- 11- IDEX-0001-02), funded by the Investissements d'Avenir project funded by the French Government, managed by the French National Research Agency (ANR). We thank Tseng for generously sharing his set of macros, under the form of a shared project in the frame of the CENTURI engineer platform (<https://centuri-livingsystems.org/multi-engineering-platform/>). The authors want to personally thank him for his dedication and help over the very troubled pandemic times.

AUTHOR CONTRIBUTIONS

F.M. did the experimental work, analyzed the data, and wrote the protocol. K.S. designed the study, performed some pilot experiments, and reviewed the protocol. P.H.P. led the experiments, implemented novel analysis, and reviewed the protocol.

DECLARATION OF INTERESTS

The authors declare no competing interests.

References

- Aramesh, M., Mergenthal, S., Issler, M., Plochberger, B., Weber, F., Qin, X.-H., Liska, R., Duda, G.N., Huppa, J.B., Ries, J., Schütz, G.J., Klotzsch, E., 2021. Functionalized Bead Assay to Measure Three-dimensional Traction Forces during T-cell Activation. *Nano Lett.* 21, 507–514. <https://doi.org/10.1021/acs.nanolett.0c03964>
- Butler, J.P., Tolić-Nørrelykke, I.M., Fabry, B., Fredberg, J.J., 2002. Traction fields, moments, and strain energy that cells exert on their surroundings. *Am. J. Physiol.-Cell Physiol.* 282, C595–C605. <https://doi.org/10.1152/ajpcell.00270.2001>
- Cazaux, S., Sadoun, A., Biarnes-Pelicot, M., Martinez, M., Obeid, S., Bongrand, P., Limozin, L., Puech, P.-H., 2016. Synchronizing atomic force microscopy force mode and fluorescence microscopy in real time for immune cell stimulation and activation studies. *Ultramicroscopy* 160, 168–181. <https://doi.org/10.1016/j.ultramic.2015.10.014>
- Dembo, M., Wang, Y.-L., 1999. Stresses at the Cell-to-Substrate Interface during Locomotion of Fibroblasts. *Biophys. J.* 76, 2307–2316. [https://doi.org/10.1016/S0006-3495\(99\)77386-8](https://doi.org/10.1016/S0006-3495(99)77386-8)
- González, C., Chames, P., Kerfelec, B., Baty, D., Robert, P., Limozin, L., 2019. Nanobody-CD16 Catch Bond Reveals NK Cell Mechanosensitivity. *Biophys. J.* 116, 1516–1526. <https://doi.org/10.1016/j.bpj.2019.03.012>
- Han, S.J., Oak, Y., Groisman, A., Danuser, G., 2015. Traction microscopy to identify force modulation in subresolution adhesions. *Nat. Methods* 12, 653–656. <https://doi.org/10.1038/nmeth.3430>
- Martiel, J.-L., Leal, A., Kurzawa, L., Balland, M., Wang, I., Vignaud, T., Tseng, Q., Théry, M., 2015. Measurement of cell traction forces with ImageJ, in: *Methods in Cell Biology*. Elsevier, pp. 269–287. <https://doi.org/10.1016/bs.mcb.2014.10.008>
- Sadoun, A., Biarnes-Pelicot, M., Ghesquiere-Dierickx, L., Wu, A., Théodoly, O., Limozin, L., Hamon, Y., Puech, P.-H., 2021. Controlling T cells spreading, mechanics and activation by micropatterning. *Sci. Rep.* 11, 6783. <https://doi.org/10.1038/s41598-021-86133-1>
- Schindelin, J., Arganda-Carreras, I., Frise, E., Kaynig, V., Longair, M., Pietzsch, T., Preibisch, S., Rueden, C., Saalfeld, S., Schmid, B., Tinevez, J.-Y., White, D.J., Hartenstein, V., Eliceiri, K., Tomancak, P., Cardona, A., 2012. Fiji: an open-source platform for biological-image analysis. *Nat. Methods* 9, 676–682. <https://doi.org/10.1038/nmeth.2019>
- Tinevez, J.-Y., Perry, N., Schindelin, J., Hoopes, G.M., Reynolds, G.D., Laplantine, E., Bednarek, S.Y., Shorte, S.L., Eliceiri, K.W., 2017. TrackMate: An open and extensible platform for single-particle tracking. *Methods* 115, 80–90. <https://doi.org/10.1016/j.ymeth.2016.09.016>
- Tse, J.R., Engler, A.J., 2010. Preparation of Hydrogel Substrates with Tunable Mechanical Properties. *Curr. Protoc. Cell Biol.* 47. <https://doi.org/10.1002/0471143030.cb1016s47>
- Tseng, Q., Duchemin-Pelletier, E., Deshiere, A., Balland, M., Guillou, H., Filhol, O., Thery, M., 2012. Spatial organization of the extracellular matrix regulates cell-cell junction positioning. *Proc. Natl. Acad. Sci.* 109, 1506–1511. <https://doi.org/10.1073/pnas.1106377109>

Cellular forces during early spreading of T lymphocytes on ultra-soft substrates

Farah Mustapha^{1,2,3,4,5}, Martine Pelicot-Biarnes^{1,2,3,4}, Remy Torro^{1,2,3,4,5}, Kheya Sengupta^{4,5,*}, Pierre-Henri Puech^{1,2,3,4,*}

Affiliations:

Laboratoire Adhésion et Inflammation (LAI)

¹ Aix Marseille University, LAI UM 61, Marseille, F-13288, France.

² Inserm, UMR_S 1067, Marseille, F-13288, France.

³ CNRS, UMR 7333, Marseille, F-13288, France.

CENTURI

⁴ Turing Center for Living systems, Marseille, France

Centre Interdisciplinaire de Nanoscience de Marseille (CINAM)

⁵ CNRS - AMU UMR 7325, Marseille, F-13288, France

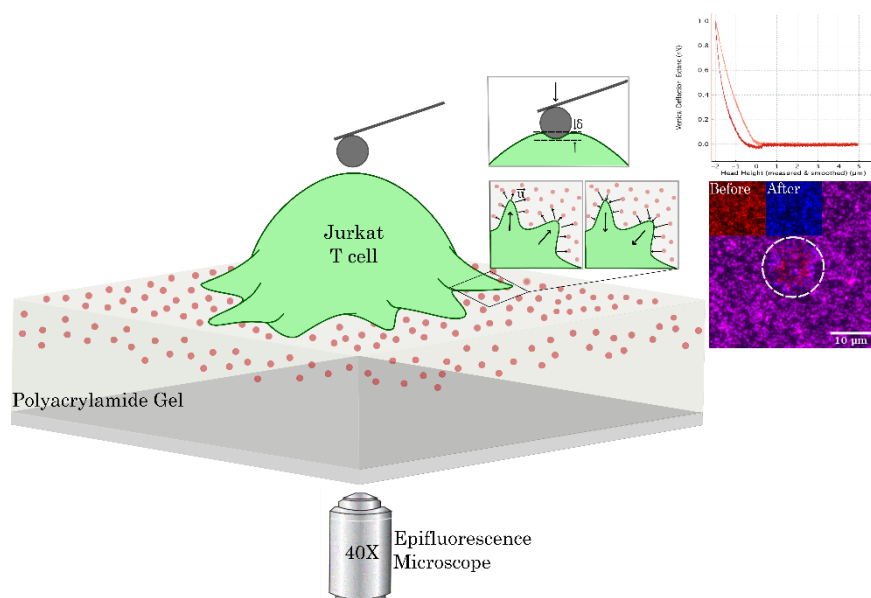
* To whom correspondence should be addressed:

sengupta@cinam.univ-mrs.fr; pierre-henri.puech@inserm.fr

Abstract:

T cells use forces to read out and act on the mechanical parameters of their microenvironment, which includes antigen presenting cells (APCs). Here we explore the early interaction of T cells with an APC-mimicking ultra-soft polymer gel exhibiting physiologically relevant stiffness in the range of 350-450 Pa. We quantify the dependence of cell spreading and stiffness on gel elasticity, and measure early time traction forces. We find that coating the surface with an antibody against the CD3 region of the TCR-complex elicits small but measurable gel deformation in the early recognition phase, which we quantify in terms of stress or energy. We show that the time evolution of the energy follows one of three distinct patterns: active fluctuation, intermittent, or sigmoidal signal. Addition of either anti-CD28 or anti-LFA1 has little impact on the total integrated energy or the maximum stress. However, the relative distribution of the energy patterns does depend on the additional ligands. Remarkably, the forces are centrifugal at very early times, and only later turn into classical in-ward pointing centripetal traction.

Keywords: T cell, Antigen presenting cells, ultra-soft polymer gel, traction forces, Early recognition



Introduction

T cells are activated when with the membrane bound T cell receptors (TCRs) recognize foreign antigenic peptides presented by the major histocompatibility complexes (pMHCs) of antigen presenting cells (APCs), within a small cell-cell contact area termed the immune synapse (IS) (Reichardt, Dornbach, and Gunzer 2010; Grakoui et al. 1999; Monks et al. 1998). This interaction bridges the innate and adaptive immune responses, as the activated T cells multiply and further differentiate, depending on their sub-type, into Cytotoxic T cells that directly kill virally infected cells and cancer cells, and Helper and Regulatory T cells that activate and tune the effector functions of other cells in the immune system. In either case, a given T cell has the formidable task of identifying a particular cognate pMHC against a very noisy environmental background of endogenous self-pMHCs, and to do so quite rapidly as to avoid any potential damage to healthy tissue. Today, an extensive body of research exists describing the biochemical signaling pathways triggered upon the pMHC-TCR interaction, however, further work is needed to unravel the precise mechanism(s) of T-cell activation (He and Bongrand 2012; Malissen and Bongrand 2015; Puech and Bongrand 2021). The formation of the IS is preceded by very dynamic processes whereby the T cell deforms and spreads over the surface of the APC, by extensively reorganizing its cytoskeleton. Such elegant observations were the first indication that physical forces may potentially play a critical role in T cell activation (B.-C. Chen et al. 2014).

Indeed, early work on tissular cells, such as fibroblasts, has demonstrated that individual cells do have the capacity to generate forces (Pelham and Wang 1997). Similar cells were shown to generate relatively large forces, transmitted through well-defined adhesion structures such as focal adhesions or focal complexes (B. Geiger and Bershadsky 2001; Solon et al. 2007; Engler et al. 2006; Elosegui-Artola et al. 2016). This body of work brought to light the relative roles of actin and myosin in force generation and transduction, as well as the existence of cross-talk with adhesion molecules, other mechanosensitive proteins and different

signaling pathways, making cell mechanobiology a complex corner-stone in understanding not only adhesion and migration but virtually all aspects of cellular physiopathology (Benjamin Geiger, Spatz, and Bershadsky 2009; Schwarz and Safran 2013; Janmey et al. 2009; Vogel and Sheetz 2006; Martino et al. 2018).

Immune cells on the other hand, including T cells, do not form focal-adhesion-like structures per se but do exert or feel forces during their physiological action. The forces exerted by these cells are expected to be comparatively feeble and less localized. Nevertheless, the ability of immune cells to generate and respond to forces is at the heart of their function in a variety of situations, ranging from phagocytosis (Herant 2006; Vorselen et al. 2020; 2021; Jaumouillé and Waterman 2020) and stop/go signal for migration (Jannat, Dembo, and Hammer 2011; S. H. J. Kim and Hammer 2021; Huse 2017), to antigen extraction and maturation by B cells (Spillane and Tolar 2018; Kumari et al. 2019) and early activation of T cells (Hu and Butte 2016; Thauland et al. 2017; Klotzsch and Schütz 2013; Y. Liu et al. 2016).

Indeed, recent studies have shown that T cells are not only sensitive, but also responsive, to forces acting at both the molecular and cellular scale (Huse 2017; Limozin and Puech 2019; Puech and Bongrand 2021).

At the molecular scale, the modification of the kinetics of the pMHC-TCR bond under force is thought to be implicated in its ability to distinguish different peptidic antigens (Limozin and Puech 2019; Y. Chen et al. 2017). Measuring single pMHC-TCR rupture forces using Atomic Force Microscopy did not reveal any strong differences upon peptide variation (Puech et al. 2011), however, Biomembrane Force Probe experiments did identify the bond lifetime as a potential key parameter in determining the outcome of the interaction (Ju et al. 2017). It has also been proposed that pMHC-TCR bond may function as a catch bond (B. Liu et al. 2014), whereby the lifetime of the bond is prolonged upon the application of physical force; nevertheless, this point, and in particular the origin of such a complex behavior, is still a matter of debate (Limozin et al. 2019; B. Liu, Kolawole, and Evavold 2021). Even more, the geometry of the applied force has also been investigated using Optical Tweezers and Micropipettes (S. T. Kim et al. 2012; 2009), and led to the proposal that its evaluation by the cell is another important modulator of recognition.

The importance of mechanics at the cell-scale has also been demonstrated (Judokusumo et al. 2012; O'Connor et al. 2012; Wahl et al. 2019; Hivroz and Saitakis 2016; Saitakis et al. 2017), and recently emphasized by showing that immune cells, in particular APCs, possess particular mechanical features that can be modulated as a function of the inflammatory conditions (Bufi et al. 2015), and that T cells are capable of probing and reacting to this modulation (Judokusumo et al. 2012; O'Connor et al. 2012; Wahl et al. 2019). Interestingly, T cells have also been shown to sense resistance to forces parallel to their membrane plane, thus being able to respond to ligand mobility (Dillard et al. 2014; Jankowska et al. 2018; Comrie, Babich, and Burkhardt 2015), as well as readily modulate their viscoelastic properties in response to specific signals at very short scales compared to the ones recorded for calcium fluxes, a hallmark of internal signal transduction (Zak et al. 2021).

Despite the highly detailed knowledge we have gathered thus far, it seems that the full description of cell-scale mechanosensitivity, as well as its link to molecular scales, is still far from being achieved. Clearly, an important aspect of understanding cell-scale mechanosensitivity is obtaining a reliable and early measurement of forces exerted by T cells when contacting a cognate surface. As mentioned above, T cells do not exhibit focal adhesion like structures, and moreover at short contact times, the traction forces applied by leukocytes in general, and T cells in particular, are expected to be comparatively low in magnitude and deployed on small, less defined, contact zones as compared to that of large fibroblasts or epithelial cells. From a physiological point of view, T cells are very reactive cells and may also exist in different initial states, ranging from naive to anergized (i.e. non-reactive state). This potentially leads to force amplitude and patterns that differ even within a given cell population. This in itself portrays a challenge for quantification, analysis, and interpretation, even in hybrid *in vitro* systems such as cells interacting with deformable gels.

Here we use well-characterized and reproducible ultra-soft polyacrylamide gels (PAGs) of variable elasticity (0.4-200kPa) to quantify the stresses exerted by T cells during their early spreading (first 15-30 minutes). We employ Traction force microscopy (TFM, (Style et al. 2014; Lekka et al. 2021)) to follow the dynamics, magnitude, and directionality of the stresses generated during the first minutes of T cell engagement with PAGs of stiffness similar to that of non-activated DCs and B cells, that is to say, about 400 Pa (Bufi et al. 2015). The cells are specifically engaged via the CD3 domain of the TCR complex, and/or the co-receptor CD28, and/or the T cell integrin LFA. To our knowledge, TFM at such a low elasticity and early interaction time is novel for T cells. We compare these results to those generated on stiffer, yet still biologically relevant, gels (≈ 2 kPa, similar to activated DCs and macrophages (Bufi et al. 2015)). Our dynamic force measurements reveal new patterns of force application over time, that are modulated as a function of substrate mechanics and functionalization, and that are also impacted by the genetic manipulation of cells to introduce fluorescent reporters at the membrane or in the cytoskeleton.

Results and discussion

1. Characterization of soft PAA gels with and without nano-beads

Our goal was to reach ultra-soft substrate rigidities compatible with the ones of physiological APCs (Bufi et al. 2015), laterally homogeneous on length scales similar to the T cell size, and in glass bottom petri dish compatible with our AFM setup and sample heating systems. We optimized the protocols readily available in literature, mainly focusing on that from (Tse and Engler 2010), to obtain thin, but thick enough, films of well-defined and reproducible rigidity (Mustapha, Sengupta, and Puech 2022). We systematically quantified the relative intra- and inter-gel variation of elasticities using AFM microindentation with soft AFM cantilevers, each decorated with a bead of a radius compatible to typical T cells size (~ 5 - $10\mu\text{m}$ in diameter, Fig. 1A,B).

On Fig.1, we present our measurement strategy. The typical measured thickness of the gels was $\sim 80\mu\text{m}$. Fig. 1C presents a typical force curve obtained while pushing (light red) then pulling (dark red) with the Hertz model fit superimposed (in green). Note that all data presented in Fig. 1C-E was obtained on bead-free gels. The pulling part of the curve shows that very little adhesion is present, allowing us to use a Hertz-like model on the pushing part for quantifying the Young modulus of the gel (the larger the Young modulus, the stiffer the gel). By laterally displacing the indenter, one can map the Young modulus to record the lateral homogeneity. Here we used beads of the same size as the T cells (5 to $10\mu\text{m}$ diameter) and a similar lateral spacing for the indentation zones (typically $8\mu\text{m}$). Such a map is shown on Fig1D for a 400Pa nominal rigidity gel. The maps revealed rather homogeneous elasticities, with a dispersion within a given gel being of the same order as the one in between samples (Fig.1E, insert is a zoom on 0.4kPa repeats). As such, using our refined protocol, we were able to produce gels with a very large range of well-defined and reproducible rigidities (nominal 0.4kPa - 200kPa), encompassing the reported range for macrophages and dendritic cells at different moments of the inflammatory process (0.4kPa - 4kPa , Fig. 1E). While cell spreading and cell elasticity measurements were done on the entire gel-elasticity range, we selected the softer gels corresponding to reported APC elasticities for TFM experiments. This also maximizes the displacement of reporter-nanobeads for feeble applied forces as expected for the early interaction of the cells with the gels (Kumari et al. 2019). We verified that these gels are elastic within our experimental margins (Suppl. Fig. 1).

Next, we characterized the very soft PAA gels when doped with fluorescent nanobeads. As reported before (Mustapha, Sengupta, and Puech 2022), a layer of nanobeads is formed close to each of the two interfaces of the gel (Fig. 1F). The typical position of the top layer, facing the cells, was found to be $\sim 2\mu\text{m}$ from the gel surface, allowing us to observe, at $40\times$, the nanobeads and the cells simultaneously. The density of nanobeads in the upper layer was observed to be fairly homogeneous (Fig 1G), and rather high, which is an advantage for performing TFM based on PIV analysis (see Material and Methods). Typically, we had four beads in an area of $2.5 \times 2.5 \mu\text{m}^2$ ($16 \times 16 \text{ px}^2$).

We observed an increase of the Young modulus of the doped gels by a factor ~ 2 , due to the presence of the nanobeads (Fig. 1I). Since the nanobeads were washed before inclusion in the gels, this could not be attributed to modification of gel chemistry by an agent in the bead solution. We therefore concluded that at the moderate indentation forces used here, we were probing a zone close to the one dense in beads, in the vertical 'z' direction. Since we expect similar forces and therefore similar probing of depth from the cells, this apparent value of Young modulus (400Pa) was used in the TFM calculations, instead of the nominal value for bead-less gels. In addition, we note that using unwashed nanobeads makes the gels less reproducible, and also usually produces softer gels (not shown). We attributed this to the presence of chemicals (in particular sodium azide for preventing bacterial growth) which most likely perturb the polymerization of PA. Interestingly, for the 2kPa gel, elasticity was only very weakly perturbed by the presence of the nanobeads (not shown).

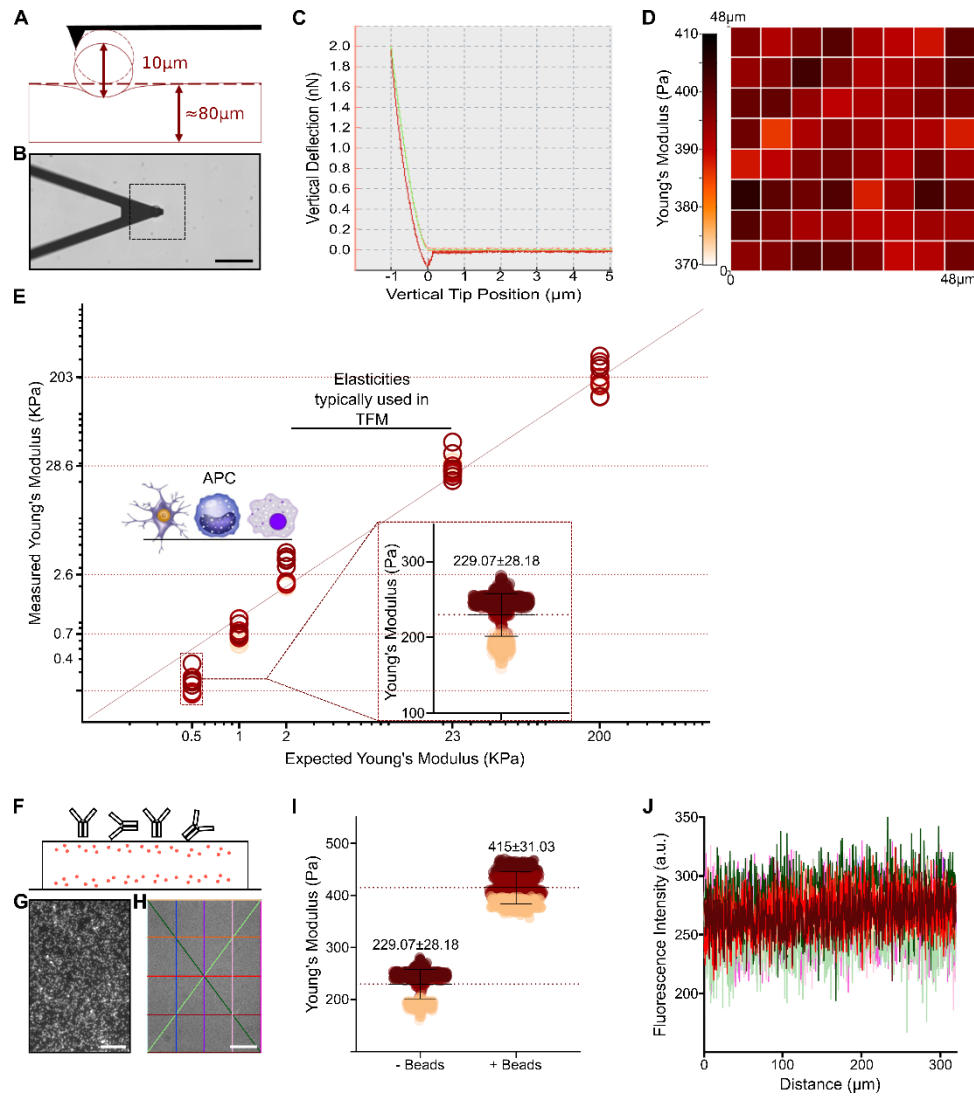


Fig. 1: Gel characterization using atomic force microscopy. A: Schematics of gel indentation using a bead modified AFM cantilever. B: Transmission micrograph showing the cantilever on the gel. C: Representative force vs. indentation curve (light red) with a Hertz-like adjustment (green). The retract curve (dark red) shows very little adhesive hysteresis. D: Representative map of the Young modulus, each pixel being of a size comparable to a T cell. E: Measured Young modulus vs. expected modulus from the gel composition (see Material and Methods) with the region of interest corresponding to APCs (Bufi et al. 2015) indicated together with the traditional range used in TFM; insert represents the dispersion between three gels obtained three different days. F: Schematic of the antibody decorated gels, doped with fluorescent nanobeads. Two layers are seen close to the two interfaces. G: Fluorescence image at the focus on the upper nanobeads layer (bar = 50 μm). H: Image taken from the upper substrate interface when coated with a fluorescent antibody (bar = 50 μm). I: Effect of the presence of the nanobeads on the apparent Young modulus of the softest gels. J: Intensity profiles of the image in H, color coded as the lines in H, showing the homogeneity of the fluorescence intensity in the image.

Covalent binding of fluorescent antibodies to the gels ensured a homogeneous lateral (x,y) coating (Fig. 1H and J). The measured fluorescent signal was confined to the surface,

indicating that the gels have negligible porosity. We subsequently quantified the amount of grafted antibodies using fluorescence microscopy following (Hornung et al. 2020) to be ~ 640 molecules/ μm^2 for a 2 hrs of incubation with a 30 $\mu\text{l/ml}$ solution of antibody (Suppl.Fig 1).

As a conclusion, we revealed that, for these very soft gels, the local elasticity in the vicinity of the surface is influenced by the presence of beads over the depths that are of the order of the ones probed by the stress generated by the cells. This again underlines that the impact of any reporter molecule or other object included in a mechanosensory study needs to be carefully investigated and reported, as we have previously shown for fluorescent calcium reporters (Cazaux et al. 2016; Sadoun et al. 2021).

2. Cell adhesion, spreading, and mechanics are modulated by PAA gels elasticity

To quantify the effect of substrate rigidity on cell spreading and mechanics, we seeded Lifeact-GFP transfected cells on nanobead-free gels of various rigidities, which were surface grafted with aCD3. The apparent spreading area of the cells was quantified, at a given time point, using fluorescence microscopy. In separate experiments, their young modulus was measured by indenting them with a moderate force by AFM, leading to depths of indentation $< 1 \mu\text{m}$, which represents $\sim < 10\%$ of cell diameter.

Fig.2A shows a sketch of the spreading experiments. The blue band depicts the depth at which we set the focus by detecting small defects or dust-particles on the gel surface by transmission microscopy. A typical cell fluorescence image is shown on Fig. 2B, after 20 min of sedimentation and contact. We made sure that the cells we evaluated were mostly adherent by gently tapping on the microscope base and observing their immobility. After image acquisition, we delineated using Fiji freehand selection tool, the contour of the cell to extract the apparent cell (contact) area (Fig. 2C). The measured area of the cells was widely distributed, and the median values were weakly, but significantly, dependent on substrate elasticity. We observed that the cells have a tendency to spread, on average, more on the softer, more physiological substrate. This observation is in good agreement with (Wahl et al. 2019). However, one should note that here we report the apparent area whereas it would be more rigorous to measure the contact area using a surface technique like reflection interference or total reflection microscopy (Wahl et al. 2019). However, PAA gels are not amenable to either technique, since their index is close to that of the medium, and they have a non-negligible thickness.

In separate experiments, the elasticity of the cells was measured after they interacted with a surface for 20 min. For the measurements, the AFM head has to be lowered towards the surface through the medium using stepper motors so that the cantilever can be close to the surface (Fig. 2D, E). The resultant mechanical perturbations lead to the lifting of almost all cells from the substrate for the softest gels. In this case, reproducible indentations were impossible to perform; cells appeared to slide away from the AFM cantilever bead tip and the indentation force curves looked distorted. We therefore cannot report a reliable value for this

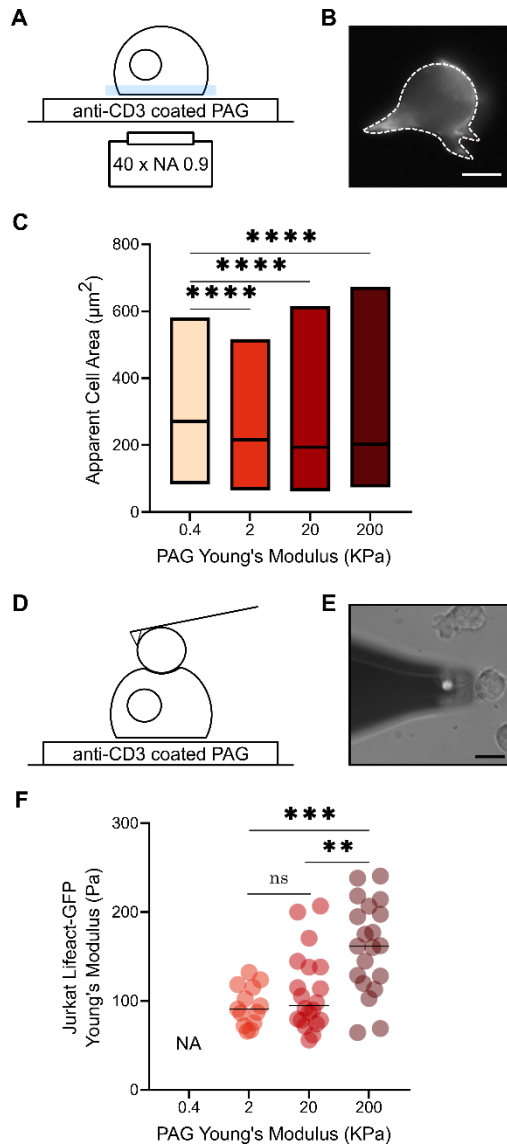


Fig. 2: T cell spreading on gels and mechanical properties A: Schematics of the spreading experiments on antiCD3 coated gels of variable rigidity, the colored zone indicates the zone on which the focus is made to measure the cell's apparent area. B: Micrographs of a Lyf-GFP cell showing the presence of cellular extensions. C: Quantification of the apparent area of cells on the different substrates. Please note that this area is *not* the contact area per se. Typically ~ 200 cells were used in total per case. D: Schematics of the AFM indentation experiments on cells adhered on similar substrates as for spreading experiments. E: Micrograph showing the bead (white round spot) glued on the cantilever (dark gray triangle) in close proximity to a cell. F: Young modulus measurements as a function of substrate rigidity. The Young modulus has not been measured faithfully on cells adhered on the softest substrate (see text) and led us to report a NA here. Typically, ~ 20 cells were used per condition.

case (Fig. 2F). In all the other cases, cells were not visibly perturbed by the approach of the AFM head, and the measured Young modulus is typical for Jurkat cell line and other lymphocytes (Cazaux et al. 2016; Sadoun et al. 2021; Zak et al. 2021). The value of the Young modulus does not show strong variation with substrate elasticity, except for the harder gels (Fig. 2F), which could indicate that the deformation of the gel under the cells can be neglected (Rheinlaender et al. 2020). The order of magnitude of the cell Young modulus, when spread on our aCD3 gels, should then be taken as the average of the ones measured over the two “softer” gels (namely 2 and 20 kPa here), leading to a value ~ 100 Pa. On the stiffer gels that do not mimic per se any relevant APC (Bufi et al. 2015), the situation of the spreading could be very different, similar to what we reported for the effect of relaxing any shape constraint (Sadoun et al. 2021). Nevertheless, one has to note that the order of magnitude of the Young modulus stays very close to the one usually reported as it is here (~ 100 Pa), far more than what has been reported to be measured using dynamic AFM modes (>10 kPa, (Jung et al. 2021)) which strengthen our conclusion above.

In the first part of this work, we produced well controlled PAA gels and laterally characterized their mechanical properties using indentation maps in AFM with moderate forces, on scales that are compatible with immune cell dimensions. These properties are homogeneous, tunable over a large range of elasticities, and down to physiological antigen presenting cell ones (Bufi et al. 2015). Such approaches are consistent with the work of others, on B lymphocytes and neutrophils in particular, in terms of gel or substrate elasticity (Kumari et al. 2019; 2020; Henry et al. 2015). Nevertheless, we used antibody-only substrate decorations, and softer substrates as compared to previous reports on Jurkat cells, where polylysine was used as an underlying layer, which likely increased the spreading of the cells via non-specific, charge-based interactions (Hui et al. 2015). By doing so, we were looking to compare situations where only specific signals, with a nonspecific interaction background as low and controlled as possible, were made available to the cells as in (Dillard et al. 2014; Wahl et al. 2019). As such, potential smaller spreading areas were expected, together with reduced stresses as when superimposed with nonspecific e.g. electrostatic interactions, since the PAA gels are intrinsically non-fouling substrates, i.e. essentially not adherent for cells in general, which applies to T cells (not shown here, but see below for IgG2a coated gels).

3. Early spreading on very soft gels reveals three distinct force application behavior

On Fig. 3A, we summarize our strategy for performing traction force microscopy with open-source tools (Mustapha, Sengupta, and Puech 2022). To capture the first moments of recognition, image acquisition is started before seeding cells, which allows us to use the first frame of our movies as a reliable reference for the unperturbed state of the nanobeads in the gel. Taking simultaneous images of the cells (fluorescence or transmission) and the nanobeads (fluorescence) (Fig 3B), we tracked the changes in the position of the nanobeads under a given cell. This was done by calculating the displacement of the beads at each time point using PIV (Fig. 3C, normalized). The first frame was used as a reference, and sample drift was quantified and compensated for. By applying FTTC, we were able to obtain maps of stress vectors, from which we plotted maps of stress-norms for given time points, in order to observe lateral distribution and magnitude of the stress (Fig. 3D). We summarized these series of snap-shots of stress maps into graphs that track, as a function of time, either the sum of the stress-norms over the whole image, (Fig. 3E top, 'stress-sum' in Pa), or the scalar product of the displacements and forces at each reconstituted pixel (Fig. 3E bottom, 'Energy' in J). The latter was offset to zero from a baseline, whose value appeared to be robust between experiments (not shown here), and was defined using the first few time points recorded before the arrival of a cell. In the following discussion, we shall focus on the time dependent evolution of the Energy (time-energy curves), and the peak value of the stress-sum (Max Stress Sum). The regularization factor, always required for TFM quantification, was optimized for our experiments (Suppl. Fig. 2) and set to the empirically obtained value of $9\text{E-}10$ (Mustapha, Sengupta, and Puech 2022), which is coherent with previous reports using the same data processing procedure (Tseng et al. 2012).

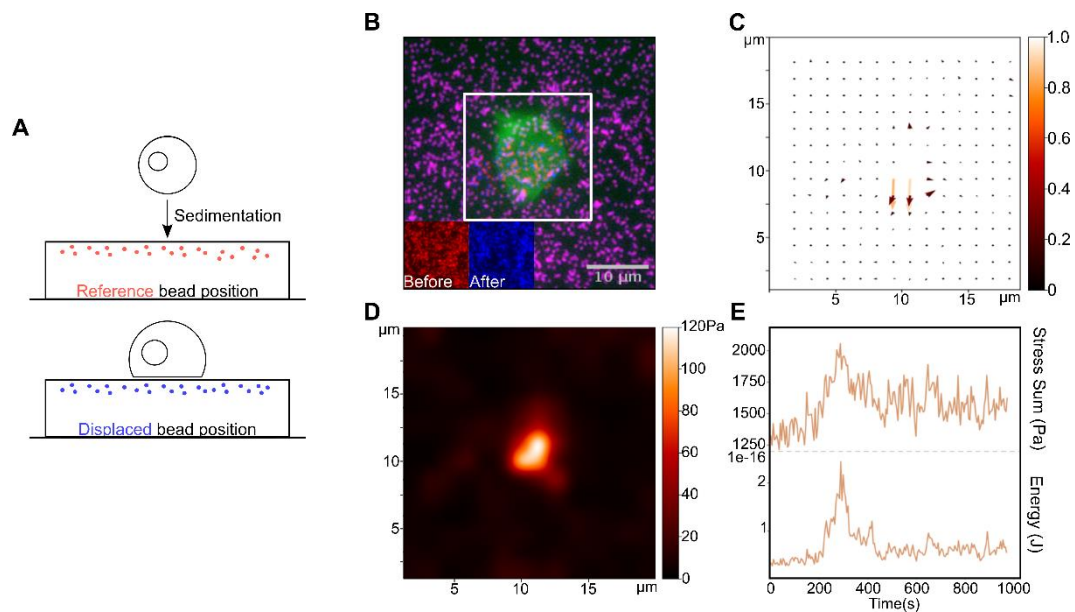


Fig. 3: Traction Force Microscopy. A: TFM experiment schematics, with the reference image taken before cell landing. B: Merged image of nanobeads (before displacement in cyan, after in blue) and of the cell sitting on the gel. C: Normalized map of PIV obtained from the nanobeads displacement. D: Stress norm map as calculated by FTTC with a regularization factor of $9\text{e-}10$. E: Typical curve of sum of stresses (bottom) and total stored energy (top) on the entire map vs. time during the early recognition of the substrate by the cell. Typically, the two curves have the same overall morphologies.

Experimentally, we first verified that no significant nanobead motion was detected on IgG2a (isotype control) coated gels. In contrast, all cells, with some rare exceptions, caused small but visible nanobead displacements when the substrate was coated with the activating antibody aCD3, which was used either alone, or with aCD28 against the coreceptor CD28 or with aCD11a that targets the integrin LFA1. This demonstrates that the cell-gel interaction is highly specific, and that no non-specific interaction occurs with the PAA, decorated or not with a non-relevant antibody.

Next, we focused on gels that were functionalized with aCD3. Interestingly, the time evolution of the energy shows three distinct and typical patterns (Fig. 4A). In the first case, which we call sigmoidal signal, the energy remains low for a whole and then jumps to a value whose magnitude is large compared to the small fluctuations visible before the arrival of the cell, and stays at this value during the remaining entire time (15 minutes) of experiment. In the second case, the energy slowly climbs to a high magnitude (comparable to sigmoidal signal) but then decreases again. We call this the intermittent signal. Finally, the third case is where the signal fluctuates around a low value which is nevertheless higher than the noise detected before arrival of cells (see below). We call this the active fluctuation case. To our knowledge, the time evolution of traction forces was never followed during early spreading events, especially for leukocytes, and such temporal patterns were never reported before.

The three types of time-energy profiles were seen also in cases where either aCD28 or aCD11a was present in addition to aCD3. However, in case of IgG2a, a small noisy fluctuating signal was obtained, which was indistinguishable from the noise before seeding of the cells.

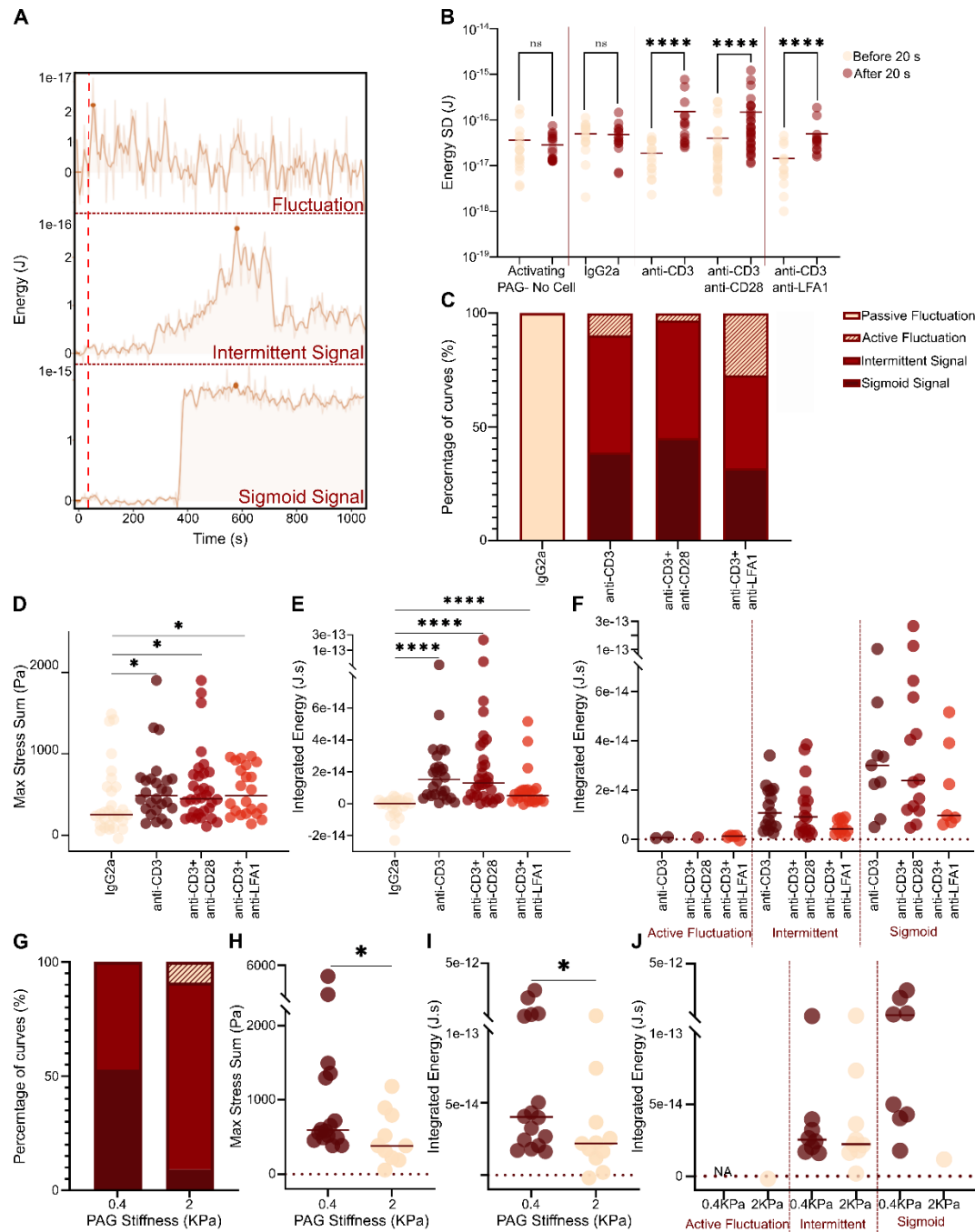


Fig. 4: Traction Force Microscopy of Lyf-GFP cells on different substrates. A: Three types of energy vs. time curves are typically observed, of very different morphologies (here with their baseline offset to zero after calculation before a 20 sec cut-off, red dashed line). B: Quantification of the SD of the fluctuating curves obtained for different coatings, at the very beginning of the experiments, where the cells are not exerting forces, and later, when they may do. This shows that fluctuating curves observed for bare or IgG2a coated substrates and aCD3 based ones are different, the latter exhibiting larger fluctuations of energy more likely due to cell interactions. C: Relative occurrence of the types of curves obtained in the different

situations with antibody decorated substrates. D: Pooled maximum of the sum of stresses as a function of substrate coating. E: Pooled integrated energy over the time of the experiment (15 min). F: Integrated energy as a function of curve type and substrate (same data as in E). G: Relative occurrence of energy curve morphology for the same cell preparations seeded on gels of two gels of different rigidities, coated with aCD3. Note the small variability of the relative proportions of events introduced by cell culture, compared with C. H: Pooled max stress sum and I: Pooled integrated energy for cells sitting on these gels. J: Same data as in I, separated by energy curve morphology and gel elasticity.

To ascertain the ‘active fluctuation’ case was indeed not noise, we analyzed the standard-deviation of the fluctuating energy curves obtained from under cells seeded on IgG2a and the aCD3 combinations and compared them to cell-free zones of aCD3 coated gels, since the last can be considered to be a robust readout of the noise level of the measurements. Interestingly, we observed that in the control case, as for IgG2a, the standard deviation did not vary between before cell seeding or after 20 sec of cell introduction, while it was significantly increased for the aCD3 combinations (Fig. 4B). The 20 sec time cut-off corresponds to the typical time needed for the cells to sediment on the gel. We can therefore distinguish the signal on IgG2a that we qualify as “passive noise” and the aCD3 combinations that we call “active fluctuations”, as stated above. The observation of only passive, noise-like fluctuations under cells on IgG2a confirms our previous conclusion that, as expected, no interaction occurs between the cell and the surface on the isotype control.

We note that the fluctuations we observed are reminiscent of the tiptoeing of cells above substrates before the cells make any decision to spread or not (Pierres et al. 2008; Brodovitch, Bongrand, and Pierres 2013). Unfortunately, due to the loss of lateral resolution imposed by the PIV/FTTC methodology, we could not resolve the real lateral size of the zones where these oscillations were present. Most likely, the active fluctuations could arise due to active dynamics of microvilli, the tip of which is meant to be a mechanosensitive probe of substrates (Brodovitch, Bongrand, and Pierres 2013) which can even penetrate the target cell to probe its mechanics while increasing the effective contact area of the functional structures (H.-R. Kim et al. 2018; Sage et al. 2012). Interestingly, the PIV movies of the 3 behaviors exhibited marked differences in the relative orientation and dynamics of the bead displacements (which will lead to the same behavior of the stress vectors after FTCC calculation. Interestingly, we observed vectors of small norms which orientation was randomly changing between frames for the fluctuating cases, outward vectors at the beginning of the intermittent cases that eventually cancel out after quickly pointing inward for only a few frames, and, for sigmoid cases, the vectors were pointing outward and stayed stable for the duration of the experiment (15 min) (not shown)).

Quantifying the occurrence of the three types of time-energy curves, we observed that the relative frequency of each type depends on the molecular coating of the gel (Fig. 4C). Intermittent and sigmoid signals, with large magnitude, dominate on aCD3 and aCD3/aCD28 coatings, whereas active fluctuations, of relatively smaller magnitude, are significantly present for the aCD3/aCD11a coating. As already mentioned, cells on IgG2a coating only presented very small magnitude, passive and noisy fluctuations.

Ignoring for the moment the various time-energy curve types, we pooled the entire population of cells for each antibody case. The Max Stress Sum (Fig. 4D) and the integrated energy (Fig. 4E) were, as expected, significantly higher for the aCD3 combinations than for the IgG2a control. Note that for the integrated energy, slightly negative values were sometimes obtained for the fluctuations (both passive and active) due to the baseline correction which did not take the slow decreases of the average signal observed on certain curves into account. Of note, we did not observe on the pooled populations (Fig. 4D, E) a strong dependence of either Max Stress Sum or integrated energy on the molecular details of the substrate for the activating substrates. Moreover, we observed that the time when the maximal force peak occurs was delayed for the aCD3 combinations compared to IgG2a (not shown), coherent with the typical times needed for the cells to be activated (Sadoun et al. 2021).

Intermittent signals were for each substrate, as expected, of lower integrated energy than for sigmoid ones, aCD3/aCD11a being the lowest, while aCD3 and aCD3/aCD28 were of a similar and higher magnitude. Nevertheless, for these latter, the medians showed the same tendency for the two substrate types, aCD3 being slightly higher than aCD3/aCD28. This not so strong role of aCD28 together with aCD3 is reminiscent of our recent observation that aCD28 did not strongly influence the spread area of the same cell line on soft substrates (Wahl et al. 2019), while it could be different for primary cells (Judokusumo et al. 2012).

As a consequence, we can hypothesize that the modulations we observed on the integrated energies when pooling the data for all curves is a combination of the magnitude of the TFM characteristic signals we detected and of the relative occurrence of the fluctuating vs. intermittent vs. sigmoid behaviors. We can therefore propose that the substrate type dictates not only the morphology but also the magnitude of the displacements and resulting stresses generated for the early recognition of a given substrate.

Our data, per se, do not push us to link the observed difference in both the relative fractions and integrated energies of the three energy morphologies with the cells being in different pre-activation states, since we used the Jurkat cell line as model T lymphocytes. It much more reveals the relative effects of substrate decoration on their early recognition by these cells. Aside, such variability of behavior has rarely, if ever, been reported in literature, but could be present in any TFM-like experiment when the processes are occurring early in the interaction with the substrates, followed over time and not at a single, later time point, which may complexify the description and understanding of the data.

We then compared in coupled experiments the behaviors of the same Lifeact cells on CD3 coated substrates with a Young modulus of $\sim 400\text{Pa}$ vs $\sim 2\text{kPa}$. Interestingly, we observed that the fraction of intermittent morphology was dominating the more rigid gel (Fig. 1G). Consequently, the pooled maximal stress sum and integrated energy were lower in this later case (Fig. 4H and I). The separation of the integrated energies per morphology is shown on Fig. 4J.

These observations underline the necessity of using very soft gels, and show why using typical “soft” gels in the range of 2-5kPa as for adherent cells is surely not optimal: the intermittent population may be missed depending on the moment where the exploration of the samples are performed, leading to the false impression that very little cells are indeed pulling / pushing on the gels, if any.

4. Stress vectors are initially pointing outwards while the cell spreads, then reverse their direction at longer time intervals

When extending the observation duration from 15 to 30 min, we observed that the cells may change their behavior over time. Below 15min, they mainly spread, and as consequence the beads below them displace outward (Suppl. Fig. 4A), the resulting stresses pointing also outwards (Suppl. Fig. 4B). The number of PIV calculated pixels exhibiting a displacement above the noise level detected outside the zone below the cells increased with the accumulated energy (Suppl. Fig. 4C). For longer times, cells start to pull, potentially retract, and bead displacements will point inward, with the resulting stress vectors pointing inwards. Eventually, as exemplified in Suppl. Fig. 4, the cell may stop interacting, or at least, to generate detectable beads motions. This is coherent with the observations made with soft micropillar experiments with different cellular systems (Bashour et al. 2014; Henry et al. 2015; Jin et al. 2019) and with micro-mechanical manipulations (Husson et al. 2011; Sawicka et al. 2017; Hu and Butte 2016; Thauland et al. 2017). Such a contraction at later times during a contact is reminiscent of typical observation for activating T cells: they stop migrating first, and then change shape by rounding while becoming polarized; when micro-manipulated against an activating bead or an AFM cantilever, they start to push, then pull on the object.

5. Fluorescent reporters may modulate TFM energy patterns

In the bulk of this study, Jurkat cells transfected with a cytoskeletal fluorescent reporter (Lifeact-GFP) were used. The use of fluorescent cells in TFM eases their detection and allows the use of multiband filter sets and diodes for changing the illumination without introducing any mechanical action on the microscope which may perturb the lateral/vertical position of the sample compared to the control image. However, though often these labelings are used as simple reporters, without verifying their impact on the biophysical or even biochemical properties of interest, they may in fact impact the final readout.

To assess the possible impact of using genetically modified cells, we compared the behavior of Jurkat WT (non-fluorescent, carrier cell line), Jurkat transfected with a membrane fluorescent construct (Lck-GFP) or with a cytoskeletal fluorescent construct (Lifeact-GFP, which had been used for the rest of our study). The cells were allowed to interact with aCD3 coated 400Pa PAA gels. The first observation was that the WT cells and the two modified cell lines exhibited the same type of shapes in energy vs. time curves. Nevertheless, their relative proportions varied depending on the cell type, from having the three populations in Jurkat Lck-GFP to only two in the Jurkat Lifeact-GFP and WT cases (Fig. 5A). Thus, in the

Lck-GFP case, the intermittent behavior dominates, while for WT it is the sigmoid one. The behavior of Lifeact-GFP cells is close to that of the WT.

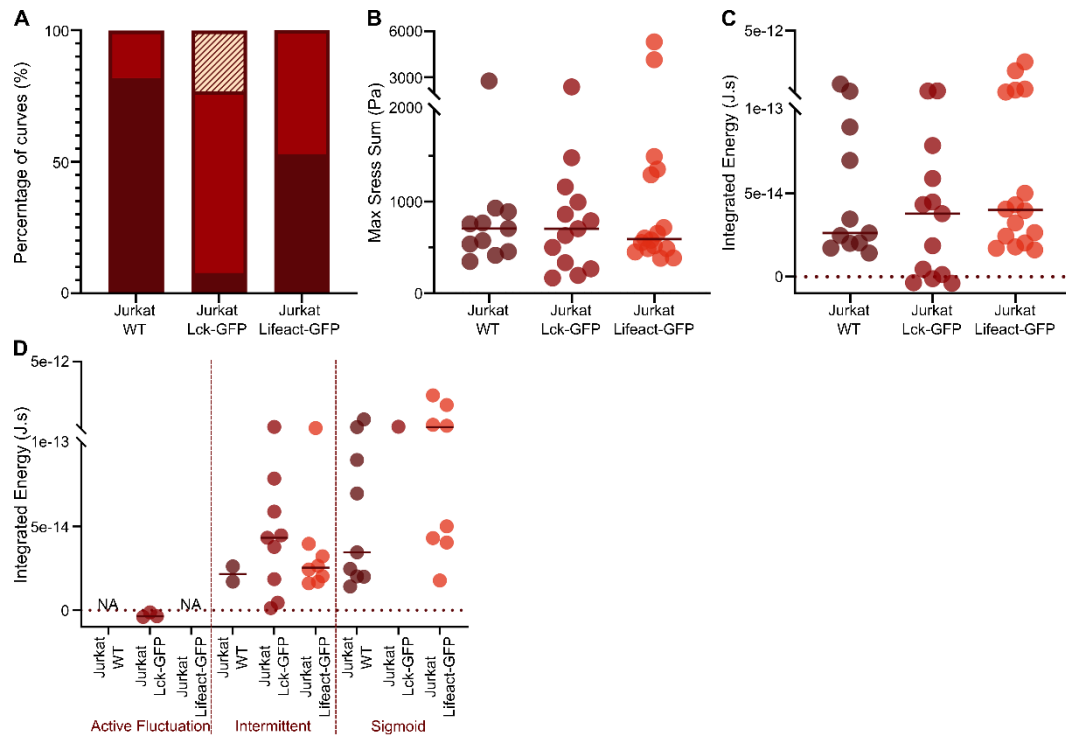


Fig. 5: Effect of transfection on the levels of stresses exerted by the cells on aCD3 coated gels. A: Quantification of the types of morphologies of energy curves. B: Pooled maximum of the sum of stresses and C: Pooled integrated energy as a function of the cell type. D: same data as in C, separated by energy curve morphology and cell type. Note that due to the coupling of experiments per cell culture lots, the data presented here for Lifeact-GFP cells is the same as in Fig. 4G to J.

Even if no significant difference is detected in either the pooled maximum stress (Fig. 5B) or integrated energy (Fig. 5C), trends do appear. The Lifeact-GFP variant does have a lower median value of maximal stress than that of the WT, coherent with the impact of intercalating a dye in the actin cytoskeleton, which may impair its capacity to exert local forces. Nevertheless, when considering the integrated energy, the signals which are present are more of a long-lasting morphology for the Lifeact-GFP, leading to larger values. Interestingly, the Lck-GFP variant, which is often used as a simple membrane reporter, appears to behave more like the WT case for the max stress sum, since its cytoskeleton is not affected by the labeling, but shows strong modulations of the energy signal morphologies, towards short lived or only fluctuating ones, and very few sustained, sigmoid signals : this results in a large dispersion of the energies, with very low values and very high ones.

The two variants then show a visible difference compared to WT cells. When separating the integrated energy along the different signal types, the spreading of the data leads us to conclude that for this parameter, the median data was not strongly influenced by the cell type, on aCD3 (Fig. 5D). As such, we may propose that the introduction of the fluorescent reporters may indeed have a subtle impact on the local capacities of cells to exert forces, but the major effect is on the capability to add up these forces to build up consequent

stress signals over an early time frame. The absence of fluctuating signals for Lifeact-GFP tagged cells in this set of data may indicate that they potentially cannot exert small forces, while for Lck-GFP cells, the membrane modification creates something unfavorable to large and long lasting signals (see Fig. 5D where intermittent low integrated energy cells are present, pointing towards the existence of short-lived transitory events).

As a matter of fact, the large dispersion we observe also underlines the possibility for the expression level of the two constructs to play a role on the stress levels and resulting morphologies of energy curves. Further experiments, eg. using scanning confocal microscopy to quantify the entire cell fluorescence level as a reporter of expression of a given reporter, together with obtaining sub populations with clearly separated fluorescence levels by cell sorting, will be needed to clarify that very precise point.

The fact that stresses and energies morphologies were modified for Lifeact-GFP cells as a comparison to WT cells, in our experiments, is well in line with the observations that Lifeact is not a simple reporter and that its expression can deeply affect the cell mechanics and biophysical responses as reported recently (Flores et al. 2019; Sliogeryte et al. 2016).

As a summary, we observed here the existence of differences in behavior due to labeling different compartments of the cells that have a strong implication either in cell contact to the substrate and its organization (the membrane), or the forces that can be exerted via ligand/receptor interactions (the actin cytoskeleton), pointing to the necessity of being careful when using labeled cells as surrogates of WT ones, in particular when performing single cell based biophysical assays. Again, as already discussed above, the introduction of a modification such as here the expression of a marker, which in many studies is thought to be benign and the modified cells considered to be faithful reporters of the WT cell line, may have profound effects in the case of mechano-transduction studies with very sensitive cells such as lymphocytes (Cazaux et al. 2016; Sadoun et al. 2021). As such, these modifications that are often used to observe cell position or shape may modify their initial state and initial response upon activation, as exemplified here with micromechanical measurements over time. Since we observe such effects on a cell line that is considered by many as a robust model for T cells, we raise the pitfall that such effects could be more important on primary cells, which may have a different, more subtle, activation history.

Conclusion

We presented traction force microscopy experiments with well-characterized, ultra-soft, poly acrylamide gels. Using open source software solutions, we quantified the early stresses that model T lymphocytes of the Jurkat cell line applied when interacting with aCD3, or aCD3 in combination with an antibody against a coreceptor (aCD28) or an adhesion molecule (aCD11a).

We observed that the patterns of time-evolution of stress and energy can be classified into three distinct categories, the frequency of each depends on the specific antibody or

antibodies used to coat the gel. One of these morphologies consists of enhanced fluctuations as compared to controls, reminiscent of cells tiptoeing on substrates before taking a decision to spread or not, as reported by others. The two other categories were an intermittent signal, which grows then disappears in the 15 min observation frame, and a sigmoid signal which, once started, lasts until the end of the experiment, the cell reaching a kind of steady state in stress application. Such observations of the cell early dynamics stress modulations have not been reported in the literature for T cells or, to our knowledge, any cell type with continuous gels.

The distribution of the categories as well as the magnitude of stress or energy are affected concomitantly by the molecular details of the coating of the gel surface. Also, we demonstrated that the ultra-soft gels we produced and characterized were needed to detect cellular action at early interaction times, in the frame of T cell activation; slightly stiffer gels resulted in mainly transient signals which are very prone to be missed by the experimentalist, depending on the time frame of the observation or the sensibility of the method in use.

When extending the observation windows to longer times, we observed that the stress vectors point outwardly when the cell spreads but often reverse direction at longer times, with the cells starting to pull on the substrate. This was coherent with reports on neutrophils on a bed of deformable nano-pillars by others (Henry et al. 2015).

Importantly, we observed modulations of the cellular behavior, in terms of time-energy morphologies as well as magnitudes, when using variants of the Jurkat cell line, expressing a membrane or cytoskeletal reporter. We highlighted the fact that such modifications may have a profound and crucial impact on cell mechanotransduction, in particular in the early moments of the cell's interaction with a target surface, potentially even more if it is a real APC, even if such cellular modifications are often thought to be benign and used to facilitate imaging of certain cellular compartments or organizations. Such a word of caution is, to our mind, crucial to be raised for the mechanobiology community, in an effort of openness and reproducibility of studies.

Overall, here we reveal that at early times, and on ultra-soft gels of physiological stiffness, spreading T cells exert stresses in centripetal, rather than centrifugal, direction, and that the resulting energies follow three distinct time patterns. Our results provide a new insight into early stages of mechanotransduction of lymphocytes.

Material and methods

Cell line, culture and modifications Human Jurkat T cells (clone E6-1, ATCC TIB-152), as a model for lymphocytes, were obtained from ATCC. Cells were counted and cultured three times a week, and their viability assessed by the use of Trypan Blue labeling. The cell culture medium (RPMI 1640) and complements (10% FBS, 1% Hepes 1M, 1% Glutamax, 1% Pen/Strep) were obtained from Gibco (Life technologies). Cells were monthly tested for the presence of mycoplasma.

Cell transfection & cytometry *LifeActGFP* transfected Jurkat was obtained in the following manner: Lentivirus expressing LifeAct-GFP were produced in HEK 293T cells by cotransfecting the lentiviral plasmids pLenti.PGK.LifeAct-GFP.W (a gift from Rusty Lansford, Addgene plasmid #51010; Watertown, MA) with psPAX2 and pMD2. G (a gift from Didier Trono, Addgene plasmid #12260 and #12259). Jurkat cells were transduced by spinoculation of virus using polybrene. The expression of LifeAct-GFP was controlled by flow cytometry using LSRFortessa X20 (BD Biosciences, Franklin Lakes, NJ). Cells expressing high levels of Life-Act GFP were sorted with BD FACSMelody cell sorter (BD Biosciences, Franklin Lakes, NJ).

Lck-GFP transfected Jurkat was obtained thus: Jurkat cells were electroporated with 1µg of DNA plasmid pcDNA3.1_mLck_GFP (produced in the lab, AM Lellouch) with Nucleofector 2b device (Lonza), and selected by antibiotic G418. The expression of Lck-GFP was controlled by flow cytometry using LSRFortessa X20 (BD Biosciences, Franklin Lakes, NJ). Cells expressing high levels of mLck-GFP were sorted with BD FACSMelody cell sorter (BD Biosciences, Franklin Lakes, NJ).

Fabrication and Functionalization of Polyacrylamide gels PAGs were casted between APTES/Glutaraldehyde treated glass-bottom petri dishes (FD35-100, World Precision Instruments) and cholo-silanized glass coverslips (12mm glass coverslips, Fischer Scientific). The detailed procedure can be found in a companion protocol (Mustapha, Sengupta, and Puech 2022). Hereafter, we give the main reactants and directions.

Solutions of acrylamide (40% wt/vol, A4058, Sigma) and N, N-methylene-bis-acrylamide (BIS, 2% wt/vol, M1533, Sigma) were mixed with PBS to obtain: (i) 3% acrylamide and 0.06% BIS (for a stiffness of 0.4 kPa), (ii) 3% acrylamide and 0.1% BIS (for a stiffness of 1 kPa), (iii) 4% acrylamide and 0.1% BIS (for a stiffness of 2 kPa), (iv) 10% acrylamide and 0.225% BIS (for a stiffness of 20 kPa), and (v) 10% acrylamide and 10% BIS (for a stiffness of 200 kPa). To these formulations, 0.7% of orange fluorescent beads (0.2µm, carboxylate modified, F8809, Thermo Fisher) was incorporated.

Crosslinking was initiated through the addition of 1% ammonium persulfate (A3678, Sigma) and 0.1% Tetramethylethylenediamine (T7024, Sigma). The entire assembly was then turned upside down (to allow the beads to move closer to the surface) and left to polymerize at 4°C. After 1hr, the petri dishes were immersed in PBS for 20 min and the top coverslips were carefully peeled off using a needle-tip.

The obtained gels were then stored overnight in PBS at 4°C and used the day after fabrication to ensure reproducible polymerization. The thickness of the obtained gels was measured to be typically $\approx 80 \mu\text{m}$, using a motorized inverted microscope.

Prior to experimentation, antibodies of choice were covalently attached to the surface of the gels using the photoactivatable heterobifunctional reagent sulfo-SANPAH (sulfosuccinimidyl 6 (4-azido-2-nitrophenyl-amino) hexanoate, 803332, Sigma). Briefly, the PBS was drained off the surface of the PAGs and 200 μl of sulfo-SANPAH (1 mM in 50 mM HEPES, pH 8.5) was applied. The surface of each gel was then exposed to a 365 nm UV radiation for 2min at 100% power in a UV-KUB 2 oven. The darkened sulfo-SANPAH solution was rinsed off using PBS and the photoactivation procedure was repeated a second time. Once the photoactivation was done, the gels were immediately incubated with anti-CD3 (OKT3, 14-0037-82, Thermo Fisher), anti-CD28 (14-0289-82, Thermo Fisher), anti-LFA-1 (14-0119-82, Thermo Fisher), anti-IgG2a (14-4724-85, Thermo Fisher) or a 1:1 combination of anti-CD3 and CD-28 or anti-CD3 and anti-LFA1-1, always to a final concentration of 30 $\mu\text{g}.\text{mL}^{-1}$ each and for 2hrs at room temperature. After 2hrs, the gels were rinsed 3 times with PBS and the petri dishes were transferred to the microscope holder, pre-heated to 37°C, for imaging.

Fluorescence quantification of antibody density Alexa Fluor 488 conjugated anti-human CD3 OKT3 (eBioscience by Thermo Fisher Scientific) antibody was used for the quantification of polyacrylamide gel coatings. A bulk calibration data was initially set up by measuring the fluorescence intensity of 41- μm -thick channels passivated with 1% Pluronic F127 (Sigma-Aldrich) and filled with antibody solutions at concentrations of 3.75, 7.5, 15, and 30 $\mu\text{g}.\text{mL}^{-1}$. In parallel, polyacrylamide gels were coated with 30 $\mu\text{g}.\text{mL}^{-1}$ of the anti-human CD3 OKT3 Alexa Fluor 488 antibody for 2 hrs at room temperature, and then imaged using the same microscope configuration as for the channels. Images were then analyzed by Fiji software and the average fluorescence intensity at three different positions was converted into surface density using the bulk calibration following (Hornung et al. 2020).

AFM set-up The set-up has been described in previous reports (Puech et al. 2011; Cazaux et al. 2016; Sadoun et al. 2021). It consists of an AFM head (Nanowizard I, JPK Instruments, Berlin) mounted on an inverted microscope (Zeiss Axiovert 200). The AFM head uses a 15 μm z-range linearized piezoelectric scanner for motion and an infrared laser for detection. The set-up sits on an active damping table (Halcyonics). AFM measurements were performed in closed loop, constant height feedback mode. Bruker MLCT-UC cantilevers, which are not gold coated, hence less sensitive to thermal drift (Cazaux et al. 2016) were used ; glass beads (5 μm or 10 μm in diameter, silica beads from Kisker Biotech GmbH, larger than cantilever tip) were glued at their extremity using micropipette micromanipulation and UV optical glue (OP-29, Dymax) cured in a UV oven (10 min at maximal power , BioForce Nanosciences). To reduce adhesion to the gels, decorated cantilevers were passivated with 2% Pluronic F127 (in Milli-Q water) for 30 min at 4°C. Alternatively to MLCT-UC, SAA-HPI cantilevers (6 μm in diameter) were used without passivation since they proved experimentally to have a very small adhesion to gels or cells (not shown). The sensitivity of the optical lever system was calibrated on a glass substrate, in PBS at 37°C temp, together with the cantilever spring constant (by using the thermal noise method (Butt and Jaschke 1995), using JPK SPM software routines

(JPK Instrument)) at the start of each experiment. The calibration procedure for each cantilever was repeated three times to rule out possible errors and spring constants were found to be consistently close to the manufacturer's nominal values.

The inverted microscope was equipped with 10x (used for laser alignment) and 40xNA0.9 (used for tip positioning and TFM measurements) objectives and a CoolSnap HQ2 camera (Photometrics). Bright field images were used to select the zone of interest on the gels. Images were obtained through either Zen software (Zeiss) or μ Manager (A. Edelstein et al. 2010; A. D. Edelstein et al. 2014). A Petri Dish Heater module (JPK Instruments) allows setting the temperature at the desired value, with a stability of a fraction of a degree over hours.

Gels and T cell mechanics using AFM First, the AFM cantilever bearing the bead was positioned above a selected region of the gel or on the center of an adhered cell. The maximal force to be applied was set at 2000pN for gels and 500 pN for cells (leading to indentation depths of the order of one μm for cells) using a contact duration of 0 sec. If not stated explicitly, the speed of pressing and pulling was $2\mu\text{m.s}^{-1}$, with an imposed maximal displacement of $7\mu\text{m}$. Then, either (i) a single force curve or a laterally resolved map (of $48 \times 48 \mu\text{m}^2 = 6 \times 6$ zones, each corresponding roughly to the size of a single T cell) was obtained and repeated on several zones of the gels (up to 5 maps at 5 locations for a given gel) or (ii) a single or up to 5 force curves were recorded for each adhered T cell tested. Data was typically recorded at 2048 Hz.

For determination of the Young modulus for T cells, each experimental force curve was examined by eye (to reject evident “bad” curves) and processed with the “Hertz model procedure” for a spherical tip included in JPK DP software (JPK Instruments), with the hypothesis that the cell behaves as an incompressible material ($\nu \sim 0.5$). Here, only a subset of the entire force span (from the baseline to the maximal contact force) was fitted: for cells we chose to fit over $0.5 \mu\text{m}$ of indentation to minimize contributions from the nucleus (Sadoun et al. 2021). Young modulus was found to be coherent with published ones for T cells specifically and immune cells in general (Cazaux et al. 2016; Zak et al. 2021; Sadoun et al. 2021; Bufi et al. 2015).

For the gels, the JPK-DP software was used to convert the (compressed) force curves to text files and remove bad curves as detected by the experimentalist eye if needed. They were then batch processed using an in-house Python script similar to JPK-DP fitting procedures. Young modulus maps are then rebuilt together with histograms. We verified that the values obtained by this method are in good agreement with the ones of the manual processing using JPK-DP (the difference was observed to be less than 2% in absolute value (not shown)).

For evaluating the visco-elasticity of the gels, experiments were performed with varying the speed of the indentation between 0.1 and $10 \mu\text{m.s}^{-1}$. It is expected that if the Young modulus is largely not dependent on speed, then the material can be considered as mainly elastic for the range of speeds/frequencies tested.

A median value per gel or cell was then calculated and tabulated in each condition. We validated this way of pooling the data experimentally since no obvious correlation between

the Young modulus and the force curve number (corresponding to the « mechanical history » of the cell or gel) was observed (not shown).

All experiments were performed at 37°C.

T cell spreading experiments After the gels were fabricated and functionalized as described above, they were then transferred to the pre-heated epi-fluorescence microscope (described below) and left to equilibrate at 37°C for approximately 20 min before the Jurkat Lifeact-GFP cells were added. The cells were left to interact with the gels for 20 min before image acquisition started. The system was focused just above the gel surface (Fig. 2A). The images were captured through Zen software (Zeiss), and the imaging parameters were set to 25% excitation power, 100 ms exposure time for the GFP-labeled cells (488 nm). The obtained images were processed using Fiji/ImageJ (Schindelin et al. 2012), as shown on Fig. 2B, by delineating the contour of the cells to quantify the apparent cell area.

TFM set-up and experiments The optical microscope set-up described above (for the AFM) was used, with a 40xNA0.9 air objective and a CoolSnap HQ2 camera (Photometrics). The microscope was also equipped with a LED illumination system (Colibri 2, Zeiss) and suitable filter sets (Cazaux et al. 2016) for fluorescence imaging, as well as the Petri Dish Heater module (JPK Instruments) for experimentation at 37°C. To measure the traction forces generated by Jurkat T cells, movies of live cells and fluorescent beads were acquired typically every 5 sec during T cell spreading for 15min in phase contrast for the WT Jurkat T cells, in the 488 nm channel for the GFP-labeled Jurkat T cells, and in the 555nm channel for the orange/red beads. For some movies, the duration was extended to 30min and/or the time between frames set to 2.5 sec.

The polyacrylamide gels were mounted on the microscope and left to equilibrate at 37°C for approximately 20min before the cells were added. Beads were brought into focus. Note that since the layer of microspheres is only a couple of microns beneath the gel surface (due to the flipping of the gel during the polymerization step above), the cells can still be easily seen and tracked while the focus is set on the bead layer. Image acquisition started a few seconds before cell addition, allowing us to obtain the relaxed state of the gel without the need for cell detachment using trypsin.

The movies were captured through Zen software (Zeiss), and the imaging parameters were set to: 20 ms exposure time for the non-labeled cells (phase contrast), 25% excitation power 100 ms exposure time for the GFP-labeled cells (488 nm), and 50% excitation power 200 ms exposure time for the orange beads (555 nm) (Cazaux et al. 2016).

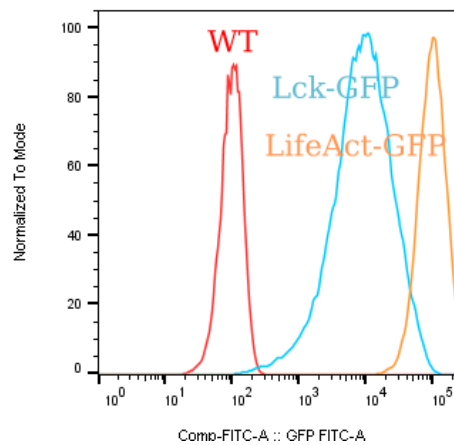
Traction Force Microscopy Image sequences of the fluorescent beads were first aligned to correct experimental drift by first extracting the trajectories of the beads on the full field images using the ImageJ “TrackMate” plugin, and then utilizing the obtained trajectories to align the images with the help of the following in-house Python 3.8 Jupyter Notebook <https://github.com/remyeltorro/SPTAlign>. 128x128 px² (equivalent to 20x20µm²) regions of interest were then selected and cropped out using ImageJ’s ROI 1-click tool and the MultiCrop macro (<https://github.com/phpuech/TFM>) respectively. The displacement fields

in the selected regions were subsequently calculated using the ImageJ “PIV” plugin (<https://sites.google.com/site/qingzongtseng/piv>; give the ref of the PNAS paper from QT), specifically the Advanced Iterative PIV option. The following parameters were set for the iterations: IW1= 64 SW1= 128 VS1= 32, IW2= 32 SW2= 64 VS2= 16, IW3= 16 SW3= 32 VS3= 8 (where IW: Interrogation window, SW: Search window, VS: Vector spacing) and a correlation threshold of 0.6. The resulting final grid size for the displacement field was $\sim 2.5 \times 2.5 \mu\text{m}^2$, with an average of four beads per interrogation window. Then the traction stress fields were reconstructed using the Fiji “FTTC” plugin (<https://sites.google.com/site/qingzongtseng/tfm>). The regularization parameter was set at 9×10^{-10} for all traction stress reconstructions. Since the ImageJ “PIV” and “FTTC” Plugins only process two images at a time and our experimental data consists of movies (made up of ≈ 200 frames), we wrote a function to consecutively run the two plugins over the full length image sequences of all the selected regions, always taking the first frame in each segment as the reference frame (<https://github.com/phpuech/TFM>). From this data, the sum of stress moduli, the stored energy as defined in (Butler et al. 2002) and the integrated energy over time (after a baseline correction for the beginning of the curve) were calculated and plotted using Python macros (<https://github.com/phpuech/TFM>). We described the entire detailed procedure in a recently published protocol (Mustapha, Sengupta, and Puech 2022).

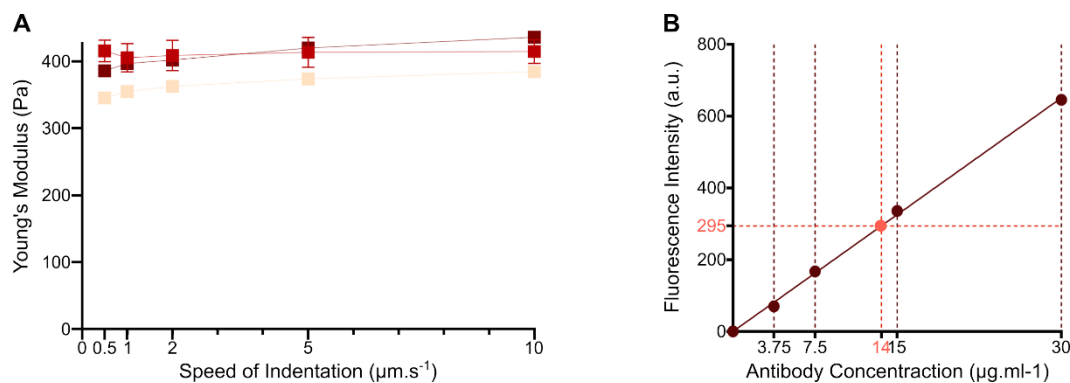
Data processing, visualization and statistics AFM data was processed partly using JPK-DP (JPK Instruments, Berlin) and partly using an in-house Python 3.8 set of functions to quantify and represent the Young modulus maps and distributions.

TFM movies were processed using a combination of Fiji/ImageJ (Schindelin et al. 2012) and in-house Python 3.8 functions. Alignment of images was performed using Trackmate (Tinevez et al. 2017) together with an in-house Python code, while PIV and FTTC calculations were performed using modified versions of Q. Tseng set of functions for FIJI/ImageJ (<https://sites.google.com/site/qingzongtseng/>; (Tseng et al. 2012)), with further plotting and calculations made using Python 3.8 homemade functions (<https://github.com/phpuech/TFM>). We used the Anaconda Python distribution (<https://www.anaconda.com/>), with the packages Seaborn, Matplotlib, Scipy, Numpy, Scikit as main dependencies. All data analysis was performed on Linux 64 bits machines.

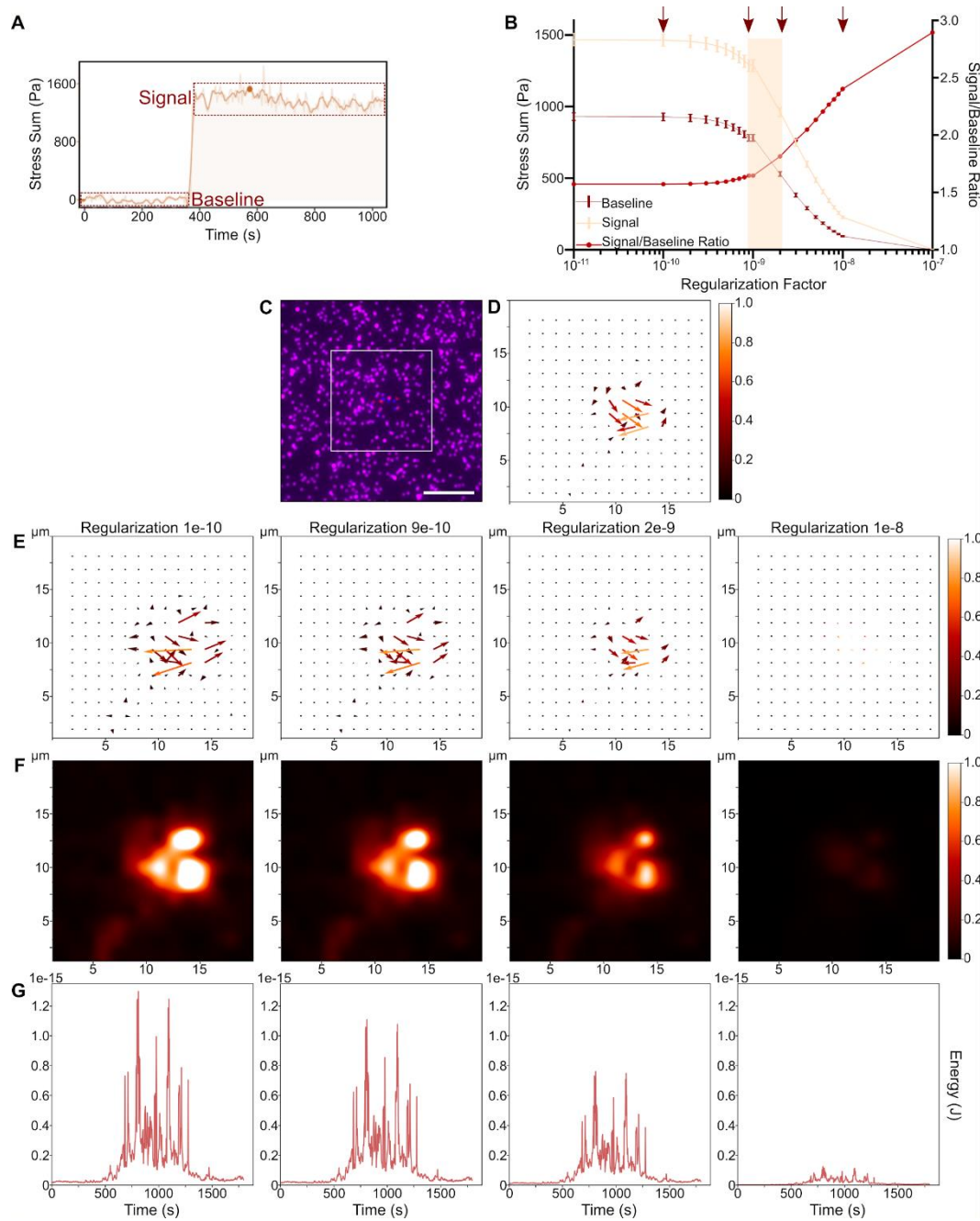
Data plotting and significance testing were performed on Linux or Windows 64 bits machines using Python, R and/or Graphpad Prism (6 or 7). We used nonparametric tests by default since our data was observed to be often largely distributed and not gaussian. If not stated otherwise, one data point corresponds to one measurement, that is, either one median value for a gel or a cell (AFM), or the one value calculated for a cell (spreading, TFM).



FigS1: Cytometry. Spectra for Jurkat WT, Lck-GFP (membrane labeling) and LifeAct-GFP (actin labeling) transfected Jurkat after cell sorting for high levels of expression post transfection.



FigS2: Gels mechanics and coating. A: Young moduli of the softest gels as a function of the indentation speed in the range accessible by classical AFM indentation on our set-up, with the same typical contact force (2 nN). No large variation is observed, pointing toward a rather elastic behavior. B: Calibration curve (see text and (Hornung et al. 2020)) that allows us to determine the average density of grafted antibodies from the intensities as measured in I. The red point corresponds to the average fluorescence intensity of the surface of the gel (>3 samples), which allows us to estimate the coating density reported in the main text.



FigS3: Optimization of the regularization parameter for FTTC. A: Type of data (Force vs. time) that was used to optimize the parameter, with the regions where baseline (noise) and signal were analyzed. B: Variation of the signal, noise and signal/noise as a function of the regularization factor. An evident change in intensity for both signals (decrease of the noise faster than the signal; increasing S/N) was observed around 10^{-9} . C: Beads images (overlay) and calculated PIV for a given time frame of a movie used for A, in the 'signal' zone. D: Reconstructed normalized force vector fields using FTTC and different regularization factors showing zones of interests. Left to right, as the regularization factor increases: decrease of the noise levels out of the higher signal zone, decrease of badly oriented force vectors, disappearance of bad vectors, loss of all signals. E: Energy values calculated vs. time for different regularization factors, showing the same patterns, but absolute levels decreasing as the regularization factor is increased. As a consequence, we choose to use the higher factor

before the transitions observed in A, namely 9×10^{-9} (Mustapha, Sengupta, and Puech 2022), which is consistent with values reported in the literature for similar cellular systems (B cells, (Kumari et al. 2020)) and by the published works of the developer of the FTTC Fiji plugin we used (Martiel et al. 2015; Tseng et al. 2012).

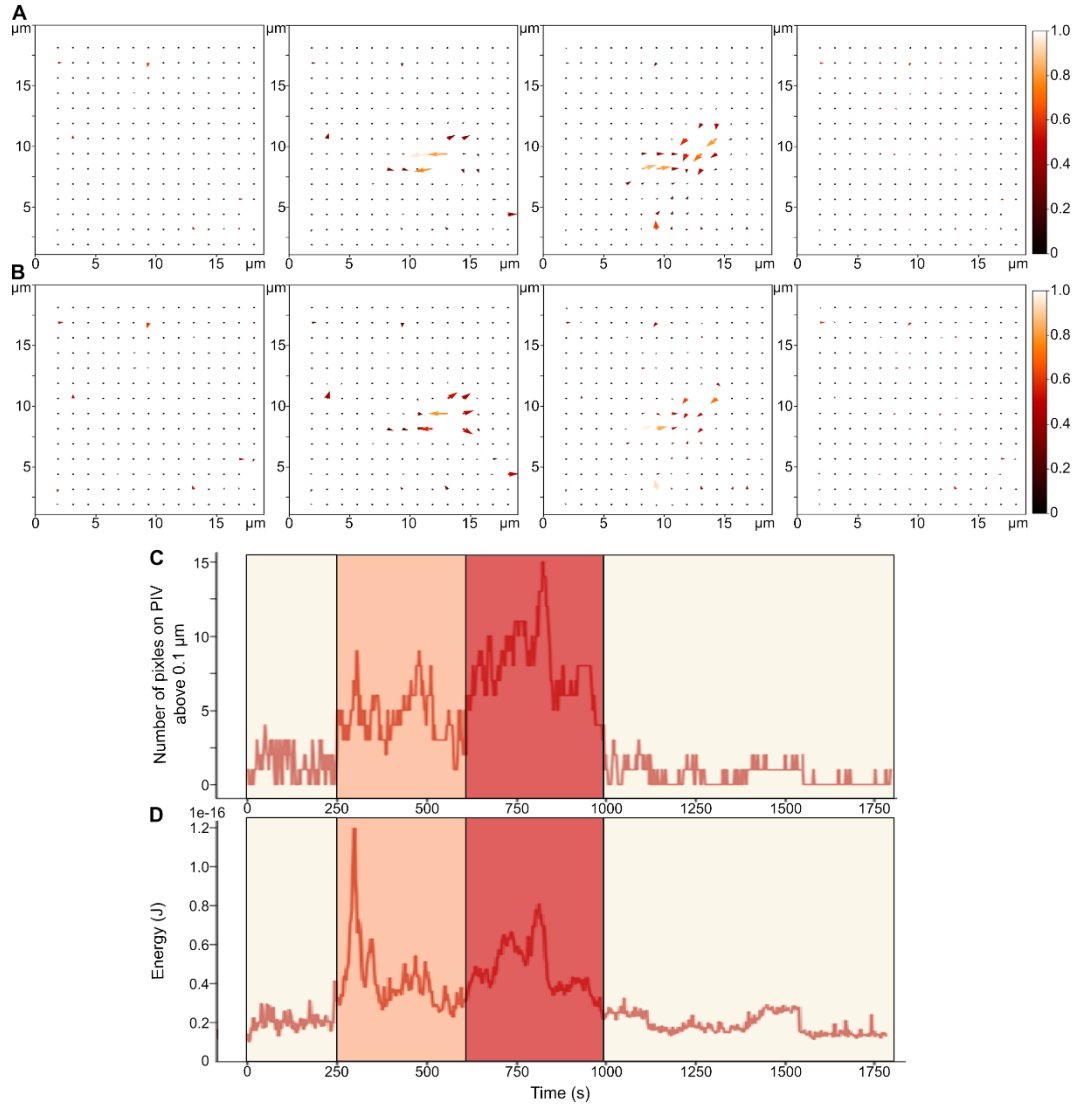


Fig. S4: From spreading to contracting. A: Normalized PIVs and B: Corresponding normalized stress maps for different times points, one for each colored zone in C (number of pixels having a displacement norm larger than the noise in the initial image, vs. time) and D (corresponding calculated energy vs time). The cell spreads first (outward arrows in the second columns of vector maps) then pulls on the gel (inward arrows on the third column). The number of apparent pixels on which noticeable stresses are occurring increase (light yellow, orange, red) then decreases (red, light yellow) as the cell detaches, the energy coming back to its initial level, and even less (the noise here almost canceled in the end, and the cell had move away from the zone, the system then behaving as a cell free system, see Fig. 4).

References

- Bashour, Keenan T, Jones Tsai, Keyue Shen, Joung-Hyun Lee, Eileen Sun, Michael C Milone, Michael L Dustin, and Lance C Kam. 2014. 'Cross Talk between CD3 and CD28 Is Spatially Modulated by Protein Lateral Mobility.' *Molecular and Cellular Biology* 34 (6): 955–64. <https://doi.org/10.1128/MCB.00842-13>.
- Brodoivitch, Alexandre, Pierre Bongrand, and Anne Pierres. 2013. 'T Lymphocytes Sense Antigens within Seconds and Make a Decision within One Minute'. *Journal of Immunology (Baltimore, Md.: 1950)* 191 (5): 2064–71. <https://doi.org/10.4049/jimmunol.1300523>.
- Bufl, Nathalie, Michael Saitakis, Stéphanie Dogniaux, Oscar Buschinger, Armelle Bohineust, Alain Richert, Mathieu Maurin, Claire Hivroz, and Atef Asnacios. 2015. 'Human Primary Immune Cells Exhibit Distinct Mechanical Properties That Are Modified by Inflammation'. *Biophysical Journal* 108 (9): 2181–90. <https://doi.org/10.1016/j.bpj.2015.03.047>.
- Butler, James P., Iva Marija Tolić-Nørrelykke, Ben Fabry, and Jeffrey J. Fredberg. 2002. 'Traction Fields, Moments, and Strain Energy That Cells Exert on Their Surroundings'. *American Journal of Physiology-Cell Physiology* 282 (3): C595–605. <https://doi.org/10.1152/ajpcell.00270.2001>.
- Butt, H.-J., and M. Jaschke. 1995. 'Calculation of Thermal Noise in Atomic Force Microscopy'. *Nanotechnology* 6 (1): 1. <https://doi.org/10.1088/0957-4484/6/1/001>.
- Cazaux, Séverine, Anaïs Sadoun, Martine Biarnes-Pelicot, Manuel Martinez, Sameh Obeid, Pierre Bongrand, Laurent Limozin, and Pierre-Henri Puech. 2016. 'Synchronizing Atomic Force Microscopy Force Mode and Fluorescence Microscopy in Real Time for Immune Cell Stimulation and Activation Studies'. *Ultramicroscopy* 160 (January): 168–81. <https://doi.org/10.1016/j.ultramic.2015.10.014>.
- Chen, Bi-Chang, Wesley R. Legant, Kai Wang, Lin Shao, Daniel E. Milkie, Michael W. Davidson, Chris Janetopoulos, et al. 2014. 'Lattice Light-Sheet Microscopy: Imaging Molecules to Embryos at High Spatiotemporal Resolution'. *Science* 346 (6208): 1257998. <https://doi.org/10.1126/science.1257998>.
- Chen, Yunfeng, Lining Ju, Muaz Rushdi, Chenchao Ge, and Cheng Zhu. 2017. 'Receptor-Mediated Cell Mechanosensing'. *Molecular Biology of the Cell* 28 (23): 3134–55. <https://doi.org/10.1091/mbc.E17-04-0228>.
- Comrie, William A., Alexander Babich, and Janis K. Burkhardt. 2015. 'F-Actin Flow Drives Affinity Maturation and Spatial Organization of LFA-1 at the Immunological Synapse'. *The Journal of Cell Biology* 208 (4): 475–91. <https://doi.org/10.1083/jcb.201406121>.
- Dillard, Pierre, Rajat Varma, Kheya Sengupta, and Laurent Limozin. 2014. 'Ligand-Mediated Friction Determines Morphodynamics of Spreading T Cells'. *Biophysical Journal* 107 (11): 2629–38. <https://doi.org/10.1016/j.bpj.2014.10.044>.
- Edelstein, Arthur, Nenad Amodaj, Karl Hoover, Ron Vale, and Nico Stuurman. 2010. 'Computer Control of Microscopes Using MManager'. *Current Protocols in Molecular Biology / Edited by Frederick M. Ausubel ... [et Al.]* Chapter 14 (October): Unit14.20. <https://doi.org/10.1002/0471142727.mb1420s92>.
- Edelstein, Arthur D., Mark A. Tsuchida, Nenad Amodaj, Henry Pinkard, Ronald D. Vale, and Nico Stuurman. 2014. 'Advanced Methods of Microscope Control Using MManager Software'. *Journal of Biological Methods* 1 (2): e10. <https://doi.org/10.14440/jbm.2014.36>.
- Elosegui-Artola, Alberto, Roger Oriá, Yunfeng Chen, Anita Kosmalska, Carlos Pérez-González, Natalia Castro, Cheng Zhu, Xavier Trepát, and Pere Roca-Cusachs. 2016.

- 'Mechanical Regulation of a Molecular Clutch Defines Force Transmission and Transduction in Response to Matrix Rigidity'. *Nature Cell Biology* 18 (5): 540–48. <https://doi.org/10.1038/ncb3336>.
- Engler, Adam J., Shamik Sen, H. Lee Sweeney, and Dennis E. Discher. 2006. 'Matrix Elasticity Directs Stem Cell Lineage Specification'. *Cell* 126 (4): 677–89. <https://doi.org/10.1016/j.cell.2006.06.044>.
- Flores, Luis R., Michael C. Keeling, Xiaoli Zhang, Kristina Sliogeryte, and N ria Gavara. 2019. 'Lifeact-TagGFP2 Alters F-Actin Organization, Cellular Morphology and Biophysical Behaviour'. *Scientific Reports* 9 (1). <https://doi.org/10.1038/s41598-019-40092-w>.
- Geiger, B., and A. Bershadsky. 2001. 'Assembly and Mechanosensory Function of Focal Contacts.' *Curr Opin Cell Biol* 13 (5): 584–92.
- Geiger, Benjamin, Joachim P. Spatz, and Alexander D. Bershadsky. 2009. 'Environmental Sensing through Focal Adhesions'. *Nature Reviews Molecular Cell Biology* 10 (1): 21–33. <https://doi.org/10.1038/nrm2593>.
- Grakoui, A., S. K. Bromley, C. Sumen, M. M. Davis, A. S. Shaw, P. M. Allen, and M. L. Dustin. 1999. 'The Immunological Synapse: A Molecular Machine Controlling T Cell Activation.' *Science* 285 (5425): 221–27.
- He, Hai-Tao, and Pierre Bongrand. 2012. 'Membrane Dynamics Shape TCR-Generated Signaling'. *Frontiers in Immunology* 3: 90. <https://doi.org/10.3389/fimmu.2012.00090>.
- Henry, Steven J., Christopher S. Chen, John C. Crocker, and Daniel A. Hammer. 2015. 'Protrusive and Contractile Forces of Spreading Human Neutrophils'. *Biophysical Journal* 109 (4): 699–709. <https://doi.org/10.1016/j.bpj.2015.05.041>.
- Herant, M. 2006. 'Mechanics of Neutrophil Phagocytosis: Experiments and Quantitative Models'. *Journal of Cell Science* 119 (9): 1903–13. <https://doi.org/10.1242/jcs.02876>.
- Hivroz, Claire, and Michael Saitakis. 2016. 'Biophysical Aspects of T Lymphocyte Activation at the Immune Synapse'. *Frontiers in Immunology* 7 (February). <https://doi.org/10.3389/fimmu.2016.00046>.
- Hornung, Alexander, Thomas Sbarrato, Nicolas Garcia-Seyda, Laurene Aoun, Xuan Luo, Martine Biarnes-Pelicot, Olivier Theodoly, and Marie-Pierre Valignat. 2020. 'A Bistable Mechanism Mediated by Integrins Controls Mechanotaxis of Leukocytes'. *Biophysical Journal* 118 (3): 565–77. <https://doi.org/10.1016/j.bpj.2019.12.013>.
- Hu, Kenneth H., and Manish J. Butte. 2016. 'T Cell Activation Requires Force Generation'. *The Journal of Cell Biology* 213 (5): 535–42. <https://doi.org/10.1083/jcb.201511053>.
- Hui, King Lam, Lakshmi Balagopalan, Lawrence E. Samelson, and Arpita Upadhyaya. 2015. 'Cytoskeletal Forces during Signaling Activation in Jurkat T-Cells'. *Molecular Biology of the Cell* 26 (4): 685–95. <https://doi.org/10.1091/mbc.E14-03-0830>.
- Huse, Morgan. 2017. 'Mechanical Forces in the Immune System'. *Nature Reviews Immunology* 17 (11): 679–90. <https://doi.org/10.1038/nri.2017.74>.
- Husson, Julien, Karine Chemin, Armelle Bohineust, Claire Hivroz, and Nelly Henry. 2011. 'Force Generation upon T Cell Receptor Engagement'. Edited by Javed N. Agrewala. *PLoS ONE* 6 (5): e19680. <https://doi.org/10.1371/journal.pone.0019680>.
- Jankowska, Katarzyna I., Edward K. Williamson, Nathan H. Roy, Daniel Blumenthal, Vidhi Chandra, Tobias Baumgart, and Janis K. Burkhardt. 2018. 'Integrins Modulate T Cell Receptor Signaling by Constraining Actin Flow at the Immunological Synapse'. *Frontiers in Immunology* 9 (January). <https://doi.org/10.3389/fimmu.2018.00025>.

- Janmey, Paul A., Jessamine P. Winer, Maria E. Murray, and Qi Wen. 2009. 'The Hard Life of Soft Cells'. *Cell Motility and the Cytoskeleton* 66 (8): 597–605. <https://doi.org/10.1002/cm.20382>.
- Jannat, Risat A., Micah Dembo, and Daniel A. Hammer. 2011. 'Traction Forces of Neutrophils Migrating on Compliant Substrates'. *Biophysical Journal* 101 (3): 575–84. <https://doi.org/10.1016/j.bpj.2011.05.040>.
- Jaumouillé, Valentin, and Clare M. Waterman. 2020. 'Physical Constraints and Forces Involved in Phagocytosis'. *Frontiers in Immunology* 11. <https://doi.org/10.3389/fimmu.2020.01097>.
- Jin, Weiyang, Fella Tamzalit, Parthiv Kant Chaudhuri, Charles T. Black, Morgan Huse, and Lance C. Kam. 2019. 'T Cell Activation and Immune Synapse Organization Respond to the Microscale Mechanics of Structured Surfaces'. *Proceedings of the National Academy of Sciences* 116 (40): 19835–40. <https://doi.org/10.1073/pnas.1906986116>.
- Ju, Lining, Yunfeng Chen, Kaitao Li, Zhou Yuan, Baoyu Liu, Shaun P. Jackson, and Cheng Zhu. 2017. 'Dual Biomembrane Force Probe Enables Single-Cell Mechanical Analysis of Signal Crosstalk between Multiple Molecular Species'. *Scientific Reports* 7 (1). <https://doi.org/10.1038/s41598-017-13793-3>.
- Judokusumo, Edward, Erdem Tabdanov, Sudha Kumari, Michael L. Dustin, and Lance C. Kam. 2012. 'Mechanosensing in T Lymphocyte Activation'. *Biophysical Journal* 102 (2): L5–7. <https://doi.org/10.1016/j.bpj.2011.12.011>.
- Jung, Philipp, Xiangda Zhou, Sandra Iden, Markus Bischoff, and Bin Qu. 2021. 'T Cell Stiffness Is Enhanced upon Formation of Immunological Synapse'. *ELife* 10 (July): e66643. <https://doi.org/10.7554/eLife.66643>.
- Kim, Hye-Ran, YeVin Mun, Kyung-Sik Lee, Yoo-Jin Park, Jeong-Su Park, Jin-Hwa Park, Bu-Nam Jeon, et al. 2018. 'T Cell Microvilli Constitute Immunological Synaptosomes That Carry Messages to Antigen-Presenting Cells'. *Nature Communications* 9 (1). <https://doi.org/10.1038/s41467-018-06090-8>.
- Kim, Sarah Hyun Ji, and Daniel A. Hammer. 2021. 'Integrin Cross-Talk Modulates Stiffness-Independent Motility of CD4+ T Lymphocytes'. *Molecular Biology of the Cell* 32 (18): 1749–57. <https://doi.org/10.1091/mbc.E21-03-0131>.
- Kim, Sun Taek, Yongdae Shin, Kristine Brazin, Robert J. Mallis, Zhen-Yu J. Sun, Gerhard Wagner, Matthew J. Lang, and Ellis L. Reinherz. 2012. 'TCR Mechanobiology: Torques and Tunable Structures Linked to Early T Cell Signaling'. *Frontiers in Immunology* 3: 76. <https://doi.org/10.3389/fimmu.2012.00076>.
- Kim, Sun Taek, Koh Takeuchi, Zhen-Yu J. Sun, Maki Touma, Carlos E. Castro, Amr Fahmy, Matthew J. Lang, Gerhard Wagner, and Ellis L. Reinherz. 2009. 'The Alphabeta T Cell Receptor Is an Anisotropic Mechanosensor'. *J Biol Chem* 284 (45): 31028–37. <https://doi.org/10.1074/jbc.M109.052712>.
- Klotzsch, Enrico, and Gerhard J. Schütz. 2013. 'Improved Ligand Discrimination by Force-Induced Unbinding of the T Cell Receptor from Peptide-MHC'. *Biophysical Journal* 104 (8): 1670–75. <https://doi.org/10.1016/j.bpj.2013.03.023>.
- Kumari, Anita, Judith Pineau, Ana-Maria Lennon-Duménil, Martial Balland, and Paolo Pierobon. 2020. 'Traction Force Microscopy to Study B Lymphocyte Activation'. *JoVE (Journal of Visualized Experiments)*, no. 161 (July): e60947. <https://doi.org/10.3791/60947>.
- Kumari, Anita, Judith Pineau, Pablo J. Sáez, Mathieu Maurin, Danielle Lankar, Mabel San

- Roman, Katharina Hennig, et al. 2019. 'Actomyosin-Driven Force Patterning Controls Endocytosis at the Immune Synapse'. *Nature Communications* 10 (1): 2870. <https://doi.org/10.1038/s41467-019-10751-7>.
- Lekka, Małgorzata, Kajangi Gnanachandran, Andrzej Kubiak, Tomasz Zieliński, and Joanna Zemła. 2021. 'Traction Force Microscopy – Measuring the Forces Exerted by Cells'. *Micron* 150 (November): 103138. <https://doi.org/10.1016/j.micron.2021.103138>.
- Limozin, Laurent, Marcus Bridge, Pierre Bongrand, Omer Dushek, Philip Anton van der Merwe, and Philippe Robert. 2019. 'TCR-PMHC Kinetics under Force in a Cell-Free System Show No Intrinsic Catch Bond, but a Minimal Encounter Duration before Binding'. *Proceedings of the National Academy of Sciences of the United States of America* 116 (34): 16943–48. <https://doi.org/10.1073/pnas.1902141116>.
- Limozin, Laurent, and Pierre-Henri Puech. 2019. 'Membrane Organization and Physical Regulation of Lymphocyte Antigen Receptors: A Biophysicist's Perspective'. *The Journal of Membrane Biology* 252 (4–5): 397–412. <https://doi.org/10.1007/s00232-019-00085-2>.
- Liu, Baoyu, Wei Chen, Brian D. Evavold, and Cheng Zhu. 2014. 'Accumulation of Dynamic Catch Bonds between TCR and Agonist Peptide-MHC Triggers T Cell Signaling'. *Cell* 157 (2): 357–68. <https://doi.org/10.1016/j.cell.2014.02.053>.
- Liu, Baoyu, Elizabeth M. Kolawole, and Brian D. Evavold. 2021. 'Mechanobiology of T Cell Activation: To Catch a Bond'. *Annual Review of Cell and Developmental Biology* 37 (1): 65–87. <https://doi.org/10.1146/annurev-cellbio-120219-055100>.
- Liu, Yang, Lori Blanchfield, Victor Pui-Yan Ma, Rakieb Andargachew, Kornelia Galior, Zheng Liu, Brian Evavold, and Khalid Salaita. 2016. 'DNA-Based Nanoparticle Tension Sensors Reveal That T-Cell Receptors Transmit Defined PN Forces to Their Antigens for Enhanced Fidelity'. *Proceedings of the National Academy of Sciences* 113 (20): 5610–15. <https://doi.org/10.1073/pnas.1600163113>.
- Malissen, Bernard, and Pierre Bongrand. 2015. 'Early T Cell Activation: Integrating Biochemical, Structural, and Biophysical Cues'. *Annual Review of Immunology* 33 (1): 539–61. <https://doi.org/10.1146/annurev-immunol-032414-112158>.
- Martiel, Jean-Louis, Aldo Leal, Laetitia Kurzawa, Martial Balland, Irene Wang, Timothée Vignaud, Qingzong Tseng, and Manuel Théry. 2015. 'Measurement of Cell Traction Forces with ImageJ'. In *Methods in Cell Biology*, 125:269–87. Elsevier. <https://doi.org/10.1016/bs.mcb.2014.10.008>.
- Martino, Fabiana, Ana R. Perestrelo, Vladimír Vinarský, Stefania Pagliari, and Giancarlo Forte. 2018. 'Cellular Mechanotransduction: From Tension to Function'. *Frontiers in Physiology* 9. <https://www.frontiersin.org/article/10.3389/fphys.2018.00824>.
- Monks, Colin R. F., Benjamin A. Freiberg, Hannah Kupfer, Noah Sciaky, and Abraham Kupfer. 1998. 'Three-Dimensional Segregation of Supramolecular Activation Clusters in T Cells'. *Nature* 395 (6697): 82–86. <https://doi.org/10.1038/25764>.
- Mustapha, Farah, Kheya Sengupta, and Pierre-Henri Puech. 2022. 'Protocol for Measuring Weak Cellular Traction Forces Using Well-Controlled Ultra-Soft Polyacrylamide Gels'. *STAR Protocols* 3 (1): 101133. <https://doi.org/10.1016/j.xpro.2022.101133>.
- O'Connor, Roddy S, Xueli Hao, Keyue Shen, Keenan Bashour, Tatiana Akimova, Wayne W Hancock, Lance C Kam, and Michael C Milone. 2012. 'Substrate Rigidity Regulates Human T Cell Activation and Proliferation.' *Journal of Immunology (Baltimore, Md.: 1950)* 189 (3): 1330–39. <https://doi.org/10.4049/jimmunol.1102757>.

- Pelham, Robert J., and Yu-li Wang. 1997. 'Cell Locomotion and Focal Adhesions Are Regulated by Substrate Flexibility'. *Proceedings of the National Academy of Sciences* 94 (25): 13661–65. <https://doi.org/10.1073/pnas.94.25.13661>.
- Pierres, Anne, Anne-Marie Benoliel, Dominique Touchard, and Pierre Bongrand. 2008. 'How Cells Tiptoe on Adhesive Surfaces before Sticking.' *Biophysical Journal* 94 (10): 4114–22. <https://doi.org/10.1529/biophysj.107.125278>.
- Puech, Pierre-Henri, and Pierre Bongrand. 2021. 'Mechanotransduction as a Major Driver of Cell Behaviour: Mechanisms, and Relevance to Cell Organization and Future Research'. *Open Biology* 11 (11): 210256. <https://doi.org/10.1098/rsob.210256>.
- Puech, Pierre-Henri, Damien Nevoltris, Philippe Robert, Laurent Limozin, Claude Boyer, and Pierre Bongrand. 2011. 'Force Measurements of TCR/PMHC Recognition at T Cell Surface'. Edited by Daniel J. Muller. *PLoS ONE* 6 (7): e22344. <https://doi.org/10.1371/journal.pone.0022344>.
- Reichardt, Peter, Bastian Dornbach, and Matthias Gunzer. 2010. 'APC, T Cells, and the Immune Synapse'. *Current Topics in Microbiology and Immunology* 340: 229–49. https://doi.org/10.1007/978-3-642-03858-7_12.
- Rheinlaender, Johannes, Andrea Dimitracopoulos, Bernhard Wallmeyer, Nils M. Kronenberg, Kevin J. Chalut, Malte C. Gather, Timo Betz, Guillaume Charras, and Kristian Franze. 2020. 'Cortical Cell Stiffness Is Independent of Substrate Mechanics'. *Nature Materials* 19 (9): 1019–25. <https://doi.org/10.1038/s41563-020-0684-x>.
- Sadoun, Anaïs, Martine Biarnes-Pelicot, Laura Ghesquiere-Dierickx, Ambroise Wu, Olivier Théodoly, Laurent Limozin, Yannick Hamon, and Pierre-Henri Puech. 2021. 'Controlling T Cells Spreading, Mechanics and Activation by Micropatterning'. *Scientific Reports* 11 (1): 6783. <https://doi.org/10.1038/s41598-021-86133-1>.
- Sage, Peter T., Laya M. Varghese, Roberta Martinelli, Tracey E. Sciuto, Masataka Kamei, Ann M. Dvorak, Timothy A. Springer, Arlene H. Sharpe, and Christopher V. Carman. 2012. 'Antigen Recognition Is Facilitated by Invadosome-like Protrusions Formed by Memory/Effector T Cells'. *The Journal of Immunology* 188 (8): 3686–99. <https://doi.org/10.4049/jimmunol.1102594>.
- Saitakis, Michael, Stéphanie Dogniaux, Christel Goudot, Nathalie Bufi, Sophie Asnacios, Mathieu Maurin, Clotilde Randriamampita, Atef Asnacios, and Claire Hivroz. 2017. 'Different TCR-Induced T Lymphocyte Responses Are Potentiated by Stiffness with Variable Sensitivity'. *ELife* 6 (June). <https://doi.org/10.7554/eLife.23190>.
- Sawicka, Anna, Avin Babataheri, Stéphanie Dogniaux, Abdul I. Barakat, David Gonzalez-Rodriguez, Claire Hivroz, and Julien Husson. 2017. 'Micropipette Force Probe to Quantify Single-Cell Force Generation: Application to T-Cell Activation'. *Molecular Biology of the Cell* 28 (23): 3229–39. <https://doi.org/10.1091/mbc.E17-06-0385>.
- Schindelin, Johannes, Ignacio Arganda-Carreras, Erwin Frise, Verena Kaynig, Mark Longair, Tobias Pietzsch, Stephan Preibisch, et al. 2012. 'Fiji: An Open-Source Platform for Biological-Image Analysis'. *Nature Methods* 9 (7): 676–82. <https://doi.org/10.1038/nmeth.2019>.
- Schwarz, Ulrich S., and Samuel A. Safran. 2013. 'Physics of Adherent Cells'. *Reviews of Modern Physics* 85 (3): 1327–81. <https://doi.org/10.1103/RevModPhys.85.1327>.
- Sliogeryte, Kristina, Stephen D. Thorpe, Zhao Wang, Clare L. Thompson, Nuria Gavara, and Martin M. Knight. 2016. 'Differential Effects of LifeAct-GFP and Actin-GFP on Cell Mechanics Assessed Using Micropipette Aspiration'. *Journal of Biomechanics* 49 (2): 310–17.

<https://doi.org/10.1016/j.jbiomech.2015.12.034>.

Solon, Jérôme, Ilya Levental, Kheya Sengupta, Penelope C. Georges, and Paul A. Janmey. 2007. 'Fibroblast Adaptation and Stiffness Matching to Soft Elastic Substrates'. *Biophysical Journal* 93 (12): 4453–61. <https://doi.org/10.1529/biophysj.106.101386>.

Spillane, Katelyn M., and Pavel Tolar. 2018. 'Mechanics of Antigen Extraction in the B Cell Synapse'. *Molecular Immunology* 101 (September): 319–28. <https://doi.org/10.1016/j.molimm.2018.07.018>.

Style, Robert W., Rostislav Boltyskiy, Guy K. German, Callen Hyland, Christopher W. MacMinn, Aaron F. Mertz, Larry A. Wilen, Ye Xu, and Eric R. Dufresne. 2014. 'Traction Force Microscopy in Physics and Biology'. *Soft Matter* 10 (23): 4047–55. <https://doi.org/10.1039/C4SM00264D>.

Thauland, Timothy J., Kenneth H. Hu, Marc A. Bruce, and Manish J. Butte. 2017. 'Cytoskeletal Adaptivity Regulates T Cell Receptor Signaling'. *Science Signaling* 10 (469): eaah3737. <https://doi.org/10.1126/scisignal.aah3737>.

Tinevez, Jean-Yves, Nick Perry, Johannes Schindelin, Genevieve M. Hoopes, Gregory D. Reynolds, Emmanuel Laplantine, Sebastian Y. Bednarek, Spencer L. Shorte, and Kevin W. Eliceiri. 2017. 'TrackMate: An Open and Extensible Platform for Single-Particle Tracking'. *Methods (San Diego, Calif.)* 115 (February): 80–90. <https://doi.org/10.1016/j.ymeth.2016.09.016>.

Tse, Justin R., and Adam J. Engler. 2010. 'Preparation of Hydrogel Substrates with Tunable Mechanical Properties'. *Current Protocols in Cell Biology* 47 (1): 10.16.1–10.16.16. <https://doi.org/10.1002/0471143030.cb1016s47>.

Tseng, Qingzong, Eve Duchemin-Pelletier, Alexandre Deshiere, Martial Balland, Hervé Guillou, Odile Filhol, and Manuel Théry. 2012. 'Spatial Organization of the Extracellular Matrix Regulates Cell-Cell Junction Positioning.' *Proceedings of the National Academy of Sciences of the United States of America* 109 (5): 1506–11. <https://doi.org/10.1073/pnas.1106377109>.

Vogel, Viola, and Michael Sheetz. 2006. 'Local Force and Geometry Sensing Regulate Cell Functions'. *Nature Reviews Molecular Cell Biology* 7 (4): 265–75. <https://doi.org/10.1038/nrm1890>.

Vorselen, Daan, Sarah R Barger, Yifan Wang, Wei Cai, Julie A Theriot, Nils C Gauthier, and Mira Krendel. 2021. 'Phagocytic "Teeth" and Myosin-II "Jaw" Power Target Constriction during Phagocytosis'. Edited by Pekka Lappalainen, Suzanne R Pfeffer, Pekka Lappalainen, and Renaud Poincloux. *ELife* 10 (October): e68627. <https://doi.org/10.7554/eLife.68627>.

Vorselen, Daan, Yifan Wang, Miguel M. de Jesus, Pavak K. Shah, Matthew J. Footer, Morgan Huse, Wei Cai, and Julie A. Theriot. 2020. 'Microparticle Traction Force Microscopy Reveals Subcellular Force Exertion Patterns in Immune Cell–Target Interactions'. *Nature Communications* 11 (1). <https://doi.org/10.1038/s41467-019-13804-z>.

Wahl, Astrid, Céline Dinot, Pierre Dillard, Aya Nassereddine, Pierre-Henri Puech, Laurent Limozin, and Kheya Sengupta. 2019. 'Biphasic Mechanosensitivity of T Cell Receptor-Mediated Spreading of Lymphocytes'. *Proceedings of the National Academy of Sciences* 116 (13): 5908–13. <https://doi.org/10.1073/pnas.1811516116>.

Zak, Alexandra, Sara Violeta Merino-Cortés, Anaïs Sadoun, Farah Mustapha, Avin Babataheri, Stéphanie Dogniaux, Sophie Dupré-Crochet, et al. 2021. 'Rapid Viscoelastic Changes Are a Hallmark of Early Leukocyte Activation'. *Biophysical Journal* 120 (9): 1692–

1704. <https://doi.org/10.1016/j.bpj.2021.02.042>.

Rapid viscoelastic changes are a hallmark of early leukocyte activation

Alexandra Zak, Sara Violeta Merino-Cortés, Anaïs Sadoun, Farah Mustapha, Avin Babataheri, Stéphanie Dogniaux, Sophie Dupré-Crochet, Elodie Hudik, Hai-Tao He, Abdul I Barakat, Yolanda R Carrasco, Yannick Hamon, Pierre-Henri Puech, Claire Hivroz, Oliver Nüsse, Julien Husson

I participated in and coauthored the work that lead to the report (Zak et al. 2021) by making the measurement for the mechanical properties of the model APCs (COS7 cells), adhered on glass substrates the same way as they were adhered on the levers for the results of the main text, in order to answer to a referee question about the variation of these properties upon changing the presented peptide. These quantifications were made with AFM indentation either with a zero-contact time or with a non-null one to follow the force relaxation when the piezo position was kept constant. This allowed us to further propose that the origin of the relaxation modulations that were observed at the interface of T cell-model APC were mainly originating from the T cell, with little if no influence of the surrogate APC. I present the part concerning this data, sent to the referees and included in the supplementary data of the article.

Mechanics of COS-APC cells as a function of peptide loading

We performed additional experiments after COVID19 confinement to confirm our preliminary data about the relative mechanics of COS7-APC, with and without peptide, when adhered on a cantilever-like substrate.

To do so, we prepared COS-APC cells in 24 well plates and incubated them overnight in culture medium supplemented with 10 μ M HEL46.61 peptide or with carrier solution (PBS). We prepared glass bottom Petri dishes to mimic the adhesive levers by (i) plasma activating them for 1 min (ii) incubating them at 4°C with 0.25mg/mL of concanavalin A. Just before the experiment, the Petri dish was rinsed carefully with PBS, filled with HBSS/Hepes medium. Cells were trypsinized for 1 min at 37°C, then trypsin was inactivated using cell culture medium containing 10%FBS. The cells were then centrifuged and resuspended in HBSS/Hepes before seeding. They were left for \sim 30min to sediment and adhere at 37°C/5%CO₂ before mounting the Petri dish in the Petri dish Heater system (JPK Instrument).

This situation mimics the situation of the COS-APC cell on the lectin coated lever where they adhere and stay largely round for the time we use them in the Single Cell Force Spectroscopy experiment (see Suppl. Fig. S2a of the article).

MLCT-Bio levers (Bruker) were modified using a previously published process (Cazaux et al. 2016) in order to present a 2R=5 μ m bead at their extremity. Once mounted on the AFM head,

a lever was calibrated as stated in the main material and methods section in a clean Petri dish containing HBSS/Hepes at 37°C. We used the long triangular lever as in our cell-cell experiments, with a nominal spring constant of 10pN/nm. Force curves, together with transmission images of the tested cells, were gathered after exchanging the Petri dishes. The experiment was performed at 37°C and each Petri was used for no more than 1.5 hrs before exchange.

Force curve parameters were set as follows: contact force 500pN, speed to and from the contact 2μm/s, length of the force curve 7μm, duration of contact at constant height 0 sec (for Young modulus measurements) or 20 sec (for relaxation experiments). When the contact time was 0 sec, we gathered at least 5 curves per cell to obtain a median cellular value. For each cell, we positioned the bead over the center of the cell nucleus. For contact times of 20 sec, we performed only one relaxation experiment per cell, from which we extracted the Young modulus during the contact part of the curve, and the relaxation force vs. time.

We then fitted the force curves using a Hertz model over an indentation of ~1μm to stay in the lowest indentation range compared to bead radius and to be close to cell/cell contacts we present in the main body of this article. We measured 22 cells for each case and rejected curves as the ones where the Hertz model was not applicable (bad curves, bad fits in particular around the contact point). We obtained data for 21 cells for carrier experiment and 18 for peptide experiments. We obtained between 1 and 5 Young modulus values per cell and calculated the median value per cell when having more than one value. We removed one cell for the peptide case having a Young modulus of ~1.6kPa, hence being a clear outlier of the distribution, giving a total of 17 cells for that condition.

For relaxation data, we offsetted the data to a starting force of 500pN as prescribed by our protocol to take into account small variations in contact force due to slight slopes in the baseline of the force curves (the contact force is taken by the AFM as relative to the first points far from contact, before the starting of the motion). We then calculated the mean relaxation and SD over the 5 cells examined for each case and plotted the result as Force vs. time.

We then observe, as our preliminary experiments have shown to us, that no difference in the Young modulus (Fig1A) and in early relaxation pattern (for $t > 20$ sec, Fig1B) can be seen, hence suggesting that our observations from cell/cell experiments may originate mainly from modulations in T cell mechanics.

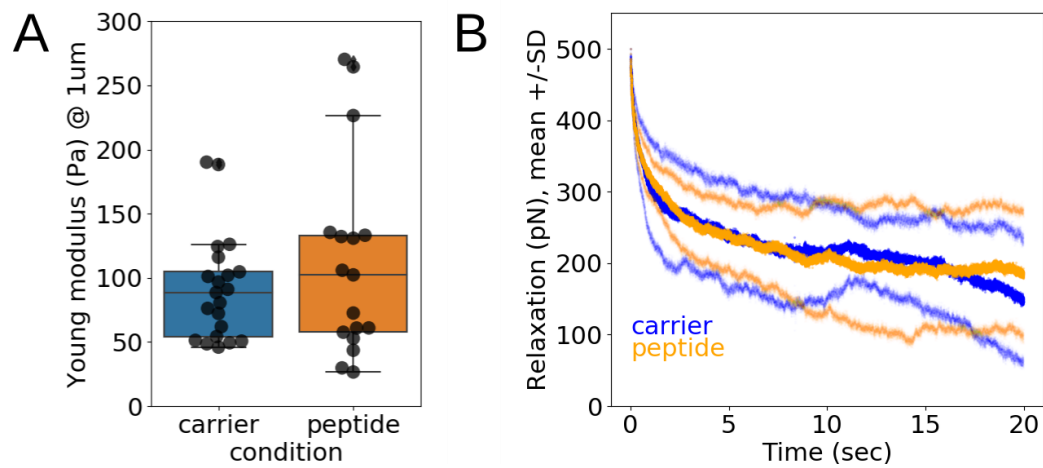


Fig.: Mechanical characterization of COS-APC cells following peptide or carrier incubation O/N with the peptide used in our study and same protocol. A. Young modulus measured for a maximal indentation depth of 1 µm. Each data point is the median value for a given cell (21 for carrier, 17 for peptide case) No significant difference is observed ($p=0.52$ Mann-Whitney test in GraphPad Prism). B. Mean \pm SD force during relaxation experiments in constant height force mode (5 cells per condition), similar to our cell-cell experiments. No difference is seen for the period 0–20 sec, the \pm SD being largely overlapping over the entire spread.

References

- Cazaux, Séverine, Anaïs Sadoun, Martine Biarnes-Pelicot, Manuel Martinez, Sameh Obeid, Pierre Bongrand, Laurent Limozin, and Pierre-Henri Puech. 2016. 'Synchronizing Atomic Force Microscopy Force Mode and Fluorescence Microscopy in Real Time for Immune Cell Stimulation and Activation Studies'. *Ultramicroscopy* 160 (January): 168–81. <https://doi.org/10.1016/j.ultramic.2015.10.014>.
- Dejardin, Marie-Julie, Arnaud Hemmerle, Anaïs Sadoun, Yannick Hamon, Pierre-Henri Puech, Kheya Sengupta, and Laurent Limozin. 2018. 'Lamellipod Reconstruction by Three-Dimensional Reflection Interference Contrast Nanoscopy (3D-RICN)'. *Nano Letters*, September. <https://doi.org/10.1021/acs.nanolett.8b03134>.
- Pérez-Calixto, Daniel, Samuel Amat-Shapiro, Diego Zamarrón-Hernández, Genaro Vázquez-Victorio, Pierre-Henri Puech, and Mathieu Hautefeuille. 2021. 'Determination by Relaxation Tests of the Mechanical Properties of Soft Polyacrylamide Gels Made for Mechanobiology Studies'. *Polymers* 13 (4): 629. <https://doi.org/10.3390/polym13040629>.
- Zak, Alexandra, Sara Violeta Merino-Cortés, Anaïs Sadoun, Farah Mustapha, Avin Babataheri, Stéphanie Dogniaux, Sophie Dupré-Crochet, et al. 2021. 'Rapid Viscoelastic Changes Are a Hallmark of Early Leukocyte Activation'. *Biophysical Journal* 120 (9): 1692–1704. <https://doi.org/10.1016/j.bpj.2021.02.042>.

Extension to human primary T cells: A preliminary study

Important limitations of the Jurkat T cell line

Most of our understanding of T cell signaling has been established from studies performed on E6.1 Jurkat T cells. Even today, numerous laboratories still employ these for experimentation. Jurkat T cells are thymocytically derived cells exhibiting the characteristics of immature thymocytes. The original Jurkat cells were obtained from a 14-year-old boy with T cell acute lymphoblastic leukemia (TALL), however, the Jurkat E6.1 subclone ('Jurkat, Clone E6-1 | ATCC' n.d.) was later developed in the 1980s (Bunnell et al. 2001). Over the years, the E6.1 cell line has proven to be extremely useful for several reasons. These include the existence of pre-established or newly developed mutant sublines, their relatively unchallenging genetic manipulation with the possibility of attaining high transfection rates, as well as their ease of growth and maintenance. Additionally, for cell mechanobiology studies, these cells undergo extensive spreading, in comparison to primary T cells (see for example (Brodovitch, Bongrand, and Pierres 2013) vs. (Brodovitch et al. 2015)), and display highly ordered cytoskeletal elements, which greatly facilitates the documentation of protein dynamics. For the aforementioned reasons, as well as the fact that using cell lines in general substantially reduces donor to donor variation and that the use of a specific cell line allows for an easier interpretation of different experiments using these cell lines, we have decided to employ first the Jurkat E6.1 subclone for the development of our TFM setup (see previous chapter).

However, the practicality of using these cells comes at a price; even if this cell line recapitulates some of the hallmark events of T cell activation, there still exists some essential differences between them and primary T cells: E6.1 cells lack the expression of PTEN (phosphatase and tensin homologue) and SHIP (SH2-domain-containing inositol polyphosphate 5' phosphatase), lipid phosphatases that regulate phosphoinositide-3 kinase (PI3K) function (a key molecular regulator of T cell differentiation (Han, Patterson, and Levings 2012)). More importantly, from a mechanobiology perspective, E6.1 do not express the force-sensing protein lymphocyte-specific Crk-associated substrate (Cas-L), that has been recently shown to mechanically link TCR MCs to the underlying actin network (Santos et al. 2016). Moreover, the F-actin protrusions that have been readily observed in primary T cells, and which are presumed to play an important role in TCR-pMHC interaction (Cai et al. 2017), have not been documented in Jurkat cells (Kumari et al. 2015). These genetic and morphologic distinctions most likely underline the differences found in IS architecture in Jurkat T cells in comparison to primary CD4⁺ T cells (Kumari et al. 2019).

All these concerns have led us, just like other T cell biologists (Chakraborty and Weiss 2014; Bartelt et al. 2009) to question the physiological relevance and implications of the data

that we have collected using Jurkat E6.1 T cells on primary T cell behavior. As such, we have decided to extend our experiments to human primary T cells. As this work is still in progress, we will present here only some of the preliminary data that we have collected thus far.

The present chapter contains its own material and methods section, mainly concerning the primary cell subtype preparation and sorting. For the gel preparation and data processing, the same methodology detailed in the previous chapters (Mustapha, Sengupta, and Puech 2022) has been employed for these experiments as well, and as such they will not be repeated here. However, it is important to mention that all data presented here is obtained using the ultra-soft polyacrylamide gel i.e. 400 Pa PAG functionalized only with the anti-CD3 antibody OKT3 (aCD3).

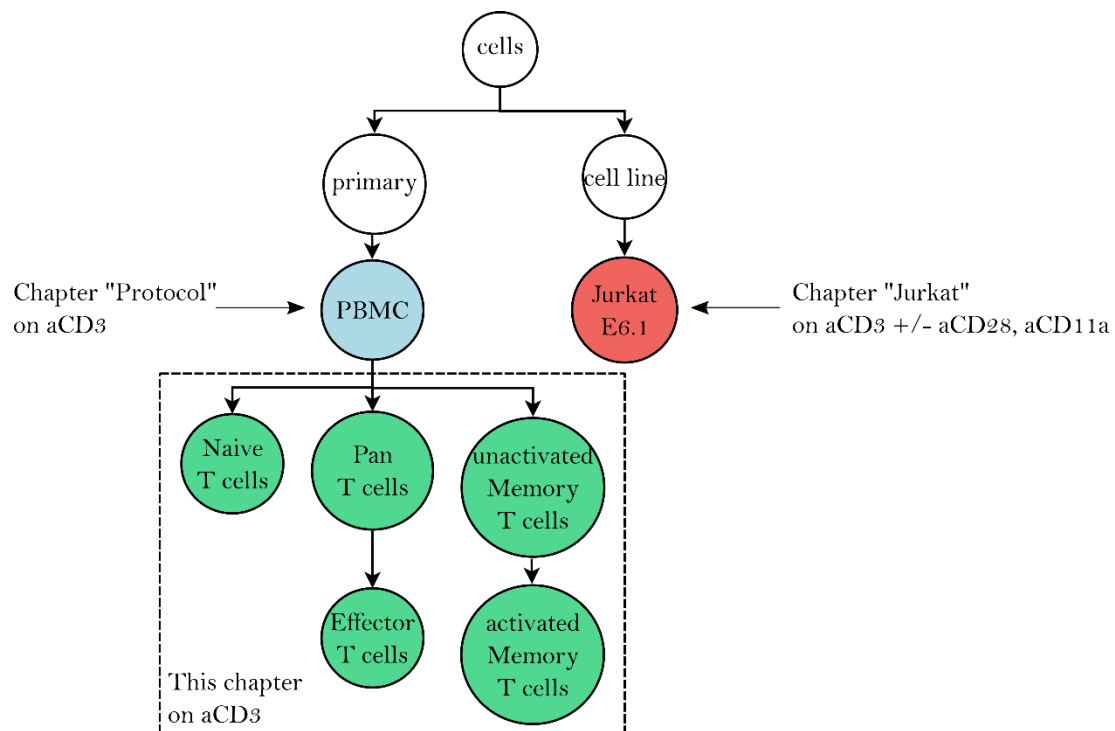


Fig. 1: Schematics of the different cell types and molecules that have been utilized in the traction force microscopy (TFM) experiments presented in this manuscript. Peripheral blood mononuclear cells (PBMCs) were used for the data presented with the main protocol in the previous chapter (Mustapha, Sengupta, and Puech 2022) and Jurkat T cells were used, with variants, in their dedicated chapter. Here, we will focus on the data acquired with subtypes of primary human T cells that have been sorted from blood bags.

Questions arising from our previous work

We kept in mind the following questions, when proceeding from the E6.1 Jurkat T cell line experiments to human primary T cell experiments:

- How do human primary T cells compare to the E6.1 Jurkat T cell line, which is, as we have mentioned before, often used as a bio-tool by biophysicists for prototyping mechanobiology experiments?
- Can our methodology reveal any differences concerning the intensity and dynamics of stress exertion for the different subtypes of primary T cells?
- If yes, who is pushing/pulling the most? The non/least (naive/unactivated memory T cells) or the most activated cells (effector/activated memory T cells)? Previously “trained” cells (memory T cells) or those who have never been activated (naive T cells)?

Cells and reagents

Blood from healthy volunteers was obtained through a formalized agreement with the French Blood Agency (Établissement Français du Sang, agreement 2017-7222), after receiving the informed consent of the donors, in accordance with the Declaration of Helsinki. All experiments were approved by the INSERM Institutional Review Board and the Ethics Committee.

Peripheral Blood Mononuclear Cells (PBMCs) were recovered from the interface of a Ficoll-Paque PLUS (GE Healthcare, Pittsburgh, PA) gradient. Unactivated Pan T cells were then isolated from PBMCs using a Pan T cell isolation Kit (Miltenyi Biotec, Bergisch Gladbach, Germany), and subsequently cultivated in Roswell Park Memorial Institute Medium (RPMI; Gibco by Thermo Fisher Scientific, Waltham, MA) 1640 supplemented with 25 mM GlutaMax (Gibco by Thermo Fisher Scientific, Waltham, MA) and 10% fetal calf serum (Gibco by Thermo Fisher Scientific, Waltham, MA) in a 37°C incubator with 5% CO₂, and used the day of isolation.

For obtaining effector T cells, freshly isolated Pan T cells were immediately activated using the antiCD3/antiCD28 T Cell TransAct™ (Miltenyi), according to manufacturer instructions. Cells were subsequently cultivated in RPMI (Gibco by Thermo Fisher Scientific, Waltham, MA) 1640 supplemented with 25 mM GlutaMax (Gibco by Thermo Fisher Scientific, Waltham, MA) and 10% FCS (Gibco by Thermo Fisher Scientific, Waltham, MA) at 37°C, 5% CO₂ in the presence of IL-2 (50 ng/ml; Miltenyi Biotec, Bergisch Gladbach, Germany), and used 5 days after activation. At the time of use, the cells were >99% positive for pan-T lymphocyte marker CD3 and assessed for activation and proliferation using CD25, CD45RO, CD45RA and CD69 makers, as judged by flow cytometry.

For obtaining memory T cells, CD45RA negative cells were purified from freshly isolated Pan T cells, and subsequently cultivated in RPMI (Gibco by Thermo Fisher Scientific, Waltham, MA) 1640 supplemented with 25 mM GlutaMax (Gibco by Thermo Fisher Scientific,

Waltham, MA) and 10% FCS (Gibco by Thermo Fisher Scientific, Waltham, MA) at 37°C, 5% CO₂, and used the day of isolation.

For obtaining activated memory T cells, isolated memory T cells were immediately activated using the antiCD3/antiCD28 T Cell Dynabeads (Thermo Fisher Scientific, Waltham, MA), according to manufacturer instructions. Cells were subsequently cultivated in RPMI (Gibco by Thermo Fisher Scientific, Waltham, MA) 1640 supplemented with 25 mM GlutaMax (Gibco by Thermo Fisher Scientific, Waltham, MA) and 10% FCS (Gibco by Thermo Fisher Scientific, Waltham, MA) at 37°C, 5%, and used 2 days after activation.

Naïve T cells were isolated using a Naive CD4+ T Cell Isolation Kit (Miltenyi Biotec, Bergisch Gladbach, Germany). Cells were subsequently cultivated in RPMI (Gibco by Thermo Fisher Scientific, Waltham, MA) 1640 supplemented with 25 mM GlutaMax (Gibco by Thermo Fisher Scientific, Waltham, MA) and 10% FCS (Gibco by Thermo Fisher Scientific, Waltham, MA) in a 37°C incubator with 5% CO₂, and used the day of isolation.

Results and discussion

As in our previous TFM experiments, we captured the first moments of the T cells landing and interacting with the aCD3-functionalized 400 Pa PAGs by starting image acquisition immediately before cell seeding. We tracked the displacement of the nanobeads under the cells (using PIV) by capturing consecutive fluorescence image sequences with similar frequencies as in previous experiments (1 frame every 5 seconds, \approx 15-minutes movies). The obtained bead displacement fields were then used for the reconstruction of the stress fields exerted by the cells at each time point (using FTTC).

This data was then used to plot graphs that show the evolution of either the “Stress Sum” (the sum of the stress-norms over the whole image, in Pa) or the “Energy” (the scalar product of the displacements and forces at each reconstituted pixel, in J) as a function of time (Fig.2). We then used the same quantification strategy for calculating the maximal stress sum and integrated energy as that presented in the previous chapters. We added the previous corresponding data (WT Jurkat on aCD3 400 Pa gels) for comparison.

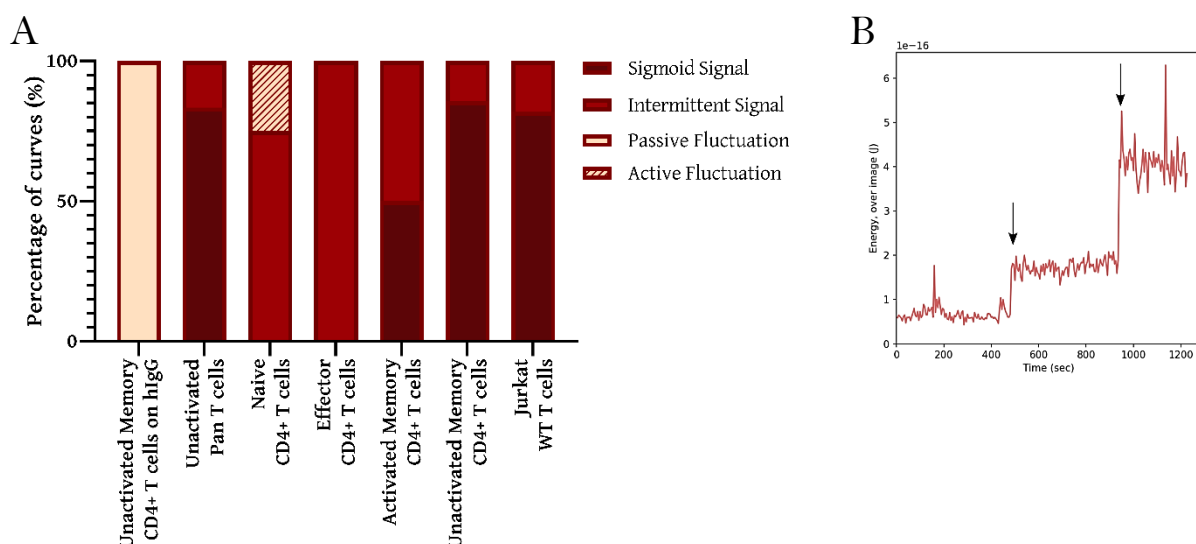


Fig. 2: Energy morphologies. A: The relative occurrence of the different energy curve morphologies obtained for the displayed T cell subsets. The data previously obtained for WT Jurkat cells on 400 Pa PAG coated with on aCD3 are here presented for comparison. B: A new energy curve morphology was frequently observed, with two (or more) steps in the “sigmoid” shaped energy curve. We do not incorporate, for the moment being, this morphology as a separate class in our analysis.

As expected, we observe, for the different primary T cell populations, the same three energy curve morphologies we have previously reported for Jurkat T cells; Sigmoidal, intermittent and active fluctuations, for cells interacting with activating aCD3-functionalized gels, and purely passive fluctuation for cells interacting with IgG gels (Fig. 2 A). Thus, as seen for the Jurkat T cells, the energy morphologies visualized were indeed specific for the interaction of the cells with the aCD3 presenting substrates.

However, we do detect a new morphology, we dubbed as “multi-step Sigmoidal”- found specifically in the memory T cell subpopulation- that was not observed at all in our Jurkat T cell experiments (Fig. 2B). As this data represents preliminary results, we do not incorporate these new morphologies in the current classification, however, we will do so as we accumulate more experimental material on primary cells.

Interestingly, there seems to be a very distinct division in the morphology of the energy profiles exerted based on the T cell subpopulation used (Fig. 2 B): memory T cells exhibiting both sigmoidal and intermittent morphologies, while effector T cells exhibiting exclusively intermittent morphology, and naive T cells exhibit both intermittent and active fluctuation morphologies. Surprisingly, similar to what we see with the memory T cells, the Pan T cell population, which represents the whole T cell population, combining the naive, effector and memory T cells, exhibits only sigmoidal and intermittent morphologies. As these cells are isolated from donor blood bags, the lack of the active fluctuation morphology, which we only observe in a small percentage (25%) of the naive subset, could be simply attributed to the fact that naive T cells constitute at best 10% of all peripheral blood T cells, which is instead dominated by memory T cells (around >50%) (Xia et al. 2021).

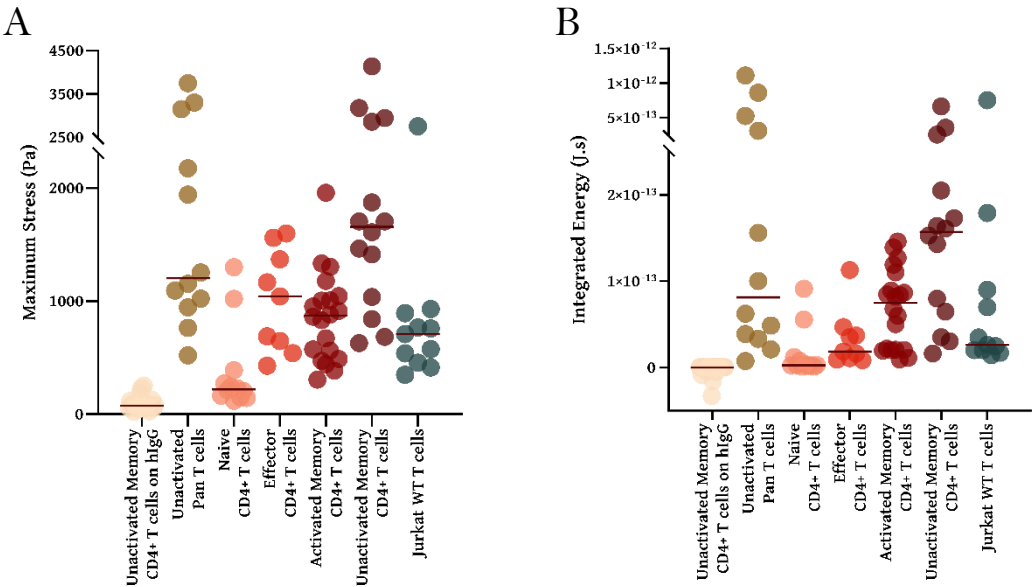


Fig. 3: A: Pooled maximum of the sum of stresses as a function of substrate coating. B: Pooled integrated energy over the time of the experiment (15 min). The data previously obtained for WT Jurkat cells on 400 Pa PAG on aCD3 are presented here for comparison. Each point corresponds to a cell, the bar presents the median of the data. Statistical comparison can be found in the table below.

| p values | Unactiv. mem. / IgG2a | Pan T cells | Naive T cells | Effector T cells | Unactiv. mem. T cells | Activ. mem. T cells | Jurkat WT T cells | Max. stress |
|-----------------------|-----------------------|-------------|---------------|------------------|-----------------------|---------------------|-------------------|-------------|
| Unactiv. mem. / IgG2a | | ***** | ***** | ***** | ***** | ***** | ***** | |
| Pan T cells | ***** | | *** | ns | ns | ** | ** | |
| Naive T cells | ***** | *** | | *** | ***** | *** | ** | |
| Effector T cells | ***** | * | * | | * | ns | ns | |
| Unactiv. mem. T cells | ***** | ns | ***** | ** | | *** | ** | |
| Activ. mem. T cells | ***** | ns | | * | ** | | ns | |
| Jurkat WT T cells | ***** | ns | ** | ns | * | ns | | |
| Integrated energy | | | | | | | | |

Table: Statistical results using the Mann-Whitney test in Graphpad Prism over the different subtypes of cells, for maximal stress and integrated energy over the entire sets of cells acquired experimentally, without any sorting on energy curve vs. time morphologies.

Previously, we have documented (see Chapter on Jurkat cells in the present report) that the sigmoidal and intermittent energy curves are correlated with higher levels of integrated energy, opposite to the active fluctuations which reflect the lowest levels of integrated energy. This applies here as well as the unactivated memory T cells, exhibiting the highest percentage ($\sim 86\%$) of sigmoidal curves between the different subtypes, display significantly higher levels of integrated energy than the remaining subtypes, conversely to the naive T cells-the only subtype comprising active fluctuation energy curves (25 %)-display the lowest (Fig. 3B).

One very intriguing observation is the significant decrease in the maximum stresses and integrated energy levels in the activated memory T cells in comparison to the unactivated ones. It is very reasonable to assume that stimulating an already activated T cell would push the cells into a state of exhaustion, however, generally exhaustion is seen over much longer time frames (days) while our experiments lasted only 15 min. Could there be an early TCR-related trigger for exhaustion? Another possibility is that, as the memory T cells were activated and then cultured in the absence of IL-2 for two days, the T cells could have entered an anergic state whereby they start downregulating their TCRs. A downregulation in the molecule we are aiming to engage to record forces would explain the decrease we observe.

In general, the differences in the maximum stresses and integrated energy levels recorded between the memory, effector, and naive T cells, which is indeed reflected in the dispersion of the data points in the Pan T cell population, hint towards the very exciting possibility that force exertion might differ based on the action carried out by a specific T cell subtype; In the physiologic context, memory T cells have been shown to exert a cytokine (CD4+)/cytotoxic (CD8+) response to re-stimulation by their cognate pMHCs irrespective of the presence of a costimulatory signal (Signal 2). Conversely, a naive T cell will never undergo stimulation and clonal proliferation outside of the lymphoid structures since it requires Signal 1 and Signal 2 from a dedicated antigen presenting cell (APC) as described in the Introduction chapter. An attractive hypothesis one could make is that the increased force exertion exhibited by memory T cells upon restimulation (in our case by aCD3 on soft-as-APC gels), in comparison to naive T cells, might contribute to their ability to undergo activation much more easily.

However, these are just speculations. As this is just preliminary data, further experimentation will be needed before we can draw firm conclusions, the first one of which could be to quantify the levels of TCR in memory unactivated and activated (in the absence of IL2 again) and see if we can correlate the level of TCR expression to force exertion. Another interesting experiment would be to probe the naïve and memory T cells on our ultra-soft gels functionalized with both stimulation (aCD3) and co-stimulation (aCD28) to see how costimulation will influence the behavior of the two. Of course, next steps will involve the introduction of adhesion (via aCD11a or ICAM1), in combination with aCD3, and potentially more complex substrates involving all three types of molecules (aCD3+aCD28+aCD11a).

We hope that these preliminary results, presented here in a condensed format, pave the way to new experiments that will lead to more detailed analysis and comprehension of the mechanisms at play during early T cell activation.

References

- Bartelt, Rebekah R, Noemi Cruz-Orcutt, Michaela Collins, and Jon C D Houtman. 2009. 'Comparison of T Cell Receptor-Induced Proximal Signaling and Downstream Functions in Immortalized and Primary T Cells.' *PloS One* 4 (5): e5430–e5430. <https://doi.org/10.1371/journal.pone.0005430>.
- Brodoivitch, Alexandre, Pierre Bongrand, and Anne Pierres. 2013. 'T Lymphocytes Sense Antigens within Seconds and Make a Decision within One Minute'. *Journal of Immunology (Baltimore, Md.: 1950)* 191 (5): 2064–71. <https://doi.org/10.4049/jimmunol.1300523>.
- Brodoivitch, Alexandre, Eugene Shenderov, Vincenzo Cerundolo, Pierre Bongrand, Anne Pierres, and Philip Anton van der Merwe. 2015. 'T Lymphocytes Need Less than 3 Min to Discriminate between Peptide MHCs with Similar TCR-Binding Parameters'. *European Journal of Immunology*, n/a-n/a. <https://doi.org/10.1002/eji.201445214>.
- Bunnell, S C, V Kapoor, R P Tribble, W Zhang, and L E Samelson. 2001. 'Dynamic Actin Polymerization Drives T Cell Receptor-Induced Spreading: A Role for the Signal Transduction Adaptor LAT.' *Immunity* 14 (3): 315–29.
- Cai, En, Kyle Marchuk, Peter Beemiller, Casey Beppler, Matthew G. Rubashkin, Valerie M. Weaver, Audrey Gérard, et al. 2017. 'Visualizing Dynamic Microvillar Search and Stabilization during Ligand Detection by T Cells'. *Science* 356 (6338): eaal3118–eaal3118. <https://doi.org/10.1126/science.aal3118>.
- Chakraborty, Arup K, and Arthur Weiss. 2014. 'Insights into the Initiation of TCR Signaling.' *Nature Immunology* 15 (9): 798–807. <https://doi.org/10.1038/ni.2940>.
- Han, Jonathan M., Scott J. Patterson, and Megan K. Levings. 2012. 'The Role of the PI3K Signaling Pathway in CD4(+) T Cell Differentiation and Function'. *Frontiers in Immunology* 3: 245. <https://doi.org/10.3389/fimmu.2012.00245>.
- 'Jurkat, Clone E6-1 | ATCC'. n.d. Accessed 2 March 2022. <https://www.atcc.org/products/tib-152>.
- Kumari, Sudha, Huw Colin-York, Darrell J. Irvine, and Marco Fritzsche. 2019. 'Not All T Cell Synapses Are Built the Same Way'. *Trends in Immunology*, October. <https://doi.org/10.1016/j.it.2019.09.009>.
- Kumari, Sudha, David Depoil, Roberta Martinelli, Edward Judokusumo, Guillaume Carmona, Frank B Gertler, Lance C Kam, et al. 2015. 'Actin Foci Facilitate Activation of the Phospholipase C- γ in Primary T Lymphocytes via the WASP Pathway', 1–31. <https://doi.org/10.7554/eLife.04953>.
- Mustapha, Farah, Kheya Sengupta, and Pierre-Henri Puech. 2022. 'Protocol for Measuring Weak Cellular Traction Forces Using Well-Controlled Ultra-Soft Polyacrylamide Gels'. *STAR Protocols* 3 (1): 101133. <https://doi.org/10.1016/j.xpro.2022.101133>.
- Santos, Luís C, David A Blair, Sudha Kumari, Michael Cammer, Thomas Iskratsch, Olivier Herbin, Konstantina Alexandropoulos, Michael L Dustin, and Michael P Sheetz. 2016. 'Actin Polymerization-Dependent Activation of Cas-L Promotes Immunological Synapse Stability'. *Immunology and Cell Biology* 94 (10): 981–93. <https://doi.org/10.1038/icb.2016.61>.
- Xia, Ying, Aqing Liu, Wentao Li, Yunhe Liu, Guan Zhang, Songshan Ye, Zhijieruo Zhao, et al. 2021. 'Reference Range of Naïve T and T Memory Lymphocyte Subsets in Peripheral Blood of Healthy Adult'. *Clinical and Experimental Immunology*, December, uxab038. <https://doi.org/10.1093/cei/uxab038>.

Concluding Remarks and Perspectives

In the preceding thesis manuscript, we have presented the work that has been done over the course of the past three years. Unfortunately, the COVID-19 pandemic hit in the midst of the project and introduced some unexpected constraints on our experiments. Most importantly, the acquisition of human blood bags for primary T cell isolation from the hospital. As such, we had to shift our focus to Jurkat T cells, and simply make do with what was available.

However, now that we have gained access to blood bags again, our chief objective is to transition back to primary cells, and build on our preliminary findings to further to investigate the differences in force exertion between the naïve, effector and memory T cell subpopulations. We would also like to study the CD4+ and CD8+ populations separately as a systematic comparison, in the context of forces during early recognition, between these two cell types has never been reported in literature.

Another interesting avenue to explore would be the influence of co-inhibitory molecules (also known as immune checkpoint, e.g. CTLA-4 and PD1) on the mechanobiology for early T cell recognition; if we would think of the T cell as a car, pMHC binding to the TCR would be the key in the ignition, co-stimulatory molecules would be the gas inducing clonal expansion and differentiation, and co-inhibitory molecules would be the brakes, abrogating the T cell response and preventing inappropriate activation events such as those directed against self-antigens. Even though checkpoint blockade is now an approved and highly utilized medical approach in cancer and autoimmune diseases, the mechanism behind their action is still a mystery. It would be therefore worthwhile to see the influence, if any, of these molecules on early T cell recognition, in the frame of force exertion.

A crucial puzzle piece still missing in our experiments is the link between the stress intensities and the energy morphologies we observe and T cell activation. One method we are currently trying to implement to address this problem is to couple TFM with calcium imaging. Calcium fluxes are indeed a hallmark of early T cell activation, however, it is important to bear in my mind that it is not a definitive marker of complete activation. Another concern of ours regarding the use of calcium dyes, is the possible effect that such dyes might have on T cell mechanics. If significant discrepancies do arise, one possible solution would be to resort to genetically expressed calcium reporters instead.

Clearly, imaging is a limitation in our approach as we rely on epifluorescence microscopy. It would be definitely beneficial to employ higher resolution imaging techniques (such as Total Internal Reflection Fluorescence microscopy), the problem with those however, is that we would most likely be forced to replace our polyacrylamide gels with substrates having a retractive index similar to glass, such as Polydimethylsiloxane (PDMS). Though using PDMS-TIRFM would surely increase our spatial resolution, we would lose our ultra-soft feature that allowed us to observe the distinctive energy profiles to begin with (for Jurkat

T cells). If we do manage to observe the same behaviors for primary T cells on stiffer substrates (2 KPa), switching to PDMS would be a very real possibility. Aside from increasing our imaging resolution, this would allow us to implement one of our initial project objectives which was to micropattern the gels for controlling cell geometry. Several attempts at that were made, including using patterned molds, nanopatterns and even Alveole UV laser technology, however they all failed, most likely to the high hydrophilicity of the ultra-soft PAA gels. Nanopatterning PDMS, a technique already established at CINAM, would surely be more feasible and would also allow us to perform bead-less, reference-free TFM.

We would like to end this dissertation by emphasizing that the experimental setup we have developed to study the forces generated during early T cell recognition is an over simplified system that surely does not recapitulate the complexities at the T cell-APC interface, either topologically (numerous ligands-other than the ones we have focused on- with variable expression levels and mobilities are present at the contact zone) or dynamically (the Tcell-APC contact is a mobile contact). Not to mention the biggest complexity of all which is that the APC itself, opposite to our substrates, is an active player in the process. We attempted to mimic two key APC characteristics, stiffness and TCR engagement. The goal from here is to **gradually** upgrade our setup (e.g. by increasing the spatio-temporal resolution, re-creating a more complex interaction with numerous, and if possible, well-distributed molecules) in hopes of attaining a better representation of in-vivo interactions, while still being able to extract meaningful correlations.

We can only hope that the work presented here paves the way to new and interesting findings.

